

043
LAL
15127

SOME STUDIES ON MINOR NEUTRAL
CONSTITUENTS OF THE
MIDDLE ATMOSPHERE OF LOW LATITUDE

MANOHAR LAL

A THESIS SUBMITTED TO THE
GUJARAT UNIVERSITY
FOR THE DEGREE OF
DOCTOR OF PHILOSOPHY

DEPARTMENT OF PHYSICS
GUJARAT UNIVERSITY

AND

PHYSICAL RESEARCH LABORATORY

043



B15127

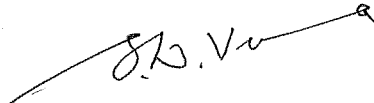
043
LAL
15127

CERTIFICATE

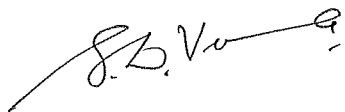
I hereby declare that the work presented in this thesis is original and has not formed the basis for the award of any degree or diploma by any University or Institution.

Manohar Lal
(Manohar Lal)

Certified by


Prof. S.D. Verma
(Professor-in-Charge)

January 1994


Head
Physics Department
Gujarat University
Ahmedabad-380009

Dedicated to my
parents

Contents

Preface	vi
Acknowledgements	viii
Publications	xi
1 Introduction	1
1.1 General Introduction	1
1.2 Aim and Scope of the Present Study	4
2 Experimental Setup	11
2.1 Introduction	11
2.2 Instruments	12
2.2.1 Monochromator	12
2.2.2 Diffraction Grating	14
2.2.3 Resolution	14
2.2.4 Stray Light	15
2.2.5 Lock-in Amplifier	16
2.2.6 Optical Chopper	17
2.3 Detector	18
2.3.1 Photomultiplier Characteristic	18
2.3.2 Dark Current	20
2.4 Filters	22

2.4.1	Absorption	22
2.4.2	Transmittance	23
2.4.3	Optical density	23
2.5	Data acquisition system	24
2.6	Operation of the instrument	25
3	Results of NO₂ Measurements	26
3.1	Introduction	26
3.2	Earlier studies	27
3.3	Methodology	31
3.3.1	Zenith sky brightness	31
3.3.2	Ratio spectrum	33
3.3.3	NO ₂ cell	35
3.4	Data reduction	36
3.4.1	Method-1	37
3.4.2	Methods 2 and 3	38
3.4.3	Method-4	39
3.4.4	Method 5	41
3.4.5	Absorption cross-sections	44
3.4.6	Conversion of slant column to vertical column	46
3.5	Sources of error	48
3.5.1	Laboratory absorption cross-sections	48
3.5.2	Tropospheric contamination	48
3.5.3	Ring effect	49
3.5.4	Enhancement factor	49
3.5.5	Resultant uncertainty	50
3.6	Results and discussion	51
3.6.1	Winter values	51
3.6.2	Decay constant	52

3.6.3	Diurnal variation	52
3.6.4	Correlation between NO_2 and O_3	53
3.6.5	Sunrisetime variation	54
3.6.6	Longterm variation and variation after Pinatubo	55
4	Results of NO_3 Measurements	57
4.1	Introduction	57
4.2	Existing observations	58
4.3	Methodology	61
4.3.1	Conversion of slant column to vertical column	62
4.3.2	Data reduction	63
4.4	Theory	67
4.4.1	Differential absorption technique	68
4.4.2	Matrix inversion technique	68
4.4.3	Absorption cross section	70
4.5	Results and discussion	72
4.5.1	Results of Ahmedabad	72
4.5.2	Results of Gurushikhar	74
4.5.3	Sunrisetime variation of NO_3 over Gurushikhar	75
4.6	Sources of error	76
4.6.1	Laboratory absorption cross-sections	76
4.6.2	Alignment of the spectrum	77
4.6.3	Water vapour interference	77
4.6.4	Ring effect	77
4.6.5	Movement of lunar image on interence slit	77
4.6.6	Enhancement factor	78
4.6.7	Resultant uncertainty	78
5	A Theoretical Model of NO_2 and NO_3	79

5.1	Introduction	79
5.2	Existing model studies	80
5.3	Scheme used in the present study	84
5.4	Input parameters	84
5.4.1	Temperature	85
5.4.2	Neutral constituents	85
5.4.3	Solar zenith angle	87
5.4.4	Reaction rate coefficients	87
5.4.5	Photolysis rate	88
5.5	Methodology and continuity equations	88
5.5.1	NO_2 continuity equation	89
5.5.2	NO_3 continuity equation	90
5.5.3	N_2O_5 continuity equation	91
5.6	Theoretical model results	91
5.6.1	NO_2 calculation	91
5.6.2	Decay factor of NO_2	93
5.6.3	Diurnal Variation of NO_2	94
5.6.4	NO_3 calculation	94
5.6.5	N_2O_5 calculation	97
6	Pinatubo Aerosols	100
6.1	Introduction	100
6.2	Existing results of Pinatubo eruption	102
6.2.1	Satellite measurements	102
6.2.2	Aircraft measurements	103
6.2.3	Ground-based experiment	104
6.3	Earlier twilight brightness measurements	105
6.4	Observations (Instrumentation)	105
6.5	Zenith sky twilight brightness	106

6.6	Theory	108
6.7	Results and discussion	110
6.7.1	Correction due to atmospheric refraction	110
6.7.2	Height of the aerosol layer	111
6.7.3	The aerosol layer thickness	112
6.7.4	Aerosol strength variation	112
6.7.5	Spectral response of twilight intensity	114
6.7.6	Zenith sky intensity at different look angle	114
6.7.7	Multiple aerosol layer	115
6.8	Uncertainty in results	116
7	Concluding Remarks	119
7.1	Achievements	119
7.2	Scope and suggestions for future work	122
	References	125

Preface

This thesis is a presentation of work carried out at Physical Research Laboratory, Ahmedabad, India, on minor neutral constituents of the middle atmosphere. Both experimental and theoretical studies have been made. Experimental studies have been conducted by ground-based technique at Ahmedabad (23°N, 73°E), India and Gurushikhar (24°N, 73°E), India. The experimental work has three parts viz: (a) NO₂ study, (b) NO₃ study and (c) Volcanic aerosol study and theoretical study consists of the explanation of the first two parts of the experimental work. These are described in different Chapters whose outline is given below :

The Chapter 1 is the introduction to this thesis. The scope of the thesis has also been given in this chapter.

Chapter 2 deals with the technique used, instrumental setup, and observational procedure.

Chapter 3 describes the results of NO₂ measurements over Ahmedabad and the effect of Mt. Pinatubo volcanic aerosols on NO₂ variability.

Another important species of NO_x group is NO₃. Results obtained from NO₃ measurements are presented in Chapter 4. Variability of NO₃ during nighttime and its disappearance during dawn have been studied over low latitude northern hemisphere.

The observational results of Chapter 3 and Chapter 4 are explained by theory in Chapter 5. This theoretical study has been made using one - dimensional model. The details of the scheme and comparison between model results and observational values are described in the same Chapter.

Chapter 6 deals with the study of volcanic aerosols produced in the stratosphere after Mt. Pinatubo erupted in June 1991. For this purpose zenith sky intensity

during twilight period has been measured using ground-based photometric technique. The detailed description of the technique and the results thus obtained are given in the same Chapter.

The concluding remarks and suggestions for the further study are given in Chapter 7.

Manohar Lal

Author

December 1993

Ahmedabad (India)

Acknowledgements

I am indebted to my supervisor Dr. D. K. Chakrabarty for his encouragement and invaluable support throughout my Ph.D. tenure. Right from the days of course work, I was always fascinated by his profound depth of understanding on the variety of basic physical and chemical processes of the entire atmosphere. It was his competent and ready guidance, throughout my research work which made the entire journey a smooth sailing to reach the quay. I owe my gratitude to him for having taught me certain basic aspects of life which I found to be very useful in the process of building up my career. I am also thankful to him for critically going through the manuscript of the thesis and making several useful suggestions.

I thank Prof. S. D. Verma for his support and encouragement which enabled me to complete this work. I express my deep sense of gratitude to Prof. A.P. Mitra, Bhatnagar Fellow, and Prof. A. K. Saha, Emeritus Professor, for going through various details of this work. Their valuable suggestions and guidance have enabled me to improve substantially the presentation of this thesis.

I am grateful for the general encouragement shown to me during my Ph.D. tenure by the Director, Prof. R. K. Verma. I am grateful to Prof. B. H. Subbaraya for having shown so much care towards the improvement of my career. I have had many fruitful discussions with Prof. Harish Chandra, Prof. J. N. Desai, Prof. R. Sridharan, Dr. Shyam Lal, Dr. T. Chandrasekhar, Dr. N. M. Ashok, Dr. A. Jayaraman, Dr. K. P. Subramanian, Dr. S. A. Haider, Dr. G. Subramanian, Dr. H. S. S. Sinha, Dr. R. Sekar, and R. Narayanan for which I am grateful and above all I am thankful for their friendship and encouragement.

It is a great pleasure to acknowledge our group members who have offered their help whole heartedly throughout my thesis work, and I would like to take this

opportunity to thank them. I value the discussions I had with Mr. S. R. Das on the data acquisition system and my thanks are due to him. I am very grateful to Mr. J. S. Sidhu for his help to setup the instruments properly. I thank Mr. K. V. Pandya for his assistance in the analysis of solar/lunar spectra obtained by using monochromator. Mr. Piplapure has been helpful to me in many ways and I owe my thanks to him. I acknowledge the secretarial assistance rendered by Mr. N. R. Pillai.

I would like to thank Dr. Susan Solomon, NOAA Aeronomy Laboratory, Boulder, Colorado, for discussions on NO_2 and NO_3 results; Prof. W. B. Grant, NASA Langley Research Center, Hampton, Virginia for providing recent SAGE data and valuable discussion on the effect of Pinatubo aerosols on different minor constituents; Dr. R. L. McKenzie, NIWAR, Lauder, New Zealand, for discussion on NO_2 ; Prof. S. Chandra, GSFC, NASA, for discussions on ozone variability due to volcanic eruption; Prof. Y. Kondo, STELab, Nagoya Univ., Nagoya, Japan, for discussions on NO_2 results; Prof. G. Brasseur, NCAR, USA, for discussions on NO_2 and NO_3 chemistry. I record my gratitude to them.

I express my thanks to the personnel of the PRL workshop and in particular to Mr. P. S. Panchal who has made lot of efforts in designing and fabricating different accessories of the monochromator system. I am grateful to the staff of the computer center and the Library for their cooperation and help. I thank Mr. D. R. Ranpura of the photographic and documentation section for his meticulous work and timely delivery of photographic prints. I am also thankful to the draftsman Mr. S. C. Bhavsar for making figures and diagrams.

NO_3 measurements have also been taken from hill station, Gurushikhar. I am indebted to all the Gurushikhar staff for the success of the nighttime observations and in particular to Mr. R. Shah and Mr. Kothari. I express my gratitude to them.

opportunity to thank them. I value the discussions I had with Mr. S. R. Das on the data acquisition system and my thanks are due to him. I am very grateful to Mr. J. S. Sidhu for his help to setup the instruments properly. I thank Mr. K. V. Pandya for his assistance in the analysis of solar/lunar spectra obtained by using monochromator. Mr. Piplapure has been helpful to me in many ways and I owe my thanks to him. I acknowledge the secretarial assistance rendered by Mr. N. R. Pillai.

I would like to thank Dr. Susan Solomon, NOAA Aeronomy Laboratory, Boulder, Colorado, for discussions on NO_2 and NO_3 results; Prof. W. B. Grant, NASA Langley Research Center, Hampton, Virginia for providing recent SAGE data and valuable discussion on the effect of Pinatubo aerosols on different minor constituents; Dr. R. L. McKenzie, NIWAR, Lauder, New Zealand, for discussion on NO_2 ; Prof. S. Chandra, GSFC, NASA, for discussions on ozone variability due to volcanic eruption; Prof. Y. Kondo, STELab, Nagoya Univ., Nagoya, Japan, for discussions on NO_2 results; Prof. G. Brasseur, NCAR, USA, for discussions on NO_2 and NO_3 chemistry. I record my gratitude to them.

I express my thanks to the personnel of the PRL workshop and in particular to Mr. P. S. Panchal who has made lot of efforts in designing and fabricating different accessories of the monochromator system. I am grateful to the staff of the computer center and the Library for their cooperation and help. I thank Mr. D. R. Ranpura of the photographic and documentation section for his meticulous work and timely delivery of photographic prints. I am also thankful to the draftsman Mr. S. C. Bhavsar for making figures and diagrams.

NO_3 measurements have also been taken from hill station, Gurushikhar. I am indebted to all the Gurushikhar staff for the success of the nighttime observations and in particular to Mr. R. Shah and Mr. Kothari. I express my gratitude to them.

It would be impossible for me to name all the people and friends whose association kept me happy and cheerful during all the past six years. A few names that comes to my mind immediately are Supriyo, Seema, Raju, Watson, Someswar, Ravi Bhushan, Poulose, Jyotiranjana, Varun, Yags, Prahalad, Prashant, Shikha, Sivakumar, Gautam, Debasish, Ganguly, Ansu, Majumdar, and Mitaxi. I extend them my gratitude.

My deep appreciation and sincere thanks to Ramani, Sam, Manish, Tarun, Srinivasan, Patra, Pullam Raju, Nagesha, Dwivedi, Indumathi, and Dr. Sai Iyer for the kind help that they have extended to me regarding the typeset of this thesis in L^AT_EX.

I am pleasantly obliged to Dr [Mrs] Purobi Chakrabarty, Manoj Samal, Dr. Gurubaran, Ramchandran, and Dr. Arul for their careful and patient reading of the text and making useful suggestions.

The work covered in this thesis could not have been possible without encouragement, constant inspiration and boundless love of my parents. I am indebted to them throughout my life.

This study falls under the Indian Middle Atmosphere Program [IMAP]. I gratefully thank the IMAP authorities for financial support which made this work possible.

Finally, I thank Gayatri with love who assisted me in various phases of my thesis work particularly in coordinating and in compiling the references of this thesis.

List of Publications

- (1) A. Jayaraman, S. Lal, M. Lal, B.H. Subbaraya, S.C. Garg, T. John, K.S. Zalpuri, N. Seshadri, C.R. Sreedharan, R. Vijaykumar, V.M. Ignatov, G.A. Kokin, S.P. Perov, O.V. Shtrikov, S.V. Tishin, and A.F. Chizov.

The Indo-Soviet collaborative experiment at Thumba to study diurnal variations in the ozone vertical distributions over the tropics.

in **Ozone in the Atmosphere** Eds. R.D. Bojkov and P. Fabian, A. Deepak Publishing, 1989, pp. 113 - 116.

- (2) M. Lal, D.K. Chakrabarty, J.S. Sidhu, S.R. Das, and S.D. Verma.

Some results of ground-based measurements of atmospheric NO_2 at Ahmedabad by visible absorption spectroscopy.

Indian J. Radio Space Phys., 22, 108 - 113, 1993.

- (3) D.K. Chakrabarty, M. Lal, G. Beig, J.S. Sidhu, and S.R. Das.

Balloon measurements of ionic conductivities of the middle atmosphere in India during MAP.

In press of **J. Atmos. Terr. Phys.** (UK).

- (4) M. Lal, D.K. Chakrabarty, J.S. Sidhu, and S.R. Das.

Atmospheric NO_3 observations over low latitude northern hemisphere during night.

In press of **J. Geophys. Res.** (USA).

(5) M. Lal, D.K. Chakrabarty, J.S. Sidhu, and S.R. Das.

Near simultaneous measurements of NO_2 and NO_3 over tropics by ground-based absorption spectroscopy.

In press of proceeding of Quad. ozone symposium, Charlottesville USA, 1992.

(6) M. Lal, and D.K. Chakrabarty.

Derivation of water vapour absorption cross - sections in the red region.

In press of proceeding of Quad. ozone symposium, Charlottesville USA, 1992.

Chapter 1

Introduction

1.1 General Introduction

Man has always been interested in the atmosphere around him - in its changing weather patterns, glorious twilight phenomena, rainbows, aurora etc. The daily variation between day and night is one of the processes of nature which exerts a striking impact on the structure of organism and the way of life of every inhabitant of our planet. This atmosphere is also a vital natural resource which man has taken for granted throughout the history. To fulfill his own requirements, he has been dumping millions of tons of chemical materials into this atmosphere. Nature has its own method to remove these pollutants from the atmosphere. Often these chemicals offer resistance to nature's removal mechanism. Nature makes them interact with air and sunlight and transform them to substances which are susceptible to nature's removal mechanism. Often these are transported to suitable regions from where they are finally removed by rain. There is now evidence that these natural capabilities of the earth system are being overtaxed. The air, the ocean and the land of our earth are no longer able to keep pace with our discharges. As a result, worldwide, the amount of numerous key chemicals are increasing above their natural background amount in

this atmosphere. CO_2 , CH_4 , N_2O , lower atmosphere ozone, CFCs are some among them. Convincing data from the gases in polar ice cores tell us that the present CO_2 , CH_4 and N_2O concentrations are unprecedented, at least for the earth of the last 160,000 years. It is time that we make correct assessment of this trend, predict their impact on global change and take corrective measures before a permanent damage is done to our environment. It is in this greater perspective, that this thesis presents some work on the minor constituents of the middle atmosphere at low latitude.

The earth's atmosphere has been divided into different layers viz. troposphere, stratosphere, mesosphere, and thermosphere. The region approximately below 15 km is called troposphere, between 15 and 50 km is called stratosphere, between 50 and 95 km is called mesosphere and above mesosphere is thermosphere. Fig. 1.1 shows these regions along with their temperature nomenclature. The region between 10 and 100 km is called the middle atmosphere. In Fig. 1.2 temperature distribution below 60 km has been shown in a magnified way for tropical and polar region. Note the low tropopause temperature and high tropopause level in the equatorial region compared to mid and high latitude region. Our studies are confined to the region below 50 km.

The major constituents of the earth's atmosphere below about 100 km are N_2 (78%) and O_2 (21%), rest are minor constituents such as CO_2 , CH_4 , N_2O , H_2O , NO_2 , O_3 , NO_3 etc. and aerosol particles of size varying from 0.2μ to 20μ . But they control the climate and the way of life on earth's surface. Fig. 1.3 illustrates the height variation in number density for various chemical compounds in the middle atmosphere [Ackerman, 1979]. Although these were compiled from observational data obtained at different times and places by different methods, it shows the general trend in the height variation for each constituent. The curves 10^{-1} , 10^{-2} etc. represent the variations in number density for the case of a constant mixing ratio. Thus these minor constituents are at ppmbv and ppbbv levels.

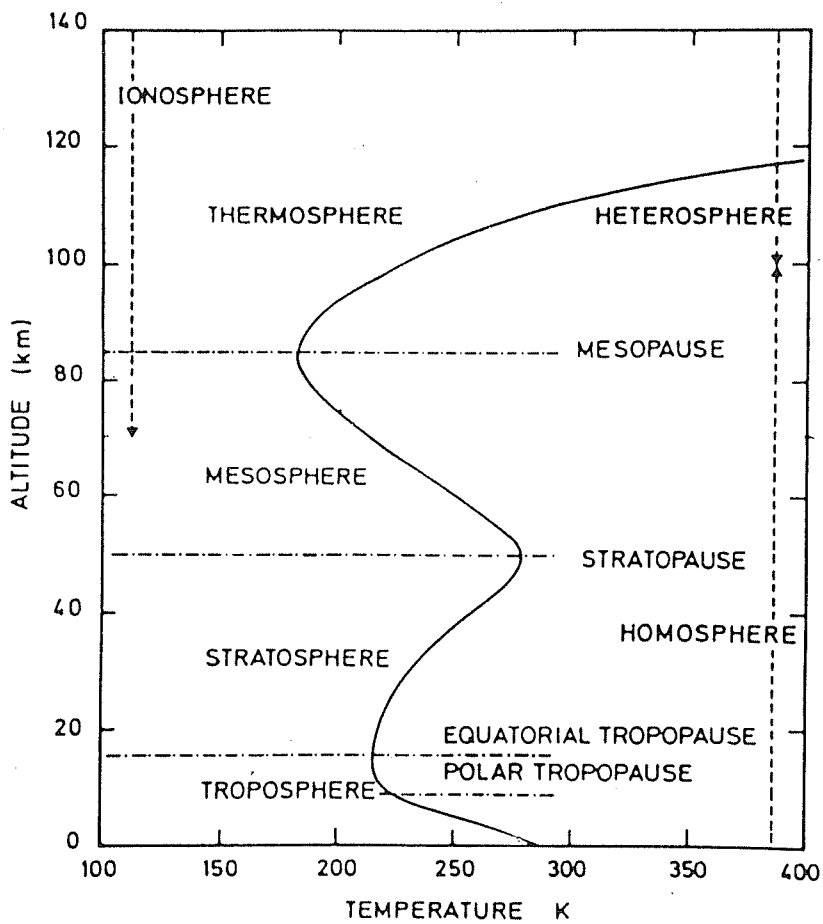


Figure 1.1 Thermal structure of atmospheric layers (Brasseur and Solomon, 1986).

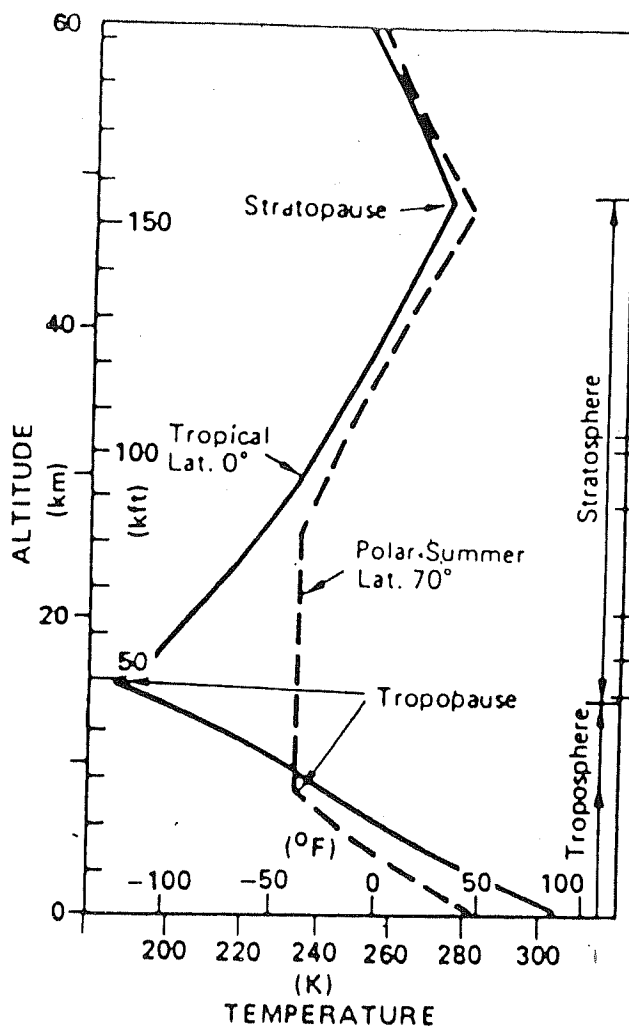


Figure 1.2 The temperature of the atmosphere below 60 km as a function of altitude.

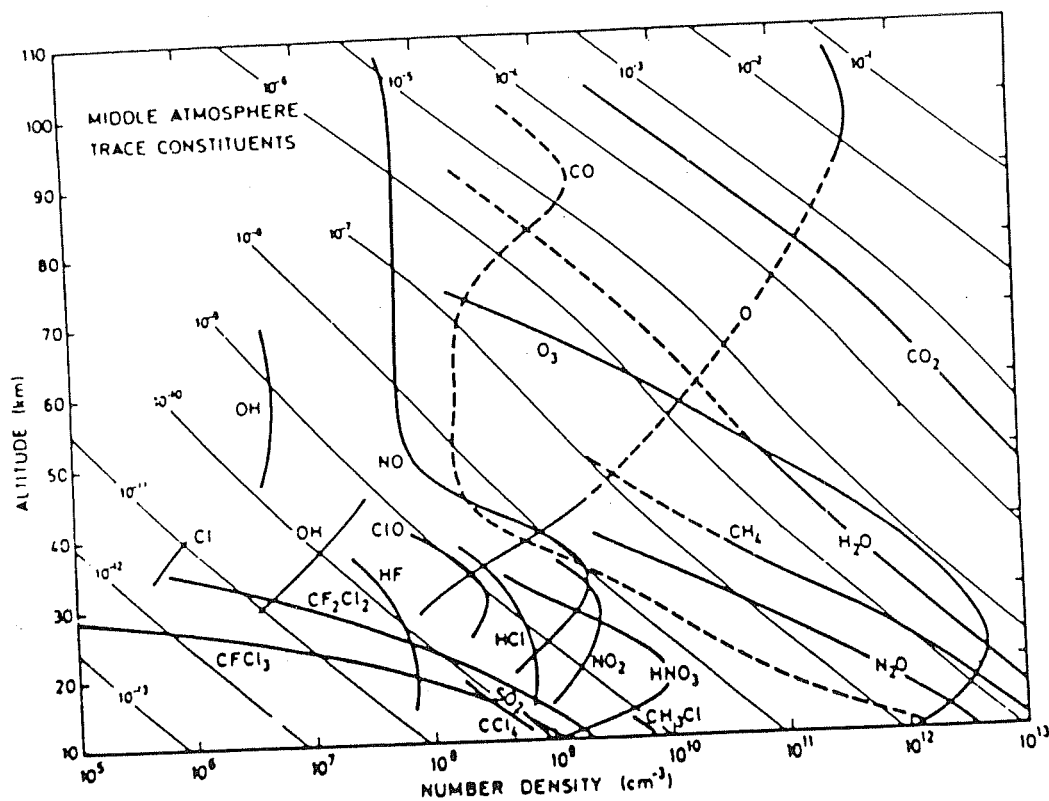
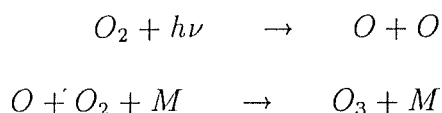


Figure 1.3 Vertical profiles of observed number densities of the typical trace constituents in the middle atmosphere (Ackerman, 1979).

The most important among the species mentioned above is O_3 which absorbs UV radiation coming from the Sun and thus prevents the harmful radiations from reaching the earth's surface. Fig. 1.4 shows the variation in the penetration height of solar radiation with wavelength. It can be seen that the radiation between ~ 200 and ~ 300 nm can penetrate to the stratosphere, and most of the energy is absorbed there. The radiation between ~ 130 and ~ 200 nm is absorbed mainly in the mesosphere, and below ~ 100 nm the radiation is absorbed mainly in the thermosphere. Fig. 1.4 also shows the main absorbing molecules over various wavelength ranges. O_3 is the main absorber at $\sim 240 - 320$ nm, O_2 at $\sim 100 - 200$ nm, and both O_3 and O_2 absorb radiation at $\sim 200 - 240$ nm. Absorption below ~ 100 nm can occur by various molecules and atoms (N_2 , O_2 , N , O). Without the protection of this ozone shield, even a lower form of animal life could not have survived on the earth's surface, as the harmful solar UV radiation would have destroyed the chromosomes of the cell nucleus, thus prohibiting cellular multiplication. The production and loss processes of O_3 were first given by Sydney Chapman in 1936. According to him, O_2 molecules get photodissociated and form O_3 molecules as follows-



At the same time O_3 absorbs the radiation and gets dissociated into O and O_2 .



But the above simple chemistry of ozone is not able to balance the ozone budget, some processes are missing. It was pointed out in 1970 by *Crutzen* [1970] and *Johnston* [1975] that the ozone concentration is greatly affected by chemical reactions with minor constituents, belonging to three groups viz. HO_X , NO_X , and ClO_X . Although concentrations of these species are very small compared to O_2 and N_2 , yet they catalytically reduce ozone by a large scale as follows:

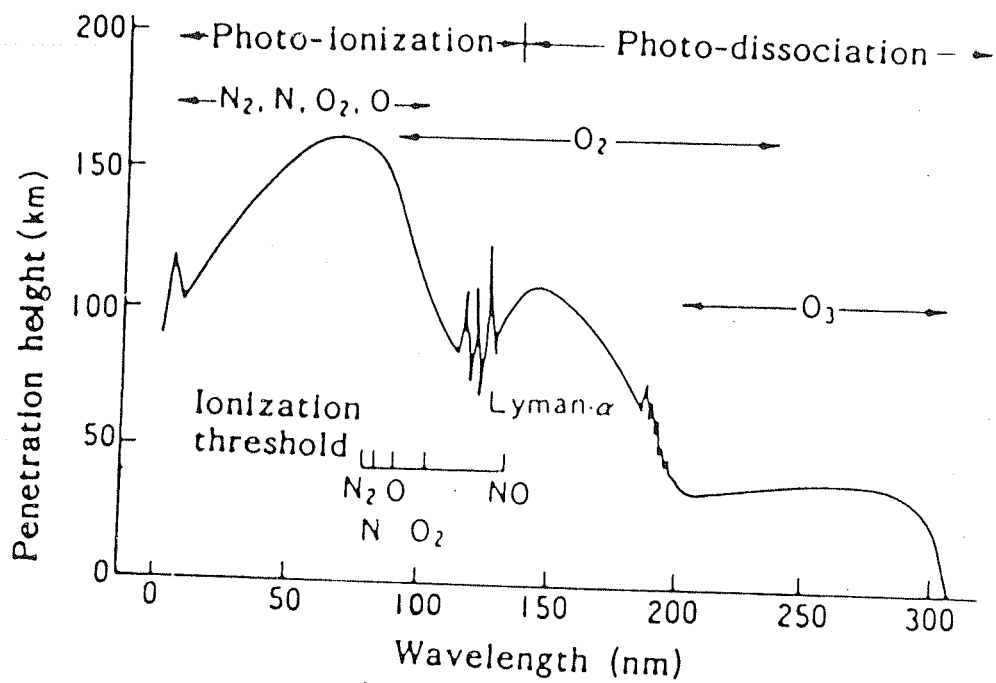
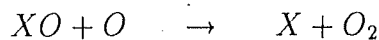
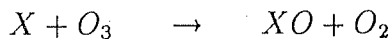


Figure 1.4 Penetration height for vertical incidence of solar radiation at various wavelengths (Shimazaki, 1985).



where, $(X = NO_X, HO_X, ClO_X)$

In the present work, characteristics of two species belonging to NO_X group viz. NO_2 and NO_3 have been experimentally and theoretically studied at a low latitude station Ahmedabad ($23^\circ N$, $72^\circ E$), India.

As mentioned above aerosols play a significant role in the radiation budget of the earth's atmosphere. The aerosol content of the atmosphere is disturbed by various processes; volcanoes are one among them. In June 1991, eruption of Mt. Pinatubo ($15^\circ N$, $122^\circ E$) volcano took place. It produced a huge amount of aerosols into the stratospheric region. In the present study, characteristics of these volcanic aerosols and their effect on the NO_2 distribution have been studied at low latitude station Ahmedabad by a ground-based technique.

1.2 Aim and Scope of the Present Study

- It has been mentioned above that NO_X group of species can catalytically destroy ozone. NO_2 is one of the important species belonging to NO_X group. Variabilities of this species are known at middle and high latitude zone. At low latitude, these have not been properly studied. This is mainly because the data at low latitude is sparse. Satellite observations are available at low latitude but these are not fully validated. We have measured NO_2 column density at low

latitude station, Ahmedabad from winter 1989 to summer 1992. One area of current interest is whether volcanic eruption affects NO_2 . A volcanic eruption which took place at Mt. Pinatubo, Philippines in June 1991 has provided us an opportunity to study its effect on NO_2 over Ahmedabad.

- NO_3 is another important species which belongs to the NO_x group. NO_3 variability has been studied at higher and mid latitude regions, but at low latitude region it has not been properly studied. Also NO_3 observational data at low latitude is very meagre. We have, therefore, studied the characteristics of this species at a low latitude station, Ahmedabad by a ground-based technique. Since NO_3 density is low during daytime, its density has been measured at night. Here, we have used direct moon as a source of light. This might introduce some tropospheric contamination in our measurements. To study this aspect, observations were taken at Gurushikhar, a hill station, 1.8 km above the mean sea level and 200 km away from the north of Ahmedabad where tropospheric pollution is less. In addition, the effect of Pinatubo volcanic aerosols on NO_3 has also been studied.

Since NO_3 gets dissociated in the presence of solar radiation, it gives us an opportunity to study the disappearance of NO_3 during twilight period. Sunrise disappearance rate of NO_3 has been observed at sunrise time by collecting scattered photons from the west horizon, opposite to the direction of sunrise.

- An attempt has been made to reproduce the features of NO_2 and NO_3 observed by us. Chemical equations are formed with production and loss terms of these species. These are solved simultaneously for steady state conditions. How far the observational results match with the theoretical model, has been studied.
- Occasionally stratospheric region is loaded by volcanic aerosols. As mentioned

earlier, a volcanic eruption took place in June 1991 at Mt. Pinatubo, Philippines. In this eruption, a huge amount of sulphur dioxide was injected into the tropical stratosphere. These SO_2 gases were converted into $\text{H}_2\text{SO}_4/\text{H}_2\text{O}$ aerosols. Characteristics of these aerosols have been studied by a ground-based technique at Ahmedabad.

This thesis has been subdivided into seven chapters, In the following sections, a brief summary and important results of the subsequent Chapters are given. These are characteristics of NO_2 and NO_3 species and volcanic aerosols. These results will contribute greatly to the global data set which will be useful not only for a better understanding of each of the basic processes, but also for obtaining an overall picture of the phenomena in the middle atmosphere.

Chapter 2 deals with the instrumental setup, observational procedure and data reduction method. Measurements of absorption spectrum in the region 436 to 448 nm for NO_2 , 655 to 667 nm for NO_3 , and 800 nm for volcanic aerosols by a ground-based technique is our aim. For that purpose we have used a McPherson UV-Visible monochromator, model-270. The details of the instrument has been described. A chopper in conjunction with a Lock-in amplifier was used to improve the signal to noise ratio. The chopper was placed in front of the entrance slit of the monochromator and Lock-in amplifier was attached to the detector system. These details are given. Photomultiplier tubes were used as detector. For NO_2 , R-372 Hamamatsu and for NO_3 and aerosol studies R-955 Hamamatsu photomultipliers were used. A cooling system was provided to R-955 tube. Scanning of the spectra was done by a computer. Data was digitized and stored in a floppy. For that purpose a software was developed by us. Besides operation of the instrument, various steps involved in the data reduction are also discussed in detail.

In Chapter 3, NO_2 and O_3 results obtained by us have been presented. Observations have been taken during twilight period. Scattered light from the zenith sky has been measured in the wavelength range 448 to 436 nm. A spectrum has also been taken near the noon time. This spectrum has been used as the back-ground spectrum. The path length covered by the solar radiation during twilight period is 20 to 30 times more than that during the noon time. The 436-448 nm wavelength region is full of Fraunhofer structure. By dividing the twilight spectrum by the back-ground spectrum, Fraunhofer component has been removed. The ratio spectrum thus obtained contains the contribution due to NO_2 , O_3 , aerosol, air, H_2O and O_4 . Using Beer Lambert's law slant column abundances of NO_2 and O_3 have been determined for sunrise and sunset times by a matrix inversion method. These slant column abundances have been converted into vertical column abundances by dividing them by the appropriate air mass factors. Diurnal and seasonal variations of NO_2 over Ahmedabad have been studied. During monsoon period observations have not been taken. NO_2 total column abundance is found to be minimum in the winter. The decay factor of NO_2 during night has also been determined. The decay factor is the ratio of $[\text{NO}_2]$ density at preceding evening to the morning $[\text{NO}_2]$ density. Correlation between NO_2 and O_3 has been examined for winter period. A weak positive correlation has been found. In addition, effect of volcanic eruption on NO_2 has also been investigated.

Chapter 4 deals with the total NO_3 column density measured by us. For these measurements we have used moon as a light source. NO_3 has strong absorption at 662 nm. Direct lunar spectrum between 655 and 667 nm region has been taken near the full moon period. Background spectrum has been taken during daytime at higher solar zenith angle with direct sun as light source. Background spectrum has also been taken with moon as source at lower lunar zenith angle. Besides NO_3 , water vapour also has absorption in this wavelength region. The contribution of water vapour has been removed by taking the ratio of the nighttime to the daytime spectra.

The nighttime spectrum is further divided by the background spectrum. The ratio spectrum thus obtained has been used to derive the NO_3 slant column abundance by using the matrix inversion technique. NO_3 slant column abundance is then converted to vertical column abundance by dividing it by the appropriate airmass factor.

Ahmedabad being an urban area, the contribution of tropospheric NO_3 is likely to be significant. Therefore, some observations have been taken on a hill station Gurushikhar (24°N , 73°E), 1.8 km above the sea level and about 200 km north of Ahmedabad. Here tropospheric pollution is negligible. Signal to noise ratio at lunar zenith angle 85° and more becomes very small in the urban area due to the presence of dust particles in the lower atmosphere. Therefore, at Ahmedabad, observations could be taken upto $\sim 85^\circ$ lunar zenith angle only and at Gurushikhar, observations were possible up to $\sim 90^\circ$ lunar zenith angle. Tropospheric and stratospheric contributions can be distinguished in slant column abundance for lunar zenith angle greater than 83° . Slant column abundance of NO_3 obtained at Gurushikhar shows stratospheric contribution. NO_3 values obtained at Ahmedabad appears to have some tropospheric component. A large scatter in the values of NO_3 is noticed. These could be because of highly temperature dependence of NO_3 production rate.

Vertical column abundance of NO_3 remains constant throughout the night. After sunrise, NO_3 starts getting photodissociated. The decreasing rate of NO_3 after sunrise has been studied by measuring the scattered photons coming from the west horizon in the morning. As the solar depression angle decreases, the amount of atmospheric illumination increases and the NO_3 value starts decreasing. Using this feature, lower limiting value of NO_3 has been determined for Gurushikhar.

An attempt has been made to reproduce theoretically the features of NO_2 and NO_3 observed by us. Chemical equations are formed with production and loss terms of these species. These are solved simultaneously for steady state conditions and

the results of this study has been presented in Chapter 5. Calculations have been made at an interval of 5 km for day and nighttime conditions. Calculated vertical distribution of these species have been converted into total column abundance and compared with the values of NO_2 and NO_3 observed by us. It appears that nighttime NO density plays a crucial role in the distributions of NO_2 and hence NO_3 at least in 1 D model. Calculation of decay factor has been carried out for winter at 200 K and 220 K stratospheric temperatures. Values obtained for 220 K and O_3 abundance observed along with NO_2 show very good correlation with the observed decay factor. Similarly observed and calculated diurnal variations of NO_2 agree with 220 K.

Occasionally the stratospheric region is loaded by volcanic aerosols. A volcanic eruption took place in June 1991 at Mt. Pinatubo, Philippines and injected huge amount of SO_2 into the tropical stratosphere. These SO_2 gases were converted into $\text{H}_2\text{SO}_4/\text{H}_2\text{O}$ aerosols through condensation. Physical characteristics of these aerosols have been studied by a ground-based technique at Ahmedabad and has been discussed in detail in Chapter 6. Normally, after sunset the twilight intensity decreases exponentially with the increase of solar depression angle. However, due to an additional aerosol loading after volcanic eruption, the twilight radiation intensity after sunset again increases and then decreases. Using this anomalous twilight intensity variation, lower altitude of aerosol layer, layer thickness, aerosols strength (which is proportional to the total aerosol mass in the stratospheric region) have been determined in the same way as done by *Ashok et al.* [1982]. Most of the observations have been taken at 800 nm wavelength by a photometer looking in the zenith direction. Scattered intensity has been measured on the ground from 0° to $\sim 8^\circ$ solar depression angle.

Aerosols strength Q is proportional to the total stratospheric air mass of aerosols. Observations have been taken since November 1991. A monotonic increase

in the Q values have been obtained upto December 1991. This agrees with the optical depth results of SAGE-II. Height of the aerosols layer has been found to vary between 22 and 28 km which agrees with lidar observations taken near the equator by *Grant et al.* [1992]. Sometimes multiple layers have also been observed. Thickness of the single aerosol layer shows seasonal variation, decreasing as winter progresses and increasing as summer approaches.

Chapter 7 gives the conclusions of the present study and some suggestions for future study.

Chapter 2

Experimental Setup

2.1 Introduction

In any measurement an experimental setup is needed. The experimental setup used in this thesis is described in this Chapter. The main aim is to measure solar / lunar incoming flux in a certain range of wavelengths. For that purpose, we have used a monochromator and a detector. A controller controls the scanning. Scanning has been done by a personal computer. Data has been digitized and recorded in a floppy. In Section 2.2 instruments have been described in detail. Section 2.3 deals with the detector system. Since the strength of the signal we deal with is very low, attempt has been made to improve the signal to noise ratio by using a chopper and a Lock-in amplifier. This has also been described in Section 2.2. To avoid interference of other wavelengths in the wavelength range of our interest filters have been used. These are described in Section 2.4. The methodology used for data acquisition has been described in Section 2.5. In Section 2.6 we have described the operation of the instrumental setup.

2.2 Instruments

The ray diagram of the experimental setup is given in a simple form in Fig. 2.1. Scattered light from zenith enters into the monochromator in a horizontal direction after reflection by a plane mirror kept at 45° elevation. The entrance of the monochromator slit which is rectangular in shape is vertical. Inside the monochromator a parabolic mirror collimates this light on the grating. Light after passing through the grating becomes near monochromatic. This monochromatic radiation is then focussed on the exit slit (also rectangular in shape) by another parabolic mirror. After coming out of the monochromator through its exit slit, this monochromatic light enters into a photomultiplier tube. The output current of the photomultiplier tube is the desired signal. This signal is stored in a floppy through a data acquisition system. A photograph of the whole experimental setup is shown in Fig. 2.2.

2.2.1 Monochromator

A McPherson 0.35 meter UV visible spectrometer has been used. Internal structure of this monochromator is shown in Fig. 2.3. This has a single-pass Czerny-Turner mounting with two folding mirrors to provide entrance and exit beam on a common optic axis. Both the mirrors are identical plane mirrors having a dimension of 25 mm x 25 mm each. Their first surface is coated with aluminium and MgF_2 . The optical surface of these mirrors are corrected to $\lambda/4$ mercury green line at 546.07 nm. Two parabolic mirrors are also used, one as a collimating mirror and other as a focussing mirror. Both the parabolic mirrors are of 50 mm diameter, 350 mm focal length and aluminium coated. To prevent deterioration of the optical images of relatively large off-axis angles, parabolic mirrors are used instead of the common spherical mirrors. The only significant image aberration resulting from the use of

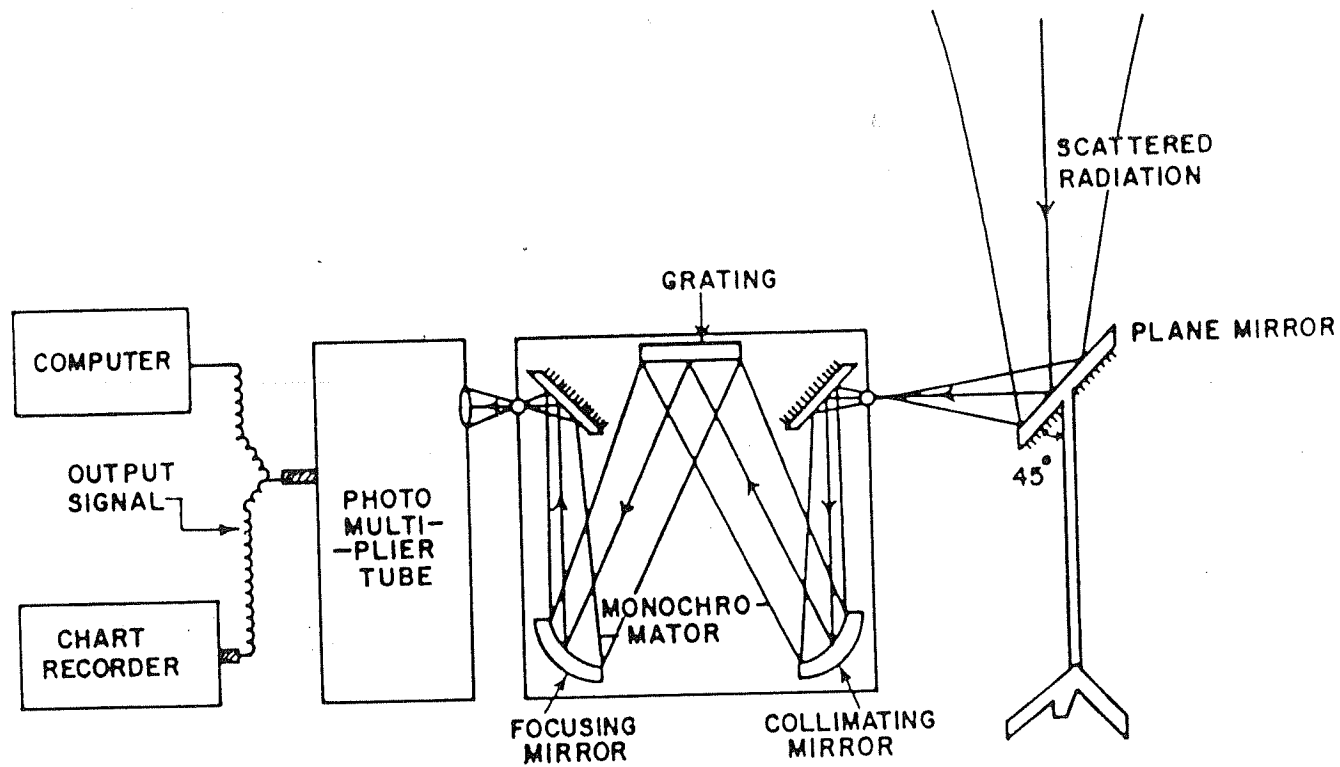


Figure 2.1 Schematic diagram of the monochromator system.

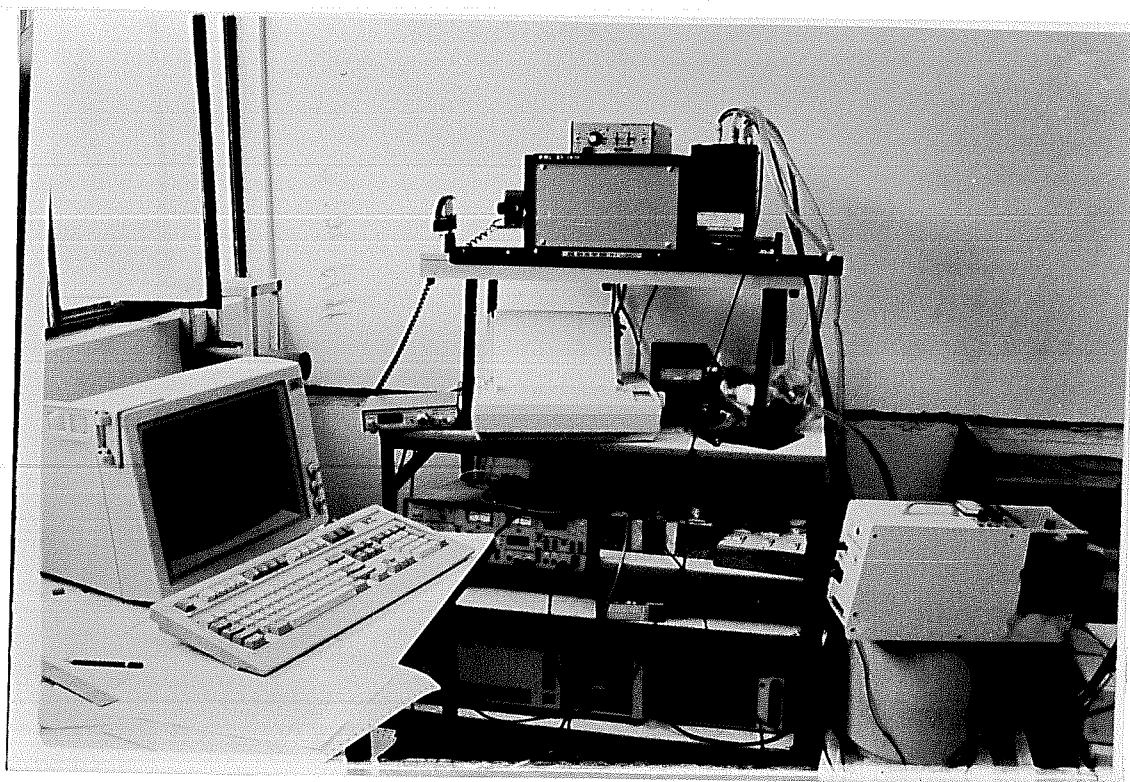


Figure 2.2 Photograph of the whole experimental setup.

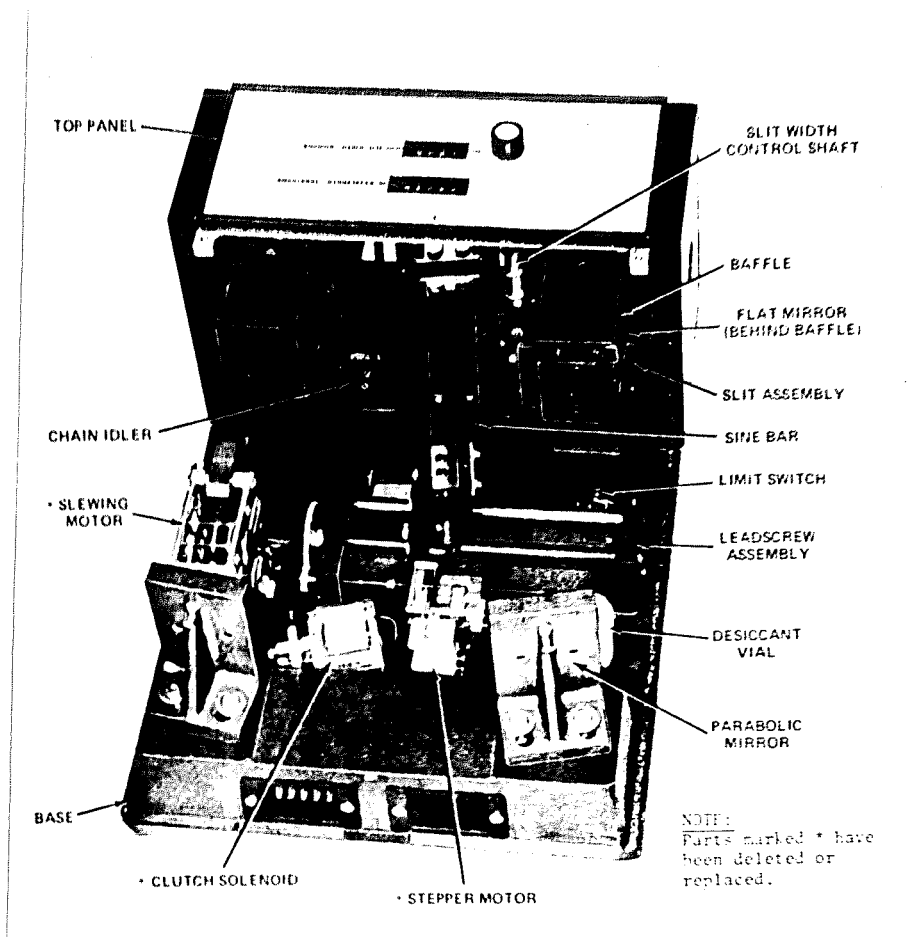


Figure 2.3 Layout of high resolution Monochromator for atmospheric studies.

parabolic mirrors is astigmatism. However, the monochromator designed to critically transfer only the width of the entrance slit image, astigmatic lengthening of this image is not detrimental to its performance. To avoid the instrumental scattering, baffles have been used with the following conditions :

- (i) The entrance and the exit slits do not see the focussing and the collimating mirrors respectively.
- (ii) The entrance or the exit slits do not directly see the grating, and
- (iii) The maximum projected area of the grating only remains open for the mirrors.

The projection of the beams at their extreme positions is taken into consideration to decide the shape of the baffles. The inner surface of the system other than the optical components is covered by dull black paint which works as anti-reflecting surface.

The monochromator has two counters. One gives the slit width reading and other the wavelength reading. In this monochromator, inlet and outlet slit widths are kept same and they are controlled by a single knob and the counter gives the reading of the slit width. The accuracy of the slit width counter is .01 nm. This counter has been factory calibrated by using a mercury emission lamp. Since the slit widths are not played with, the accuracy of the slit width counter given by the factory is not likely to change. The wavelength counter is used for the scanning. This has also been calibrated in the factory. This has been done by coinciding the mercury emission of green line at 546.07 nm with counter reading at 54607. Since the scanning has been done for a large number of times, the counter reading and actual wavelength could become different after several scannings. This has been checked by using a mercury lamp.

2.2.2 Diffraction Grating

The wavelength dispersing element of this monochromator is a plane diffraction grating. This precision plane grating has 48 mm x 48 mm ruled area. The number of grooves in the grating are 1200 lines per mm and blazed at 500 nm. This type of grating has three main advantages :

1. The plane grating permits an optical system with fixed position entrance and exit slits, yet allows fixed focus scanning without the need for compensation of focal plane or slit plane during scan. This is shown in Fig. 2.4. The fixed exit-beam angle is the viewing angle and the angles of concave mirrors from the normalcy of the grating. In this case, the grating equation can be written as

$$n.\lambda = d.(Sin\alpha \pm Sin\beta) \quad (2.1)$$

which is independent of the rotation angle of the grating, and thus is independent of the wavelength being observed as the grating is rotated.

2. The plane grating permits a linear relationship between mechanical movement and wavelength presentation. This linearity permits easy identification of spectral lines and provides ready synchronization with recorder.

3. Wavelength dispersion, and consequently resolution and bandwidth, is essentially constant over the entire scanning range.

2.2.3 Resolution

In any solar /lunar spectrum measurement, the resolution of the monochromator plays a vital role. The ability of an optical instrument, expressed in numerical measure, to resolve the images of two nearby points is termed as its resolving power. According to Rayleigh criterion, two nearby images are said to be resolved if the

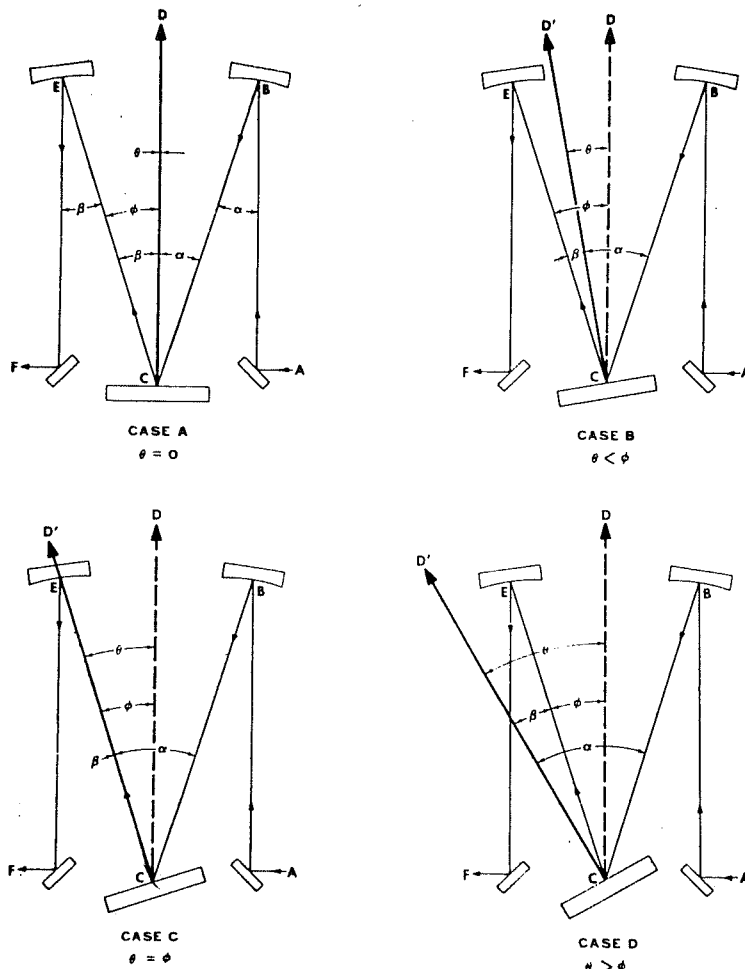


Figure 2.4 Optical configuration of Monochromator.

position of the central maximum of one coincides with the first secondary minimum of the other and vice versa. In case of monochromator, employing plane grating as the dispersing element, the resolving power is defined as the ratio of the wavelength of any spectral line and a neighboring line such that the two lines appear to be just resolved. Thus, the resolving power of a grating is equal to $\frac{\lambda}{\Delta\lambda}$. In this case, $\Delta\lambda$ is the minimum wavelength separation which can be resolved by the monochromator at a wavelength λ of spectral line. $\Delta\lambda$ is called the resolution or instrumental bandwidth of the monochromator. The quantity $\frac{\lambda}{\Delta\lambda} = nN$ measures the resolving power of a grating. Thus, the resolving power of a grating is independent of the grating constant. The resolving power is directly proportional to (i) the order of the spectrum (n) and (ii) the total number of lines on the grating surface (N). Virtually for all small monochromators, the spectral band width is linearly dependent on slit width, while slit height affects the spectral line straightness or curvature. Both slit height and slit width are limiting factors to the resolution of the instrument. In most cases, the resolution is represented in terms of full width at half maximum (FWHM) for a spectral line. At the slit width of $500\ \mu$ for both entrance and exit slits of the above monochromator, an average resolution of about 1 nm has been observed with the He-Ne laser source at 632.8 nm wavelength region. A resolution of 0.5 nm has been used for the measurements of solar spectrum while keeping the entrance as well as exit slit width equal to $200\ \mu$. In case of lunar spectrum, 1.0 nm resolution has been used for enhancing the signal to noise ratio.

2.2.4 Stray Light

Another factor indirectly related to the resolution of a monochromator is stray light. This factor includes radiation of wavelengths other than the specific band width corresponding to the wavelength setting. Such background radiation is usually of the nature of a spectral continuum, without discrete line structure, and is distributed in

varying degrees throughout the spectral range. This stray light can be defined as the ratio of amount of stray light to the desired radiation intensity, and is usually expressed as a percentage. The principle source of the stray light is light scattered from the grating when it acts as a simple mirror instead of perfect diffractive surface and light scattered by imperfect, damaged, dirty, or low efficiency optical system. To prevent the grating from receiving any off-axis light, two stage light baffles at the entrance and exit slits have been used.

2.2.5 Lock-in Amplifier

The Lock-in amplifier is an exceptionally useful instrument for extracting signals from noise, when noise and signal frequencies are close. A Lock-in amplifier can also make accurate measurements of small signals when the signals are obscured by noise source. We have used a Lock-in amplifier of model SR - 530 (Stanford Research System) for the present study. The heart of a Lock-in amplifier is a phase-sensitive detector, a circuit that gives preferential treatment to the desired signal based on information about the signal's phase. This has been used at the output port of the detector system. The output of the detector is ac current which is input for the Lock-in amplifier. The dc light signal coming from the Sun / Moon has been converted into ac light signal through a chopper used in front of the entrance slit of the monochromator. The chopper frequency has been controlled by the Lock-in amplifier. The ac signal which works as an input for the Lock-in amplifier is in the form of a square wave, maxima contain the information of true signal radiance and experimental noise, and minima correspond to instrumental noise. Maxima and minima of square wave are subtracted. Then the residual signal contains only signal radiance. This signal is amplified through a high gain amplifier. The Lock-in amplifier used by us can amplify a 10 nanovolt signal to 10 volt, i.e., a gain of one billion. Essentially, Lock-in amplifier is a filter with an arbitrary narrow bandwidth which is tuned to the frequency of the signal.

Such a filter rejects most unwanted noise to allow the signal to be measured.

2.2.6 Optical Chopper

Model SR-540 optical chopper has been used for converting continuum light signal into square wave. This unit can chop light source at rates from 4 Hz to 4 KHz. Versatile, low jitter reference outputs provide the synchronizing signals required for our operating mode. The chopper which has been used in the present work contains two rows, inner and outer. Inner row contains 5 slots whereas the outer row contains 6 slots. The diameter of the chopper is 10 cm. Aperture sizes of the inner and outer slots are 1.55 cm and 2.1 cm respectively. The frequency of the chopper is controlled by the chopper controller. Light emitting diode is used for counting chopper frequency. The position of the chopper setup along with the Lock-in amplifier and experiment is shown in Fig. 2.5. Slots of outer row have been used for converting signal from continuous to square wave form. The chopper is painted black to avoid scattering effect from its surface. The frequency of the chopper should be low, because the low frequency increases the exposure time. But it should not be that low so that 60 Hz pick up from ac mains, Lock-in amplifier noise at lower frequency, phase jitter of chopper and other background noise become dominant. The frequency of the chopper in the present work remains constant throughout the experiment, and it is 152 Hz. The entrance slit size of the monochromator is kept less than the size of the chopper aperture because the field of view covered by the monochromator should be well inside the chopper aperture.

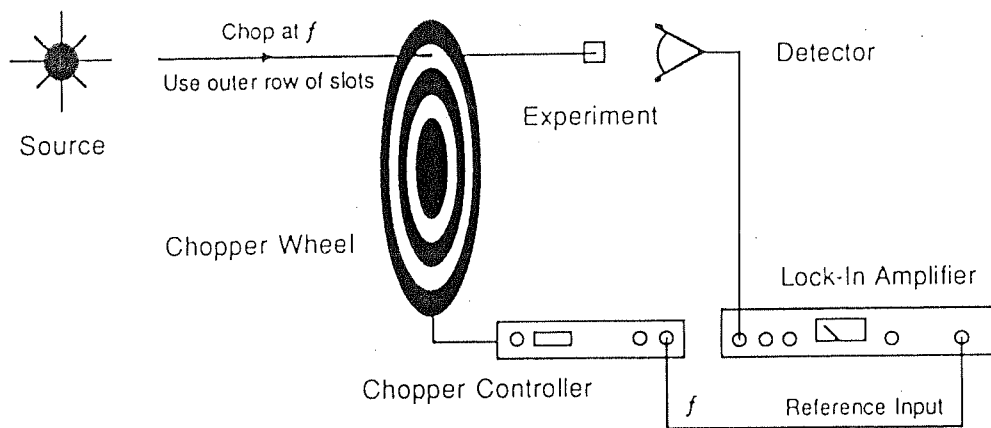


Figure 2.5 Chopper setup with Lock-in amplifier for single beam experiment.

2.3 Detector

The solar/lunar radiation dispersed by the monochromator is detected by a photomultiplier tube. R-372 Hamamatsu photomultiplier tube is used for NO_2 measurements and R-955 Hamamatsu photomultiplier tube is used for NO_3 measurements as well as aerosol measurements. R-955 Photomultiplier is cooled up to -20°C for enhancing the signal to noise ratio and minimizing the thermal noise. The primary function of the photomultiplier is to convert an input light intensity (luminous flux) to an output current that can be measured. The relationship between the light energy input and energy of the output photoelectrons is given in the form of Einstein's equation.

$$E = 1/2.m.v^2 = h\nu - \phi \quad (2.2)$$

This equation shows how the maximum energy $1/2.m.v^2$ of the photoelectron is proportional to the energy of the incident photon $h\nu$ minus the energy ϕ required (work function) to remove the photoelectron from the surface of the photo sensitive material.

2.3.1 Photomultiplier Characteristic

A photomultiplier amplifies the primary photocurrent to a level which could be measured and utilized for photometric applications. The amplification process in a photomultiplier tube is initiated by radiant-energy photons which interact with electrons on a photosensitive cathode surface to emit secondary electrons. These secondary electrons are elastically directed to a succession of dynode surfaces, each of which emits several secondary electrons for each primary electron contacting the dynode surface. The secondary electrons emitted from a preceding dynode become the primary electrons of the next, and so on through 9 dynode stages comprising a typical photomultiplier. The total gain of a given tube is an exponential relationship between the number of stages (n), and the number of secondary electrons emitted per stage

as given by the following idealized equation-

$$\text{Gain} = (\text{electrons emitted per stage})^n \quad (2.3)$$

The resultant gain of a photomultiplier tube is typically of the order of 10^5 to 10^7 .

The photomultiplier tube (PMT) R-372 has a maximum sensitivity at 340 nm. Its spectral type is S-5. Red-enhanced bialkali photocathode has been used in this PMT. The response of this PMT is from 185-730 nm region. UV glass has been used as a window material. Optimum voltage of this PMT is 1000 volts dc, therefore, most of the observations have been taken around this voltage. Another PMT, R-955, has spectral response from 160-900 nm with maximum sensitivity at 400 nm. Its spectral type is S-20. Multialkali material for photocathode and synthetic Silica for the window have been used. Number of dynodes in each PMT is 9. Similar to earlier PMT, anode to cathode supply voltage used in this PMT is also 1000 volt dc. We have used the side-on photomultiplier tubes to illuminate the surface of the cathode. While using these PMTs, following precautions have been taken :

1. Radiation may be directed so that the perimeter of the ray bundle is sharply focussed on a minimum area of the photocathode surface. The sensitivity of the photocathode surface is not same at all the points. Therefore, the light falling at different points of the surface might show different intensity, even if the input intensity is the same. While focussing the light at the smallest possible area of the photocathode, sensitivity of the photocathode increases tremendously and very weak signal also can be detected.

2. Radiation is confined in such a way that the width of the ray bundle should fall between one half and three-fourth of the total width of photocathode surface. While doing this, the wide dynamic range has been used because if there is any shift in the image, the resultant current does not show much variation and this geometry lends

itself to relatively simple and reliable optical arrangements.

3. Each photomultiplier has some limitation of receiving the amount of intensity. To control the strong light signal coming to the photomultiplier, very thin unfolded wire mesh has been used. Putting a diffuser such as a frosted plate of glass or quartz in the optical path length will distort the path of the light. It will result in linearity loss and higher noise level. Due to these reasons, neutral density filter has not been used for reducing the intensity of incoming solar/lunar radiation.

2.3.2 Dark Current

A small amount of current that flows in a photomultiplier tube even when the tube is operated in complete darkness, is called the “dark current of the photomultiplier”. The value of this current is critical for determining the lower limit of the signal. There are different sources of dark current which can be characterized as follows :

Thermionic emission of electrons

Since the material used for photocathode and dynode surfaces have very low work function, they emit thermionic electron even at room temperature. Most of the dark current originates from the thermionic emissions, especially from the photocathode. It is then multiplied by the dynodes and becomes large. To minimize dark current due to thermionic emission, R-955 PMT has been cooled up to -20°C .

Ionization of residual gases

Residual gases inside a photomultiplier tube can be ionized by the flow of photo-electrons. When these ions strike the photocathode or dynode, secondary electrons

will be emitted. And these secondary electrons will be multiplied by many stages of dynode, resulting in a large amount of noise. This noise is the abrupt noise and is usually observed as after pulses. The output of the photomultiplier tube contains signal followed by after pulse. This may cause problem in the detection of very weak signal, but the PMT is constructed in such a way that it minimizes the possibility of after pulse sources.

Glass scintillation

When positive voltage is applied on the anode, electrons will move from cathode to anode. Sometimes, at lower applied potential, electrons deviate from its original path and strike the glass envelope of the PMT, causing dark pulse generation. This can affect the actual output signal. To avoid the deviation of the electrons emitted from the cathode a high voltage at anode is necessary. Hence the cathode is kept at ground potential and the anode at the maximum possible voltage.

Ohmic leakage

Ohmic leakage resulting from imperfect insulation of the glass stem base and socket may be another source of dark current, especially when the anode voltage is at lower potential. The presence of dust or humidity on the surface of PMT glass results in ohmic leakage. Therefore, R-955 Hamamatsu PMT has been fitted into the Hamamatsu cooling system of Model C959-S. The temperature of the cooling system is maintained through water circulation system, upto about -20°C . Photomultiplier tube socket is kept isolated from the rest of PMT housing, and a quartz window is used to prevent the photomultiplier tube from dust or humidity.

There are two ways in which a photomultiplier tube can be used. These are

analog mode and photon counting mode. In analog mode, dark current accumulates with the signal current, and the output is the resultant of signal and dark currents. It is difficult to separate the dark current from the signal current in the analog mode. If the signal to noise ratio is very high then the dark current becomes insignificant compared to the actual signal. Since solar/lunar intensity is very strong, it can be easily detected in analog mode. On the other hand, in the photon counting mode very weak signal can be detected. If the dark current is greater than the signal strength, it can be easily subtracted by using a discriminator. Therefore, photon counting method is appropriate for detecting the weak signal.

Optimization test of signal to noise ratio has been done for both the photomultiplier tubes used. A standard tungsten lamp has been used as input light source. The anode voltage has been varied. The output current increases as the voltage increases and is found to be maximum at about 1000 volt dc in both the PMTs used.

2.4 Filters

Filters are used to prevent unwanted radiation from entering the monochromator. Different types of filters are available in the market. Their characteristics determine their suitability for a particular line or band of wavelengths. These characteristics are described in Sections 2.4.1 to 2.4.3 below. Filters are mounted in front of the entrance slit of the monochromator. Size of the filter is larger than size of the entrance slit.

2.4.1 Absorption

All material absorb radiation in some part of the electromagnetic spectrum. The amount of absorption depends on the wavelength of radiation, the amount of absorbing material in the path of the radiation, and the absorbance of the material at that

wavelength. Absorption occurs when the electric field of the light wave interacts with the absorbing atoms or molecules. Electrons of the atoms or molecules get excited due to the interaction with photons and go to higher energy level. This is a resonant process and it occurs only at the resonant wavelengths. In a solid or liquid absorber, the excitation energy is soon dissipated as heat. If this heat is very intense then it causes local heating which can lead to structural damage.

2.4.2 Transmittance

As a beam of light passes through the absorbing medium, the amount of light absorbed in the medium is proportional to the intensity of incident light, absorption coefficient of the medium and the path length covered by the light. Consequently, the intensity of the incident beam drops exponentially as it passes through the absorber. This is often expressed as Lambert's law :

$$T_I = 10^{-\alpha \cdot c \cdot X} \quad (2.4)$$

where T_I is the internal transmittance, α is the absorption coefficient, c is the concentration of absorbers and X is the path length covered by light in medium. Clearly α and T_I are wavelength dependent.

This transmittance is defined as the transmittance of an optical element when surface losses are ignored. The overall transmittance of the element, i.e., the measured transmittance, is termed the external transmittance T_E .

2.4.3 Optical density

The optical density can be defined as the logarithm of the opacity

$$D = \log\left(\frac{1}{T}\right) \quad (2.5)$$

Thus, greater the optical density, greater is the amount of light blocked by the filter. The optical density is additive. If several filters are stacked in series, the combined optical density is given by the sum of the individual optical densities. The filter characteristics are also defined on the basis of the light that it blocks, and the inverse of the light that it transmits.

For NO_2 measurements, quartz filter has been used to cut off UV radiation. For NO_3 measurements and twilight intensity measurements at 800 nm, quartz and red cutoff filters have been used to remove the second order spectrum of the monochromator.

2.5 Data acquisition system

This system gives the raw data in the final form for further analysis. Data acquisition system includes preamplifier, A/D converter, along with RS-232 interface to a personal computer through a Lock-in amplifier. Monochromator operation is also controlled by the same computer. The entire software for operation of the system and data storage has been developed by us. Block diagram of our data acquisition system is shown in Fig. 2.6. A monitor has been used for display, a floppy for storing and a printer for hard copy.

The output of the PMT is in the form of a current. This is fed to a current / voltage converter. The output of the converter goes to a preamplifier which precedes the input of the Lock-in amplifier. This voltage preamplifier has gains of 10, 20, 50 or 100. The Lock-in amplifier controls this gain to a maximum value and at the same time it maintains the selected dynamic range. Signal output of the Lock-in amplifier is converted to digital form by an A/D converter (PCL-205 PCB) with 12 bit resolution through a personal computer. Scanning of wavelength is also controlled

DATA ACQUISITION / CONTROL FOR A
SPECTROMETER (BLOCK DIAGRAM)

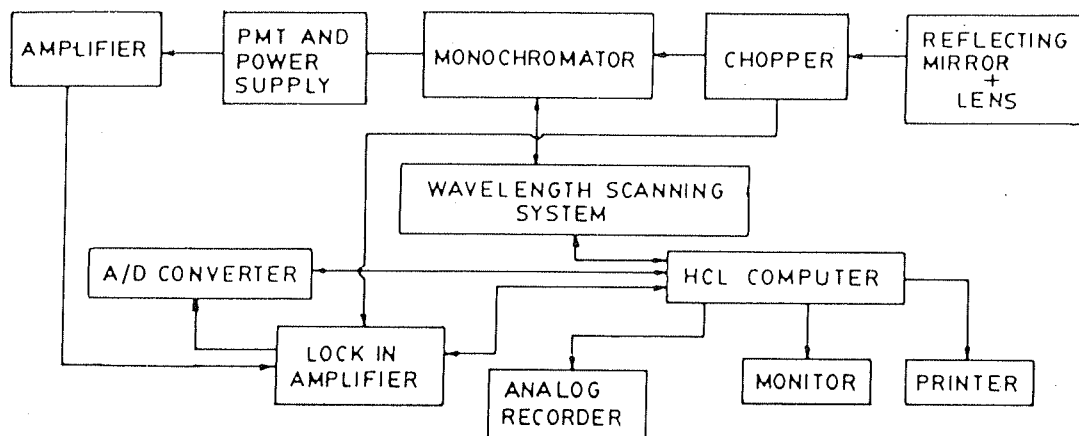


Figure 2.6 Block-diagram of complete experimental setup and data acquisition system for atmospheric studies.

this computer. Both forward and backward scanings have been done for a couple of times. The data has been recorded at the interval of 0.01 nm.

2.6 Operation of the instrument

Prior to 120 minutes of measurements, cooling system of the detector was turned on. The cooling system has a thermoelement for cooling. The outer surface of the PMT housing is cooled by water circulation. Before switching on the power supply of the cooling system, water circulation is started with the help of a water pump. In about two hours, the temperature of PMT decreases to a stable value of about -20°C . After that the photomultiplier supply is switched on. Lock-in amplifier system along with chopper is made operational. Sensitivity of the Lock-in amplifier has been fixed according to the signal to noise ratio values. And finally monochromator is switched on for scanning. Monochromator operation is controlled by a personal computer. Before scanning the system, the grating is kept at an appropriate angle which corresponds to the desired wavelength. Before starting the scanning of the spectrum, a dummy program is executed to optimize the signal to noise ratio. If signal intensity is very high, neutral density filter such as the wire mesh is used for attenuating the signal strength. If the signal is weak then the PMT voltage value is increased by a reasonable amount. After optimizing the signal, actual program for scanning the spectrum is loaded in the computer and executed for scanning in the forward and backward directions. The scanning rate of the spectrum is controlled by the software used for scanning the spectrum. The signal spectrum, thus obtained is then plotted on the monitor, and checked with the reference spectrum taken at noon time. If the difference between the noon time spectrum and the signal spectrum is under permissible limit, then the signal spectrum is stored for further analysis.

Chapter 3

Results of NO₂ Measurements

3.1 Introduction

In the NO_x group of species NO₂ is most widely studied. We have measured NO₂ content at Ahmedabad (23°N, 72°E), India, at low latitude. As mentioned in Chapter 2, we have used a ground-based absorption spectroscopy technique. The radiation reaching the ground is a function of wavelength and different wavelengths are attenuated by different amount by different species. Since NO₂ has a number of structures in the visible region, we have used this spectral region for the measurement of columnar density of this gas in the atmosphere. The present Chapter deals with the results of these measurements. In Section 3.2 we have surveyed the existing results on NO₂. The methodology used is described in Section 3.3. Section 3.4 deals with the data reduction. The errors that come in these measurements are given in Section 3.5. Results are given in Section 3.6. They are also compared with other available data and discussed in the same section.

3.2 Earlier studies

Brewer et al. [1973] were, probably the first to initiate NO₂ total column abundance measurements by using a ground-based absorption spectroscopy technique. Later observations of stratospheric nitrogen species using ground-based visible absorption spectroscopy began with the seminal work of Noxon and coworkers in the late 1970s [*Noxon*, 1975, 1978b, 1979; *Noxon et al.*, 1979]. Their measurements employed the sun, moon, or twilight sky as the light source and determined the total atmospheric column abundance. The wavelength range used was 430 to 450 nm. They found NO₂ column abundance between 2 and 5 x 10¹⁵ cm⁻² with minimum in winter and maximum in summer. *Noxon* [1979] studied latitudinal variation and reported several features for NO₂ : an equatorial minimum, a seasonal variation in the northern hemisphere, a polar maximum in summer, an abrupt drop in abundance near 50° N in winter etc. But in this technique absorption due to species other than NO₂ is also present. *Harrison* [1979] developed an algorithm in which absorption due to O₃ and water vapour, and scattering due to aerosols and Rayleigh atmosphere have been taken into account. This method was modified further by *Syed and Harrison* [1980] who developed a scattering model to calculate NO₂ enhancement factor for different solar zenith angles. *Syed and Harrison* [1981] observed maximum NO₂ in summer - about 5 x 10¹⁵ cm⁻² and minimum in winter about 2.5 x 10¹⁵ cm⁻². *McKenzie and Johnston* [1982a] developed an automatic scanning spectrometer at Lauder (45°S) for scanning the zenith sky intensity during twilight period between 436 and 448 nm for NO₂ measurements. This method was used later by many workers for NO₂ total column measurements [*McKenzie and Johnston*, 1983, 1984; *Noxon et al.*, 1983; *Keys and Johnston*, 1986]. *Solomon et al.* [1987] developed a matrix inversion technique to derive column density of atmospheric species. *Pommereau and Goutail* [1988b] measured NO₂ over Antarctica and found NO₂ to be about 2 x 10¹⁵ cm⁻² in winter.

Further, *Mount et al.* [1987], *Sanders et al.* [1989], *Johnston and McKenzie* [1989], *McKenzie et al.* [1991] etc. studied NO₂ variability over mid and high latitude zones. *Johnston and McKenzie* [1989] observed seasonal variation of NO₂ slant column at 45°S and found its value to lie between 3 and 12 x 10¹⁶ cm⁻². Most of these observations are for mid and high latitude zones. Recently *Bhonde et al.* [1992] made some measurements at Pune (15°N) and found NO₂ slant column density between 0.6 and 1.3 x 10¹⁶ cm⁻² at 90° solar zenith angle (SZA). In addition, the effect of volcanic aerosols on NO₂ has also been studied by *Johnston and McKenzie* [1989] and *Johnston et al.* [1992].

Besides ground-based measurements, satellites have also been used to measure NO₂ density. The satellites which have given results of NO₂ are Nimbus-7, Atmospheric Explorer-II (AEM-II), Solar Mesospheric Explorer (SME) and Earth Radiation Budget (ERBS) satellites. A comprehensive near global data base on the odd nitrogen (NO_x) chemistry is available from the Nimbus-7 Limb Infrared Monitor of the Stratosphere (LIMS) experiment, the Stratospheric and Mesospheric Sounder (SAMS), the Solar Mesosphere Explorer (SME), and the AEM-II Stratospheric Aerosol and Gas Experiment (SAGE) which collectively provided data on vertical profiles of temperature, O₃, NO₂, N₂O, HNO₃, CH₄, CO and aerosols. SAGE-II zonal averages between 42.5° and 47.5°S have been compared with ground-based data from Lauder (45°S) by *Cunnold et al.* [1991]. They found good agreement between the annual cycles in the SAGE-II and Lauder NO₂ column. The average difference between the adjusted Lauder and SAGE -II columns is $1 \pm 2.5 \times 10^{14}$ cm⁻²; however, the SAGE-II data shows a long term decrease in NO₂ which is not shown in the Lauder data.

In the early 1970s infrared absorption technique on - board balloon was used by many workers [*Ackerman and Muller*, 1972, 1973; *Farmer*, 1974; *Murcray et al.*, 1974;

Fontanella et al., 1975; *Ackerman et al.*, 1975] to measure NO₂ vertical distribution. *Ackerman et al.* [1975] found NO₂ peak around 25 km with a value about $2 \times 10^9 \text{ cm}^{-3}$. *Kerr and McElroy* [1976], *Evans et al.* [1978], and *Goldman* [1978] used techniques similar to that developed by *Brewer* [1973] and observed NO₂ distribution over high latitude. *Kerr and McElroy* [1976] found maximum NO₂ volume mixing ratio around 28 km and its value was about 10^{-8} . *Blatherwick et al.* [1980], *Naudet et al.* [1980], and *Roscoe et al.* [1981] used long-path pressure - modulated infrared radiometer for day-night observation of NO₂. *Roscoe et al.* [1981] found maximum NO₂ around 35 km and its value was about 2 ppbv. *Kerr et al.* [1982] determined NO₂ profile by measuring NO₂ absorption of sunlight from a balloon platform during sunrise and sunset. They found average NO₂ concentration at sunset to increase from about 0.3 ppbv at 10 km to 10 ppbv at 35 km. At sunrise the concentration was found to increase from 0.2 ppbv at 10 km to 5 ppbv at 35 km. *Pommereau* [1982] found mean concentration of NO₂ between 22 and 33.5 km to be about $8.7 \pm 3.2 \times 10^9 \text{ cm}^{-3}$. *Louisnard et al.* [1983] found maximum NO₂ at about 25 km and its value was $1.2 \times 10^9 \text{ cm}^{-3}$ at 44° N. *McFarland et al.* [1986] measured NO₂ using chemiluminescence technique and found about 4 ppbv NO₂ at 30 km. *Shibasaki et al.* [1986] measured NO₂ profile over Antarctica and found maximum NO₂ around 25 km and its value about $4 \times 10^9 \text{ cm}^{-3}$. *Ridley et al.* [1987] measured NO₂ at 50°N and found an increase in NO₂ with an increase of altitude.

Aircraft measurements of NO_x species are also available at different latitudes. Perhaps first air craft NO₂ column density measurement was made by *Harries* [1973] and he found its value about $5 \times 10^{16} \text{ cm}^{-2}$ above 15 km altitude. *Girard et al.* [1978] made aircraft measurements of NO₂ column density at several latitude regions and found its value in tropical latitude to be about $2.2 \pm 0.3 \times 10^{15} \text{ cm}^{-2}$. *Coffey et al.* [1981] studied latitudinal variation of NO₂ in the northern hemisphere and found NO₂ column density to be about $3 \times 10^{15} \text{ cm}^{-2}$ above 15 km in equatorial region.

NO₂ of Polar region has been measured under Airborne Antarctic Ozone Experiment (AAOE) by many workers [Toon *et al.*, 1989; Coffey *et al.*, 1989; Wahner *et al.*, 1989]. Wahner *et al.* [1989] reported average NO₂ vertical column to be about $2 \pm 1 \times 10^{15} \text{ cm}^{-2}$. Arctic NO₂ measurements were also made by many workers [Carroll *et al.*, 1990, 1992; Wahner *et al.*, 1990; Mankin *et al.*, 1990]. Mankin *et al.* [1990] found marginal latitudinal variation of NO₂ column density. Their value was about $0.4 \times 10^{15} \text{ cm}^{-2}$. Wahner *et al.* [1990] found NO₂ below detection limit. Carroll *et al.* [1992] measured NO_x species during the Mauna Loa Observatory Photochemistry Experiment (MLOPEX) and found NO₂ to lie between 0 and 50 pptv.

Long path absorption spectroscopic technique has also been used for the study of tropospheric NO₂ by several workers [Platt *et al.*, 1979; McMahon and Simmons, 1980; Platt and Perner, 1980; McKenzie and Johnston, 1982b; Johnston and McKenzie, 1984]. Platt *et al.* [1979] measured tropospheric NO₂ in 6.3 km pathlength and found NO₂ mixing ratio to vary between 1 and 3 ppbv over Dagebull, Germany. Platt and Perner [1980] measured different tropospheric species at the maritime sites in Germany and found NO₂ mixing ratio to lie between 0.5 and 2 ppbv. McKenzie and Johnston [1982b] measured NO₂ at 45°S using ground-based long path absorption spectroscopy. They found evening value of NO₂ column to be between 3.2 and $6.4 \times 10^{15} \text{ cm}^{-2}$ and morning value of NO₂ to be between 2 and $4.5 \times 10^{15} \text{ cm}^{-2}$. Johnston and McKenzie [1984] measured NO₂ using 9.2 km path length and found nighttime tropospheric NO₂ mixing ratio to be between 200 and 800 pptv.

We have made a survey of existing measurements of NO₂ in the previous paragraphs. One can see that a large number of observations exist for the Antarctic. A good number of observations are also available at mid latitude. Some observations are also available at the Arctic and high latitude zone. But only one or two good observations are available for low latitude region. Obviously, these observations are

not sufficient to draw a clear picture of the global NO₂ variability. We have, therefore, done some measurements of NO₂ at Ahmedabad (23°N, 72°E), a low latitude station.

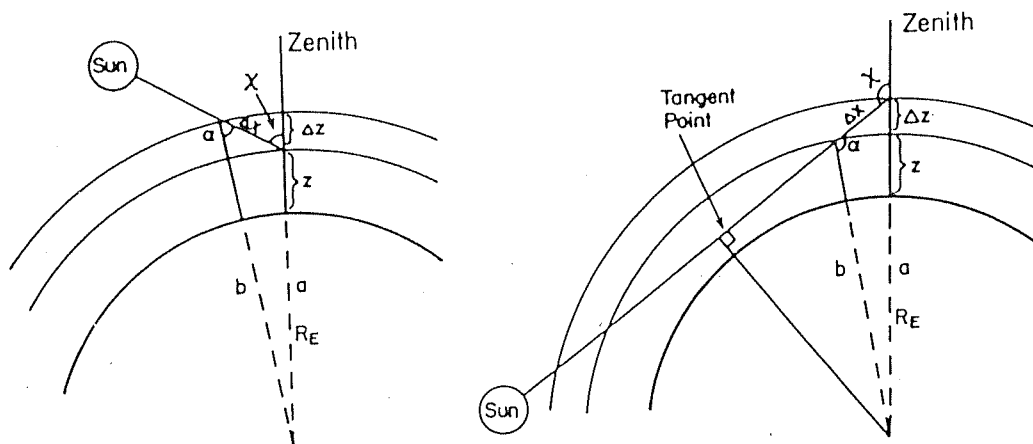
3.3 Methodology

The experimental setup used in the present study has been described in detail in Chapter 2. We measure the scattered intensity of the sun in the zenith direction. The wavelength region which we have considered for the present study extends from 436 to 448 nm. This part of the solar spectrum contains a number of Fraunhofer absorption structures. It also contains absorption structures by NO₂. Besides NO₂, species like O₃, H₂O and O₄ also have absorptions in this wavelength region but relatively weak compared to NO₂. Measurements have been taken for two positions of the sun : (1) during twilight period when solar zenith angle is greater than 85° and (2) during noontime when solar zenith angle is minimum. As the solar zenith angle increases, the atmospheric path covered by the solar radiation increases. Because of this increase in the path length covered by the solar radiation, twilight spectrum will have greater absorption due to atmospheric species compared to that at noontime.

3.3.1 Zenith sky brightness

When the zenith sky is observed, the photons detected by the instrument, have been scattered at least once. Let us consider the case of single scattering. The relevant geometry is depicted in Fig. 3.1 [Solomon *et al.*, 1987]. The contribution to the intensity of scattered radiation by an infinitesimally thin layer at altitude z is given by :

$$I_{z,s} = I_z s_r [M]_z L \Delta z \quad (3.1)$$



(a) $X \leq 90^\circ$

$$a = R_E + z, \quad b = R_E + z + \Delta z$$

$$\alpha = \sin^{-1} \left[\frac{a}{b} \sin X \right]$$

$$\Delta x = [a^2 + b^2 - 2ab \cos (X - \alpha)]^{1/2}$$

(b) $X > 90^\circ$

$$a = R_E + z + \Delta z, \quad b = R_E + z$$

Figure 3.1 Twilight geometry for (a) zenith angle (χ) less than 90° and (b) zenith angle (χ) greater than 90° (Solomon et al., 1987).

where I_z is the intensity of radiation reaching the layer at altitude z , s_r is the Rayleigh - scattering cross section for the wavelength of interest, $[M]_z$ is the air density at altitude z , and $I_{z,s}$ is the intensity of the radiation scattered at the layer z and L is the airmass factor which is the ratio of slant path to vertical path covered by solar radiation. If the atmosphere is optically thin at the wavelength considered, then all factors except $[M]_z$ in eqn. 3.1 are independent of height, and it follows that the scattered flux varies with altitude as the air density. Under these circumstances, most of the singly scattered photons measured by an upward looking spectrometer will have been scattered in the lowest few kilometers of the atmosphere. However, for photons at large solar zenith angles ($\geq 85^\circ$) in the wavelength range of our interest, the atmosphere is not optically thin. This is due to the attenuation of solar radiation by Rayleigh scattering, so that the radiation reaching a particular altitude is reduced according to

$$I_z = I_o \cdot \exp(-s_r \cdot \int_z^\infty [M]_z \cdot L_z \cdot dz) \quad (3.2)$$

The intensity, therefore, varies according to the atmospheric density profile. It also varies strongly with wavelength, since the Rayleigh - scattering cross section varies as the inverse of the wavelength to the fourth power. Combining eqn. 3.1 and eqn. 3.2, we obtain for any assumed infinitely thin layer :

$$I_{z,s} = s_r \cdot [M]_z \cdot I_o \cdot \exp(-s_r \cdot \int_z^\infty [M]_z \cdot L_z \cdot dz) \quad (3.3)$$

The change in atmospheric densities with height thus has nonlinear effects on the scattered flux, and there will be some height z at which maximum scattered intensity occurs. At large solar zenith angles, increases in the optical path inhibit the propagation of solar radiation to low altitudes, but the radiation that does arrive there will be more strongly scattered. Thus there will be some altitude z from which most of the radiation reaching the surface is scattered, and this will depend upon the wavelength and air density profile. The scattered flux coming from the zenith has been calculated

by many workers [Solomon *et al.*, 1987; Bhonde *et al.*, 1992]. Solomon *et al.* [1987] calculated scattered flux at the surface by an upward looking spectrometer at 440 nm for 55°N in winter, as a function of the altitude. They found that the scattered flux simply decreases exponentially with height, but at, for example, 90° most of the sky brightness, or flux arriving at the ground, does so by scattering above 5 km. Similar calculation was done by Bhonde *et al.* [1992] for low latitude. They found most of the scattered flux received on the ground at 90° comes from 10 km altitude at low latitude and decreases exponentially above that altitude. Thus the scattered solar flux which is reaching the surface of the earth during twilight period has the major contribution from the altitude about 15 km and it follows Gaussian distribution with height. Thus, the species which is being measured during twilight period, by absorption in the lower wavelength region, will be of the stratospheric region. This situation has been shown in Fig. 3.2.

The radiation reaching the earth surface is also scattered by aerosols. The contribution of molecular scattering is very high at lower wavelength region. On the other hand, the aerosol contribution is dominant over higher wavelength region. This is because Rayleigh scattering is proportional to the λ^{-4} and aerosol scattering is inversely proportional to the wavelength.

3.3.2 Ratio spectrum

We have taken eight scans - four in the forward direction and four in the backward direction. Each scan takes 12 sec. We have taken the average of these eight scans. Each spectrum has been normalized by the intensity of Fraunhofer line at 437.9 nm. Each spectrum has been made to coincide at 438.36 nm for matching.

An example of twilight zenith sky solar spectrum taken by us is shown in Fig. 3.3 by solid line. The spectrum taken during noontime is also shown in Fig.

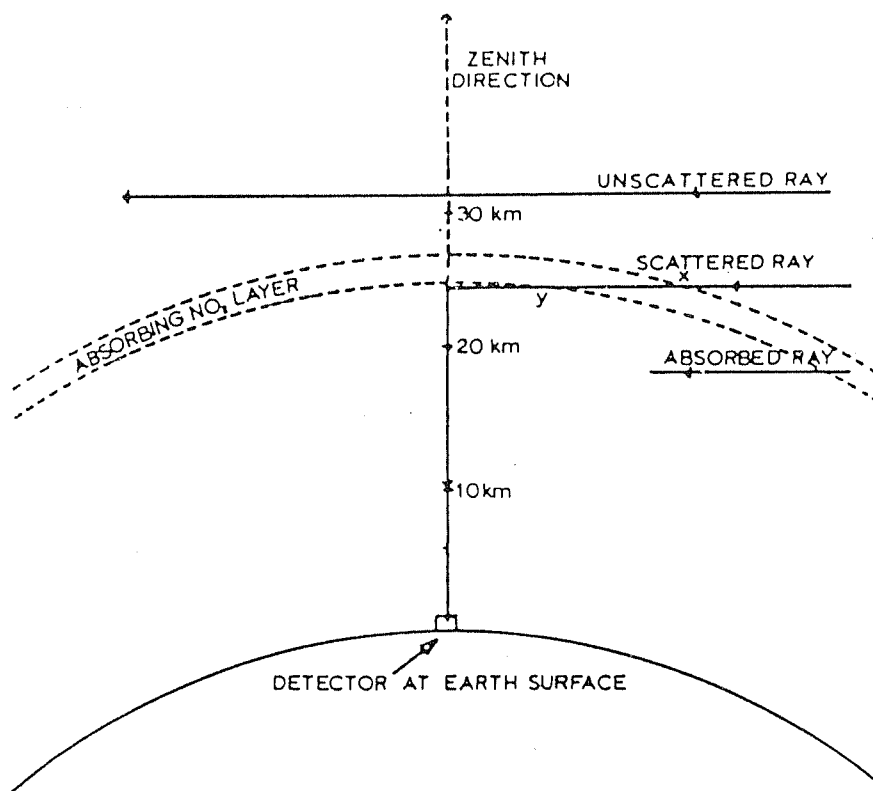


Figure 3.2 Path geometry for twilight rays scattered from the zenith sky (McKenzie and Johnston, 1982)

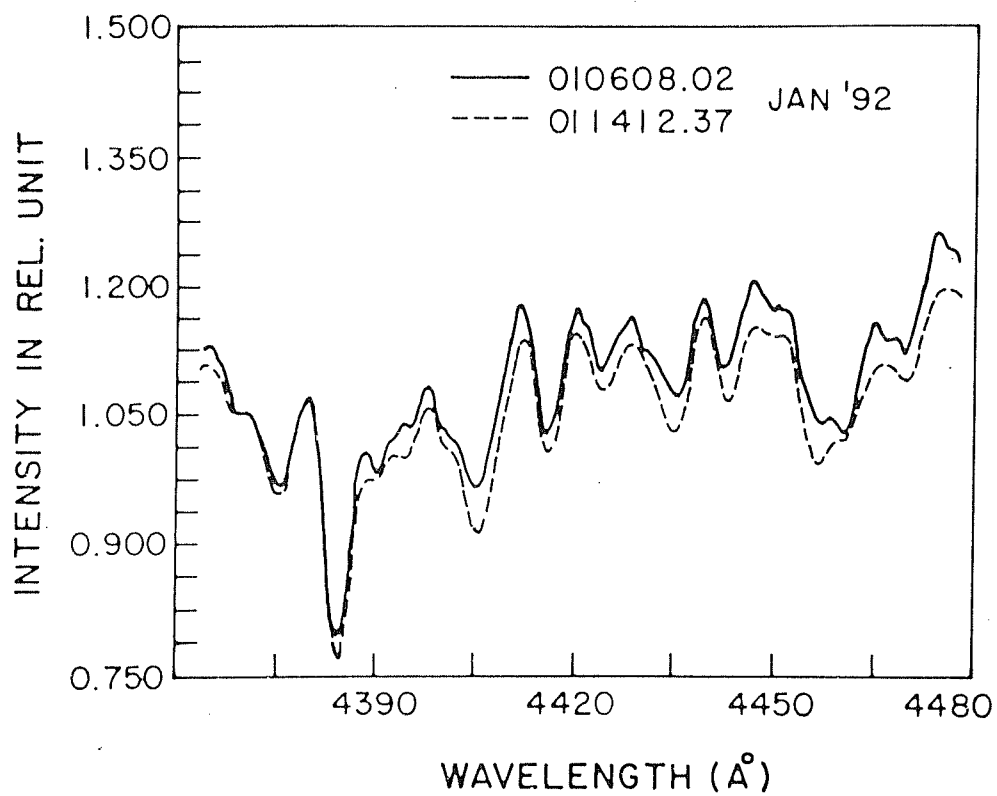


Figure 3.3 Zenith sky spectra obtained in the range of 436 - 448 nm during noontime (1237 IST, dotted line) and morningtime (0802 IST, solid line).

3.3 by dotted line. These are the averages of 8 spectra. An examination of two spectra plotted in Fig. 3.3 shows that both twilight and noontime spectra are very similar. This is owing to the presence of strong Fraunhofer structure in the incident sunlight. Absorption due to NO_2 in the noontime spectrum is less than 0.1% of the signal, but during twilight period this value is about 2.0% . However, the Fraunhofer absorptions are up to 25% of the signal. Therefore, it is necessary to remove the Fraunhofer component from the observed signal. Since the contribution of NO_2 during noontime is negligible, we have taken the ratio of the observed twilight spectrum to the noon time spectrum. This should remove the Fraunhofer component present in twilight spectrum and leave in it the signature of absorption due to atmospheric species. Before taking the ratio, noontime and twilight spectra have been adjusted for maximum correlation and then positioned at 438.36 nm Fe-II Fraunhofer line.

A typical example of the ratio spectrum is shown in Fig. 3.4. An examination of two spectra plotted in Fig. 3.3 shows that Fraunhofer absorption in the twilight spectrum is shallower than the noontime spectrum. This is known as the Ring effect, named after its discoverer. Due to this reason, the ratio spectrum reveals a smaller amount of residual Fraunhofer component. This effect has been minimized by smoothing the ratio spectrum by 50 point running average. In the wavelength region used here for the NO_2 study the Ring effect is apparent at the levels of a few tenths of a percent [Solomon *et al.*, 1987].

The absorption features seen in Fig. 3.4 can be compared with the absorption cross-section values of NO_2 and O_3 of this region. Fig. 3.5 shows the absorption cross-section values of NO_2 and O_3 given by Harrison [1979]. The ratio spectrum shows pronounced structure at points A, B, C and D. In these, A and D occur at 439.5 and 445.0 nm respectively. These two prominent features are due to NO_2 . They coincide with the maximum NO_2 absorption cross section values shown in Fig. 3.5. In the

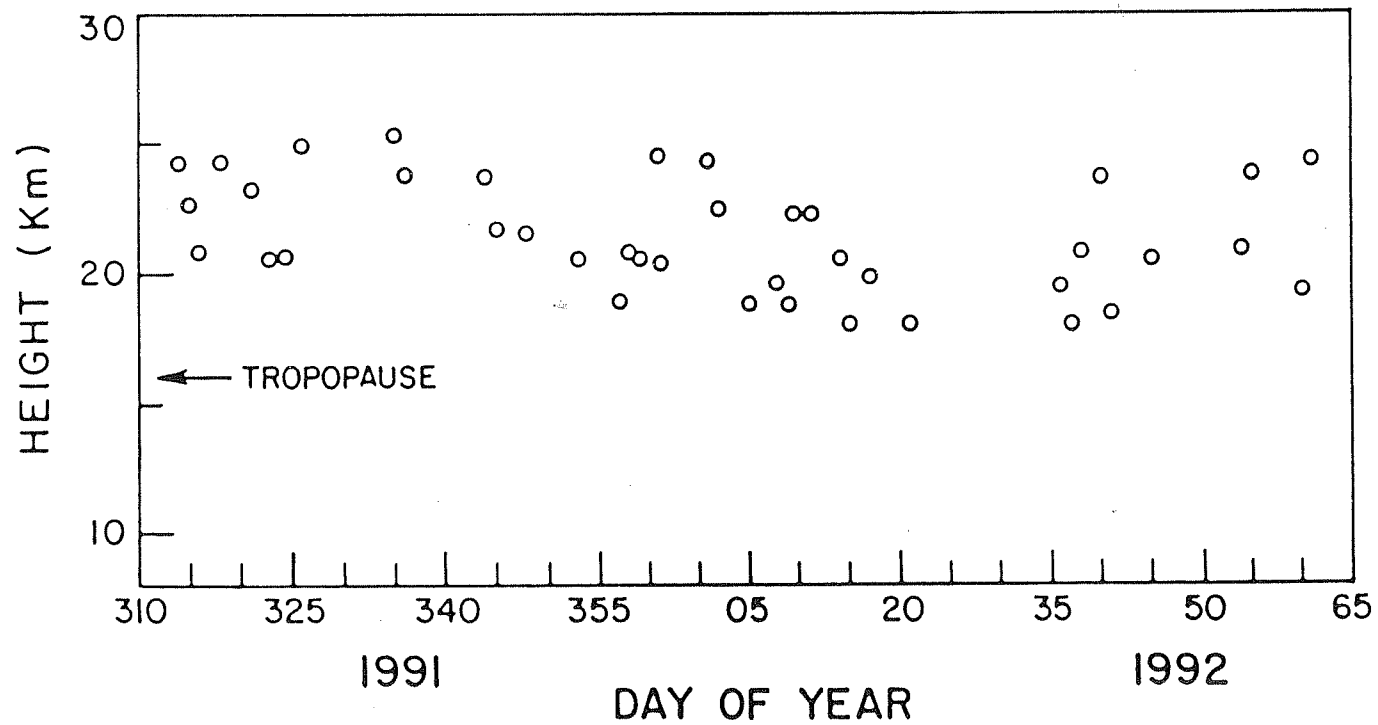


Figure 6.5 Height of the lower end of the aerosol layer (H_L).

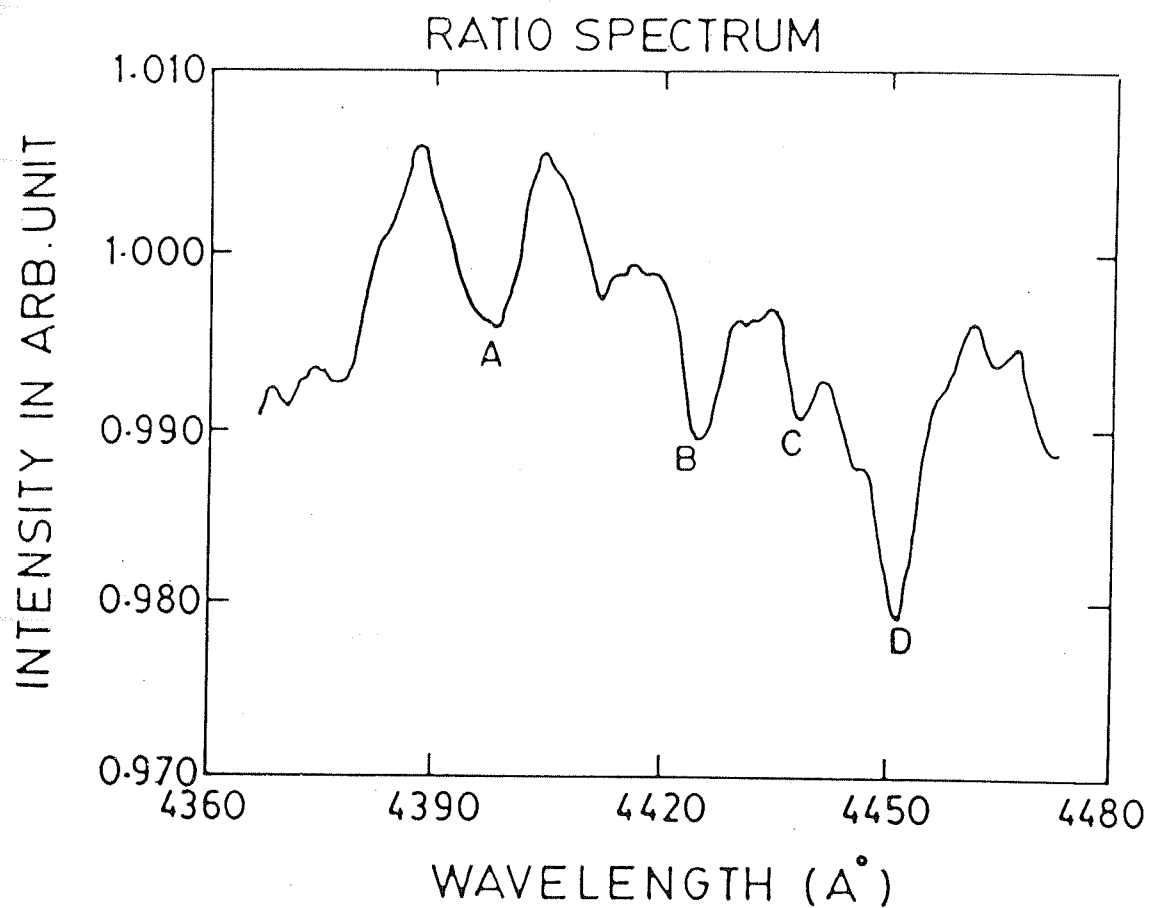


Figure 3.4 Curve showing the ratio of morningtime to noontime spectra.

ratio spectrum, another dip is seen at 442.5 nm (point B). This is mainly due to water vapour. Our ratio spectrum can be compared with the ratio spectrum obtained by *Harrison* [1979]. The dips occurring at point A and D are also observed by *Harrison* [1979]. However, water vapour absorption feature (i.e., the depth of the dip at B) at our latitude is large compared to the water vapour feature (the depth of the dip at 442.5 nm) obtained at high latitude region. This could be due to the reason that low latitude region contains more atmospheric water vapour compared to that at mid and high latitude regions. Another difference in the absorption feature is seen at C at 443.5 nm region (Fig. 3.4). This is due to O_3 present in the atmosphere. The dip at C is relatively less pronounced (at low latitude) compared to that obtained by *Harrison* [1979] (at mid latitude). This could be due to the reason that ozone content at mid latitude is more compared to that at low latitude. An examination of Fig. 3.4 shows that there is a tilt in the ratio spectrum. This tilt is due to aerosols present in the atmosphere. Such type of tilt has also been observed by other workers [*Noxon*, 1978b; *Harrison*, 1979]. This tilt can be on either side, because it mainly depends upon the amount of aerosols present during the observation period. O_4 also contain absorption in this wavelength region but its contribution is less significant compared to other species. The components due to aerosol and Rayleigh scattering and O_4 in the ratio spectrum must be removed. This procedure has been described in Section 3.4.

3.3.3 NO_2 cell

To verify that the observed residual spectrum of the atmosphere contains NO_2 feature, a NO_2 cell has been made in the laboratory. This NO_2 cell is made up of a glass tube having inlet and outlet openings. The length of the tube is 10 cm and diameter 1 cm. NO_2 has been prepared in the laboratory by reaction of HNO_3 with $FeSO_4$. After evacuating the NO_2 cell to 10^{-6} Torr of pressure, NO_2 was filled in it and was

properly sealed. Although care was taken to keep NO₂ in the cell as pure as possible, formation of N₂O₄ inside the tube can not be ruled out [Sanders *et al.*, 1989]. This might affect the shape of the NO₂ absorption spectrum. Tungsten lamp has been used as a source. First monochromator has been scanned to get the background spectrum without using NO₂ cell. Then monochromator has been scanned by putting the NO₂ cell in front of it. The spectrum has been scanned between 436 and 448 nm region. 12 nm wavelength region has been scanned in about 6 minutes. This cell spectrum has been divided by the background spectrum and is shown in Fig. 3.6. Clearly in this spectral scan, two major dips around 439.5 and 445.0 nm are seen. Similar NO₂ cell spectrum has been observed by many workers [e.g., Noxon *et al.*, 1979; Syed and Harrison, 1980].

3.4 Data reduction

The fundamental principle underlying absorption measurements is Beer's law, wherein the attenuation of monochromatic radiation is related to the number of absorbing molecules in the optical path, so that

$$I = I_B \cdot \exp(-s[A]\Delta x) \quad (3.4)$$

where I is the measured flux, I_B is the incident or background flux, s is the molecular cross section of the absorbing species, $[A]$ is the absorbing species density, and Δx is the distance over which absorption takes place, or optical path. In atmospheric application, Δx is often rewritten as $L \cdot \Delta z$, where Δz is the vertical thickness of the optical path and L is a geometrical factor which relates the slant path length to its thickness. In the atmosphere, $[A]$ and L are generally functions of altitude, so that the absorption seen at the ground represents an integral over the absorbing path :

$$I = I_B \cdot \exp(-s \cdot \int_z^\infty [A]_z \cdot L_z \cdot dz) \quad (3.5)$$

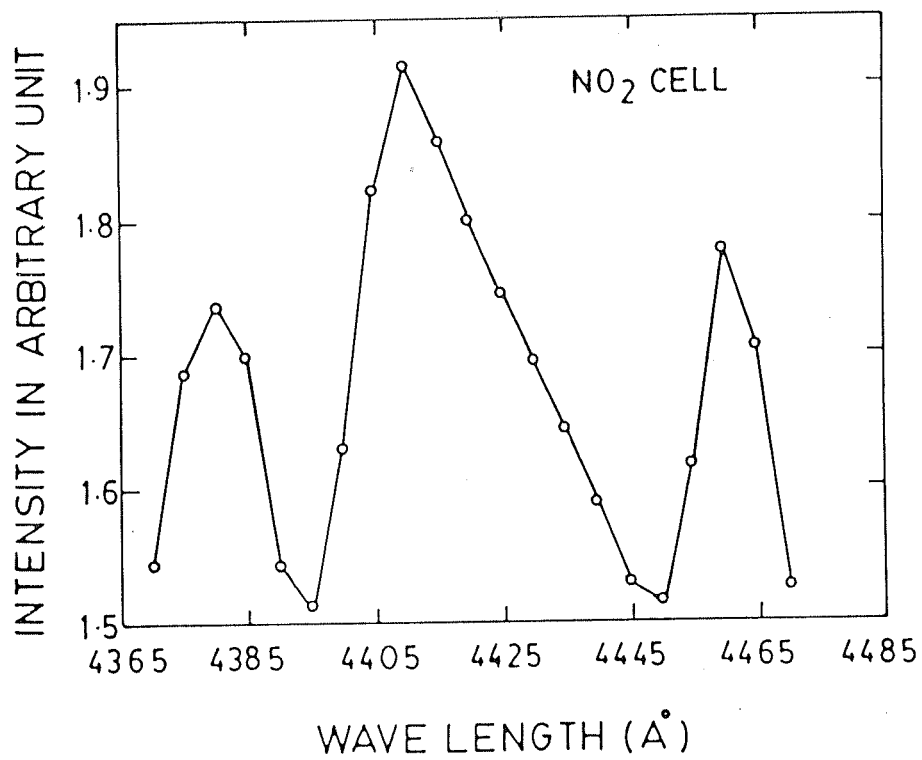


Figure 3.6 A scan of 436.5 to 448.5 nm with NO₂ cell.

The quantity measured in atmospheric absorption spectroscopy is the slant column abundance, $\int_z^\infty [A]_z \cdot L_z \cdot dz$. Since all the parameters except $\int_z^\infty [A]_z \cdot L_z \cdot dz$ are known in eqn. 3.5, the value of this quantity can be determined.

To derive the slant column density of NO₂ from ratio spectra several methods are available. These have been summarized by *Syed and Harrison* [1980]. They also have studied the relative merits and demerits of these methods. The latest method, however, is the matrix inversion method introduced by *McKenzie and Johnston* [1982b] and also used in the present study. In this section, we have given a brief description of these methods.

3.4.1 Method-1

This method is similar to that used by *Brewer et al.* [1973]. In Brewer's method the spectral radiant intensity of the sky is measured at three wavelengths and only NO₂ absorption and Rayleigh scattering are taken into account. Later J.B. Kerr has modified this method to use five wavelengths. These wavelengths are : 437.6 (λ_1), 439.3 (λ_2), 442.0 (λ_3), 444.9 (λ_4), and 450.1 (λ_5) nm. In this method, O₃ absorption has also been taken into account.

The spectral radiant intensity of sunlight after passing through the atmosphere at wavelength λ_n is given by

$$\log_{10} I_n = \log_{10} I_{on} - \alpha_n \cdot Y - \delta_n \cdot Z - \beta \cdot m \quad (3.6)$$

where, I_{on} is the value of I_n at the top of the atmosphere

α_n the NO₂ absorption coefficient at λ_n , cm^{-1} ;

Y the effective path length of NO₂ , cm;

δ_n the O₃ absorption coefficient at λ_n , cm^{-1}

Z the effective path length of O₃ , cm;

β the Rayleigh scattering coefficient at λ_n , atm^{-1}

m the effective airmass, atm

The light intensities at the five wavelengths given by eqn. 3.6 can be combined linearly to form the following expression [Ridley *et al.*, 1984] :

$$F = F_o - \Sigma\alpha.Y - \Sigma\beta.m \quad (3.7)$$

where,

$$F = \log_{10} I_1 - 1.28 \log_{10} I_2 + 0.97 \log_{10} I_3 - 1.29 \log_{10} I_4 + 0.61 \log_{10} I_5$$

$$F_o = \log_{10} I_{o1} - 1.28 \log_{10} I_{o2} + 0.97 \log_{10} I_{o3} - 1.29 \log_{10} I_{o4} + 0.61 \log_{10} I_{o5}$$

$$\Sigma\alpha = \alpha_1 - 1.28\alpha_2 + 0.97\alpha_3 - 1.29\alpha_4 + 0.61\alpha_5 = 8.16 \text{ cm}^{-1}$$

$$\Sigma\delta = \delta_1 - 1.28\delta_2 + 0.97\delta_3 - 1.29\delta_4 + 0.61\delta_5 = 0.0$$

$$\Sigma\beta = \beta_1 - 1.28\beta_2 + 0.97\beta_3 - 1.29\beta_4 + 0.61\beta_5 = 0.0$$

The values of $\Sigma\alpha$, $\Sigma\delta$, $\Sigma\beta$ are derived by using appropriate absorption coefficient values. From measurements of F , the amount of NO_2 can be deduced provided F_o is known which can be measured by using noontime sky spectrum.

3.4.2 Methods 2 and 3

Noxon [1975] proposed a method in which an unambiguous identification of NO_2 was possible by taking the complete spectrum into account. The procedure involves direct measurements of NO_2 differential absorption in the complete spectrum. It takes account of NO_2 absorption and scattering (Rayleigh and aerosol). Also, it uses a method for reducing the Ring effect. As has been explained earlier, first a ratio spectrum is obtained from the raw spectra. Then the maximum and minimum absorptions of NO_2 in the ratio spectrum are used for the calculation of NO_2 column

abundance. Since there are several such minima in the spectral region of interest, several pairs of minima can be used for analysis. In method 2, 437.9 and 442.0 nm wavelength pair was used and in method 3, 437.9 and 446.6 nm wavelength pair was used to derive the magnitude of absorption at 439.5 nm [Syed and Harrison, 1980]. In the absence of ozone contribution or other perturbing effects, NO₂ obtained by methods 2 and 3 are equal.

The NO₂ differential absorption at 439.5 nm is then converted to slant column abundance Y, using the corresponding value of the differential absorption coefficient. The required relation, obtained using Bouguer's law is :

$$Y = \frac{-\ln(1 - \Delta X \cdot 10^{-2})}{2.76 \cdot 10^{-19}} \quad (3.8)$$

where ΔX is the value of depth in the ratio spectrum caused by the NO₂ absorption.

3.4.3 Method-4

This method was introduced by Harrison [1979]. In this method contribution due to ozone and aerosols and Rayleigh scattering have been taken into account. The measurement of spectral radiant intensity is needed only at five wavelengths. These wavelengths have been selected in such a way that the effect of Ring component is minimum. These wavelengths are 437.9, 439.5, 441.2, 443.5, and 446.6 nm. Here 439.5 and 443.5 nm wavelengths correspond to the maximum absorption of NO₂ and O₃ respectively. If the spectral radiant intensities of the zenith sky at twilight and at midday are $I(\lambda)$ and $J(\lambda)$ respectively, and if $K(\lambda)$ is the solar spectral irradiance at the top of the atmosphere then one can write

$$I(\lambda) = K(\lambda) \cdot l\beta \cdot \exp[-(\beta \cdot x + \delta \cdot y + \sigma \cdot z)]$$

and

$$J(\lambda) = K(\lambda) \cdot m\beta' \cdot \exp[-(\beta' \cdot p + \delta \cdot q + \sigma \cdot r)]$$

where x , y , and z and p , q , and r are net effective attenuation optical path lengths for scattering (aerosol and Rayleigh), NO_2 absorption, and O_3 absorption, respectively. The factors $l\beta$ and $m\beta'$ take account of the different geometries and different scattering angles in the field of view of the observer during twilight and at midday. The scattering coefficients β and β' will not necessarily be equal in magnitude but can be expected to have nearly the same wavelength dependence. The absorption coefficients for NO_2 and O_3 are δ and σ , respectively, and like β and β' they are wavelength dependent. Here it is assumed that compared to the twilight NO_2 absorption, $J(\lambda)$ contains negligible NO_2 absorption. Since $x \gg p$, $y \gg q$, and $z \gg r$ then if $R(\lambda) = \frac{I(\lambda)}{J(\lambda)}$, one can write :

$$R(\lambda) = \left[\frac{l\beta}{m\beta'} \cdot \exp(-\beta \cdot x) \right] \cdot \exp[-(\delta \cdot y + \sigma \cdot z)] \quad (3.9)$$

The first term in brackets is assumed to vary linearly with wavelength over a small wavelength interval. Then eqn. 3.9 can be rewritten as -

$$R(\lambda_n) = [a + b(\lambda_n - \lambda_1)] \cdot \exp[-(\delta_n \cdot y + \sigma_n \cdot z)]$$

$$\text{or,} \quad R_n = [a + b(\lambda_n - \lambda_1)] \cdot S_n \quad (3.10)$$

$$\text{or,} \quad R_n = \rho \cdot S_n$$

$$\text{where,} \quad \rho = a + b(\lambda_n - \lambda_1)$$

$$\text{and,} \quad S_n = \exp[-(\delta_n \cdot Y + \sigma_n \cdot Z)]$$

Here S_n is the ratio which would be observed if all aerosol and Rayleigh scattering were absent.

The variations of both δ and σ with wavelength are shown in Fig. 3.5 [Harrison, 1979]. It is to be noted from this figure that $\delta_3 = \delta_5$ and $\sigma_3 = \sigma_5$ at $\lambda_3 = 441.2$ nm and $\lambda_5 = 446.6$ nm, respectively. This fact has been used for removing the effects of aerosol scattering from each spectrum. Putting $c=b/a$ and noting that $S_3 = S_5$,

we have from eqn. 3.10

$$c = \frac{(R_3 - R_5)}{[R_5(\lambda_3 - \lambda_1) - R_3(\lambda_5 - \lambda_1)]} \quad (3.11)$$

After obtaining the value of c , the following two equations can be derived :

$$\begin{aligned} \frac{S_2}{S_1} &= \frac{R_2}{R_1}[1 + c(\lambda_2 - \lambda_1)] \\ &= \exp[-(\delta_2 - \delta_1)Y - (\sigma_2 - \sigma_1)Z] \end{aligned} \quad (3.12)$$

$$\begin{aligned} \frac{S_4}{S_1} &= \frac{R_4}{R_1}[1 + c(\lambda_4 - \lambda_1)] \\ &= \exp[-(\delta_4 - \delta_1)Y - (\sigma_4 - \sigma_1)Z] \end{aligned} \quad (3.13)$$

These two equations can then be combined to give :

$$Y = \frac{(\ln(\frac{S_4}{S_1})(\sigma_2 - \sigma_1) - \ln(\frac{S_2}{S_1})(\sigma_4 - \sigma_1))}{((\delta_2 - \delta_1)(\sigma_4 - \sigma_1) - (\sigma_2 - \sigma_1)(\delta_4 - \delta_1))} \quad (3.14)$$

$$Z = \frac{(\ln(\frac{S_2}{S_1})(\delta_2 - \delta_1) - \ln(\frac{S_4}{S_1})(\delta_2 - \delta_1))}{((\delta_2 - \delta_1)(\sigma_4 - \sigma_1) - (\sigma_2 - \sigma_1)(\delta_4 - \delta_1))} \quad (3.15)$$

where Y and Z correspond the slant column abundances of NO_2 and O_3 respectively.

3.4.4 Method 5

To derive the NO_2 column abundance from the solar absorption spectrum, matrix inversion technique was introduced by *Mckenzie and Johnston* [1982b]. Since NO_2 and O_3 possess absorption feature in the blue region, maximum number of points has been used for detecting the absorption feature in detail.

Let I_I be the intensity reaching the ground at wavelength λ_I , where $I = 1, 2, 3, \dots$, then according to Lambert - Beer's law we get,

$$I_I = I_{oi} \cdot \exp[-\alpha_I \cdot M \cdot \Delta x - \beta_I \cdot N \cdot \Delta x] \quad (3.16)$$

where

I_{oi} Intensity outside the atmosphere at wavelength λ_I

α_I, β_I Absorption cross-sections of NO_2 and O_3 at wavelength λ_I

M, N Number density for NO_2 and O_3 , respectively.

Δx slant path length traversed by solar rays.

By taking the ratio of intensity of a particular wavelength at evening time to the intensity at noontime, the I_{oi} factor is eliminated.

The ratio of evening time intensity to noontime intensity is given by-

$$\begin{aligned} R_I &= \exp[-\alpha_I.M.(\Delta x_e - \Delta x_n) - \beta_I.N.(\Delta x_e - \Delta x_n)] \\ &= \exp[-\alpha_I.M.\Delta'x - \beta_I.N.\Delta'x] \end{aligned} \quad (3.17)$$

where $\Delta x_e, \Delta x_n$ are path lengths of solar radiation during evening and noontime respectively

$$\Delta'x = \Delta x_e - \Delta x_n$$

By taking the ratio of every two adjacent wavelengths, we have

$$R'_{jj} = \frac{R_I}{R_{I+1}} = \frac{\exp[-\alpha_I.M.\Delta'x - \beta_I.N.\Delta'x]}{\exp[-\alpha_{I+1}.M.\Delta'x - \beta_{I+1}.N.\Delta'x]} \quad (3.18)$$

where $jj \doteq 1, 2, 3, \dots, 1108$. Let $(\alpha_I - \alpha_{I+1}) = \alpha'_{jj}$; $(\beta_I - \beta_{I+1}) = \beta'_{jj}$; $M.\Delta'x = M'$ = slant column abundance of NO_2 during twilight time, $N.\Delta'x = N'$ = slant column abundance of O_3 during twilight time.

Thus,

$$R'_{jj} = \exp[-M'.\alpha'_{jj} - N'.\beta'_{jj}] \quad (3.19)$$

$$\ln(R'_{jj}) = [-M'.\alpha'_{jj} - N'.\beta'_{jj}]$$

or,

$$R_{jj} = -M'.\alpha'_{jj} - N'.\beta'_{jj} \quad (3.20)$$

where $\ln(R'_{jj}) = R_{jj}$

In eqn. 3.20, α'_{jj} and β'_{jj} are known. Thus, computing R_{jj} for $jj = 1, 2, 3, \dots, 1108$, the value of M' and N' can be computed. These 1108 simultaneous equations can be arranged in the form of a matrix

$$[-M' - N'] \cdot \begin{pmatrix} \alpha'_1 & \alpha'_2 & \dots & \alpha'_{1108} \\ \beta'_1 & \beta'_2 & \dots & \beta'_{1108} \end{pmatrix} = [R_1 \ R_2 \ \dots \ R_{1108}] \quad (3.21)$$

Besides NO_2 and O_3 , absorptions due to H_2O and O_4 (O_2 dimer) are also present in R. If these are taken into account, then the matrix 3.21 becomes

$$[-M' - N' - W' - P'] \cdot \begin{pmatrix} \alpha'_1 & \alpha'_2 & \dots & \alpha'_{1108} \\ \beta'_1 & \beta'_2 & \dots & \beta'_{1108} \\ \gamma_1 & \gamma_2 & \dots & \gamma_{1108} \\ \delta'_1 & \delta'_2 & \dots & \delta'_{1108} \end{pmatrix} = [R_1 \ R_2 \ \dots \ R_{1108}] \quad (3.22)$$

where W, P, γ and δ represent the terms corresponding to H_2O and O_4 .

The above matrices can be represented in the form :

$$A.B = R \quad (3.23)$$

To make B as a square matrix, we multiply its transpose for converting into a square matrix and then take the inverse of this square matrix for finding the value of A, i.e., M' and N' . Thus we get-

$$A.B.B' = R.B'$$

$$\text{or,} \quad (A.B.B').(B.B')^{-1} = R.B'.(B.B')^{-1}$$

$$\text{or,} \quad AI = R.B'.(B.B')^{-1} \quad (3.24)$$

The elements of matrix $R.B'.(B.B')^{-1}$ give the values of M' and N' . These are the slant column densities of NO_2 and O_3 .

3.4.5 Absorption cross-sections

To calculate the column density of NO_2 , we need its absorption cross-sections in the wavelength range of our interest. We also need absorption cross-section values for O_3 , O_4 and H_2O .

Absorption cross-sections of NO_2 in different wavelength regions have been reported by several groups. *Hall and Blacet* [1952] measured absorption curves for NO_2 - N_2O_4 mixtures at pressures 33, 126 and 307 Torr at 298 K, with an average spectral bandwidth of 0.4 nm, and calculated the contribution of NO_2 and N_2O_4 by using the equilibrium constant expression of Beer's Law. Individual absorption curves for NO_2 and N_2O_4 in the range 240-500 nm were calculated by deconvolution using a mechanical analog differential analyzer. *Nakayama et al.* [1959] obtained NO_2 absorption curves from 108 to 270 nm at 300 K at a resolution of 0.02 nm. *Johnston and Graham* [1974] obtained the NO_2 absorption spectrum with an 8.6 m optical path and 1.3 nm resolution at low pressures over the wavelength range 185-420 nm. *Bass et al.* [1976] measured the extinction coefficients of NO_2 in the spectral ranges 185-410 nm at 298 K and 290-410 nm at 235 K with a spectral resolution of 0.015 - 0.04 nm. The spectra were obtained in a multiple - pass variable temperature cell using NO_2 pressures varying between 30 and 600 m Torr. The absorption spectrum of N_2O_4 was also measured separately at various low temperatures. Corrections were made for the presence of N_2O_4 and the resulting NO_2 spectrum was tabulated at 0.125 nm intervals for both the temperatures. The absorption cross-sections were also measured by *Harker et al.* [1977] over the wavelength range 375-420 nm at 296 K, and by *Davenport* [1977] in the range 390 - 420 nm from 204 to 296 K. *Hicks et al.* [1979] measured the NO_2 absorption cross-sections between 425 and 450 nm at 298 and 235 K using a combined spectrograph - microdensitometer analysis system with a resolution of 0.04 nm. In the longer wavelength range, *Hsu et al.* [1978] and

Uehara and Sasada [1985] measured NO_2 absorption cross-section in the range 533-648 nm and 559 - 597 nm respectively. *Davidson et al.* [1988] made measurements of the temperature dependence of the absorption cross-section of NO_2 in the visible - ultraviolet region (264 - 649 nm). They find a small negative temperature dependence of σ over the 264 to 400 nm range and a small positive dependence over the 450 - 649 nm range. In the wavelength range of our interest, the absolute absorption cross section values, given by different workers, at 0.5 nm resolution are consistent with each other. Absorption cross-section values of NO_2 have also been given by *Harrison* [1979]. These have been taken from the unpublished work of *Johnston*. These are the most widely used values for NO_2 determination and we have also used them for the present study. Fig. 3.5 shows the values of absorption cross section of NO_2 and O_3 used in the present work.

Absorption cross section in the wavelength range of our interest for O_3 falls in Chappuis band. Very few measurements are available and they show a certain disagreement. It has been measured by various workers [*Lefebvre*, 1935; *Humphrey and Badger*, 1947; *Vassy and Vassy*, 1948; *Inn and Tanaka*, 1953; *Vigroux*, 1953; *Griggs*, 1968; *Penney*, 1979; *Chappuis*, 1980, 1982; *Nicolet*, 1980; *Amoruso et al.*, 1990]. *Chappuis* [1980, 1982], *Vassy and Vassy* [1948], and *Penney* [1979] note an important increase of the absorption coefficient when the temperature is lowered. On the contrary, *Lefebvre* [1935], *Humphrey and Badger* [1947], and *Vigroux* [1953] see a very small dependence of the ozone absorption cross section on temperature. *Inn and Tanaka* [1953] and *Griggs* [1968] have also carried out measurements of the ozone cross -section but at room temperature. *Amoruso et al.* [1990] also found ozone absorption cross -section value to be independent of temperature. Laboratory absorption cross-section of ozone has been measured by *Johnston* (unpublished data) in the visible region at room temperature, along with NO_2 . O_3 absorption cross -section used in the present study has been taken from *Harrison* [1979]. These are the

unpublished data of *Johnston*.

The absorption cross-sections of O_4 have been measured in the laboratory by *Greenblatt et al.* [1990]. They have measured the absorption spectrum of O_2 and O_2 - O_2 collision pairs over the wavelength range from 330 to 1140 nm using pressures of O_2 from 1 to 55 atm at 298 K. The absorption cross section of O_4 used in the present study are from *Greenblatt et al.* [1990].

It has been mentioned earlier that water vapour has a major absorption at 442.6 nm. The value of absorption cross -section at this wavelength is $3.1 \pm 0.3 \times 10^{-26} \text{ cm}^{-2}$ [*Johnston and McKenzie*, 1984]. Water vapour absorption spectrum has been measured by *Curcio et al.* [1955] from about 415 to 447 nm. They have given relative value of water vapour absorption cross-section. To obtain absolute value of water vapour cross-section, spectrum obtained by them has been normalized with respect to cross-section value at 442.6 nm measured by *Johnston and McKenzie* [1984].

3.4.6 Conversion of slant column to vertical column

As long as the sun is at an elevation angle greater than 15° , the increase in the path length of the solar radiation compared to the path length covered by solar radiation at 0° solar zenith angle is not very significant. In this case the enhancement factor has the value of $\text{Sec}(\chi)$, where χ is the solar/lunar zenith angle. For solar zenith angles $\chi > 75^\circ$, $\text{Sec}(\chi)$ is replaced by the Chapman function, $\text{Ch}(\chi)$. The $\text{Ch}(\chi)$ is calculated by assuming that the air density of the earth's atmosphere decreases exponentially with height. But in the case of minor constituents, the vertical distribution will be different from that of air, therefore the enhancement factor will be different for different species.

In order to convert slant column abundances to vertical column abundances, a

scattering model has been developed by many workers [Syed and Harrison, 1980; Noxon *et al.*, 1979; Solomon *et al.*, 1987; McKenzie *et al.*, 1991b; Perliski and Solomon, 1992]. Kerr *et al.* [1977] has developed multiple scattering model for the calculation of NO₂ twilight enhancement factor. This model was originally developed for ozone study by Mateer and Duetsch [1964]. In this model it has been assumed that the number of molecules per layer is 9×10^{15} molecules cm⁻², and each layer is 5.6 km thick. Similar type of model has been developed by Noxon *et al.* [1979] assuming single and double scattering. They also have assumed 9×10^{15} molecules cm⁻² per layer and the thickness of each layer is 5 km. The twilight enhancement factor calculated by second model is 1.4 times higher compared to the first one at $\chi = 90^\circ$. McKenzie *et al.* [1991b] have calculated the twilight enhancement factor by using the NO₂ vertical profile obtained over Lauder (45°S) by using visible absorption spectrometric technique. They have calculated the airmass factor by taking layer of 5 km thickness. Observations have been made by them for the clean atmosphere, therefore tropospheric contamination is almost negligible. They have calculated twilight enhancement factor with and without sunset chemistry. The enhancement factors with and without considering this chemistry are 19.1 and 20 respectively at 90° solar zenith angle. Same procedure has been used by them for the calculation of ozone enhancement factor. Recently airmass factors have been calculated by Perliski and Solomon [1992] using a spherical Monte Carlo radiative transfer model. They have considered the effect of Pinatubo aerosols and calculated the NO₂ enhancement factor by considering the 5 km thickness of NO₂ slab. They find that the enhancement factor of NO₂ changes at larger scale below 20 km altitude but above 20 km altitude the enhancement factor of NO₂ due to the presence of Pinatubo aerosols remains unchanged. The value of enhancement factor used in the present study has been taken from model developed by Syed and Harrison [1980]. This enhancement factor at 90° solar zenith angle is almost equal to the value calculated by McKenzie *et al.* [1991b]

without considering the sunset chemistry.

3.5 Sources of error

Any experimental technique used for the measurement of any parameter has some limitations and uncertainties. These, for our NO₂ measurements, are discussed in the following paragraphs.

3.5.1 Laboratory absorption cross-sections

Cross-sections for NO₂ and O₃ used in the present study were those used by *Harrison* [1979], taken from the unpublished work of H.S. Johnston at a resolution of 0.5 nm. The uncertainty in these values are about $\pm 5\%$, and according to *Syed and Harrison* [1980] these absorption cross-section values are independent of temperature and pressure. This inconsistency will lead to some error in the NO₂ density.

3.5.2 Tropospheric contamination

Since the observations have been made in the urban area, possibility of contamination due to motor-car, biomass burning and industrial pollution exists. In the zenith sky measurements during twilight period, direct solar radiation passing through troposphere is absorbed by its dense atmosphere. Thus the light reaching the surface of the earth during twilight period is the light scattered from above troposphere. Then the possibility of contamination due to tropospheric region is negligible during twilight period.

3.5.3 Ring effect

Fraunhofer filling-in was first reported by *Gringer and Ring* [1962]. The Fraunhofer lines during twilight period have been found to be shallower than those during noon-time. This is due to the unpolarized Raman-scattered photons reaching the surface. During noontime, the contribution of Rayleigh scattered photons which are polarized is higher than twilight period. The unpolarized scattered component during twilight is large compared to noon time. To remove the Ring effect, the ratio of twilight and background spectra is taken. But the contribution due to Ring component is still present in the ratio spectrum. The presence of the Ring component causes change in the wavelength positioning by which selection of particular wavelength with greater accuracy becomes difficult. To minimize this effect the cross correlation matching of two spectra has been done by a computer. Also to overcome this effect, the ratio spectrum has been further smoothened. Due to these precautions, the contribution of Ring effect becomes minimum but it is not removed completely. To incorporate the Ring component in the observed spectrum, theoretical Ring spectrum has been made by *Solomon et al.* [1987]. The error in the column abundance of NO_2 due to the effect of Ring component is found to be about 5%.

3.5.4 Enhancement factor

In order to convert slant column abundances to vertical column abundances, a model of enhancement factor is needed. This model is prepared by assuming a few stratospheric NO_2 profiles. These profiles have been obtained for mid or high latitude stations by using balloon-borne or ground-based techniques. But the vertical distribution of NO_2 for low latitude region is not properly known. This lack of information in the vertical distribution of NO_2 at low latitude region will cause some uncertainty in the vertical column abundance.

3.5.5 Resultant uncertainty

Errors which are possible in our measurements and the steps taken to minimize them have been mentioned above. The experimental set-up is such that the monochromator looks in the horizontal direction. A reflecting mirror has been kept in front of the monochromator for receiving the light from the zenith. The accuracy of the mirror position leads to the variation in height range covered during twilight period. The variation in the position of reflecting mirror by $\sim 30^\circ$ corresponds to the variation in height range ~ 5 km [Rozenberg, 1966]. Backlash error between forward and reverse scans also causes wavelength shift of the spectrum. To avoid the distortion in the shape of the spectrum, we have taken the average of both forward and backward spectra. Use of different control spectrum changes the value of column abundance because of the presence of different NO_2 absorption in different background spectra. To minimize the error caused by the background spectrum, the same background spectrum has been used for all the data spectrum. Ratio of twilight and noontime spectra has been taken after getting there maximum correlation and then positioning around Fe II line. We have also taken steps to minimize the contribution of Ring component. It has been assumed that the aerosol and Rayleigh scattering coefficients vary with wavelength as λ^{-1} and λ^{-4} respectively. This assumption is valid for the molecules and particles which have specific dimensions. But some aerosols particles are also present in the atmosphere which may not satisfy these dimensions. Corrections due to O_3 , O_4 and H_2O have also been applied as much as possible. Besides there could be some effect of refraction. But it is more pronounced in the higher wavelength region. In the wavelength region of our interest, it does not have any significant contribution to the twilight spectrum. According to Noxon *et al.* [1979], NO_2 absorption can be measured to an accuracy of about 0.3% by this technique. Since the twilight spectra usually exhibit absorption of a few percent, this accuracy is generally sufficient. Considering all the precautions taken above we place the overall

error in our measurements to be less than 25%.

3.6 Results and discussion

3.6.1 Winter values

Daily observations of atmospheric NO_2 column amounts have been made during sunrise and sunset periods at $90 \pm 1^\circ$ solar zenith angle. Fig. 3.7 (lower panel) shows a plot of morning and evening vertical column abundances obtained during December 1989 - January 1990. Sunrise values have been represented by solid circles and sunset values by open circles. These values are the averages of five consecutive days with one σ standard deviation. Ozone values obtained by the spectrometer are also shown in the upper panel. This also represents the five days running mean.

An examination of Fig. 3.7 shows that in most cases, sunrise values are less than the sunset values. On certain days, reverse feature has been seen. Our values of NO_2 lie in the range of 0.5 to $2 \times 10^{15} \text{ cm}^{-2}$. These values can be compared with the low latitude values reported in *WMO* [1985]. Our values are consistent with *WMO* values. The lower values of NO_2 during the morning hours compared to those in the evening hours are due to the decay of NO_2 at night. During nighttime, NO_2 is converted into N_2O_5 . The details of chemical processes which takes place are given in Chapter 5.

Observed values of ozone by zenith sky technique show more fluctuations as compared to the values obtained by the Dobson instrument operating at the same location. The Dobson ozone values at the same location are in the range of 240-250 DU.

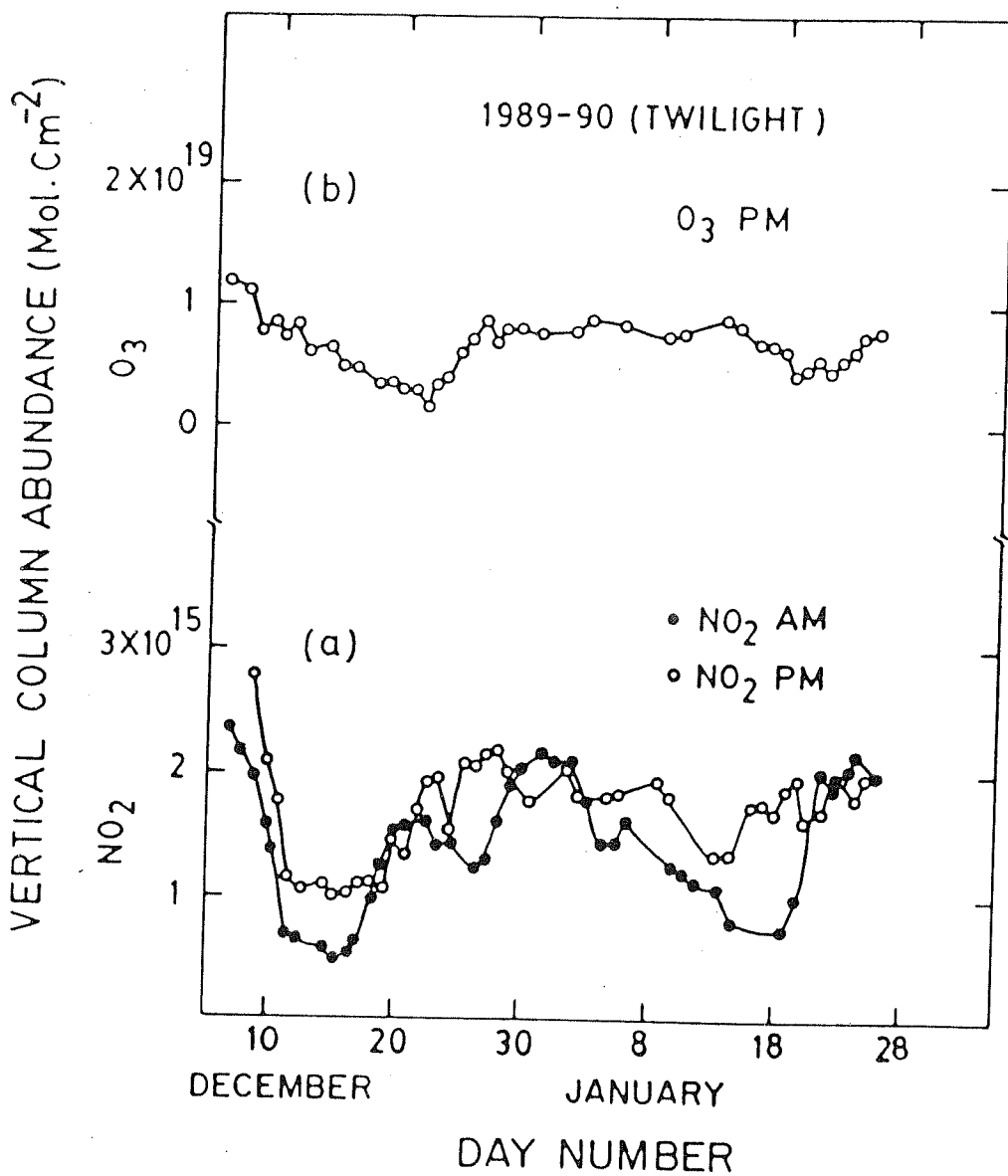


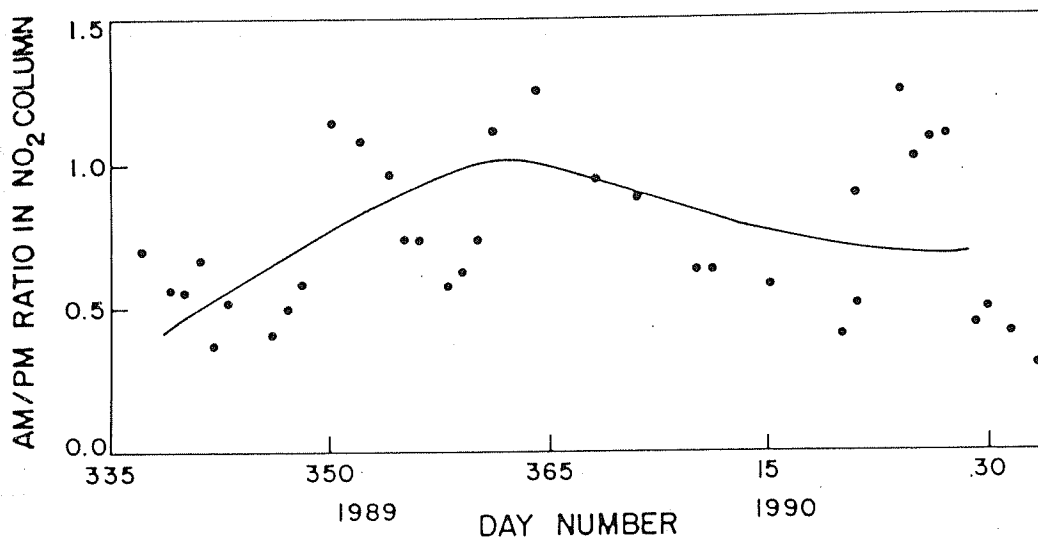
Figure 3.7 Curves showing (a) NO_2 vertical column density in December 1989 and January 1990, and (b) corresponding O_3 values.

3.6.2 Decay constant

Decay constant is defined as the ratio of NO_2 during morning to that in the preceding evening. Overnight decay of NO_2 for different days in the winter period is shown in Fig. 3.8. This figure shows that the decay factor is maximum in the last week of December and shows a decreasing tendency afterwards. For few days, NO_2 does not show much conversion and the morning values have been found to be higher than the evening values. There could be several local sources, such as transportation, bio-mass burning, etc. which are high in the tropical region. These sources could enhance the NO_2 values during the morning time. Large changes in both the abundance of NO_2 and its diurnal variation are commonly seen at mid-latitude [Noxon *et al.*, 1979]. The amount of decay during darkness is highly dependent on the length of the night. If duration of the darkness is more, the amount of decay would be more. Our observations correspond to the winter period, when the length of the night was more than that of the day. Hence, the decay factor observed by us should be the maximum decay factor at our low latitude region. This should make $[\text{NO}_2]_{AM}$ minimum and $\frac{[\text{NO}_2]_{AM}}{[\text{NO}_2]_{PM}}$ minimum in the last week of December. However, this was not observed. That is because the rate of decay of NO_2 is also directly proportional to O_3 value which is not minimum in winter.

3.6.3 Diurnal variation

The diurnal variation is a quantity which measures the rate of change of NO_2 formation during daytime. NO_2 diurnal variation, calculated as (sunset - sunrise) / sunset vs day number is shown in Fig. 3.9. It is to be seen from Fig. 3.9 that the value of diurnal variation is minimum during the last week of December 1989 and it increases before and after this week. Diurnal variation for high-latitude has been reported by Pommereau and Goutail [1988a,b]. At Arctic, they found the maximum to



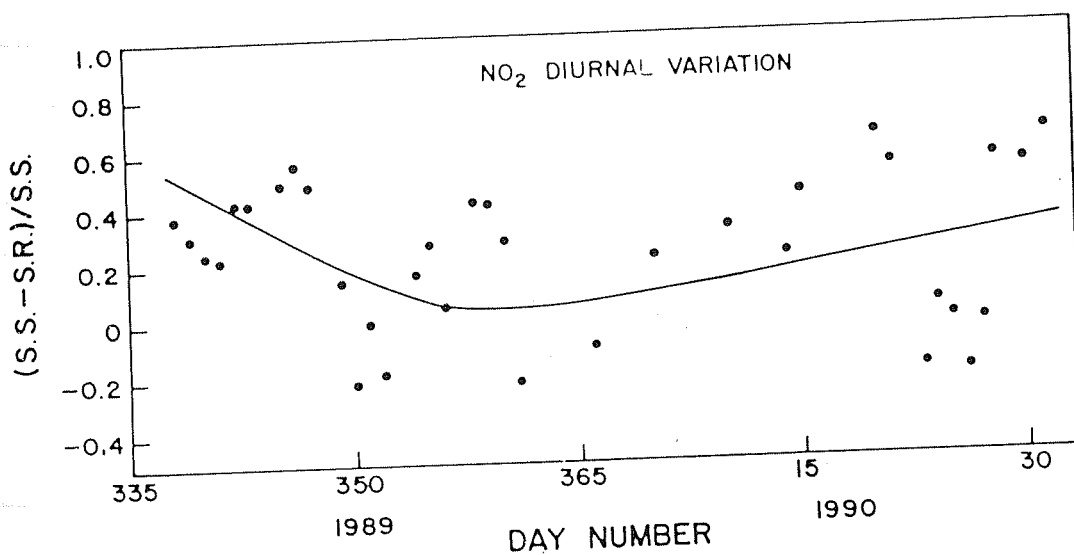


Figure 3.9 Plots showing the NO₂ diurnal variation calculated as $(\text{sunset} - \text{sunrise}) / \text{sunset}$, for different days in December 1989 and January 1990.

be around the end of March and beginning of April [*Pommereau and Goutail*, 1988a] and at Antarctica, the maximum occurs towards the end of February [*Pommereau and Goutail*, 1988b].

3.6.4 Correlation between NO_2 and O_3

Plots of NO_2 versus O_3 values obtained in this work have been made for sunrise and sunset times in Fig. 3.10 [(a) and (b)]. Although, there is a scatter in the data, a direct linear correlation appears to be existing between NO_2 and O_3 column densities. These O_3 values have been obtained along with NO_2 using the same spectral region. Both plots show positive correlation between NO_2 and O_3 . Morning NO_2 and O_3 values show a strong positive correlation compared to the evening values. A small variation in NO_2 leads to a large variation in O_3 during morning as well as evening times. These NO_2 and O_3 values are the means of five consecutive days. In this spectral region, besides NO_2 and O_3 absorptions, the possibility of O_4 absorption can not be neglected, whose absorption-cross section is highly dependant on the temperature [*Greenblatt et al.*, 1990]. The NO_2 - O_3 correlation study has been done by many workers [*Mount et al.*, 1987; *Pommereau and Goutail*, 1988a,b; *Ridley et al.*, 1984; *Chakrabarty and Chakrabarty*, 1982; *Shibasaki et al.*, 1986; *Sanders et al.*, 1989; *Johnston et al.*, 1992; *Kondo et al.*, 1987]. *Pommereau and Goutail* [1988a] have observed a positive correlation between NO_2 and temperature, but not with ozone. Similar observations have been made in Antarctica by a large number of workers [*Mount et al.*, 1987; *Pommereau and Goutail*, 1988b; *Keys and Johnston*, 1986; *Shibasaki et al.*, 1986; *Sanders et al.*, 1989; *Kondo et al.*, 1987]. *Sanders et al.* [1989] during summer showed positive correlation between stratospheric NO_2 and O_3 . Species like NO_2 , O_3 and some other meteorological parameters have been simultaneously studied by *Shibasaki et al.* [1986]. According to them, when NO_2 shows a clear increasing trend, the O_3 increasing trend is not very clear. Even when

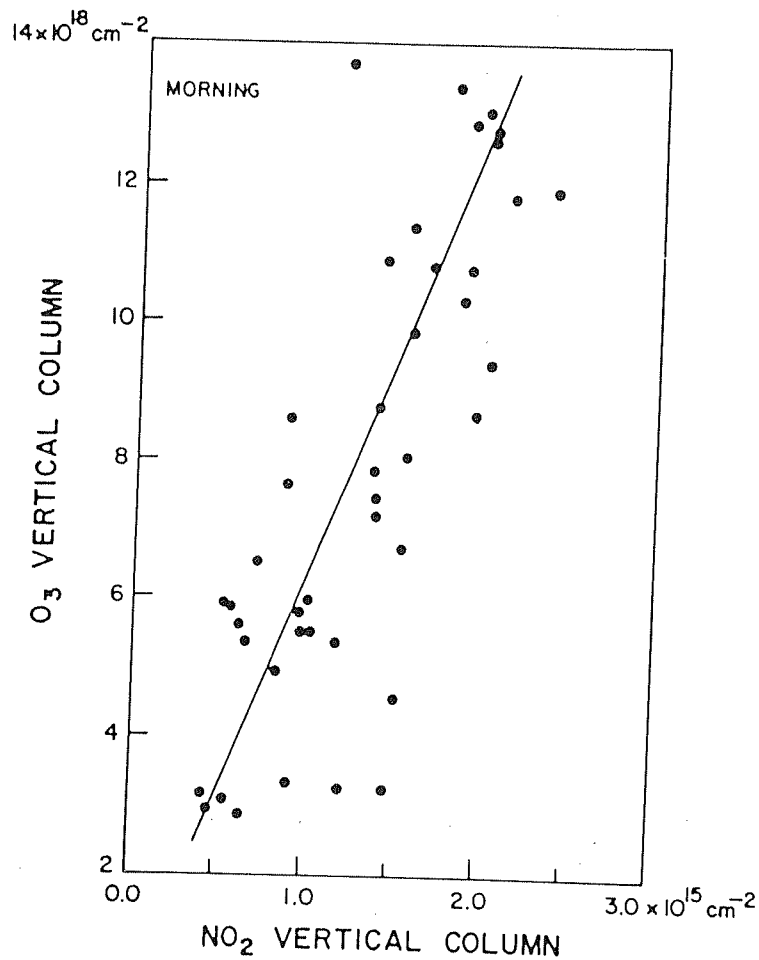


Figure 3.10a Plots showing the correlation between morning NO_2 column density and corresponding O_3 column density obtained with the same instrument.

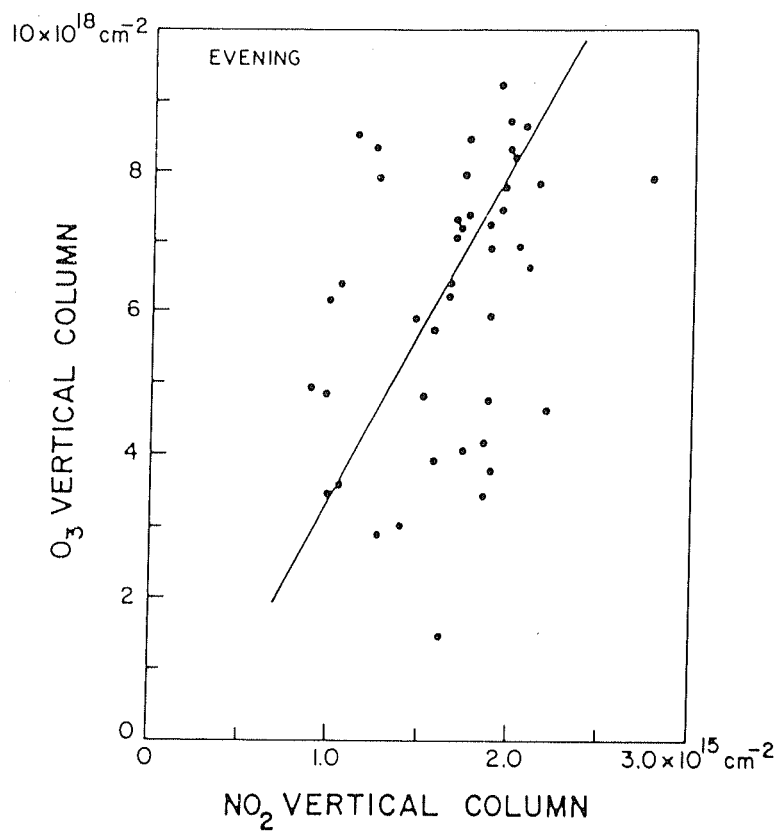


Figure 3.10b Plots showing the correlation between evening NO₂ column density and corresponding O₃ column density obtained with the same instrument.

both show a similar trend, some phase difference is noticed. *Mount et al.* [1987] have observed NO_2 and O_3 column densities and temperature at 50 mbar over McMurdo station, Antarctica. They found a negative correlation between NO_2 and O_3 column densities during September - October 1986, and a morning-to-evening variation of individual species in the same phase. The 50 mbar temperature also shows a one-to-one correlation with NO_2 values. It may be mentioned here that at Antarctic the relation between NO_2 and O_3 inside and outside the vortex is different. It is to be noticed that most of the observations mentioned above are for mid or high latitude regions. Therefore, it is not exact to compare these results with our low latitude observations.

3.6.5 Sunrisetime variation

A plot of sunrise time NO_2 vertical column abundance vs time of the day for different months for some clear days between October 1990 and January 1991 is shown in Fig. 3.11. These are also zenith sky observations. Although a large scatter in the data is noticed, yet a clear minimum around 90° solar zenith angle followed by an increase in the values of NO_2 with the decrease of solar zenith angle is discernible. The scatter in the data after sunrise could be attributed to the tropospheric contamination which might be important at low latitude for solar zenith angles less than 90° . In the presence of sunlight, N_2O_5 gets dissociated into NO_2 and NO_3 . The minimum of NO_2 around sunrise is due to the photodissociation of NO_3 . After sunrise time, the NO present in the atmosphere gets converted into NO_2 and the NO_2 density starts increasing. For the same reason, a sudden increase in NO_2 should occur near the sunset time.

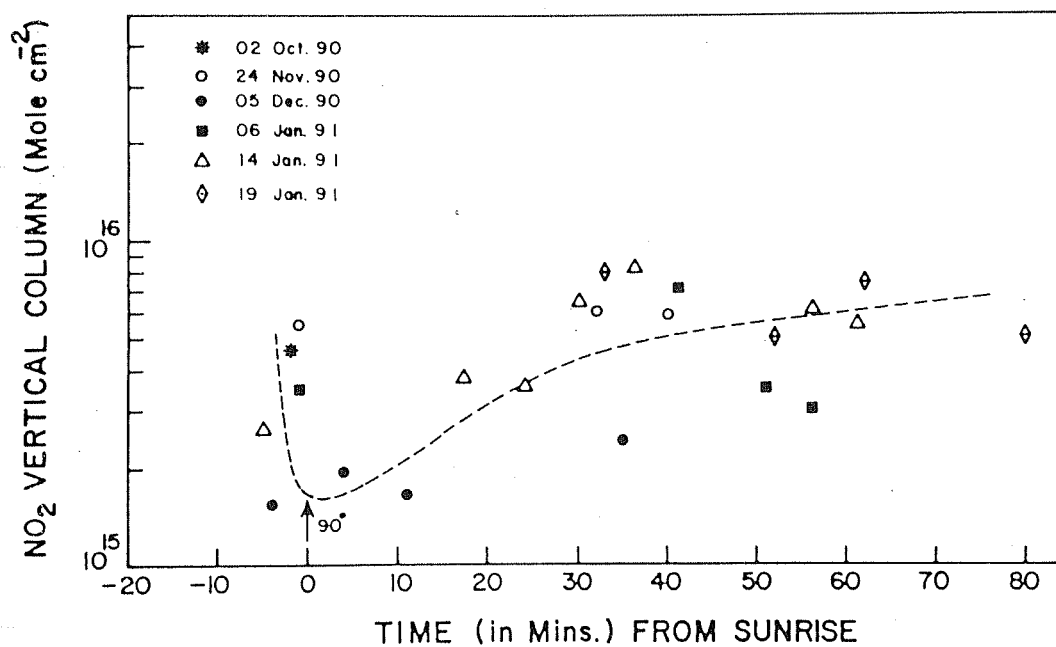


Figure 3.11 Plot of sunrisetime NO₂ vertical column abundance vs time of the day for different months for some clear days between October 1990 and January 1991.

3.6.6 Longterm variation and variation after Pinatubo

As mentioned above, the twilight abundances of stratospheric NO_2 and O_3 have been measured at Ahmedabad (23°N , 72°E) from December 1990 to February 1992. Slant column abundance of NO_2 thus observed is shown in Fig. 3.12. Sunrise and sunset values of NO_2 slant column are shown by solid and open circle respectively. These are monthly averaged values. In 1990, NO_2 slant column started decreasing after monsoon and decreases up to January 1991. Similar feature has also been observed in the next season, but the magnitude of decrease is less compared to previous year. It may be mentioned here that Mt. Pinatubo erupted in Philippines (15.4°N , 120.35°E) in June 1991. Slant column abundance of NO_2 in our site varies between 3×10^{16} and $1.2 \times 10^{17} \text{ cm}^{-2}$. A change in the slant column abundance of NO_2 after Pinatubo eruption could be possible since stratospheric temperature increased by about 4°K [Labitzke, 1992] after this event, and there are temperature dependent chemical reactions. At Lauder (45°S , 170°E) Johnston *et al.* [1992] have reported lower values of NO_2 twilight slant column (by about 30-45 %) after Pinatubo eruption. They propose that this decrease is due to heterogeneous reaction [Perliski and Solomon, 1992].

The slant column values of NO_2 shown in Fig. 3.12 have been converted into vertical column by the method described earlier. These values from January 1990 to February 1992 are plotted in Fig. 3.13. During cloudy and monsoon days (February 1990 to September 1990 and June 1991 to September 1991), observations were not taken. One can see from the figure that after September 1991, the values of NO_2 appear to be slightly higher than those obtained in the previous year during the corresponding months.

Perliski and Solomon [1992] show that volcanic aerosols can affect the ground-based visible absorption measurements in at least three ways. The first is the effective optical path or airmass factor which is likely to change due to the increased aerosol

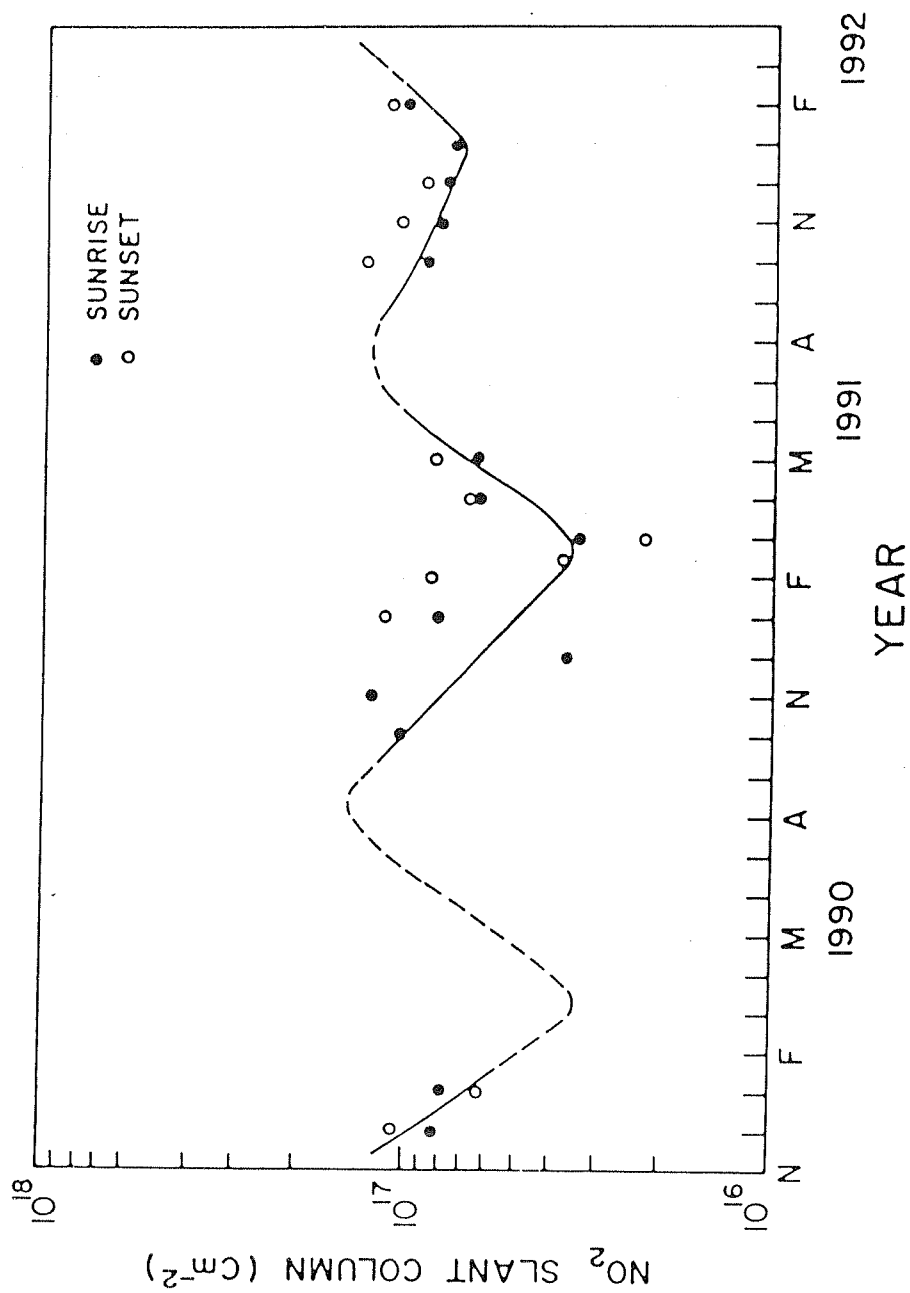


Figure 3.12 Plot of monthly averaged NO_2 slant column values since January 1990.

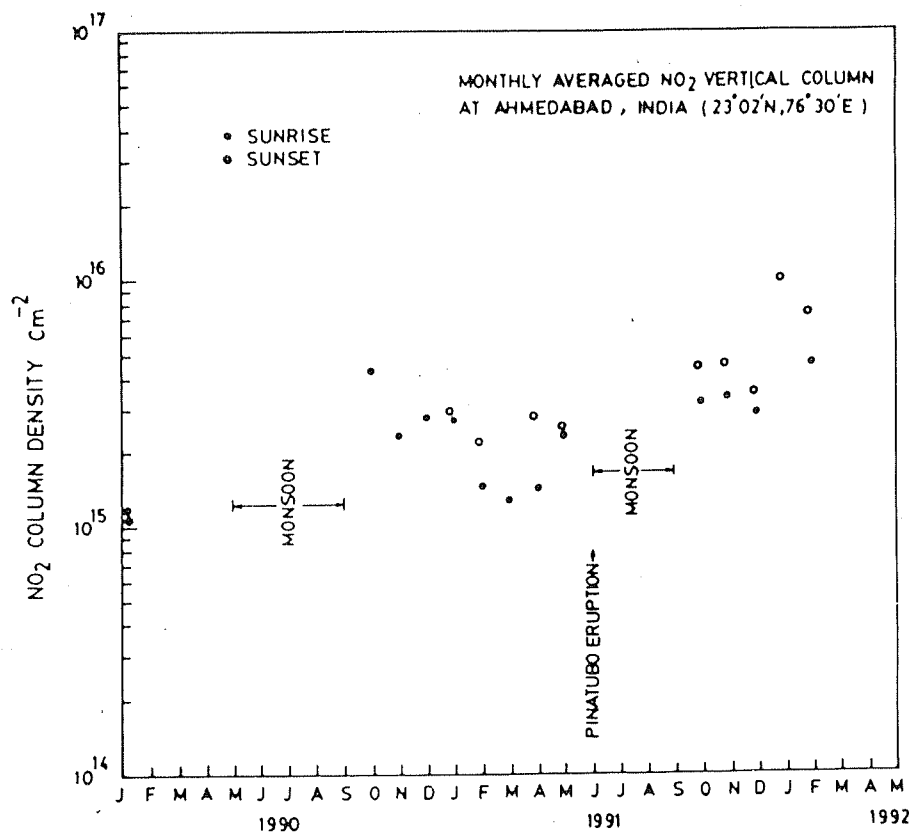


Figure 3.13 Plot of monthly averaged NO₂ vertical column values since January 1990.

scattering in the direction of observation. However, both *Johnston et al.* [1992] and *Perliski and Solomon* [1992] show that the change in the airmass factor is relatively insensitive to the presence of Pinatubo aerosols above about 20 km. The increased aerosol scattering could also increase the photolysis rate of atmospheric chemical species [*Michelangeli et al.*, 1989]. This is the second way in which volcanic aerosols could affect vertical NO_2 column abundance. An increased photolysis rate of NO_2 may change the partitioning between NO and NO_2 , resulting in a decrease in NO_2 column abundance. *Perliski and Solomon* [1992] show that the second way also does not have a significant effect on the total NO_2 column abundance after volcanic eruption. The third way in which volcanic aerosols could affect the vertical NO_2 column abundance is the heterogeneous chemical conversion of reactive nitrogen to nitric acid. This conversion is very fast on the surface of volcanic aerosols to cause significant local odd nitrogen depletion [*Hofmann and Solomon*, 1989]. Both *Johnston et al.* [1992] and *Perliski and Solomon* [1992] show that nearly all of the observed decrease in twilight NO_2 slant column abundance at Lauder after Pinatubo eruption is due to heterogeneous chemistry. *Hofmann and Solomon* [1989] also say that NO_2 depletion was much lower in middle latitude than in the tropics, in spite of greater aerosol loading there. However, we at tropics, do not find any decreasing trend in NO_2 after Pinatubo eruption even in slant column abundance. It may be mentioned here that aerosol correction exists in the present method of calculation of NO_2 .

Chapter 4

Results of NO_3 Measurements

4.1 Introduction

As mentioned earlier, the balance between ozone formation and destruction in the troposphere as well as stratosphere is largely dependent on the ambient concentrations of oxides of nitrogen, NO_x . In the NO_x group, NO , NO_2 and NO_3 are important major species. NO_3 plays the role of a buffer in the conversion of NO_2 to N_2O_5 . In the previous Chapter, results of our NO_2 measurements have been described. In this Chapter, the results of our NO_3 measurements are being presented. Experimental setup used for this measurement has been described earlier in Chapter 2. In Section 4.2 we have described the existing observational results of NO_3 . Section 4.3 deals with the methodology of the measurements. Theory has been described in Section 4.4. Results are given in Section 4.5. In the same section our results are compared with other available data. The errors that come in these measurements are given in Section 4.6.

4.2 Existing observations

Observations of stratospheric and tropospheric NO_3 using ground-based visible absorption spectroscopy began with the pioneering work of Noxon and his coworkers in the late 1970s [Noxon *et al.*, 1978a]. They used the property that NO_3 has strong absorption near 662 nm. In these measurements, sun or moon was employed as light source. The first observation of NO_3 was reported by Noxon *et al.* [1978a] who used a scanning spectrometer above the Fritz Peak Observatory (40°N) in April 1978. They reported its vertical column abundance to be $\sim 10^{14} \text{ cm}^{-2}$. Norton and Noxon [1986] studied NO_3 column abundance for 5 years at 40°N . They found seasonal variation minimum in the winter and maximum in the summer conditions. In addition, at 40°N , they also studied the effect of east-ward as well as west-ward winds. They also made observations at 19° (Mauna Loa), 31° (Continental USA), 51° (Canada), and 64°N (Alaska). According to them, NO_3 column abundance has a strong latitudinal variation. In this set of measurements NO_3 abundance varied from slightly greater than 10^{14} cm^{-2} to below the detection limit of 10^{13} cm^{-2} . Using the same spectral region, stratospheric NO_3 has been measured by several workers [Herman, 1979; Gelinas and Vajk, 1981; Naudet *et al.*, 1981; Rigaud *et al.*, 1983; Helten *et al.*, 1984; Solomon *et al.*, 1989a,b; Smith and Solomon, 1990]. Nighttime profiles at 44°N have been obtained from a balloon platform at 38.8 km in fall 1980, 1981, 1983 and in spring 1982 [Rigaud *et al.*, 1983; Pirre *et al.*, 1985] looking at the setting star Arcturus or at the rising planet Venus. Stratospheric NO_3 also has been studied during nighttime using balloon-borne technique by Naudet *et al.* [1981]. They made simultaneous nighttime observations of NO_3 and O_3 by means of a spectrophotometer pointing at the rising planet Venus from 43°N , France. In-situ diurnal variation at sunrise has been measured by Helten *et al.* [1984] using matrix isolation and electron spin resonance spectroscopy from a balloon platform at 32.7 km. They reported nighttime mixing

ratio to be 2×10^{-10} and about 30 minutes before sunrise the mixing ratio decreased to a value below 2×10^{-11} . These values tend to be about a factor of two larger than those obtained from visible spectroscopy [WMO, 1986]. WMO [1986] report has summarized all the NO_3 measurements prior to 1985. To verify the absorption spectrum of NO_3 near 662 nm, another spectral region can be used for NO_3 absorption in which NO_3 has maximum absorption near 623 nm. The spectral region used by Solomon *et al.* [1989a] for their study lies between 605 and 685 nm. This spectral region also contains water vapour absorption feature. To remove the interference of water vapour, Solomon *et al.* [1989a] have used a modified matrix inversion technique. They took observations at 40°N for all the seasons and made extensive studies of water vapour interference. They showed that NO_3 absorption feature has strong negative correlation with water vapour. Their NO_3 values lie in the range of $2 - 9 \times 10^{13} \text{ cm}^{-2}$.

Following the discovery of Antarctic ozone hole in 1985 [Farman *et al.*, 1985] and the recognition of the links between nitrogen and chlorine chemistry in the Antarctic ozone depletion phenomena, observation of nitrogen compounds in the polar region has become a subject of increased scientific importance. Sanders *et al.* [1987] reported the first measurements of NO_3 in the spring season from McMurdo station of the Antarctica (78°S). The basic technique used by this group is similar to that used by the Noxon group. Solomon *et al.* [1989b] later reported additional springtime NO_3 measurements in the Arctic and the Antarctic. Very recently Solomon *et al.* [1993] have measured NO_2 and NO_3 over McMurdo during fall, spring and winter in 1991.

During sunrise, photolysis rapidly reduces the NO_3 column abundance. Recently Smith and Solomon [1990] have experimentally studied NO_3 disappearance during dawn. Scattered solar flux coming from west horizon before sunrise period has been used as light source.

From the ground-based measurements one gets column density. It does not give density of NO_3 at different altitudes. To derive vertical distribution from the column density, *Smith and Solomon* [1990] have described a method. In this method they have used column density observations at different zenith angles.

Tropospheric NO_3 has been measured by many workers [*Noxon et al.*, 1980a; *Platt et al.*, 1980, 1981, 1984, 1990; *Noxon*, 1983; *Pitts et al.*, 1984; *Perner et al.*, 1985] by using moon or artificial lamp as a light source. Direct moon light observations can give the contribution of both stratospheric and tropospheric NO_3 . The long path absorption technique gives only tropospheric contribution. To extract the tropospheric contamination from moon light observation, direct moon light as well as long path absorption techniques have been used simultaneously by many workers. *Noxon et al.* [1980a] measured NO_3 in slightly polluted Colorado mountain. *Platt et al.* [1981] used artificial lamp as a source of light. They placed the lamp about a couple of kilometers away from the laboratory and measured the tropospheric NO_3 by using longpath absorption technique. *Noxon* [1983] studied the correlation between NO_2 and NO_3 in mid-pacific troposphere, and found positive correlation. Alongwith NO_3 , other nitrate radical concentrations in continental air have also been measured simultaneously by *Platt et al.* [1984] during nighttime. *Platt et al.* [1990] studied the formation of peroxy radicals by the reaction of NO_3 with organic compounds during night.

We have made a survey of existing measurements of NO_3 in the previous paragraphs. One can see that a large number of observations exists for the Antarctic region. A good number of observations are also available at mid latitude. Some observations are also available at the Arctic and high latitude zone. But only one or two good observations are available for low latitude region. Obviously, these observations are not sufficient to draw a clear picture of the global NO_3 variability. We

have, therefore, done some measurements of NO_3 at Ahmedabad (23°N , 72°E), a low latitude station. Since the observation site in Ahmedabad is near an urban area, tropospheric contamination could be possible in the stratospheric results. To assess the tropospheric contribution, NO_3 measurements have also been made over a hill station, Gurushikhar, near Ahmedabad, where the troposphere is very clean.

4.3 Methodology

The property that NO_3 has strong absorption around 662 nm has been used for the measurement of column density of this species in the present work. The basic technique adopted is the same as that given by *Noxon et al.* [1978a]. A spectral range has been scanned which extends from 655 to 667 nm. To verify the NO_3 absorption feature near 662 nm, another spectral region from 617 to 629 nm has also been used. During daytime, NO_3 values are low and below the detection limit of the instrument. Measurement has, therefore, been made at nighttime when NO_3 is about two orders of magnitude higher than the daytime value. Direct moon light has been used as source and observations have been taken near full moon period. The spectrum thus obtained contains absorptions by absorbing species. As the lunar zenith angle increases the atmospheric path covered by the lunar radiation increases. Because of this increase in the path length, there is an increase in the percentage of absorption by atmospheric species. This has been explained in the previous Chapter. The absorption due to NO_3 at 662 nm is of the order of few percent during night at lunar zenith angle $\sim 90^\circ$. For NO_3 derivation, we have, therefore, used the spectrum taken during nighttime at large ($> 85^\circ$) lunar zenith angle only (hereafter called as signal spectrum).

The signal spectrum contains absorption due to solar Fraunhofer component as well as absorption species. The contribution of solar Fraunhofer component is much larger than that of NO_3 . Therefore, it is necessary to remove the Fraunhofer

component from the signal spectrum. The signal spectrum also contains absorption structure by atmospheric water vapour, and scattering contributions due to aerosols as well as due to Rayleigh particles. These have to be removed.

The spectrum in which the contribution of NO_3 is negligible compared to the signal spectrum is called the control or background spectrum. During daytime NO_3 amounts are very low. Hence a daytime spectrum or a lunar spectrum for a low lunar zenith angle has been used as a control spectrum. The control spectrum also contains the Fraunhofer component. Hence, if a ratio of signal spectrum and control spectrum is taken, the Fraunhofer component will be removed from the signal spectrum. As discussed in Chapter 3, ratio spectrum reveals a smaller amount of residual Fraunhofer component. But, except for a single solar Balmer alpha feature near 657 nm, there is little solar Fraunhofer structure in the wavelength region used for NO_3 measurements. Also the Ring effect is not very significant for these measurements (as discussed, for example, by *Solomon et al.* [1987]). The ratio spectrum will, however, contain the contribution of water vapour. Water vapour airmass in the background spectrum will be the same as in the signal spectrum if taken at the same zenith angle. Since the observations have been taken at an urban area and over hill stations, corresponding background spectra have also been taken at these two stations. The components due to aerosols and Rayleigh scattering and water vapour in the ratio spectrum have to be removed. The way this has been done has been described later.

4.3.1 Conversion of slant column to vertical column

We have measured the slant column densities. These have been converted into vertical column density by dividing the slant column density by the airmass factor. Airmass factor is defined as the ratio of slant column to vertical column density. This conversion mechanism has been discussed in detail in the previous Chapter in Section 3.4.

In order to convert NO_3 slant column abundance to its vertical column abundance, calculation of airmass factor has been done by many workers [Norton and Noxon, 1986; Sanders *et al.*, 1987; Solomon *et al.*, 1989a,b, 1993; Smith *et al.*, 1993]. Norton and Noxon [1986] calculated both tropospheric and stratospheric airmass factors against lunar zenith angle by considering direct moon light measurements. Sanders *et al.* [1987] determined airmass factors appropriate to polar NO_3 measurements by considering ray geometry. They calculated stratospheric airmass factor for 40 km and tropospheric airmass factor by assuming a 5 km scale height. According to them, within the stratosphere the airmass factor for direct light observations from the ground are nearly independent of lunar zenith angle and tropospheric airmass factor increases almost exponentially above 80° lunar zenith angle. Solomon *et al.* [1989b] also did airmass factor calculation for direct light from geometric considerations. They found substantial differences in the tropospheric and stratospheric airmasses at large zenith angle. Solomon *et al.* [1993] converted slant column into vertical column by simply dividing by the stratospheric lunar airmass factor appropriate to the angle of observation after ensuring that the observed variation with lunar angle follows what is expected from geometrical considerations. More recently, Smith *et al.* [1993] have also used similar airmass factor as used by Solomon *et al.* [1993] for the derivation of vertical distribution of NO_3 over the polar region. The value of airmass factor used by us in the present study is similar to the airmass factor derived by Sanders *et al.* [1987].

4.3.2 Data reduction

Over the spectral range 655 to 667 nm and 617 to 629 nm, 8 forward and 8 reverse scans were taken. These were averaged to minimize the atmospheric scintillation effect. The average spectrum has been made to coincide at 656.3 nm (Balmer H_α line) to verify the wavelength calibration.

Fig. 4.1 (lower curve) shows the background direct solar spectrum at 81.2° solar zenith angle for 18 January 92 at 0800 hrs IST (Indian Standard Time) and the direct lunar spectrum (upper curve) at 84.3° lunar zenith angle for the same day at 0447 hrs IST. The signal modulation due to second and higher order spectrum has been removed by using a red cutoff filter. The solar spectrum appears to be smoother than the lunar spectrum. This is due to large signal to noise ratio in the solar spectrum. The dip at 656.3 nm H_α does not show variation from solar to the lunar spectra.

Fig. 4.2 shows a ratio spectrum in the 655 to 667 nm wavelength region. This ratio spectrum has been obtained by dividing the lunar spectrum obtained on 18 January 92 at 0447 hrs IST by the background solar spectrum obtained on the same day at 0800 hrs IST. Both the spectra have been taken under the same sky conditions. Modulation in the signal due to any local effect has been removed by taking the ratio of these two spectra. In the ratio spectrum, Balmer H_α line is clearly seen at 656.3 nm. Before taking the ratio of the two spectra, alignment has been done in such a way that the Balmer H_α line of the lunar spectrum coincides with that of the background solar spectrum.

The ratio spectrum shown in Fig. 4.2 has components due to aerosol and Rayleigh scattering, ozone and water vapour. To remove the component due to atmospheric aerosol and Rayleigh scattering, the spectrum shown in Fig. 4.2 has been subtracted from a straight line parallel to the slope of the ratio spectrum. It is known that the Rayleigh scattering coefficient and aerosol scattering coefficient are proportional to λ^{-4} and λ^{-1} respectively. For the ideal mid latitude atmosphere, at 660 nm, aerosol optical depth is 0.35, Rayleigh optical depth is 0.04 and the total optical depth is 0.40 [Elterman, 1968]. Thus, 90% contribution of scattering in this wavelength region is due to aerosols. The optical thickness of Rayleigh atmosphere

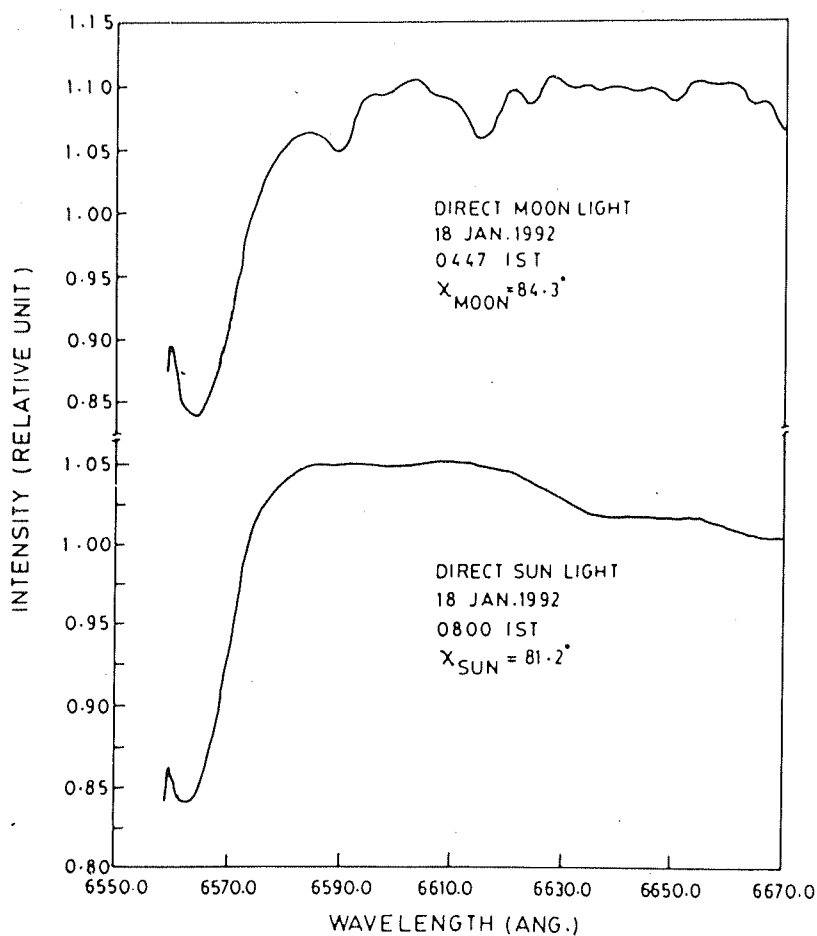


Figure 4.1 Direct solar spectrum at 81.2° solar zenith angle taken at 0800 hrs (lower curve) and direct lunar spectrum at 84.3° lunar zenith angle taken at 0447 hrs (upper curve) on January 18, 1992.

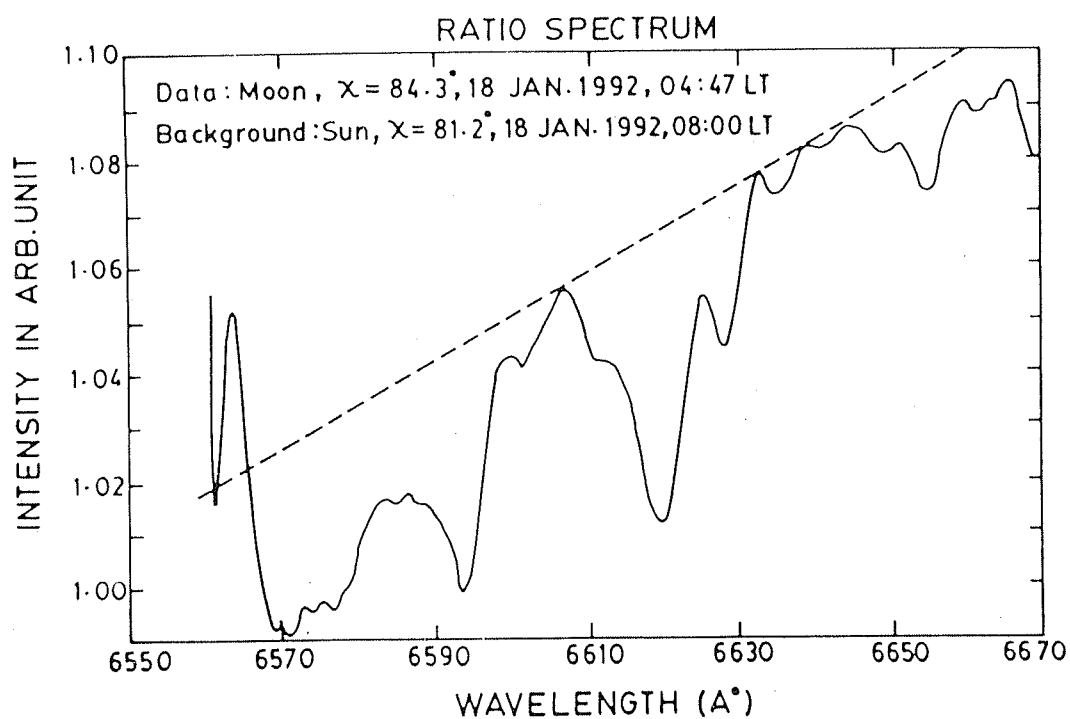


Figure 4.2 Ratio of two spectra shown in Figure 4.1.

does not vary appreciably with latitude because it is a function of the condition of the stratosphere which is relatively calm from pole to the equator. On the other hand, the aerosol contribution in the atmosphere is highly dependent on the local perturbation. Hence, optical thickness at our location will be different from that at the mid-latitude as given by *Elterman* [1968]. Besides, ozone absorption coefficient also has linear wavelength dependence in this region. Therefore, by subtracting the ratio spectrum from a straight line parallel to the slope of the ratio spectrum, aerosols scattering, Rayleigh scattering and attenuation due to ozone can be considered to have been removed from the ratio spectrum.

The residual absorption spectrum thus obtained after removing the contribution of aerosols and molecular scattering, and absorption due to ozone is shown in Fig. 4.3. This residual absorption spectrum contains absorption due to NO_3 and water vapour. NO_3 has maximum absorption at 662 nm which can be clearly seen in the residual spectrum as a prominent dip. Water vapour has absorption near 659 nm which is seen as a dip less pronounced compared to NO_3 absorption at 662 nm. Besides these absorption features, the Balmer alpha feature is also seen in the residual absorption spectrum at 656.3 nm.

To verify the absorption feature of NO_3 , observations were also taken in the 617 to 629 nm region, in which NO_3 has a strong absorption at 623 nm. Fig. 4.4 shows two linear spectra taken on 19 January 1992 at 1941 hrs IST and on 21 January 1992 at 2104 hrs IST in the 617-629 nm region. Fig. 4.5 shows the ratio of these two spectra. As in Fig. 4.2, a slope is observed in the ratio spectrum. This slope is due to Rayleigh and aerosol scattering. The effect of scattering is removed by subtracting the ratio spectrum from a straight line parallel to the slope of the ratio spectrum. The residual absorption spectrum thus obtained is shown in Fig. 4.6. In this spectrum, NO_3 has a strong absorption at 623 nm which can be clearly seen as

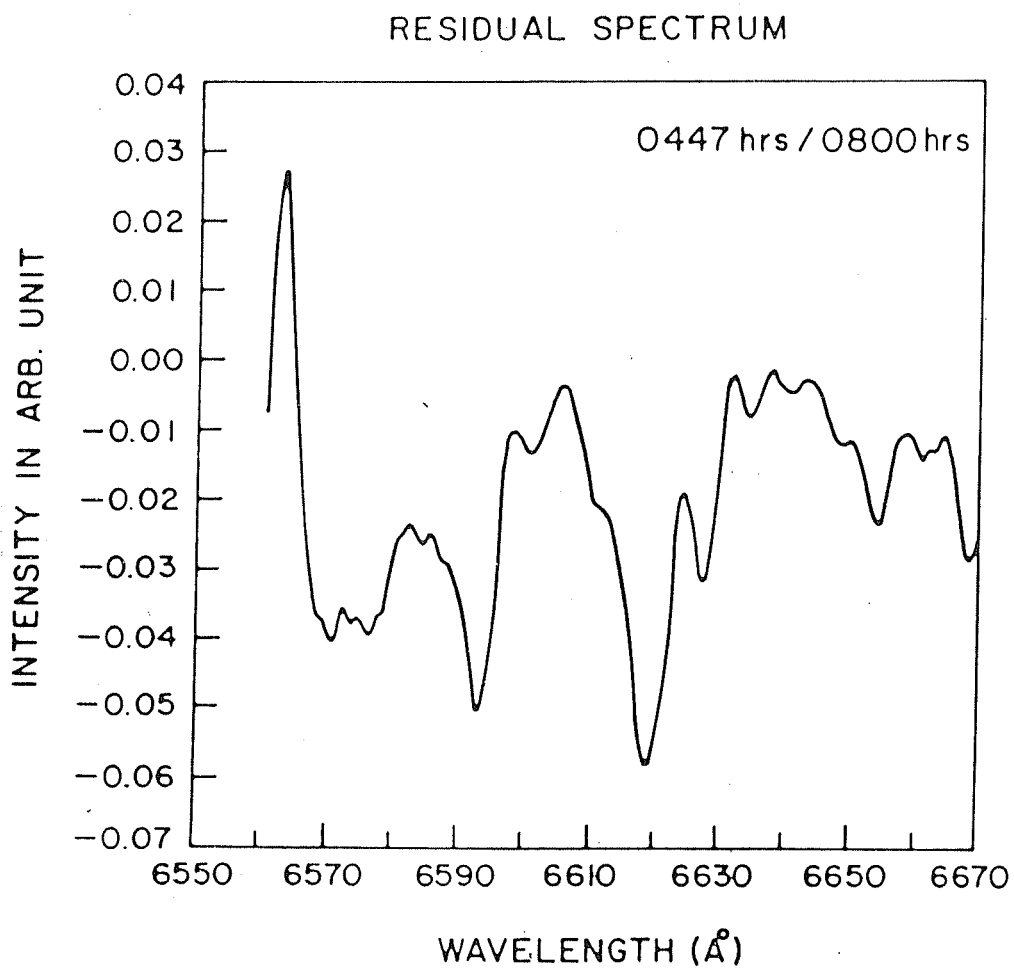


Figure 4.3 Ratio of two spectra shown in Figure 4.1 after removing the contribution of aerosols and molecular scattering.

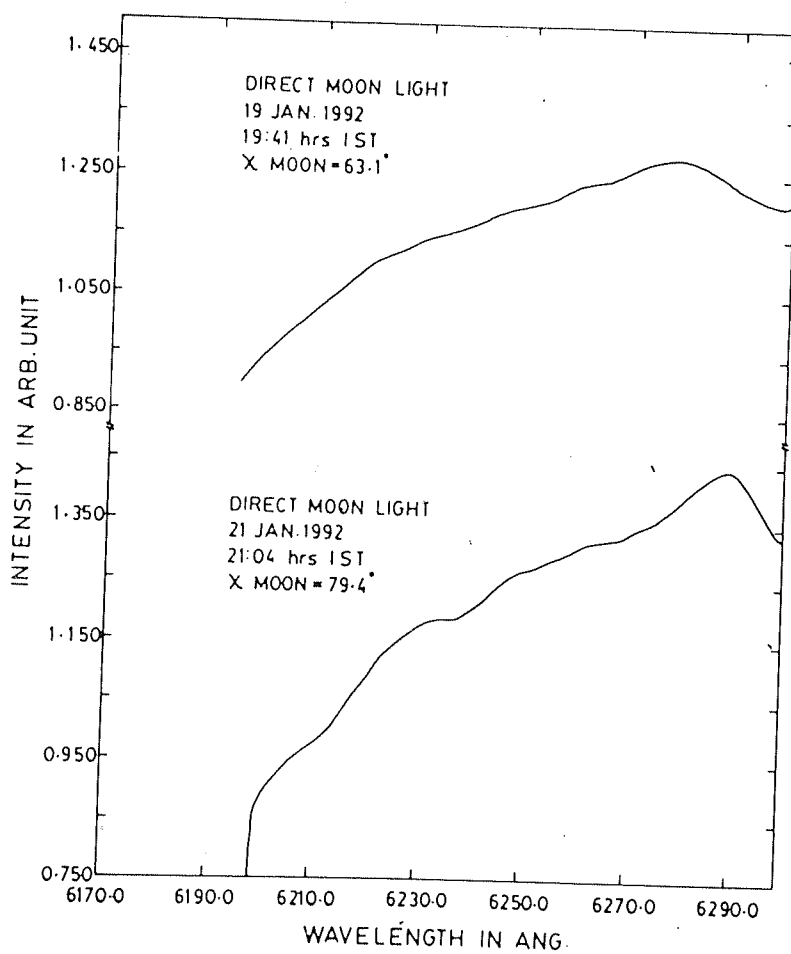


Figure 4.4 Two direct lunar spectra in the 619 to 629 nm region.

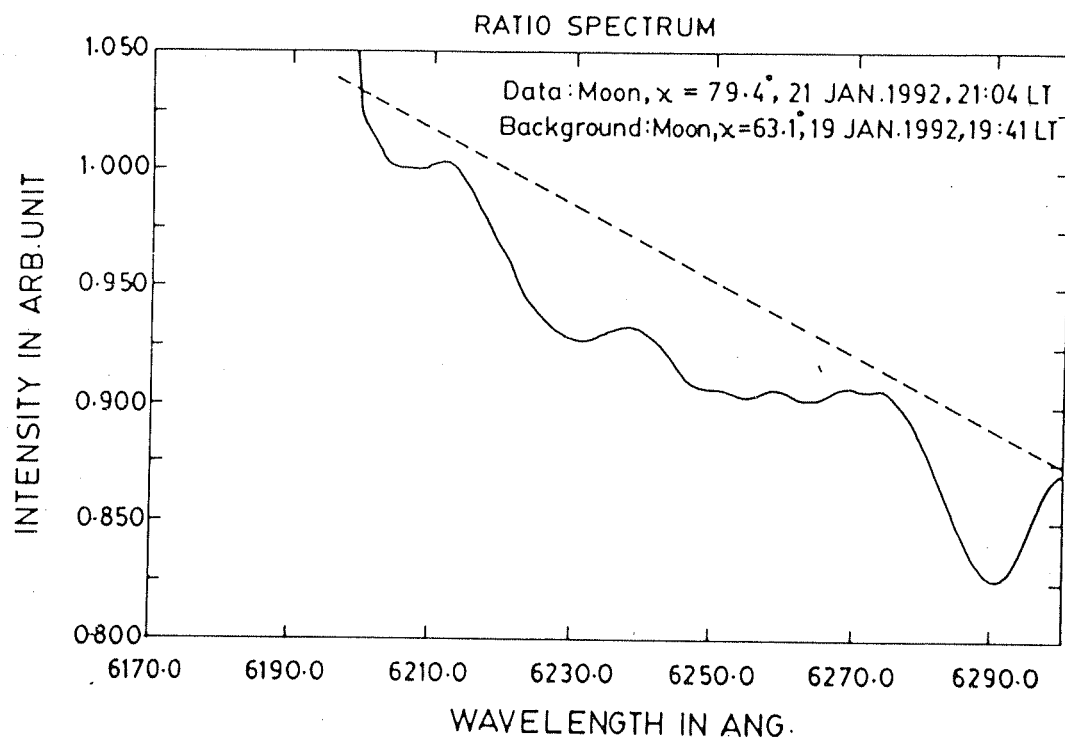


Figure 4.5 Ratio of two spectra shown in Figure 4.4.

a broad absorption dip.

Fig. 4.7 shows the ratio of two consecutive spectra taken at 0441 hrs IST and 0447 hrs IST on 18 January 92. These two spectra were taken at as close an interval of time as possible. The variation in airmass factor during this time interval is small, but, not all together negligible. Nevertheless, a lower limit of the system noise is revealed in the ratio spectrum. This ratio spectrum shows a sharp decrease with increase in wavelength up to 656.0 nm after which some small fluctuations are seen. These fluctuations are of about 0.1% from the mean value. Fluctuations in the wavelength region 658 nm to 663 nm is small compared to those in the 663 to 667 nm region. Few more consecutive spectra were taken and their corresponding ratio spectra have been calculated. All the ratio spectra were found to be nearly identical.

Spectrum in the wavelength region 655 to 667 nm contains the absorption due to water vapour and NO_3 . During daytime, the abundance of NO_3 is very small. Therefore, the ratio of two daytime spectra will give the differential absorption cross-section of water vapour. The differential absorption cross-section of water vapour thus obtained by taking the ratio of two direct solar spectra observed at 0721 hrs IST, 88.2° SZA and 0800 hrs IST, 80° SZA on 18 January 92 is shown in Fig. 4.8. Similar differential absorption cross-section in arbitrary unit has been reported by *Solomon et al.* [1989a] for July 2, 1984 from 640 to 680 nm region and our observed cross-section appears to agree with this. To verify the atmospheric water vapour cross-section, laboratory cross-section of water vapour was also measured at NASA Ames Research Center. This has been done using a 25 m white cell at NASA Ames Research Center, capable of achieving multiple pass path length as large as 5 Km. Water vapour was introduced directly into the cell, and the absorption spectrum was recorded. Attempt to measure the differential absorption cross-sections of water vapour in the spectral region of our interest was also made in our laboratory using a water vapour cell.

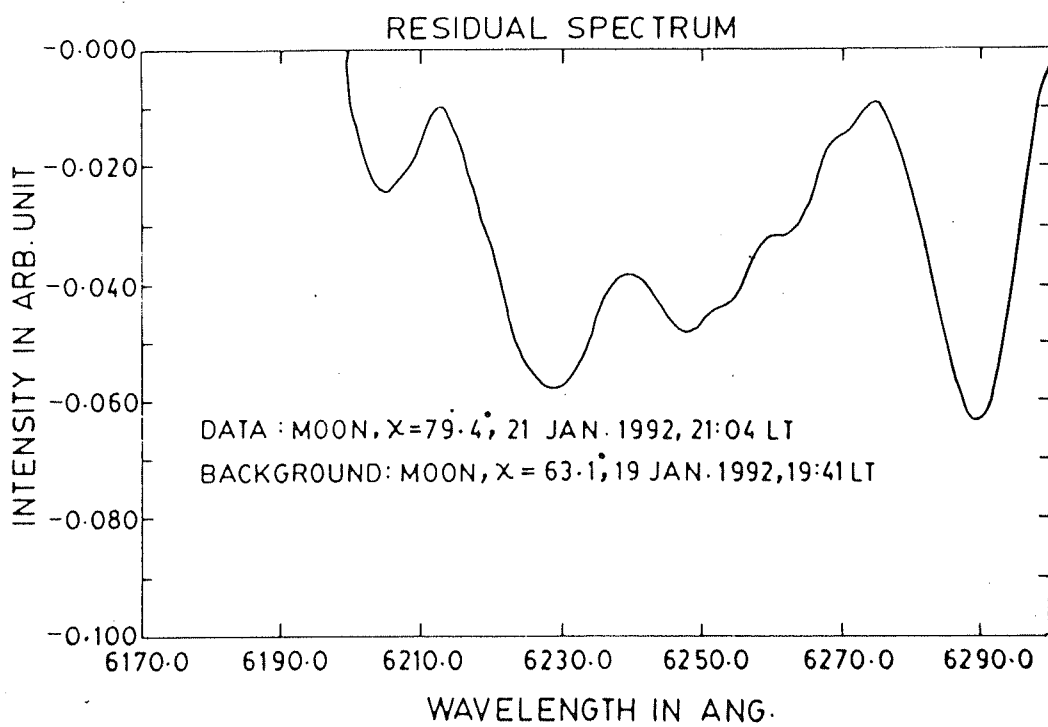


Figure 4.6 Ratio of two spectra shown in Figure 4.4 after removing the contribution of aerosols and molecular scattering.

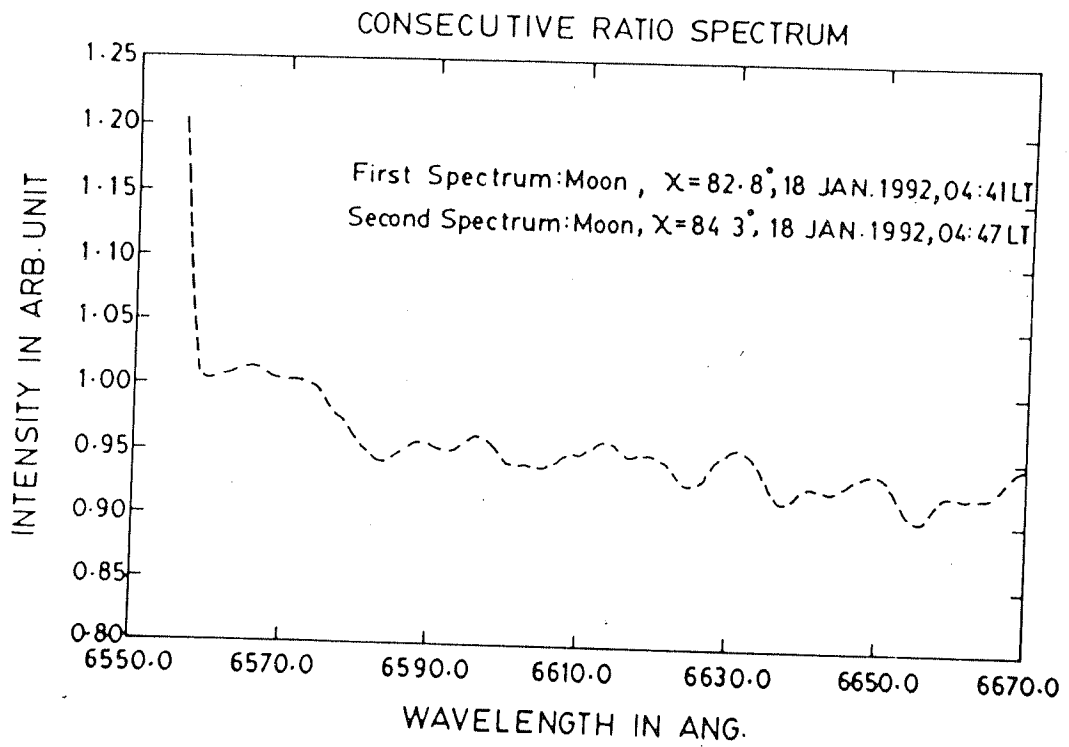


Figure 4.7 Ratio of two consecutive lunar spectra taken at 0441 hrs and 0447 hrs on January 18, 1992.

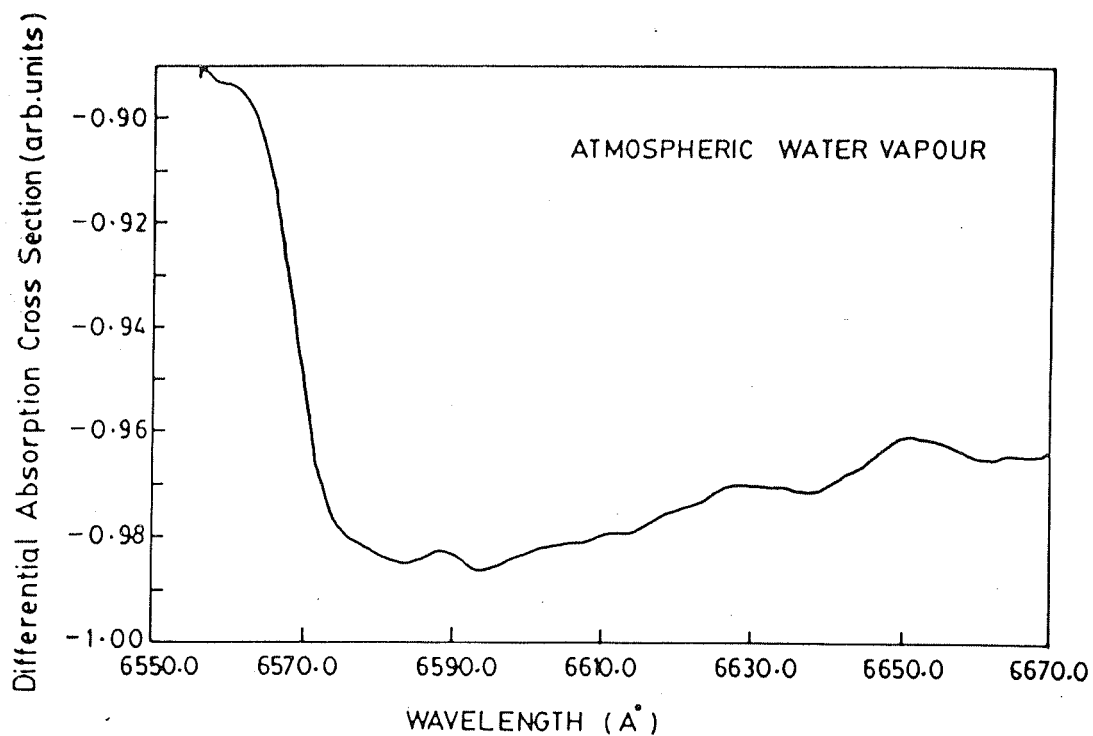


Figure 4.8 Ratio of solar spectra taken at 0724 hrs and 1345 hrs on January 22, 1992. This also represents the differential absorption cross-section of water vapour in arbitrary unit.

However, due to the fine condensation of water vapour which occurred inside the cell while taking the observations, the results were not found to be accurate. To remove the contribution of water vapour from our observed ratio spectrum shown in Fig. 4.2, we have divided this spectrum by the differential absorption cross-section spectrum observed by us shown in Fig. 4.8. Finally, we have calculated the values of NO₃ from this ratio spectrum by the matrix inversion method.

4.4 Theory

The intensity of solar radiation reaching the earth's surface basically follows Beer's law, wherein the attenuation of monochromatic radiation is related to the number of absorbing molecules in the path, so that

$$I = I_o.exp[-\sigma.N.dx] \quad (4.1)$$

where, I is the measured flux on the earth's surface, I_o is the background solar flux, σ is the absorption cross-sections of the absorbing species, N is the number density of the absorbing species and dx is the optical path length covered by the lunar/solar radiation. dx can be converted into a geometrical factor which relates the slant path length covered by the solar radiation to the geometrical thickness of the atmosphere. Thus, dx can be represented as

$$dx = L.dz \quad (4.2)$$

where L is the enhancement factor and dz is the vertical thickness of the optical path. Then the above equation can be represented as :

$$\begin{aligned} I &= I_o.exp[-\sigma.N.L.dz] \\ &= I_o.exp[-\sigma.\int_z^{\infty} N_z.L_z.dz] \end{aligned} \quad (4.3)$$

where, $\int_z^\infty N_z \cdot L_z \cdot dz$ is slant column abundance of NO_3 .

To derive the slant column density of NO_3 from the absorption spectra, so far two main techniques have been used. In the following section, we have given a brief description of these two techniques.

4.4.1 Differential absorption technique

Differential absorption technique for NO_3 measurement was described by Noxon as early as 1975 [Noxon, 1975]. In this technique, only maximum and minimum absorption points are used for the derivation of total column abundance. If δ_1 is the absorption cross - section of NO_3 at 659 nm, δ_2 is the absorption cross -section of NO_3 at 662 nm, X is the coordinate for minimum absorption, and Y is the coordinate for maximum absorption, then the differential NO_3 absorption A(%) is given by

$$\begin{aligned} A &= (1 - \exp[-(\delta_2 - \delta_1) \cdot N_{\text{NO}_3}]) \cdot 100\% \\ &= \left[\frac{(X - Y)}{X} \right] \cdot 100\% \end{aligned} \quad (4.4)$$

where N_{NO_3} is its column density. Since all the parameters except N_{NO_3} are known in eqn. 4.4. N_{NO_3} can be calculated. This simple procedure to calculate N_{NO_3} assumes that there is no interference of any other species of the atmosphere.

4.4.2 Matrix inversion technique

To derive the NO_3 slant column abundance matrix inversion technique is the second method. This has been introduced recently and has been used by several workers [Sanders et al., 1987; Solomon et al., 1989a,b, 1993]. The theory of this technique is given below :

Let I_i be the intensity of solar / lunar radiation reaching the ground at wavelength λ_i , where $i = 1, 2, 3, \dots$, then according to Lambert-Beer's law we have,

$$I_i = I_{oi} \cdot \exp[-\sigma_{NO_3} \cdot N_{NO_3} \cdot dx - \sigma_{H_2O} \cdot N_{H_2O} \cdot dx] \quad (4.5)$$

where, I_{oi} is intensity outside the atmosphere at wavelength λ_i , σ_{NO_3} and σ_{H_2O} are absorption cross-sections of NO_3 and H_2O at wavelength λ_i , N_{NO_3} and N_{H_2O} are column densities of NO_3 and H_2O respectively, and dx is slant path length traversed. As mentioned earlier we measure the background solar flux and the signal solar flux. We take the ratio of these two fluxes. This will eliminate Fraunhofer components as well as I_{oi} in the signal spectra. This ratio spectra is given by :

$$\begin{aligned} R_I &= \exp[-\sigma_{NO_3} \cdot N_{NO_3} \cdot (\Delta X_L - \Delta X_S) - \sigma_{H_2O} \cdot N_{H_2O} \cdot (\Delta X_L - \Delta X_S)] \\ &= \exp[-\sigma_{NO_3} \cdot N_{NO_3} \cdot \Delta'X - \sigma_{H_2O} \cdot N_{H_2O} \cdot \Delta'X] \end{aligned} \quad (4.6)$$

where ΔX_L , ΔX_S are path lengths in the signal spectrum and background spectrum respectively and $\Delta'X = \Delta X_L - \Delta X_S$. Now if we take the ratio of every two adjacent wavelengths, we will have

$$R'_{jj} = \frac{R_I}{R_{I+1}} = \frac{\exp[-\sigma_{NO_3} \cdot N_{NO_3} \cdot \Delta'X - \sigma_{H_2O} \cdot N_{H_2O} \cdot \Delta'X]}{\exp[-\sigma_{NO_3} \cdot N_{NO_3} \cdot \Delta'X - \sigma_{H_2O} \cdot N_{H_2O} \cdot \Delta'X]} \quad (4.7)$$

where, $jj = 1, 2, 3, \dots, 1108$. jj will have 1108 values because we have digitized 120 Å wavelength range at an interval of 0.1 Å and we have taken a running mean of 25 points. Let, $(\sigma_{NO_3} - \sigma_{NO_3+1}) = \sigma'_{NO_3jj}$; $(\sigma_{H_2O} - \sigma_{H_2O+1}) = \sigma'_{H_2Ojj}$, $N_{NO_3} \cdot \Delta'X = N'_{NO_3}$ = slant column abundance of NO_3 and $N_{H_2O} \cdot \Delta'X = N'_{H_2O}$ = slant column abundance of H_2O . Then eqn. 4.7 becomes :

$$R'_{jj} = \exp[-N'_{NO_3} \cdot \sigma'_{NO_3jj} - N'_{H_2O} \cdot \sigma'_{H_2Ojj}] \quad (4.8)$$

$$\ln(R'_{jj}) = [-N'_{NO_3} \cdot \sigma'_{NO_3jj} - N'_{H_2O} \cdot \sigma'_{H_2Ojj}]$$

$$\text{or,} \quad R_{jj} = -N'_{NO_3} \cdot \sigma'_{NO_3jj} - N'_{H_2O} \cdot \sigma'_{H_2Ojj} \quad (4.9)$$

where $R_{jj} = \ln(R'_{jj})$. In equation (4.9), σ'_{NO_3jj} and σ'_{H_2Ojj} are known. Thus, computing R_{jj} for $jj = 1, 2, 3, \dots, 1108$ from observational data, the values of N'_{NO_3} and N'_{H_2O} can be calculated. These 1108 simultaneous equations can be arranged in the form of a matrix as follows :

$$[-N'_{NO_3} - N'_{H_2O}] \cdot \begin{pmatrix} \sigma'_{NO_31} & \sigma'_{NO_32} & \dots & \sigma'_{NO_31108} \\ \sigma'_{H_2O1} & \sigma'_{H_2O2} & \dots & \sigma'_{H_2O1108} \end{pmatrix} = [R_1 \ R_2 \ \dots \ R_{1108}] \quad (4.10)$$

The above matrices can be represented in the form :

$$A.B = R \quad (4.11)$$

To make B as a square matrix, we multiply both sides of eqn. 4.11 by the transpose of B. Then we take the inverse of this square matrix for finding the value of A. These steps are as follows :

$$A.B.B' = R.B' \quad (4.12)$$

$$\text{or,} \quad (A.B.B').(B.B')^{-1} = R.B'.(B.B')^{-1}$$

$$\text{or,} \quad AI = R.B'.(B.B')^{-1} \quad (4.13)$$

The elements of matrix $R.B'.(B.B')^{-1}$ are the values of N'_{NO_3} and N'_{H_2O} .

4.4.3 Absorption cross section

That NO_3 absorbs light between 670 and 400 nm in a banded absorption was first observed by *Jones and Wulf* [1937]. This was later studied at higher resolution by *Ramsey* [1962]. The studies of *Graham and Johnston* [1978] and *Mitchell et al.* [1980] do not rely on a calculation of the NO_3 concentration to determine its absorption cross section and agree well on the integrated strength of the 662 nm band. However, the maximum absorption cross section derived by the later group is lower by about

40%. *Marinelli et al.* [1982] undertook the most detailed investigation of the band positions and line shapes of NO_3 , but the maximum absorption cross section at 662 nm and the total integrated intensity of the 662 nm band are both about 12% lower than the values derived by *Graham and Johnston* [1978]. On the other hand, in their determination of the yields of O and NO from NO_3 photolysis, *Magnotta and Johnston* [1980] derived cross sections 30 - 40% larger than those obtained by *Graham and Johnston*. *Ravishankara and Wine* [1983] generated NO_3 in a discharge flow tube and monitored the absorption with a tunable dye laser. *Cox et al.* [1984] generated NO_3 by modulated photolysis and recorded the entire spectrum of NO_3 simultaneously using an optical multichannel analyzer. However, these two later studies differ by at least 10% over the whole range. According to *Burrows et al.* [1985], although agreement existed on the positions of the absorption features in the above works, estimates of the absolute magnitude of the cross section varied by upto a factor of about 2. *Burrows et al.* [1985] measured 615 to 670 nm spectrum of NO_3 and found values close to the values of *Graham and Johnston* [1978], but are slightly larger than those of *Ravishankara and Wine* [1983]. *Ravishankara and Mauldin* [1986] and *Sander* [1986] measured the absolute cross sections of NO_3 as a function of temperature. *Sander* [1986] reported values for the 662 nm feature as 2.69×10^{-17} and $2.28 \times 10^{-17} \text{ cm}^2$ at 230 and 298 K, while *Ravishankara and Mauldin* [1986] obtained 2.31×10^{-17} and $1.90 \times 10^{-17} \text{ cm}^2$ at 240 and 298 K, respectively. *Cantrell et al.* [1987] reported a cross-section of about $2.0 \times 10^{-17} \text{ cm}^2$, independent of temperature. In this study, the absorption cross section of NO_3 has been taken from *Ravishankara and Mauldin* [1986].

4.5 Results and discussion

We have taken observations from February 25 to March 3, 1991, December 19 to 23, 1991 and January 17 to 23, 1992 near the full moon days during presunrise and postsunset periods. Background spectrum has been taken at lowest possible lunar zenith angle. Background spectrum has also been taken during daytime, using direct sun as light source. Measurements have been taken at Ahmedabad, an urban area and at Gurushikhar, a hill station. The results obtained are discussed below.

4.5.1 Results of Ahmedabad

Fig. 4.9a shows slant column abundance of NO_3 versus lunar zenith angle observed on different nights in February and March 1991. Slant column values actually correspond to the difference between higher airmass value (HAM) and lower airmass value (LAM). Stratospheric and tropospheric airmass factors as calculated by *Sanders et. al.* [1987] are also shown in Fig. 4.9a. These airmass factors have been calculated by assuming 5 Km scale height of NO_3 . The trends of observed NO_3 slant column abundance and airmass factors show that NO_3 at our location is neither fully stratospheric nor fully tropospheric. This is in agreement with the measurements made at Thule (76.5°N) during February 1988.

The slant column abundances shown in Fig. 4.9a have been converted into vertical column abundances by dividing them by the appropriate airmass factors. The vertical column abundance thus obtained are shown in Fig. 4.9b. It is to be noted from this figure that after sunset NO_3 increases rapidly for about two hours. This variation is in the agreement with the results reported by *Norton and Noxon* [1986]. Our measured values of NO_3 lie between 1 and $5 \times 10^{14} \text{ cm}^{-2}$. *Norton and Noxon* [1986] have taken NO_3 observations at different latitudes in the northern hemisphere. Their

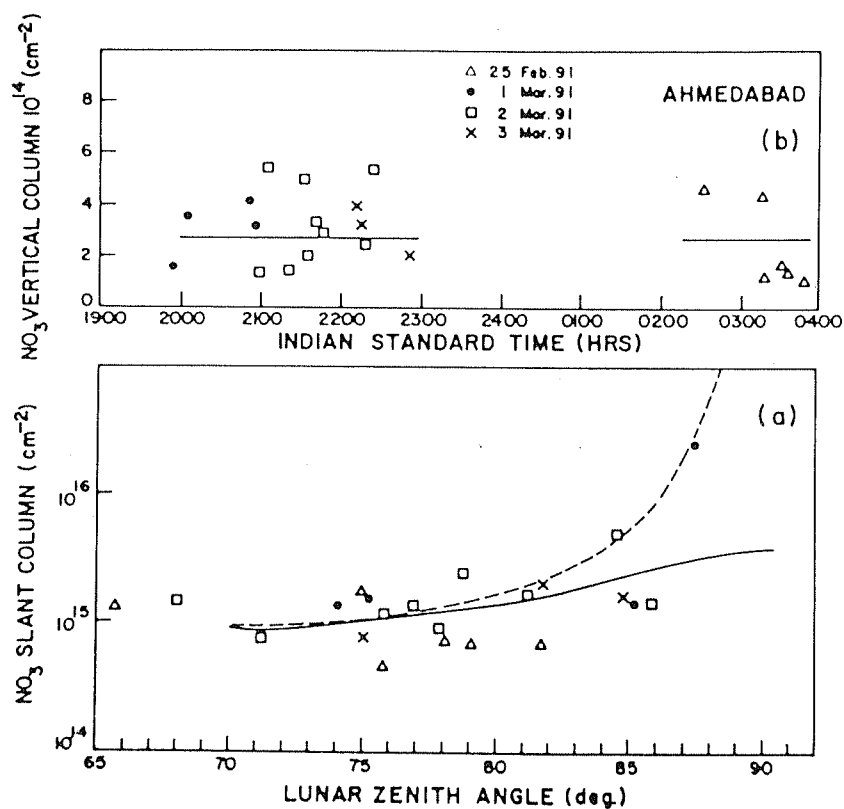


Figure 4.9 (a) Slant column abundance (lower panel) and
(b) Vertical column abundance (upper panel) of NO_3 for
February - March 1991 over Ahmedabad.

results nearest to our latitude, 19°N (Mauna Loa), show that our values are by a factor of about 10 larger than those reported by them. Even the lower value given in our work is twice the maximum value given by *Solomon et al.* [1989a]. An explanation could be that tropospheric NO₃ has affected our measurements. Both *Norton and Noxon* [1986] and *Solomon et al.* [1989a] have taken observations for a clean atmosphere, where contribution of tropospheric NO₃ is minimum. Our place of observation, on the other hand, is close to an urban area and hence our measurements might be affected by the tropospheric NO₃. If 90% of the NO₃ was in the troposphere, then its behaviour as a function of lunar zenith angle (LZA) should have been purely tropospheric. However, such a behaviour is not seen in Fig. 4.9a. Moreover, at tropospheric temperature, NO₃ increases throughout the night and the highest amounts of NO₃ are found in the morning. Such a behaviour is not seen in Fig. 4.9b. There the NO₃ reaches quickly the highest column density after sunset and the morning values are about the same and the behaviour is exactly what is expected for the stratosphere. It is therefore, argued on the basis of Fig. 4.9a and Fig. 4.9b that our measurements have stratospheric and tropospheric contributions. This argument, however, has to be taken with a little caution. Tropospheric contribution to our NO₃ measurements can be unambiguously ascertained if we have several measurements at or near 90° LZA. At this value of LZA, however, the signal to noise ratio becomes very weak at Ahmedabad due to the presence of dust particles and haze in the lower atmosphere. The highest value of LZA for which we have got only one observation is 87°.

Fig. 4.10 shows another set of observations taken at Ahmedabad during December of 1991. In this figure, bottom panel shows the slant column abundance and the top panel shows the vertical column abundance. A comparison of Fig. 4.10 with Fig. 4.9a shows that the trend of variability of NO₃ in December 1991 is identical to that in February and March 1991. However, December NO₃ values are higher than the February -March values by a factor whose average value is about 2. Another

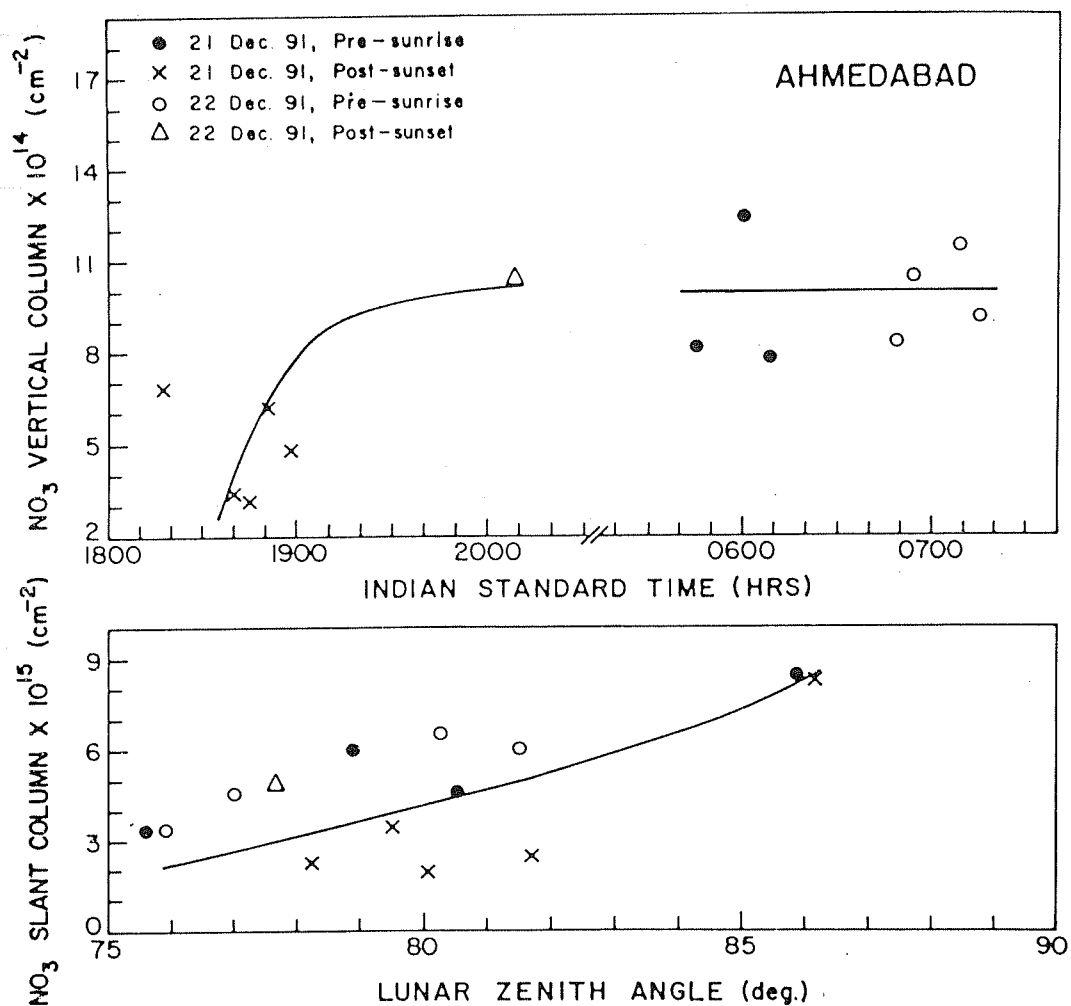


Figure 4.10 Slant column abundance of NO₃ (lower panel) for December 1991 and vertical column abundance of NO₃ (upper panel) for December 1991 over Ahmedabad.

interesting point to be noticed in Fig. 4.10 at the top panel is that in about 2 hours after sunset, NO_3 column attains a maximum value.

During daytime, the abundance of NO_3 is very low (about two orders of magnitude less than that at nighttime). This behaviour of NO_3 has been considered by many [Solomon *et al.*, 1989a] to use the solar spectrum as the background spectrum. Fig. 4.11 shows a set of NO_3 values measured in the month of January 1992 at Ahmedabad in which solar spectrum has been used as a background spectrum. This background spectrum was taken on 18 January 1992 during daytime at 80° solar zenith angle. In this figure, bottom panel shows the slant column abundance and the top panel shows the vertical column abundance. The trend of slant column variability of NO_3 in Fig. 4.11 and Fig. 4.10 appears to be the same. The value of vertical NO_3 column in Fig. 4.11 is in the range of 1.9 to $2.5 \times 10^{15} \text{ cm}^{-2}$. These values are higher than the December 1991 values (of Fig. 4.10) by a factor of about 2. December 91 and January 92 values should not differ by such a large factor. This is attributed to the different background spectra taken for the derivation of NO_3 for December and January months. The signal to noise ratio in the solar spectrum is much higher than that in the lunar spectrum.

4.5.2 Results of Gurushikhar

In order to check if our NO_3 measurements over Ahmedabad were affected by tropospheric contamination, we took our instrumental setup to Gurushikhar, a hill station about 200 km north of Ahmedabad and 1.8 km above the mean sea level. The atmosphere at Gurushikhar is absolutely clean. We intended to take observations in the months of November 1992, December 1992 and January 1993 for a few nights near the fullmoon time. Due to cloudy atmosphere and strong wind, observations could

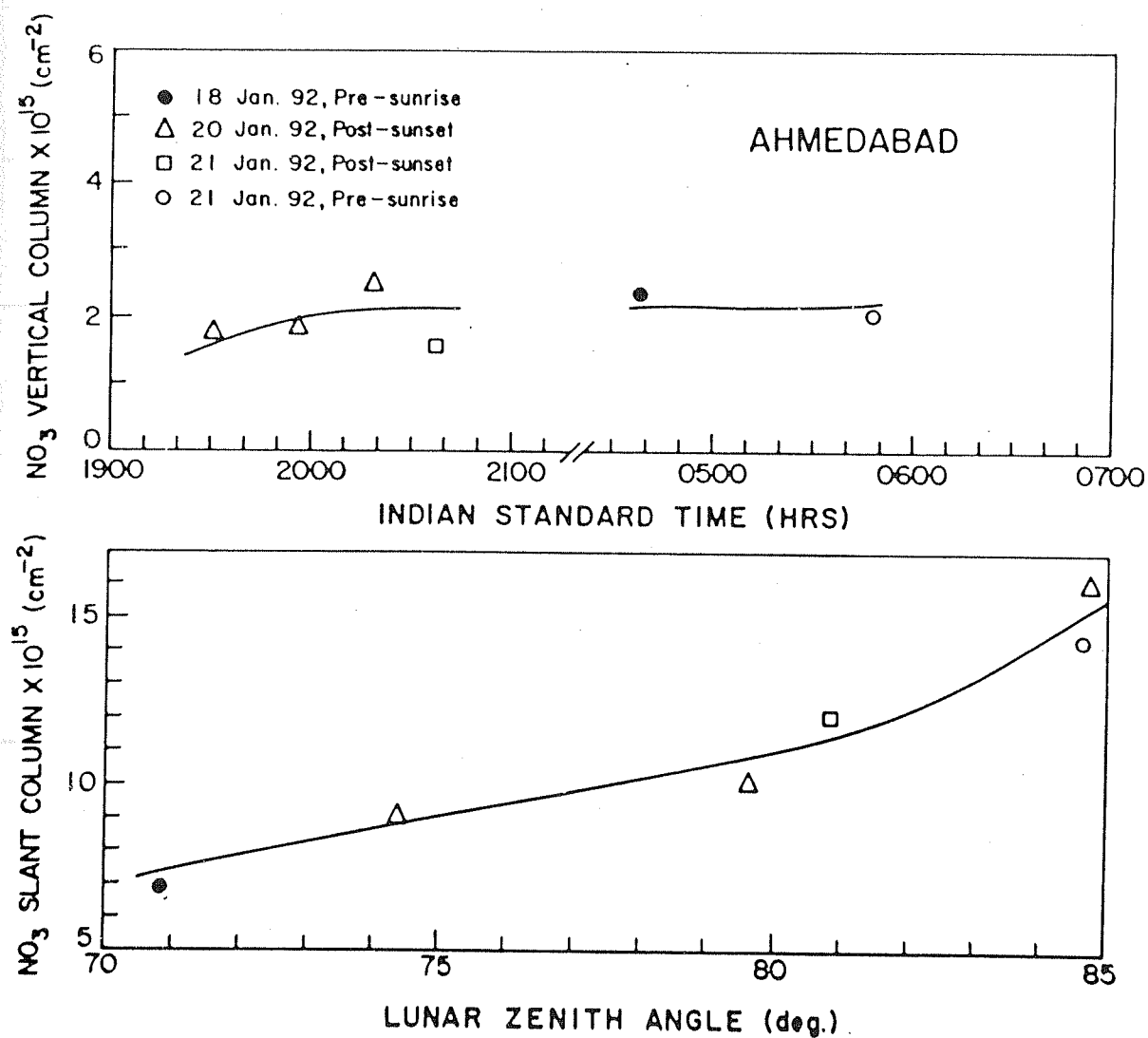


Figure 4.11 Slant column abundance of NO₃ (lower panel) for January 1992 and vertical column abundance of NO₃ (upper panel) for January 1992 over Ahmedabad.

not be taken in December 1992 and January 1993 months. The tropospheric contamination being negligible, we could take observations at Gurushikhar upto about 90° lunar zenith angle. In Fig. 4.12 we have shown a plot of NO_3 values of Gurushikhar against lunar zenith angle. In this figure the bottom panel shows the slant column and the top panel shows the vertical column abundance. The variability of slant column at Gurushikhar appears to be nearly the same as what has been observed at Ahmedabad. For Gurushikhar, we have taken the solar spectrum of November 22, 1992 as the background spectrum corresponding to 80° solar zenith angle. Gurushikhar values do not differ significantly from the Ahmedabad values of February, March, but are lower than the values obtained in the month of December 1991 and January 1992.

4.5.3 Sunrisetime variation of NO_3 over Gurushikhar

As soon as the sun appears over the horizon, NO_3 starts getting dissociated. Sunrisetime variation of NO_3 has been studied over Gurushikhar where the effect of tropospheric pollution is negligible. For that purpose, scattered light coming from the west horizon, opposite to the sun, has been measured. Measurements have been made between 0° and 8° solar depression angle during dawn from 655 and 667 nm. Slant column abundances obtained at different solar depression angles are shown in Fig. 4.13. These observations have been taken on two days in November and December 1992. From this figure it appears that total column abundance remains constant between 8° and 5° solar depression angle at a value of about $4 \times 10^{15} \text{ cm}^{-2}$. At 5° solar depression angle, earth's atmosphere at and above 30 km is illuminated by solar flux. After 5° as the solar depression angle decreases, NO_3 starts getting dissociated and the total column abundance of NO_3 starts decreasing. This decrease in NO_3 total column continues upto about 0° solar depression angle and becomes about $4 \times 10^{14} \text{ cm}^{-2}$. After sunrise as the solar zenith angle further decreases from 90° , the signal

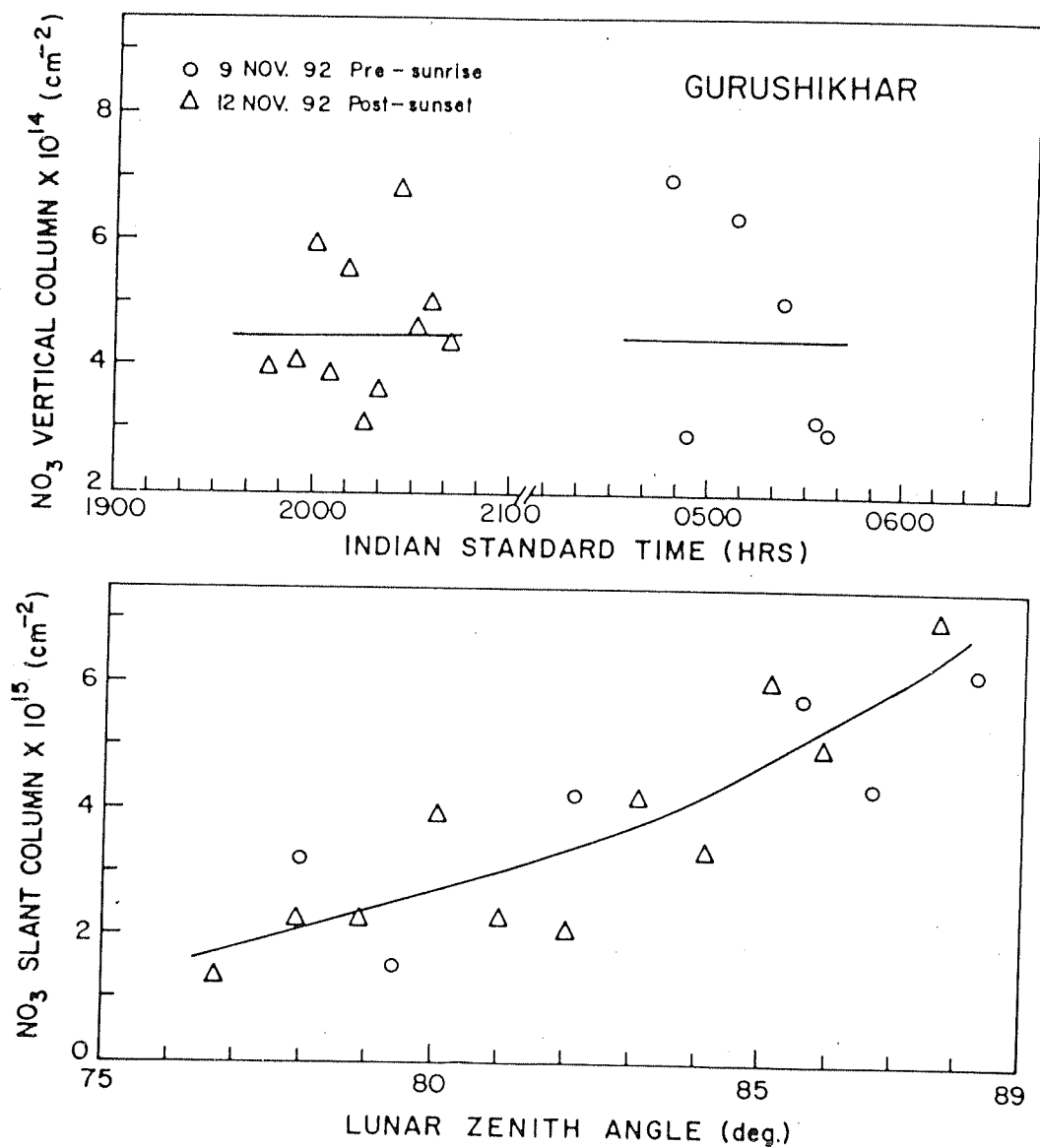


Figure 4.12 Slant column abundance of NO_3 (lower panel) for November 1992 and vertical column abundance of NO_3 for November 1992 over Gurushikhar.

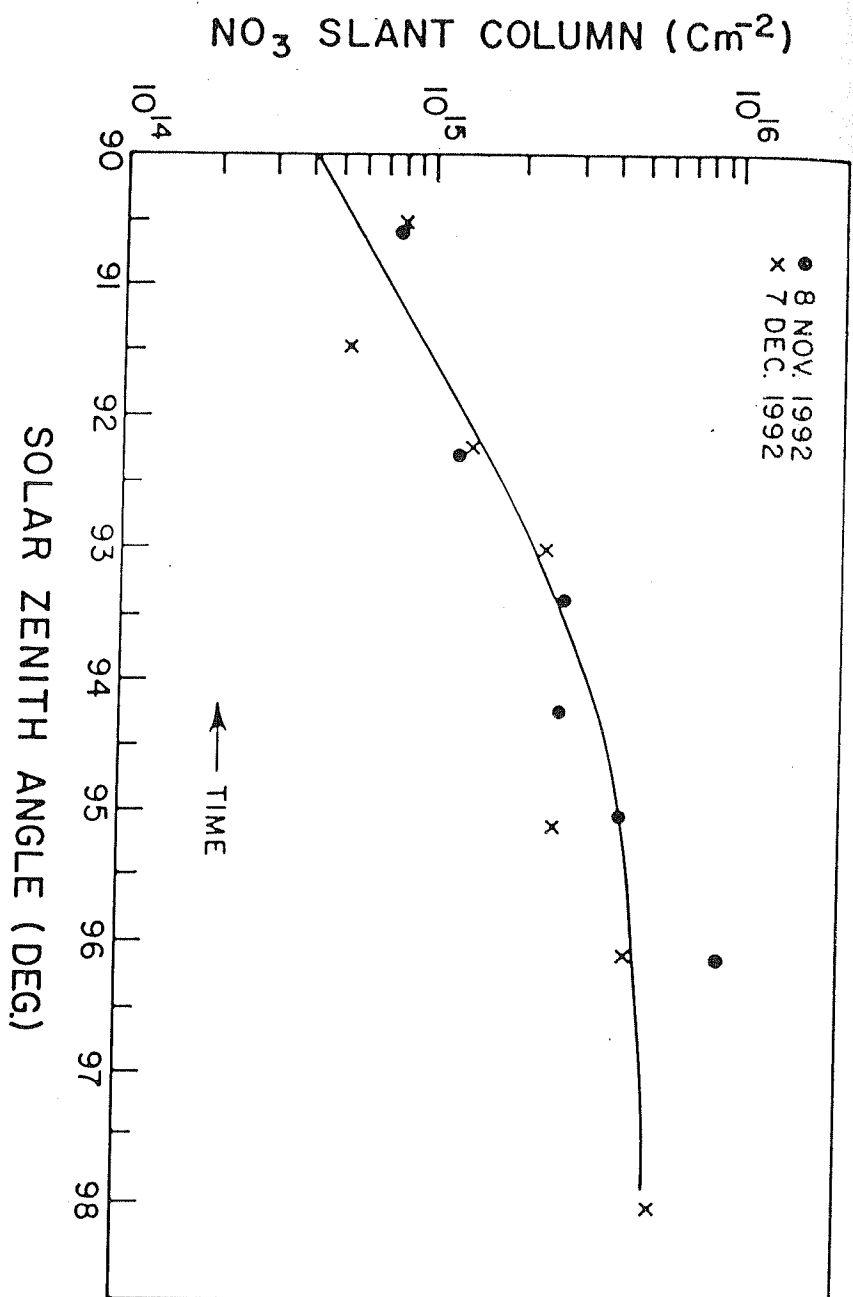


Figure 4.13 Sunrise disappearance of NO₃ observed over Gurushikhar during winter 1992.

to noise ratio decreases and goes beyond the lower limit of detection. This is because by this time NO_3 density decreases by many orders of magnitude compared to night. This trend has been found on both 8th November and 7th December 1992. Sunrise variation of NO_3 has also been studied at mid latitude [*Smith and Solomon* , 1990; *Smith et al.* , 1993]. *Smith and Solomon* [1990] found NO_3 slant column abundance to be about $3.5 \times 10^{14} \text{ cm}^{-2}$ at 6° solar depression angle which decreased upto $1 \times 10^{13} \text{ cm}^{-2}$ at 0° solar depression angle. A similar study was made by *Smith et al.* [1993]. They found NO_3 slant column to be about $2 \times 10^{14} \text{ cm}^{-2}$ at 6° solar depression angle which decreased to $1 \times 10^{13} \text{ cm}^{-2}$ at sunrise.

4.6 Sources of error

The errors described in Chapter 3 for NO_2 measurements are also present in NO_3 measurements. Some of these and some additional errors are discussed in the paragraphs that follow :

4.6.1 Laboratory absorption cross-sections

Accuracy of NO_3 measurements is directly dependent on the accuracy of the absorption cross-section value. NO_3 absorption cross-section used in this study was measured by *Ravishankara and Mauldin* [1986] which is temperature dependent. Hence, an use of inaccurate value of temperature would lead to an inaccurate value of NO_3 density. The averaged error in the value of absorption cross section is about $\pm 7\%$. This would lead to an error of NO_3 measurement of $\pm 3\%$.

4.6.2 Alignment of the spectrum

The accuracy of NO_3 also depends highly on how accurately we can determine the ratio spectra. For that purpose, we have taken maximum possible care for alignment of the spectra by cross correlation using a computer.

4.6.3 Water vapour interference

Accuracy of NO_3 will also depend on how accurately we are able to remove interference due to water vapour. In our case, we have considered no variation of water vapour from day to night. If there is any change in H_2O content during this period, then NO_3 determination will be inaccurate.

4.6.4 Ring effect

Ring effect is because of the filling of the Fraunhofer component. This effect is considerably less in the NO_3 determination spectral range compared to the NO_2 determination spectral range. According to *Solomon et al.* [1989b] ring effect could give an error of the order of 3% in the NO_3 measurement.

4.6.5 Movement of lunar image on interference slit

While scanning the spectra slit should remain fully illuminated by the lunar image. A drop in intensity due to the shift of the image from the slit will increase NO_3 density. Care was taken to see that slit remained fully illuminated for the whole range of scanning.

4.6.6 Enhancement factor

Our measurements give NO_3 slant column density. To convert them into vertical column density, it is necessary to know the exact value of NO_3 airmass factor. For that purpose the vertical distribution of NO_3 over the site of observation is needed. NO_3 enhancement factor has been calculated by *Sanders et al.* [1987] and *Solomon et al.* [1989b]. They have assumed that the bulk of NO_3 lies around 30 km and the scale height is 5 km. This may not be correct. We have used the same airmass factor as given by *Solomon et al.* [1989b] and this might have introduced some error in our vertical NO_3 column density.

4.6.7 Resultant uncertainty

Considering all the errors involved at different stages, overall error of our NO_3 measurement is put to be about 25%. In addition, as has been mentioned before, NO_3 absorption cross section is temperature dependent. A day to day variation in temperature would lead to a day to variation of NO_3 density. A variation in temperature by ± 20 K causes a variation in NO_3 column density by about 10%.

Chapter 5

A Theoretical Model of NO₂ and NO₃

5.1 Introduction

To understand various chemical processes that take place in the atmosphere a theoretical study is needed. This study should be such that it is able to reproduce the main observed features. The main features which we intended to reproduce theoretically in the present study are the NO₂ and NO₃ column densities obtained by us over Ahmedabad. Many ground-based measurements of NO₂ column density are available for different latitudes under different geophysical conditions [Brewer *et al.*, 1973; Noxon *et al.*, 1979; Noxon, 1979; Harrison, 1979; Syed and Harrison, 1980; McKenzie and Johnston, 1982b; Mount *et al.*, 1987; Sanders *et al.*, 1989]. Similarly NO₃ column abundance have also been measured by several workers for different latitude zones [Noxon *et al.*, 1978a; Noxon, 1983; Norton and Noxon, 1986; Sanders *et al.*, 1987; Solomon *et al.*, 1989a,b; Smith and Solomon, 1990]. Most of these observations are for mid and high latitude zones. How these values of NO₂ and NO₃ conform with our measurements have been discussed in Chapter 3 and Chapter 4 respectively. Several theoretical attempts have been made by various workers to reproduce NO₂

and NO_3 observed features. These have been discussed in Section 5.2. Most of these attempts are for mid and high latitude regions. NO_2 is formed in the atmosphere with a reaction of NO with O_3 and NO_3 is formed mainly in the nighttime by NO_2 combining with O_3 . The reactions which control the production and loss of NO_2 and NO_3 are described in Section 5.3. Like observations, theoretical studies are also sparse for low latitude region. A one dimensional model study has been made in the present work to examine the behaviour of NO_2 , NO_3 and N_2O_5 . In any model study, some input parameters are needed. The parameters we need in the present study have been discussed in Section 5.4. The results obtained in the present work are described in Section 5.6. These results contain NO_2 , NO_3 and N_2O_5 column densities during day and night and their vertical distributions.

5.2 Existing model studies

Since the pioneering work of *Crutzen* [1970] showing the importance of nitrogen oxides for the ozone balance in the stratosphere, considerable work has been done on the odd nitrogen in the atmosphere with one-dimensional and two-dimensional models [*Crutzen*, 1972, 1973; *Rao-Vupputuri*, 1973; *Wofsy and McElroy*, 1974; *Crutzen*, 1975; *Logan et al.*, 1978; *Penner and Chang*, 1978; *Miller et al.*, 1981; *Knight et al.*, 1982; *Evans et al.*, 1982]. *Noxon et al.* [1979] showed that the distribution of the total NO_2 column reflected the role of quasi - horizontal transport in the stratosphere on a global scale. *Miller et al.* [1981] calculated column abundance of important NO_x species for daytime. They found that the conversion of NO and NO_2 to other NO_x species took place at mid-latitudes more completely during the winter than the model calculated. *Knight et al.* [1982] and *Evans et al.* [1982] suggested that formation of N_2O_5 was important in determining the distribution of NO_2 in high latitude winter. The details of the nature of the dynamical - chemical coupling remained a

mystery, however, until laboratory measurements of the temperature dependence of the N_2O_5 absorption cross - section were made by *Yao et al.* [1982]. *Solomon and Garcia* [1983a,b] applied this laboratory data of N_2O_5 in model calculations of Noxon "cliff", and showed that the distribution of NO_2 in the cold, high latitude region depended strongly on the photochemistry of air parcels. They found that the calculated NO_2 column densities is somewhat lower than the measurements in the tropics of the summer hemisphere. *Solomon et al.* [1986] observed NO_2 from the limb infrared monitor of the stratosphere (LIMS) experiment and found that the data obtained at zenith angles greater than about 95° provided clear evidence for the night decay of NO_2 to form N_2O_5 . They also found the observed decay rate consistent with present theory. *Roscoe et al.* [1986] developed a photochemical model and compared their results with the measured stratospheric NO and NO_2 from the four flights of the Oxford radiometer. Their observations suggest agreement with model predictions of the nighttime decay of NO_2 associated with N_2O_5 production but do not fully verify them. *Brasseur et al.* [1987] developed a one-dimensional model to calculate the formation and destruction of active nitrogen in the stratosphere and indicated that transport processes played an important role in the behaviour of these species. *Flaud et al.* [1988] measured nighttime and daytime variation of atmospheric NO_2 from ground-based infrared spectrometer and compared their data with one dimensional model developed by *Brasseur et al.* [1987]. They found the build up during the night of a reservoir molecule which dissociates during the day. The formation rate deduced from the measurements seems to be more rapid than the model value and NO_2 day to night ratio was found larger than the theoretical values, suggesting a faster photodissociation of NO_2 than currently used in the model. *Douglas et al.* [1989] developed a two - dimensional residual circulation stratospheric model to study the long - term changes of trace gases for a large number of scenarios and to examine the model sensitivities to dynamical and photochemical assumptions and inputs. *McKenzie et*

al. [1991] developed an algorithm to derive altitude distribution of NO_2 from ground-based measurements at twilight. *Perliski and Solomon* [1992] studied the influences of Pinatubo volcanic aerosols on twilight observations of NO_2 column abundances. They suggested that the observed decrease in twilight NO_2 slant column abundance over mid latitude (45°S) was due to heterogeneous chemistry. *Solomon and Keys* [1992] also observed NO_2 column and its diurnal variation at two sites in the Antarctic region during fall, winter, and spring. They proposed a simple model for polar region and compared their results with NO_2 observation. They found that the rapid decline of NO_2 observed during fall is likely to be largely due to its gas phase conversion to N_2O_5 . The onset of a diurnal variation observed near day 57 and its magnitudes during the spring are also in general agreement with those anticipated from $\text{NO}_3 \rightarrow \text{N}_2\text{O}_5$ photochemistry. However, the details of the observed decay of the NO_2 column in fall and the am/pm ratio suggest problems with the present gas phase photochemical schemes. Improved agreement between the model and both observed slant column seasonal decay and am/pm ratios can be achieved either through consideration of background aerosol chemistry or substantial errors in N_2O_5 absorption cross-sections, especially at low temperatures. More recently *Solomon et al.* [1993] have determined NO_2 vertical column abundance over Antarctica (77.8°S) and compared these data with the model prediction. The observed NO_2 amounts during the fall and spring were broadly consistent with model predictions and with daytime measurements. During winter it differed from such simple predictions by factors greater than 10.

In case of NO_3 a theoretical attempt was made first, perhaps, by *Herman* [1979] to study the behaviour of the NO_3 column content as a function of time after sunset. They found that NO_3 took nearly two hours to increase from daytime values of approximately 10^{11}cm^{-2} to nighttime values of 10^{14}cm^{-2} . These results disagreed with the measured $[\text{NO}_3]$ rise time of 40 min after sunset obtained from the 662-nm

absorption data of *Noxon et al.* [1978a]. These results were discussed later in detail [*Noxon et al.*, 1980a,b; *Herman*, 1980]. Subsequently a more detailed theoretical analysis was carried out by *Gelinas and Vajk* [1981]. Their analysis indicated that the current photochemical theory was consistent with the experimental observations of total NO_3 diurnal variations. *Fabian et al.* [1982] did a 2D model study of stratospheric minor constituents as a function of latitude and season. They compared a model prediction for the latitude belt $33.2^\circ - 42.6^\circ \text{ N}$ in spring with observed values of *Noxon et al.*, [1978a] and found a reasonable agreement with the two points viz. 'end of night' and 'one hour after sunset'. *Norton and Noxon* [1986] measured the total column abundance of NO_3 in the stratosphere at night for 5 years at 40° N , with additional observations at 19° , 31° , 51° , and 64° N . At low latitude their mean abundance was found to be in general agreement with a model based upon simple NO_x chemistry, except that the summer values were smaller than spring values. At mid-latitude the variation in abundance exceeded by a factor of about 5. Very recently *Solomon et al.* [1993] have measured the vertical column abundances of NO_2 and NO_3 above McMurdo station, Antarctica (77.8° S) during the fall, winter, and spring seasons in 1991. These amounts during fall and spring were broadly consistent with model predictions. During winter, when polar night is long there was a gradual removal of NO_2 and build-up of NO_3 and N_2O_5 . The winter observations of both species differed from predictions by factors greater than ten, with the measured NO_2 being larger than the predicted and the measured NO_3 smaller than the predicted.

From the above discussion it is evident that the chemistry of NO_2 and NO_3 is different within and outside the polar vortex. It could be different in the low latitude zone compared to those of mid and high latitude zones.

5.3 Scheme used in the present study

In the stratosphere, nitric oxide (NO) is produced mostly from N_2O by reaction with an excited oxygen atom in the (1D) state. Nitric oxide is converted in to nitrogen dioxide by reaction with O_3 . This NO_2 molecule, is converted to NO during the day, either by reaction with atomic oxygen or by photolysis of itself. Reaction of NO with O_3 , followed by reaction of NO_2 with O represents a catalytic cycle which provides the major loss process of odd oxygen in the stratosphere. During night, when the above mentioned reactions do not occur, nitric oxide decreases after sunset and nitrogen dioxide is converted into nitrogen trioxide by combining with ozone. Further, NO_3 combines with another molecule of NO_2 and forms N_2O_5 , which is expected to be a temporary reservoir of odd nitrogen in the stratosphere. Thus NO_3 builds up during the nighttime. N_2O_5 is also photodissociated during the daytime, but with a time scale which is of the order of hours to days below 40 km. It is also important to note that some of the N_2O_5 formed undergoes thermal decomposition, providing a potentially time-dependent source of NO_3 , especially when thermal decomposition is relatively rapid. The major reactions of NO_2 and NO_3 used in this study and their rates are listed in Table 5.1. These are shown schematically in Fig. 5.1.

5.4 Input parameters

To reproduce the observational data theoretically, informations of some parameters such as temperature, ozone, reaction rate coefficients etc. are needed. These are described in the following sections :

TABLE 5.1

Photochemical reactions and their rates used in the present model

	Reaction	Reaction rate coefficient ^a
1	$\text{NO} + \text{O}_3 \rightarrow \text{NO}_2 + \text{O}_2$	$k_1 = 9.0 \times 10^{-13} \cdot e^{\frac{-1200}{T}}$
2	$\text{NO}_2 + h\nu \rightarrow \text{NO} + \text{O}$	$J_2 = 6.60 \times 10^{-3}$
3	$\text{NO}_2 + \text{O} \rightarrow \text{NO} + \text{O}_2$	$k_3 = 9.1 \times 10^{-12}$
4	$\text{O} + \text{O}_2 + \text{M} \rightarrow \text{O}_3 + \text{M}$	$k_4 = 1.06 \times 10^{-34} \cdot e^{\frac{510}{T}}$
5	$\text{O}_3 + h\nu \rightarrow \text{O}(^1\text{D}, ^3\text{P}) + \text{O}_2$	$J_5 = 4.26 \times 10^{-5}$
6	$\text{NO}_2 + \text{O}_3 \rightarrow \text{NO}_3 + \text{O}_2$	$k_6 = 1.1 \times 10^{-13} \cdot e^{\frac{-2450}{T}}$
7	$\text{NO}_2 + \text{NO}_3 + \text{M} \rightarrow \text{N}_2\text{O}_5 + \text{M}$	$k_7 = 1.26 \times 10^{-29}$
8	$\text{NO}_3 + h\nu \rightarrow \text{NO}_2 + \text{O}$	$J_8 = 2.20 \times 10^{-2}$
9	$\text{N}_2\text{O}_5 + h\nu \rightarrow \text{NO}_2 + \text{NO}_3$	$J_9 = 3.85 \times 10^{-5}$
10	$\text{N}_2\text{O}_5 + \text{M} \rightarrow \text{NO}_2 + \text{NO}_3 + \text{M}$	$k_{10} = 5.79 \times 10^{-27}$

^aTwo body reactions are in units of cm^3s^{-1} and three body reactions are in units of cm^6s^{-1} .

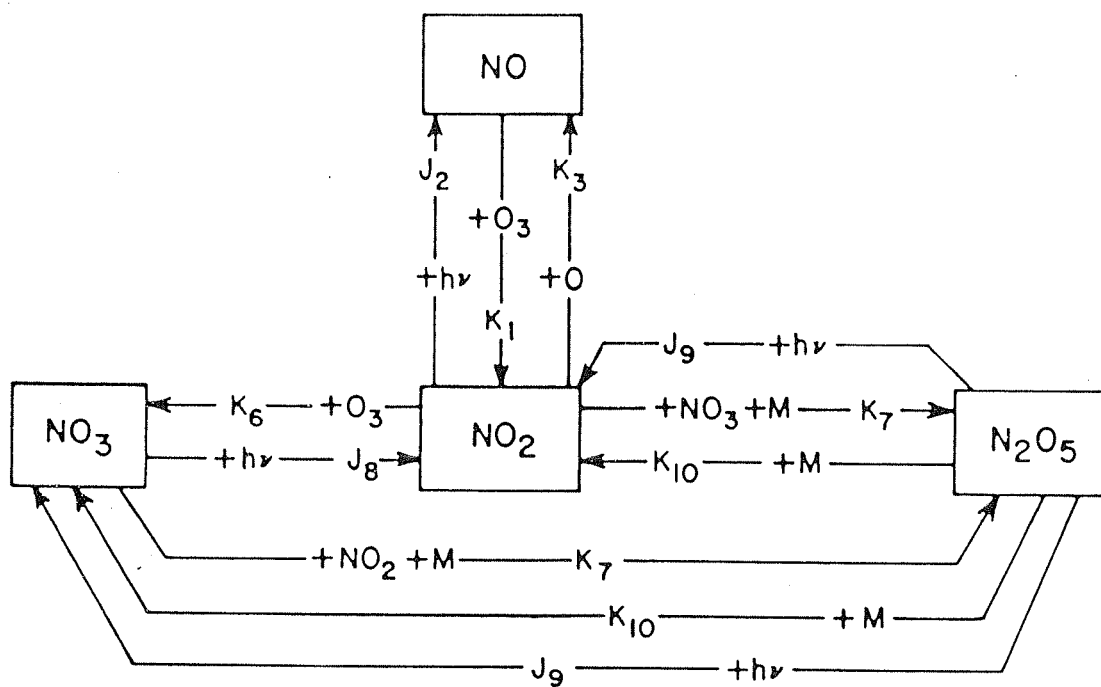


Figure 5.1 Schematic diagram of detailed chemical scheme used in the present work.

5.4.1 Temperature

Information of temperature profile is essential for developing any kind of model. Good reviews of temperature measurements by several techniques and their theoretical interpretations are available [Barnett, 1980; Knight et al., 1982; Barnett and Corney, 1984; McElroy, 1985; Russel et al., 1986]. At Thumba, several temperature profiles have been measured by Soviet M - 100 rocket for a long period of time. Mitra [1977] has compiled all these profiles and has given a standard reference profile for Indian zone. This is given in Table 5.2. We have used this temperature profile in the present study.

5.4.2 Neutral constituents

Informations about the neutral constituents both, major and minor, are also needed for any model study. Several informations of minor neutral constituents are available by rocket-borne, balloon-borne, satellite, and ground-based techniques. Mitra [1977] has made a good review of the available observational results of all the important minor constituents of the middle atmosphere. For major neutral atmospheric density, model prepared by Mitra [1977] with the M-100 rocket data of Thumba has been used. These values which have been used in the present study are shown in Table 5.2.

The concentration of ozone is needed in the present work. Information on the distribution of this species has been obtained from rocket, balloon, satellite and ground-based technique [Nagata et al., 1971; Shimabukuro et al., 1975; Llewellyn and Witt, 1977; Miller et al., 1981; Knight et al., 1982; Rigaud et al., 1983; Bhartia et al., 1984; Ridley et al., 1984; McCormick et al., 1984; Keating and Young, 1985; Russell et al., 1986; Naudet et al., 1989; Keating et al., 1990 etc]. Several theoretical profiles of O_3 are also available [Garcia and Solomon, 1983; Shimazaki, 1984]. In the equatorial

TABLE 5.2

Distributions of temperature, air and minor neutral constituents in
the middle atmosphere

Height km	Temperature °K	Air cm ⁻³	Ozone cm ⁻³	Oxygen atom cm ⁻³	Nitric oxide cm ⁻³
0	300	2.55E+19	8.60E+11	1.50E+3	7.00E+7
5	273	1.53E+19	4.70E+11	5.00E+3	8.00E+7
10	237	8.99E+18	3.30E+11	1.00E+4	2.00E+8
15	199	4.96E+18	4.20E+11	1.00E+5	6.00E+8
20	207	2.01E+18	1.78E+12	1.00E+6	6.00E+8
25	221	8.43E+17	3.14E+12	8.00E+6	8.50E+8
30	232	3.71E+17	2.81E+12	6.00E+7	6.00E+8
35	245	1.74E+17	1.33E+12	1.50E+8	6.00E+8
40	258	8.19E+16	5.42E+11	8.50E+8	5.00E+8
45	264	4.23E+16	2.04E+11	2.50E+9	4.00E+8
50	262	2.22E+16	6.84E+10	5.00E+9	1.00E+8
55	248	1.23E+16	2.86E+10	6.00E+9	7.50E+7
60	227	6.57E+15	1.25E+10	7.00E+9	4.50E+7
65	208	3.34E+15	3.00E+09	6.50E+9	2.00E+7
70	195	1.54E+15	4.50E+09	8.50E+9	5.00E+6
75	189	6.67E+14	6.00E+09	2.00E+10	4.20E+5
80	183	2.76E+14	9.00E+09	5.00E+10	3.15E+5

region O₃ has been measured by balloon and rocket-borne techniques [Mitra, 1977; Somayajulu *et al.*, 1981; Subbaraya *et al.*, 1981; Subbaraya and Jayaraman, 1987; Jayaraman *et al.*, 1989]. Using these data Subbaraya and Jayaraman [1987] have constructed a mean vertical distribution of ozone for Thumba (8.5°N) between 0 and 60 km altitude. This profile has been used in our study and is given in Table 5.2.

Nitric oxide plays an important role in the daytime stratospheric chemistry. Large amount of data are available for the nitrogen compounds NO₂ and HNO₃ from satellite; however, no such data exist for nitric oxide in the stratosphere. Our knowledge of the distribution of nitric oxide in the stratosphere is based on the discrete measurements made from the ground, from high-altitude balloons, aircraft, rockets, and space shuttle platforms [Ridley *et al.*, 1976, 1984; Blatherwick *et al.*, 1980; Roscoe *et al.*, 1981, 1985, 1986; Ridley and Hastie, 1981; Ridley and Schiff, 1981; Knight *et al.*, 1982; Webster and Menzies, 1984; Kondo *et al.*, 1985; Fabian *et al.*, 1987]. Solar occultation measurements of nitric oxide during sunset have been reported since as early as 1973 [Ackerman and Muller, 1973; Ackerman *et al.*, 1975]. To obtain the best estimate of the profile of NO at sunset, a diurnal model was developed by Boughner *et al.* [1980]. Rinsland *et al.* [1984] have developed reduction technique of solar occultation measurements. Maier *et al.* [1978] and Drummond *et al.* [1977] made balloon flight in 1977 and obtained NO profile below 32 km. Weiler *et al.* [1980] also made balloon flight up to 30 km altitude. Burkhardt *et al.* [1975], Ridley *et al.* [1977] and McFarland *et al.* [1986] have measured the growth of NO during the morning at constant altitudes. Simultaneous in-situ and long-path measurements of nitric oxide and nitrogen dioxide have been obtained by Louisnard *et al.* [1983] and McFarland *et al.* [1985]. Several high altitude measurements have been obtained by Horvarth *et al.* [1983], using a rocket-borne chemiluminescence instrument. No measurement of NO has been made in the Indian latitude zone in the stratosphere. Mitra [1977] has reviewed the observations and theoretical studies of several workers and have given a

profile of NO for low latitude. We have used this NO profile given by *Mitra* [1977] in the present study. These values of NO are given in Table 5.2.

Reliable experimental profiles of atomic oxygen are very few [*Anderson*, 1975; *Robbins and Carnes*, 1978; *Dickinson et al.*, 1980] and none are for the equatorial region. However, several theoretical profiles are available [*Logan et al.*, 1978; *Garcia and Solomon*, 1983; *Shimazaki*, 1984]. These theoretical profiles, however, do not differ much among themselves for the quiet noon time condition. Like T, O₃, NO and M, atomic oxygen profile used in the present work has been taken from *Mitra* [1977] and is given in Table 5.2.

5.4.3 Solar zenith angle

The solar zenith angle (χ) at any geometrical latitude (ϕ) has been calculated using the relation

$$\cos\chi = \sin\phi.\sin\delta + \cos\phi.\cos\delta.\cos HA \quad (5.1)$$

where δ is the declination of the sun and HA is the hour angle. This hour angle has been calculated with local sidereal time and the right ascension (RA) using the formula

$$HA = \text{Local time} + \text{Sidereal time} - RA \quad (5.2)$$

The δ and RA values are available as a function of time in the astronomical ephemerides.

5.4.4 Reaction rate coefficients

Table 5.1 lists the rate constants for all the chemical reactions used in the present work. These reaction rate constants have been determined and recommended by several panels after reviewing the laboratory data *NASA* [1979], *JPL* [1981, 1982] and

WMO [1981]. In some cases the recommended value is a simple average or a weighted mean of several qualified experimental data. N_2O_5 builds up more slowly than does NO_3 after sunset. The abundance of stratospheric NO_3 is determined largely by the ozone density and by the temperature distribution through its effect on K_7 . The rate constant K_{10} is very critical to the absolute abundance of NO_3 and has only recently been measured directly [JPL, 1987, and references therein]. Previously, K_7 was derived from measurements of K_{10} and the equilibrium constant for N_2O_5 . The directly measured value of K_{10} results in larger value for K_7 and smaller abundances for NO_3 .

5.4.5 Photolysis rate

For theoretical study we need photodissociation rates of NO_2 , NO_3 and N_2O_5 . These have been calculated by many workers [Johnston and Graham, 1974; Cogley and Borucki, 1976; Herman, 1979; Magnotta and Johnston, 1980; JPL, 1981; Shimazaki, 1985; Froidevaux et al., 1984; Demore et al., 1987; JPL, 1990; Smith and Solomon, 1990; Solomon and Keys, 1992]. NO_2 photolysis rate has been measured by Madronich et al. [1985] and Creel and Ross [1976]. N_2O_5 photolysis rate has also been measured by Yao et al. [1982]. In the present work photolysis rates used have been taken from Shimazaki [1985] for NO_2 , NO_3 , and N_2O_5 .

5.5 Methodology and continuity equations

The continuity equations for NO_2 , NO_3 , and N_2O_5 were framed and solved simultaneously for the steady state condition. These equations are listed below. The general form of these equations can be written as :

$$\frac{d[N_i]}{dt} = P - L \quad (5.3)$$

where, $[N_i]$ is the number density of the species i , P its production rate and L its loss rate. For steady state $\frac{d[N_i]}{dt} = 0$

5.5.1 NO₂ continuity equation

Using the chemical scheme shown in Fig. 5.1 and Table 5.1, the continuity equation of NO₂ with time at a particular height can be written as :

$$\begin{aligned} \frac{d[NO_2]}{dt} = & K_1.[NO].[O_3] + J_8.[NO_3] + K_{10}.[N_2O_5].[M] + J_9.[N_2O_5] \\ & - J_2.[NO_2] - K_3.[O].[NO_2] - K_6.[O_3].[NO_2] - K_7.[NO_3].[M].[NO_2] \end{aligned} \quad (5.4)$$

In the steady state, $\frac{d[NO_2]}{dt} = 0$

This gives

$$[NO_2] = \frac{K_1.[NO].[O_3] + J_8.[NO_3] + K_{10}.[N_2O_5].[M] + J_9.[N_2O_5]}{J_2 + K_3.[O] + K_6.[O_3] + K_7.[NO_3].[M]} \quad (5.5)$$

During nighttime NO₂ loss is mainly due to the reactions (6) and (7) shown in Table 5.1 [Solomon and Garcia, 1983a] and if NO₃ is considered to be in a steady state during night, then the NO₂ nighttime variation (from eqn. 5.4) will become as follows :

$$\frac{d[NO_2]}{dt} = -2.K_6.[O_3].[NO_2]$$

This gives

$$[NO_2]_{AM} = [NO_2]_{PM} \cdot \exp(-2.k_6.[O_3].\Delta T) \quad (5.6)$$

The ratio $\frac{[NO_2]_{AM}}{[NO_2]_{PM}}$ is called as decay factor of NO₂ and its value can be obtained from the following expression :

$$\begin{aligned} DF &= \frac{[NO_2]_{AM}}{[NO_2]_{PM}} \\ &= \exp(-2.k_6.[O_3].\Delta T) \end{aligned} \quad (5.7)$$

We define the diurnal variation of NO_2 as :

$$DV = \frac{([\text{NO}_2]_{PM} - [\text{NO}_2]_{AM})}{[\text{NO}_2]_{PM}}$$

Using eqn. 5.7, this becomes

$$DV = 1 - \exp(-2.k_6.[\text{O}_3].\Delta T) \quad (5.8)$$

where ΔT is the length of the night.

In the lower stratosphere the ratio between NO and NO_2 during the day is given by :

$$\frac{[\text{NO}]_{DAY}}{[\text{NO}_2]_{DAY}} = \frac{J_2}{K_6.[\text{O}_3]}$$

At night, all NO is quickly converted into NO_2 . Then one write

$$\begin{aligned} [\text{NO}_2]_{NIGHT} &= [\text{NO}]_{DAY} + [\text{NO}_2]_{DAY} \\ &= (1 + \frac{J_2}{(K_6.[\text{O}_3])})[\text{NO}_2]_{DAY} \end{aligned} \quad (5.9)$$

5.5.2 NO_3 continuity equation

Using the chemical scheme shown in Fig. 5.1 and Table 5.1, the continuity equation of NO_3 at a particular height can be written as :

$$\begin{aligned} \frac{d[\text{NO}_3]}{dt} &= K_6.[\text{NO}_2].[\text{O}_3] + K_{10}.[\text{N}_2\text{O}_5].[M] + J_9.[\text{N}_2\text{O}_5] \\ &\quad - J_8.[\text{NO}_3] - K_7.[\text{NO}_3].[\text{NO}_2].[M] \end{aligned} \quad (5.10)$$

In the steady state, $\frac{d[\text{NO}_3]}{dt} = 0$

This gives

$$[\text{NO}_3] = \frac{K_6.[\text{NO}_2].[\text{O}_3] + K_{10}.[\text{N}_2\text{O}_5].[M] + J_9.[\text{N}_2\text{O}_5]}{J_8 + K_7.[\text{NO}_2].[M]} \quad (5.11)$$

5.5.3 N₂O₅ continuity equation

Using the chemical scheme shown in Fig. 5.1 and Table 5.1, the continuity equation of [N₂O₅] can be written as :

$$\frac{d[N_2O_5]}{dt} = K_7.[NO_2].[NO_3].[M] - K_{10}.[N_2O_5].[M] - J_9.[N_2O_5] \quad (5.12)$$

In the steady state, $\frac{d[N_2O_5]}{dt} = 0$

This gives

$$[N_2O_5] = \frac{K_7.[NO_2].[NO_3].[M]}{K_{10}.[M] + J_9} \quad (5.13)$$

Equation 5.5, 5.11, and 5.13 have been solved simultaneously with arbitrary initial values of N₂O₅. Iterations have been done till the convergence at one percent is reached and the results become independent of the initial values. Calculations have been done from ground to 80 km altitudes at an intervals of 5 km. The results obtained are discussed in the next section.

5.6 Theoretical model results

In the present study vertical distributions of NO₂, NO₃ and N₂O₅ have been calculated. The calculated values of NO₂ and NO₃ have been compared with our observational values. Comparison has also been made with other theoretical values.

5.6.1 NO₂ calculation

NO₂ vertical distributions calculated from ground up to 80 km for both noontime and midnight conditions are shown in Fig. 5.2. Calculated value of daytime NO₂ density on surface is about $1.0 \times 10^8 \text{ cm}^{-3}$ (Fig. 5.2a). It increases with height, reaches maximum around 25 km and then decreases as the height further increases. Vertical

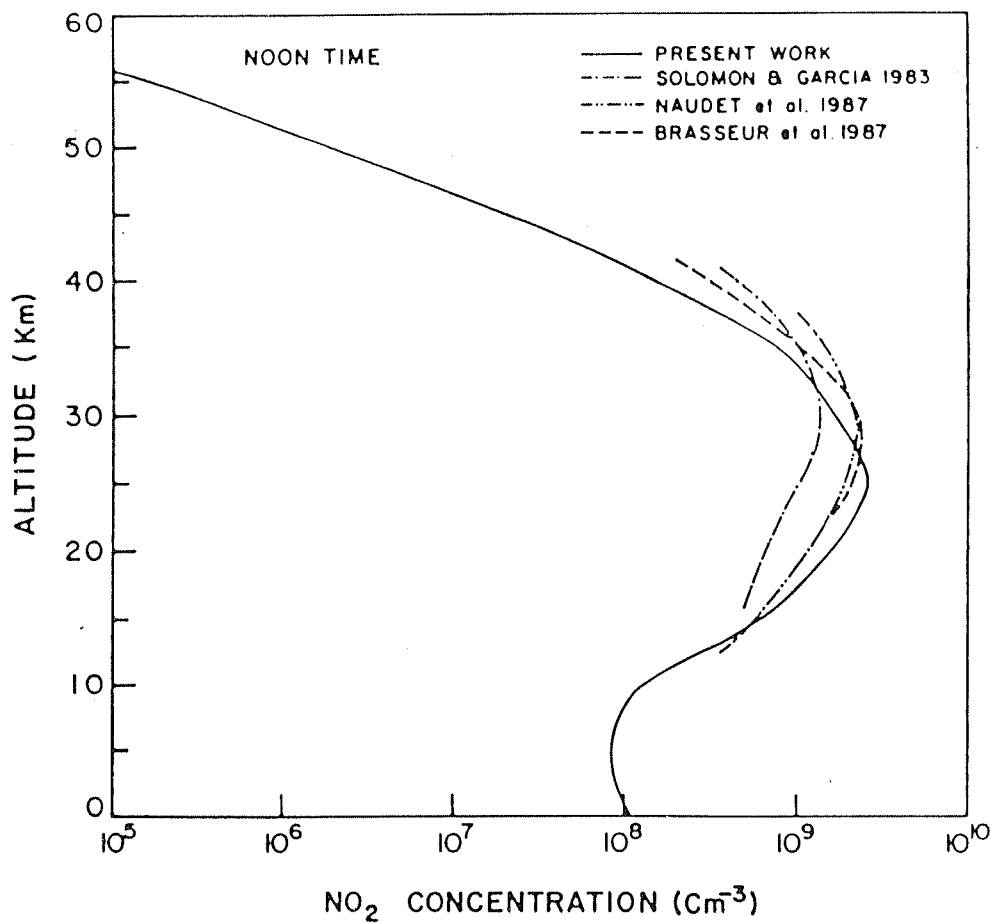


Figure 5.2a Theoretical model of NO₂ vertical distribution for daytime.

distribution of NO_2 also has been calculated by others [Garcia and Solomon, 1983; Solomon and Garcia, 1983a; Roscoe et al., 1986; Naudet et al., 1987; Brasseur et al., 1987] and they show that most of the daytime NO_2 lies between 15 and 40 km. Our calculated NO_2 daytime profile agrees with other profiles.

The calculated vertical distribution of stratospheric NO_2 has been converted into total column abundance. This comes out to be $3.1 \times 10^{15} \text{ cm}^{-2}$. The observed values of NO_2 over Ahmedabad during winter twilight 1990 lie between 0.5 and $3 \times 10^{15} \text{ cm}^{-2}$. Thus our theoretical value lies within the range of the observed values and the agreement is towards the upper limit of the observed NO_2 . This could be because of the chosen input values of NO and T. It has been found that NO_2 density is highly sensitive to initial NO density chosen. A calculation done with an increase of NO density by a factor of 10 increases NO_2 density also by a factor of 10 at 15 km. Further calculation shows that if the temperature profile is increased by 10 K the NO_2 column density increases to $3.9 \times 10^{15} \text{ cm}^{-2}$ and a decrease of temperature by 10 K decreases NO_2 column density to $2.3 \times 10^{15} \text{ cm}^{-2}$.

Our calculated values of NO_2 during night have been shown in Fig. 5.2b. A large increase in the value of NO_2 below about 40 km compared to that of daytime has to be noticed in this figure. Our calculated value of stratospheric NO_2 column density during night is $2.4 \times 10^{17} \text{ cm}^{-2}$. This value is about two orders of magnitude greater than the daytime value. In this calculation we have not invoked day - night variation of NO. NO density in the stratosphere decreases by several orders of magnitude from day to night. If this factor is taken into consideration the day to night change of column density of NO_2 becomes marginal as observed. For further study in this direction nighttime profile of NO density is needed.

An examination of all the production terms of NO_2 in eqn. 5.4 shows that $K_1 \cdot [\text{NO}] \cdot [\text{O}_3]$ is most predominant during daytime. At 20 km its value is $\sim 1.0 \times$

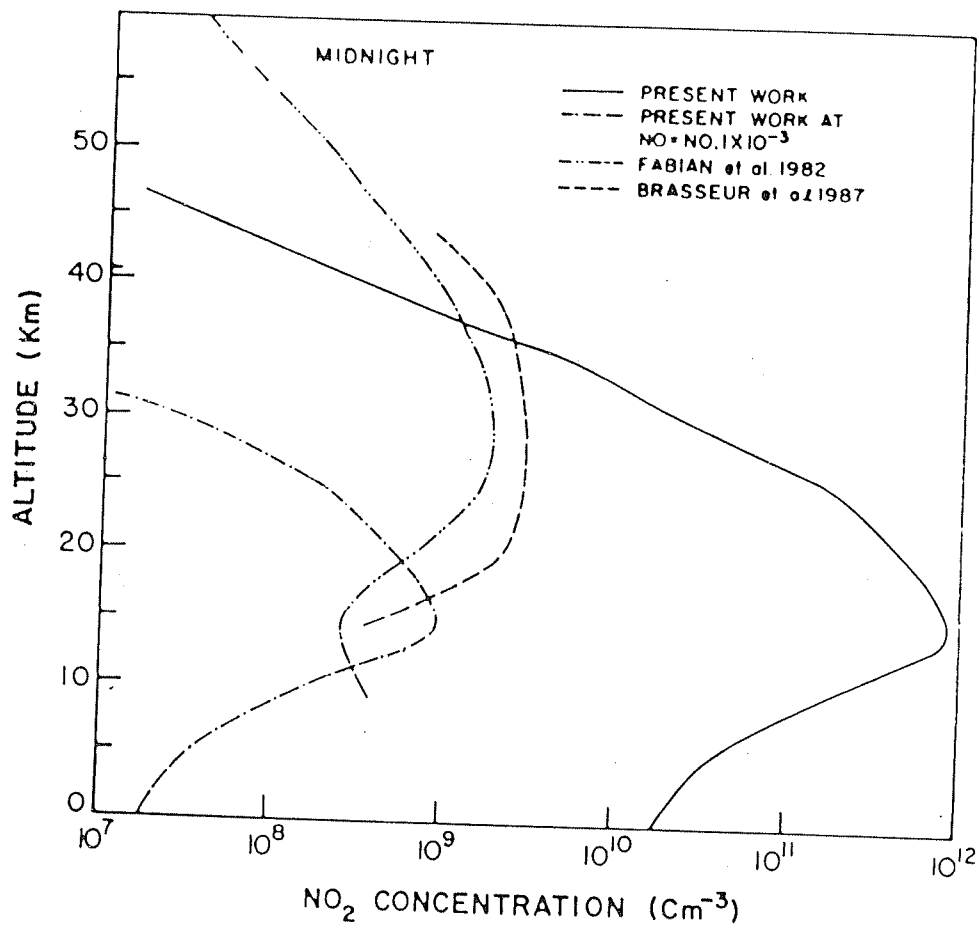


Figure 5.2b Theoretical model of NO₂ vertical distribution for nighttime.

$10^7 \text{ cm}^3 \text{ sec}^{-1}$. At night additional term $K_{10} \cdot [\text{N}_2\text{O}_5] \cdot [\text{M}]$ also becomes comparable to $K_1 \cdot [\text{NO}] \cdot [\text{O}_3]$ term. Similarly an examination of all the loss terms in eqn. 5.4 shows that during daytime J_2 is most predominant and during night all the three terms are comparable. At 20 km the value of $J_2 \sim 6.5 \times 10^{-3} \text{ sec}^{-1}$ and at night other terms are $\sim 10^{-5} \text{ cm}^3 \text{ sec}^{-1}$. If we do not consider day - night variation of NO density then production rate increases by factor of about 1.3 from day to night. The loss rate, on the other hand, decreases by about two orders of magnitude. Due to these variations of production and loss rates increase in NO_2 density at night comes to be about two orders of magnitude around 20 km (as found in Fig. 5.2a,b) and the column density also increases by about 2 orders of magnitude compared to daytime which is not observed. Thus we have to take lower values of nighttime NO compared to daytime. Decrease of NO during night in the stratosphere has been reported in both observations and theoretical works [*Patel et al.*, 1974; *Burkhardt et al.*, 1975; *Ridley et al.*, 1976, 1977; *Ridley and Schiff*, 1981; *Kondo et al.*, 1985, 1987, 1989, 1990; *Fabian et al.*, 1987].

5.6.2 Decay factor of NO_2

Decay factor has been defined in Section 5.5.1. Using the eqn. 5.7, decay factor of NO_2 has been calculated for 200 K and 220 K stratospheric temperatures. These values are shown in Fig. 5.3. In this figure cross points correspond to 200 K stratospheric temperature and open circles to 220 K stratospheric temperature. Comparison with observation shows that decay factor calculated by using 220 K stratospheric temperature is in better agreement with observation.

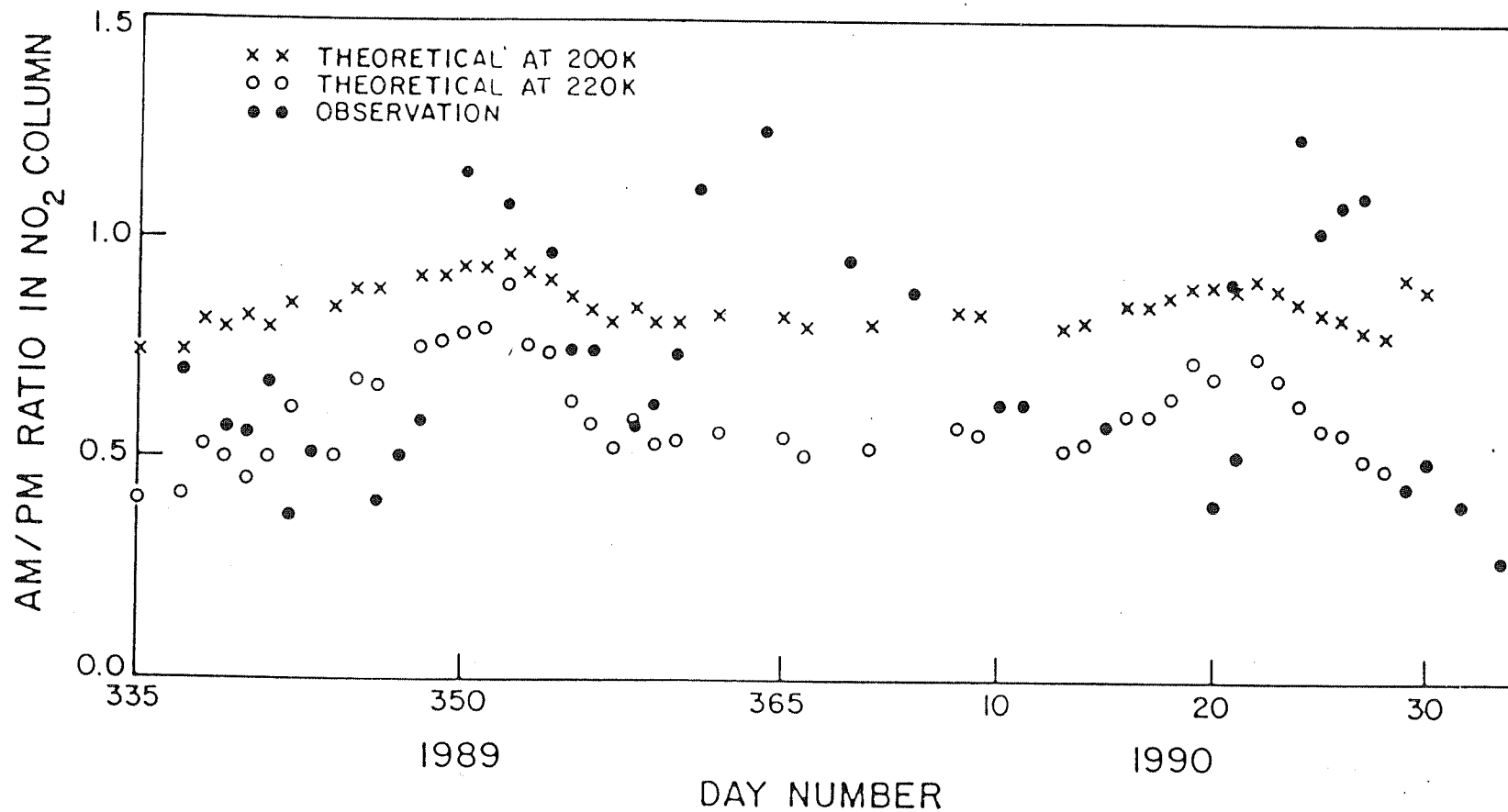


Figure 5.3 NO₂ decay factor calculated at 200 K stratospheric temperature (cross points) and 220 K stratospheric temperature (open circles).

5.6.3 Diurnal Variation of NO₂

Similar to decay factor, diurnal variation has been defined in Section 5.5.1. Diurnal variation of NO₂ also has been calculated for 200 K and 220 K stratospheric temperatures for winter period and is shown in Fig. 5.4. Here also cross points correspond to 200 K stratospheric temperature and open circle to 220 K stratospheric temperature. *Gil and Cacho* [1992] have observed NO₂ diurnal variation over Antarctica (64°S) and have calculated its variability at different temperatures. Their observed and calculated values lie between 0.1 and 0.5. Our values of diurnal variation lie between 0.1 and 0.6 which agree with the results of *Gil and Cacho* [1992]. Our computed values have been compared with the observed values taken during winter. Agreement is found to be good for 220 K stratospheric temperature.

5.6.4 NO₃ calculation

Fig. 5.5 shows the theoretical NO₃ vertical distribution obtained by us for both noon and midnight conditions. It is to be noticed from this figure that during night (Fig. 5.5a), NO₃ density on the surface is about $1.2 \times 10^5 \text{ cm}^{-3}$. It decreases as height increases, becomes minimum around 10 km, again increases, reaches maximum around 40 km. At this altitude the value of NO₃ is about $9.0 \times 10^6 \text{ cm}^{-3}$. Above this altitude NO₃ decreases with increase in height. Thus, most of the NO₃ lie between 20 and 60 km. Vertical distribution of NO₃ also has been calculated by many workers [*Fabian et al.*, 1982; *Brasseur et al.*, 1987; *Pirre et al.*, 1989; *Smith and Solomon*, 1990; *Smith et al.*, 1993]. For the sake of comparison some theoretical profiles obtained by other workers have also been shown in Fig. 5.5a. *Fabian et al.* [1982] studied diurnal variation of NO₃ at 47°N and found NO₃ to lie between 25 and 60 km with maximum density around 35 km at midnight. *Pirre et al.* [1989] compared their model calculation with observed values of *Naudet et al.* [1989] and they interpreted

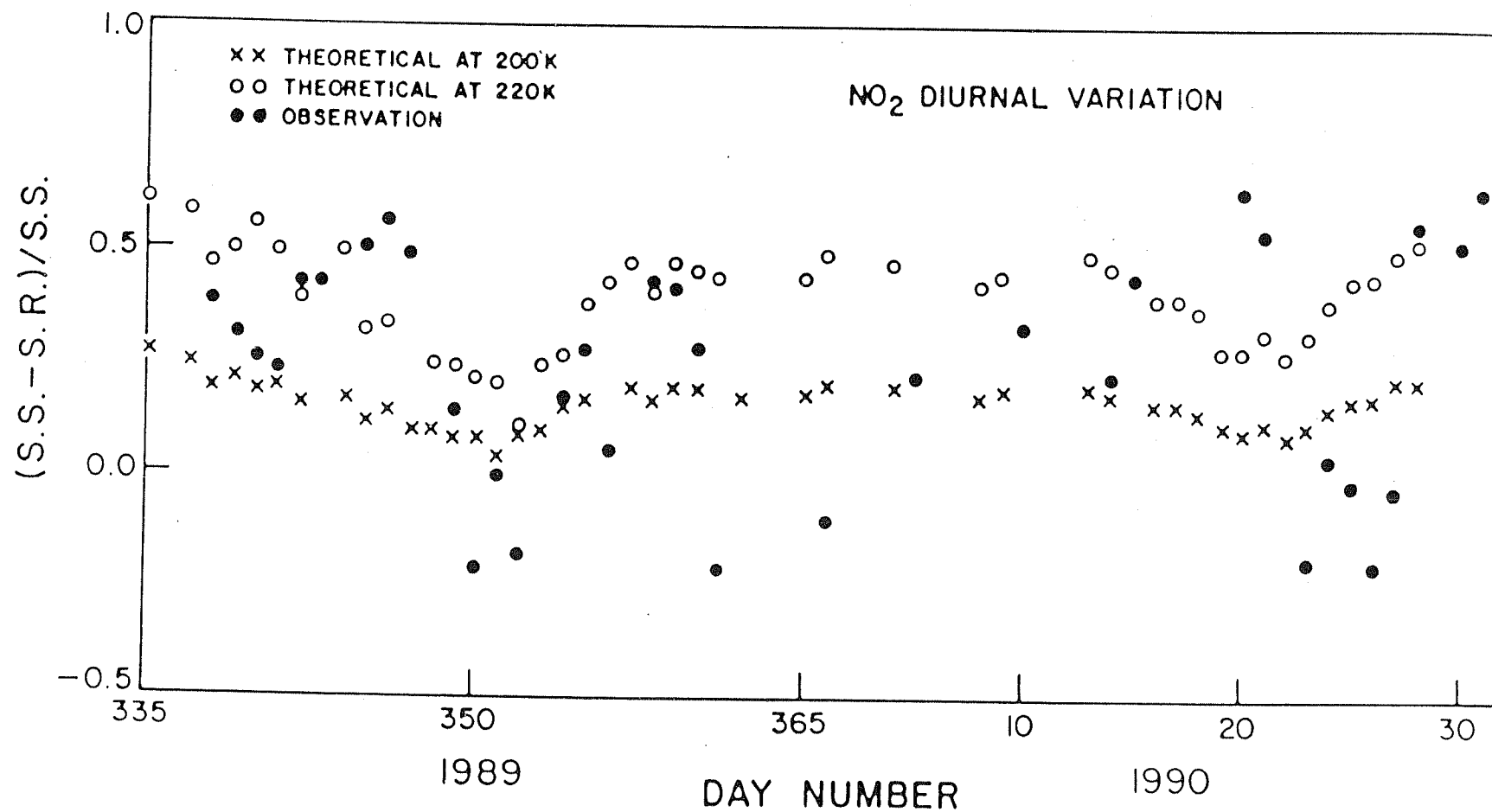


Figure 5.4 NO₂ diurnal variation calculated at 200 K stratospheric temperature (cross points) and 220 K stratospheric temperature (open circles).

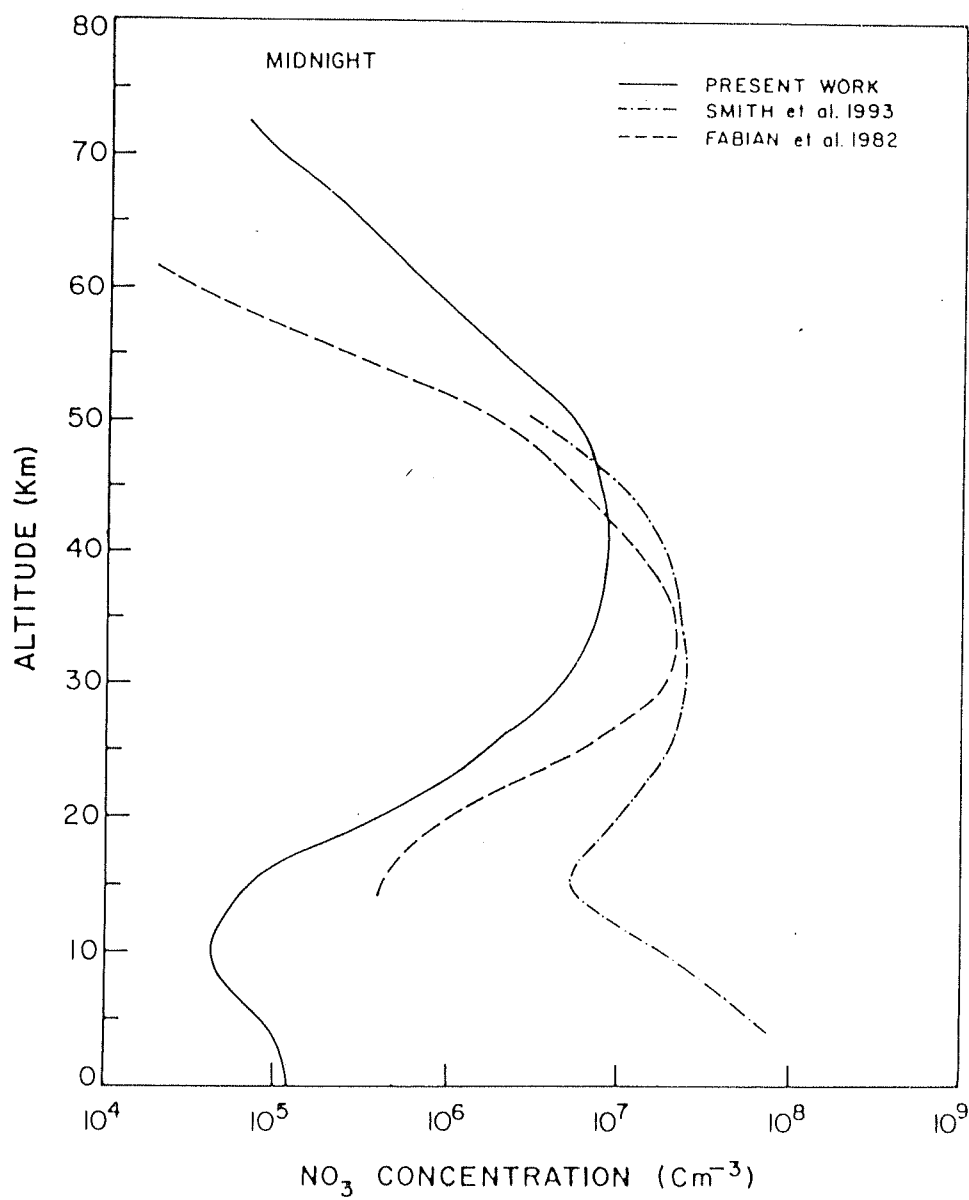


Figure 5.5a Theoretical model of NO₃ vertical distribution for nighttime.

maximum NO₃ in summer to be due to larger stratospheric temperature. *Smith and Solomon* [1990] and *Smith et al.* [1993] derived algorithm for NO₃ vertical distribution using ground-based technique and found maximum NO₃ between 20 and 50 km. Also they observed an increase in NO₃ density below 15 km altitude. Similar to *Smith et al.* [1993] our calculated vertical profile also shows increase in NO₃ density below 15 km. Our values are in good agreement with the other profiles in the region 40 - 50 km, above which altitude they are overestimated and below that altitude they are underestimated.

Our calculated vertical distribution of NO₃ has been converted into total column abundance. The value of total column abundance obtained is $2.0 \times 10^{13} \text{ cm}^{-2}$. It has been found that NO₃ is very much sensitive to ambient temperature. A change of stratospheric temperature by 10 K changes column density by 25%. NO₃ vertical column abundance has been measured over Ahmedabad for different periods. NO₃ vertical column obtained in early 1991 is found to lie between 1 and $5 \times 10^{14} \text{ cm}^{-2}$. Similar observation was made in December 1991 and NO₃ vertical column obtained during this period was found to be about 2 times higher compared to early 1991 values. During daytime, the abundance of NO₃ is very low, therefore, solar spectrum has been used as background spectrum in which NO₃ contribution is almost negligible. Using this background spectrum, NO₃ vertical column has been obtained in January 1992 and its value has been found to lie in the range of 1.9 to $2.5 \times 10^{15} \text{ cm}^{-2}$. Measurements have also been made over Gurushikhar, a hill station, 1.8 km above sea level. Here vertical column abundance of NO₃ is found to be between 2.5 and $7.0 \times 10^{14} \text{ cm}^{-2}$. Thus we find that our calculated values of NO₃ are about an order of magnitude less than our observed NO₃ values. Part of this could be because of temperature profile chosen. Scattering noticed in observed NO₃ data in Chapter 4 could be due to the day to day variation of stratospheric temperature.

The daytime vertical distribution of NO_3 calculated in this work has been shown in Fig. 5.5b. Calculated value of daytime NO_3 density on the surface is about $5.0 \times 10^4 \text{ cm}^{-3}$. It decreases with height, reaches minimum around 10 km, again increases and reaches maximum around 25 - 30 km. At this altitude the value of NO_3 is about $7.0 \times 10^5 \text{ cm}^{-3}$. Above this altitude NO_3 decreases with increase in height. Thus, most of the NO_3 lie between 10 and 40 km. Vertical distribution of daytime NO_3 has also been calculated by many workers [Fabian *et al.*, 1982; Shimazaki, 1985]. Fabian *et al.* [1982] studied diurnal variation of NO_3 at 47°N and found daytime NO_3 to lie between 15 and 45 km with maximum density around 32 km at noontime. Our profile lies between the profiles of Fabian *et al.* [1982] and Shimazaki [1985].

Our computed vertical distribution of noontime NO_3 has been converted in to total column abundance. The value of total column abundance of noontime NO_3 obtained is $1.0 \times 10^{12} \text{ cm}^{-2}$. This value can not be compared with experimental value because experimental value during daytime is not available. This is about one order of magnitude less than the nighttime calculated value of NO_3 column abundance.

It is to be seen from Fig. 5.5a, and b that in the lower stratosphere (below about 25 km) day - night variation of NO_3 is not very significant. But in the upper stratosphere this variation is large, e.g. at 45 km, the decrease from night to day is by about 3 orders of magnitude. At night the main loss of NO_3 is by $K_7 \cdot [\text{NO}_2] \cdot [\text{M}]$. During day NO_3 is photolyzed. Calculation shows that the loss rate of NO_3 during noon is about $5.0 \times 10^{-2} \text{ cm}^3 \text{ sec}^{-1}$ and during midnight it is about $1.2 \times 10^1 \text{ cm}^3 \text{ sec}^{-1}$. In the production of NO_3 main term is $K_6 \cdot [\text{NO}_2] \cdot [\text{O}_3]$. At 20 km its value is $\sim 7.8 \times 10^3 \text{ cm}^3 \text{ sec}^{-1}$ during daytime and increases to $\sim 2.6 \times 10^6 \text{ cm}^3 \text{ sec}^{-1}$ during nighttime. Due to these variations in the production and loss rates, there is no significant change in NO_3 density at night compared to day in the lower stratosphere. In the upper stratosphere, e.g. around 40 km, the production rate of NO_3 does not

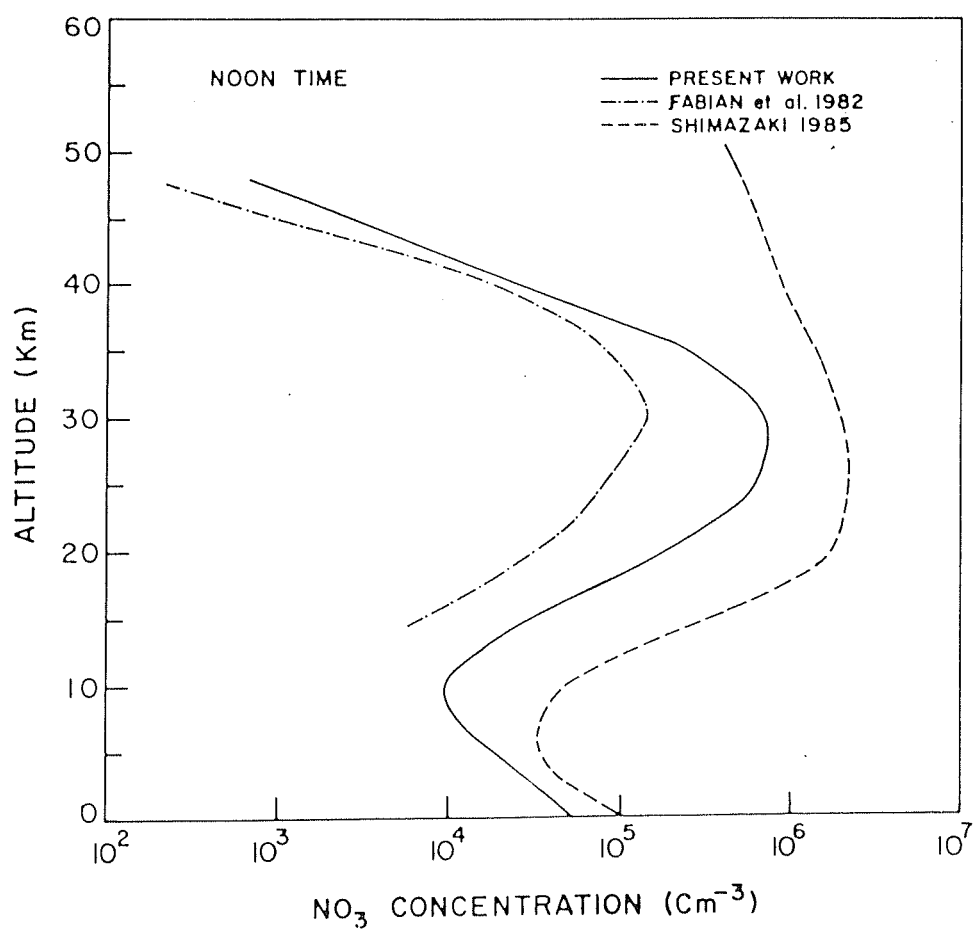


Figure 5.5b Theoretical model of NO₃ vertical distribution for daytime.

significantly change from day to night, but the loss rate decreases by about two orders of magnitude. As a result NO_3 increases by about two orders of magnitude in the upper stratosphere at night compared to day. This agrees with the work of *Fabian et al.* [1982].

5.6.5 N_2O_5 calculation

Similar to NO_2 and NO_3 , N_2O_5 vertical distributions have also been calculated for day and nighttime conditions. These are shown in Fig. 5.6. One can see from Fig. 5.6a that at night on the ground, N_2O_5 density is about $2.3 \times 10^{12} \text{ cm}^{-3}$. This value increases with height and becomes maximum around 25 km. At this level the value of N_2O_5 is $4.0 \times 10^{14} \text{ cm}^{-3}$. Above this height, it again decreases as the height increases. Vertical distribution of N_2O_5 has also been calculated by many workers [*Wofsy*, 1978; *Fabian et al.*, 1982; *Solomon and Garcia*, 1983a; *Shimazaki*, 1985; *Toon et al.*, 1986; *Allen and Delitsky*, 1990]. *Wofsy* [1978] has calculated N_2O_5 vertical profile for noon at different latitude region. He finds that N_2O_5 lies between 20 and 35 km at 30°N . *Fabian et al.* [1982] calculated N_2O_5 profile for different time of the day and found that it lies between 10 and 50 km with maximum density during night at about 30 km. *Toon et al.* [1986] analyzed ATOMS experiment data and obtained N_2O_5 vertical profile. They found N_2O_5 to lie between 10 and 52 km region with peak volume mixing ratio around 35 km. Our calculated value of N_2O_5 is much larger than that reported in these works. Our large value of N_2O_5 is due to the fact that we have not changed the value of NO at night compared to daytime. NO density in the stratosphere decreases by several orders of magnitude from day to night. Calculation has been done by changing NO by different amounts. Curve 2 represents N_2O_5 by decreasing NO by six order of magnitude compared to daytime. Curve 2 now comes close to other profiles given in Fig. 5.6a. With that profile of N_2O_5 the vertical column density comes out to be $4.4 \times 10^{14} \text{ cm}^{-2}$. We do not have any measurement

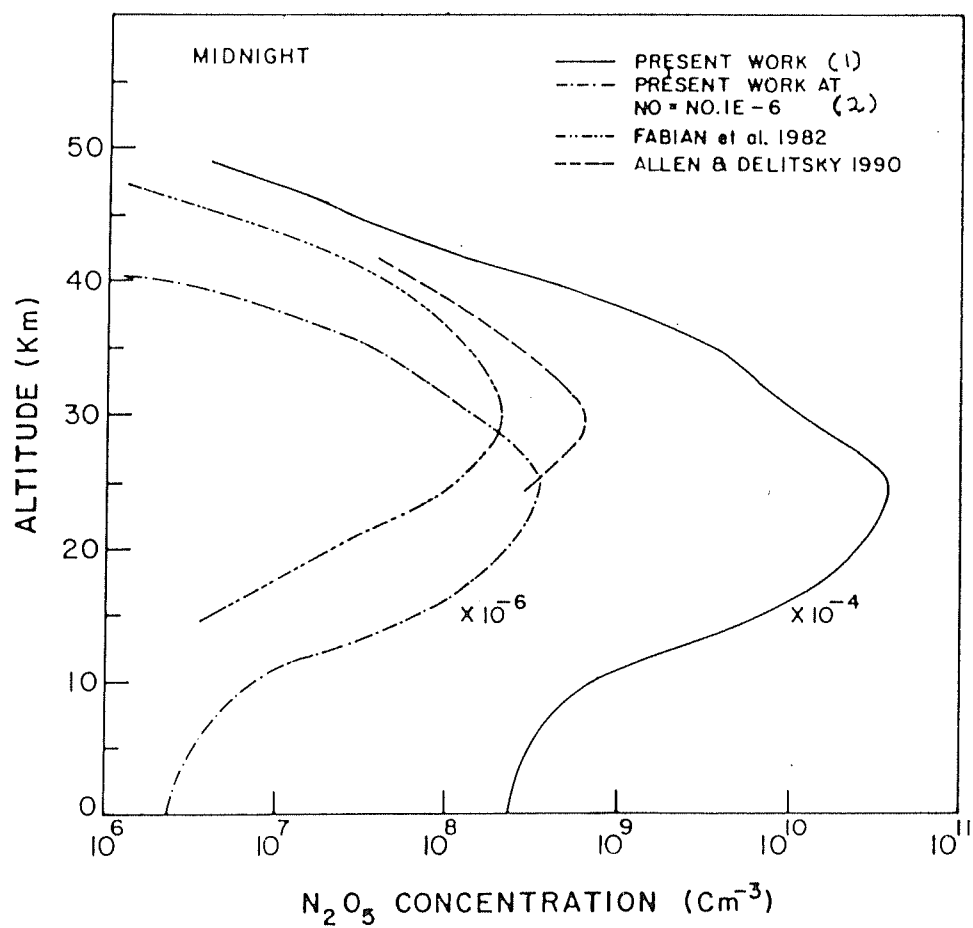


Figure 5.6a Theoretical model of N_2O_5 vertical distribution for nighttime.

of column density of N_2O_5 to compare with our results. Also comparison would be meaningful only when accurate nighttime NO profile is available.

Calculation has also been done by changing T profiles. It has been found that like NO_2 , N_2O_5 is also sensitive to T. An increase of stratospheric temperature by 10 K increases column density by a factor of about 3 and a decrease of temperature by 10 K, decreases column density by a factor of about 3 compared to normal temperature.

The daytime vertical distribution of N_2O_5 calculated in this work has also been shown in Fig. 5.6b. Calculated value of daytime N_2O_5 density on the surface is about $3.0 \times 10^7 \text{ cm}^{-3}$. It decreases with height, reaches minimum around 10 km, again increases and reaches maximum around 25 km. At this altitude the value of N_2O_5 is $2.5 \times 10^8 \text{ cm}^{-3}$. Above this altitude N_2O_5 decreases with increase in height. Thus, most of the daytime N_2O_5 lie between 10 and 35 km. Daytime vertical distribution of N_2O_5 has also been calculated by many workers [Fabian *et al.*, 1982; Solomon and Garcia, 1983]. Fabian *et al.* [1982] studied diurnal variation of N_2O_5 at 47°N with a two-dimensional model and found daytime N_2O_5 to lie between 15 and 40 km with maximum density around 27 km at noontime. Solomon and Garcia [1983] also used a two-dimensional model to study the behaviour of N_2O_5 at mid latitude. They found most of the daytime N_2O_5 to be between 15 and 35 km at 32°N . Our N_2O_5 profile agrees with the profile of Fabian *et al.* [1982].

Our vertical distribution of daytime N_2O_5 has been converted into total column abundance. The value of total column abundance of daytime N_2O_5 obtained is $2.33 \times 10^{14} \text{ cm}^{-2}$. This value is only marginally less than the nighttime value obtained with curve 2 in Fig. 5.6a. However, this difference has to be much more. An examination shows that the production term of N_2O_5 is $K_7 \cdot [\text{NO}_2] \cdot [\text{NO}_3] \cdot [\text{M}]$. If we assume that NO_2 decreases by about an order of magnitude and NO_3 increases by two order of magnitude, then the effective increase of N_2O_5 production rate is by one order of

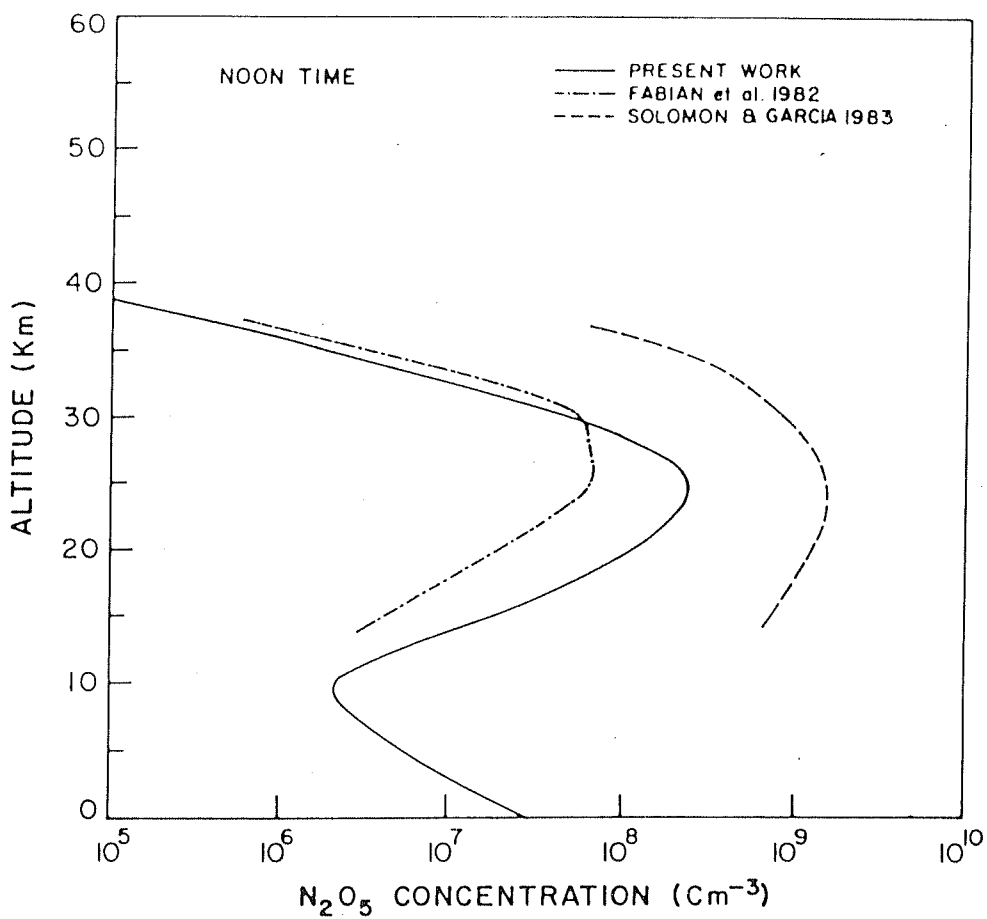


Figure 5.6b Theoretical model of N_2O_5 vertical distribution for daytime.

magnitude from day to night. At night the loss of N_2O_5 is by $K_{10}[\text{M}]$. During day N_2O_5 is photolyzed. These will give the decrease in the loss rate of N_2O_5 by three orders of magnitude from day to night. Due to these variations in the production and loss rates, N_2O_5 density at night should be about four orders magnitude larger than the daytime.

Although, we have done calculations for steady state condition, the results are to be taken with a little caution. NO_2 near the noon reaches a steady state value and hence a steady state calculation of NO_3 and N_2O_5 during day are probably exact. Also NO density during day is reasonably known. At night, however NO is rapidly converted into NO_2 . Then the NO_2 is also quickly converted into NO_3 and N_2O_5 which then decreases throughout the night. Thus a condition of steady state is probably a too simplified approach to calculate NO_3 and N_2O_5 distributions during nighttime. It could be that in most of the cases probably by midnight the production of species is cutoff. This problem can be studied in more detail by a time dependent model which is beyond the scope of this thesis. And for that we also need an accurate nighttime measured profile of NO .

Chapter 6

Pinatubo Aerosols

6.1 Introduction

Stratospheric aerosols play an important role in determining the radiation budget of the earth's atmosphere. They reflect a part of incoming solar radiation back into the space and thus control the solar heating of the earth. These aerosol distributions are disturbed by various activities, volcanoes are one among them. In this natural phenomenon, a huge amount of SO_2 is injected into the atmosphere along with other materials. This gas is then converted into sulphate aerosols within a couple of weeks. Evidences exist in two huge 19th century volcanoes viz. Tambora in 1815 which was followed by "the year without a summer" and Krakatau in 1883, which was followed by the coolest year [Stommel and Stommel, 1983]. Volcanic eruption, therefore, affects the climate. Pollack *et al.* [1976] have reported that an increase in the optical depth of about 0.1 lasting for a sufficiently long time would lead to a cooling of about 1 K averaged over the globe. It is, therefore, worth to study the characteristics of aerosols produced by volcanoes. The effect of volcanic eruption was first studied extensively after the eruption of El Chichón [Orme, 1982; Barth *et al.*, 1983; Livingston and Lockwood, 1983; Hirono and Shibata, 1983; Thomas *et al.*, 1983; Knollenberg and

Huffman, 1983; Pollack and Ackerman, 1983; Hofmann and Rosen, 1983, 1984; Labitzke et al., 1983; Ashok et al., 1982, 1984; Heath and Schlesinger, 1984; Shibata et al., 1984; Spinhirne and King, 1985; Deluise et al., 1983; Jäger and Carnuth, 1987; Michelangeli et al., 1989; Chandra and Stolarski, 1991]. Livingston and Lockwood [1983] reported a maximum extinction in visible wavelengths of over 40% or 0.4 in optical depth over Tucson ($32^{\circ} 2' \text{N}$) on 15 May 1983. Lidar measurements by Hirono and Shibata [1983] at two wavelengths, $1.06 \mu\text{m}$ and $0.53 \mu\text{m}$, over Fukukoa (33°N , 130°E) showed a high concentration of aerosols in the altitude region 15-33 km, with highest concentrations between 21 and 30 km. In situ measurements of the dust cloud by balloon borne particle counters at Laramie (41°N) and in Southern Texas ($27\text{-}29^{\circ}\text{N}$) have shown the presence of 2 layers, one at ~ 25 km and the other at ~ 18 km. From these measurements the total mass thrown up into the stratosphere by the eruptions has been estimated to be $\sim 20 \text{ T}_g$ ($1 \text{ T}_g = 10^{12} \text{ g} = 1 \text{ megaton}$) [Hofmann and Rosen, 1983]. As a result of the injection, a stratospheric temperature increase of $4.5^{\circ} - 5^{\circ} \text{ C}$ over the previous 18 year average was detected at 10°N at the 30 mbar level [Labitzke et al., 1983]. Very recently, eruption of Mount Pinatubo (15.4°N , 120.35°E) took place in Philippines between 3 June and 15 June 1991. In this eruption, the amount of SO_2 injected into the atmosphere was reported to be two to three times more than that of El Chichón [Bluth et al., 1992]. This event must have caused more perturbation in atmosphere compared to El Chichón volcanic eruption. We have studied the aerosol characteristics of this volcanic eruption at Ahmedabad. The results are described in this Chapter.

The solar radiation which penetrates the atmosphere during twilight period serves as a source of illumination on the earth's surface. As the sun moves below the horizon, the path length of atmosphere covered by the solar radiation increases. The earth's shadow gradually rises upward and the atmospheric region coming in the earth's shadow starts increasing. This leads to a monotonic decrease in twilight

intensity due to exponential decrease in air density with altitude. However, the presence of an additional layer (as for example due to aerosols) causes perturbation in the twilight brightness variation with solar depression angle. Also the twilight sky was found to remain reddish for a longer period of time after a volcanic eruption. Anomalous variation of twilight brightness after volcanic eruption has been reported earlier [Rosen 1969; Volz 1969, 1974; Cadle and Grams, 1975; Ashok et al., 1982, 1984]. We have measured this twilight brightness by a ground-based technique after Pinatubo eruption at Ahmedabad. The analysis of the variation of this brightness has given information about the characteristics of the aerosols of this event.

6.2 Existing results of Pinatubo eruption

Volcanic aerosols formed in the stratospheric region, after the eruption of Mt. Pinatubo, encircled the globe within three weeks [Bluth et al., 1992; Stowe et al., 1992]. These aerosols have been monitored by ground-based Lidar, photometric and spectrometric technique, aircraft, and different satellites such as SAGE-II, NOAA/11, NIMBUS-7/TOMS (see special January issue of GRL, 1992). Some of these measurements are described below :

6.2.1 Satellite measurements

This eruption produced plumes which reached as high as 40 km, with ash canopy reaching altitudes between 25 and 30 km [Labitzke and McCormick, 1992]. SAGE-II satellite has been measuring the aerosol optical depth and extinction coefficient at 1020 nm wavelength region. SAGE-II satellite measurements in early August 1991 show that aerosols in the tropics reached as high as 29 km altitude with most of the cloud between 20 and 25 km. The aerosol clouds reached still higher altitudes in

the equatorial region. These aerosols spreaded over higher latitude region through advection and also transported into upward direction by eddy diffusion. In the month of September and October 1991, between equator and 30°N the stratospheric temperature increased by about 3.5°C [Labitzke and McCormick, 1992]. Before Pinatubo eruption, NOAA/11 satellite was used for the measurements of Sahara dust, haze from industrialized urban areas and smoke from forest fires and agriculture burning [Stowe *et al.*, 1992], and after eruption Advanced Very High Resolution Radiometer (AVHRR) has been used to measure the reflected radiation from the atmospheric aerosols at 0.5 μ for spatial and temporal variability of the aerosol layer and its optical thickness. NIMBUS-7 satellite contains Total Ozone Mapping Spectrometer (TOMS) which measured total ozone. After Pinatubo volcanic eruption, SO₂ interference took place in O₃ measurements. Bluth *et al.* [1992] reported that the SO₂ tonnage of Mt. Pinatubo was the greatest ever recorded by satellite, almost three times that of 1982 El Chichón eruption.

6.2.2 Aircraft measurements

Just after Pinatubo volcanic eruption, an aircraft mission was conducted [McCormick, 1992]. In this mission, several experiments have been performed to study the dynamical, chemical and radiative behaviour of volcanic aerosol cloud. On July 7, three weeks after the eruption, NASA Wallops Flight Facility Electra aircraft was airborne and headed for Barbados to intercept and characterize the clouds as they moved over the Caribbean. Instruments which had been used in studies of previous eruptions such as Mount St. Helens and El Chichón were selected for the aircraft mission to facilitate comparisons with data from these earlier eruptions : an upward-looking Lidar; a side-looking Fourier Transform Interferometer; an upward- and downward-looking Total, Direct and Diffuse multichannel Radiometer; and an upward looking correlation spectrometer. Six flights were conducted between July 7 and 14; four out

of Barbados and two ferry flights conducted between Wallops Island, Virginia, and Barbados. Observations covered latitudes from 4.5°S to 37°N and longitudes from 80°W to 45°W [McCormick, 1992]. In this mission, effective particle radius was determined. It was found to be between 0.18 μm at 16 - 17 km and 0.35 μm at 22 - 23 km with a corresponding columnar mass loading between 35 and 80 $\text{mg}\cdot\text{m}^{-2}$. This gave an opportunity to study the clouds in the early stage of their evolution.

6.2.3 Ground-based experiment

Besides satellite and Aircraft measurements Mt. Pinatubo aerosols have also been measured by using ground-based technique over the globe. At Mauna Loa observatory, Hawaii, the Pinatubo plume was first observed by Lidar on 1 July 1991 [Defoor *et al.*, 1992]. They found a decrease of about 13% in a broad band atmospheric transmission factor. At mid - latitude station Garmisch-Partenkirchen (47.5°N, 11.1°E), stratospheric plume from the explosive eruption of Pinatubo had been observed since July, 1991 [Jäger, 1992]. NOAA Lidars at wavelengths of 0.574, 0.694, and 1.591 μ have observed ejecta from the eruption of Mt. Pinatubo both in the troposphere and stratosphere over Boulder, Colorado, since July 1991 [Post *et al.*, 1992]. These data provide valuable information on size distribution and the wavelength dependence of backscatter and optical depth. Pinatubo volcanic aerosol has also been observed by using photometric and IR absorption spectroscopic techniques [Goldman *et al.*, 1992]. They found SO₂ total column upper limit to be about 0.9×10^{16} molecules cm^{-2} from measurements on September 20-24, 1991. Their measurement is close to the total columns of 2.0×10^{16} to 3.7×10^{16} molecules cm^{-2} obtained using IR solar absorption spectroscopy [Mankin *et al.*, 1992].

6.3 Earlier twilight brightness measurements

Twilight brightness can be measured with simple, inexpensive, and sensitive ground-based optical methods. This type of measurement has been done by many workers [Ashburn, 1952; Bigg, 1956; Volz and Goody, 1962; Rozenberg, 1966; Dave and Mateer, 1968; Volz, 1969, 1973, 1974; Ashok *et al.*, 1982, 1984; Coulson, 1988 and references there in; Sarkissian *et al.*, 1991; Perliski and Solomon, 1992] mainly for the determination of additional layer present in the atmosphere. Colour ratio also has been used for identifying the aerosol layer height and the strength of aerosols by measuring the twilight intensity at different wavelength regions [Sarkissian *et al.*, 1991]. Stratospheric dust has been measured in terms of colour ratio by Volz [1969, 1970, 1974] and spectral colour ratio has been measured at the polar region for the identification of polar stratospheric cloud [Sarkissian *et al.*, 1991]. Logarithmic gradient of twilight intensity has been measured or theoretically interpreted by many workers [Bigg, 1956; Volz and Goody, 1962; Rozenberg, 1966; Dave and Mateer, 1968; Volz, 1969; Ashok *et al.*, 1982, 1984; Coulson, 1988] for the derivation of aerosol layer height and its thickness. By monitoring this brightness, information about the properties of stratospheric aerosols during El Chichón eruption were obtained by Ashok *et al.* [1982, 1984]. They used radiation at 870 nm for their studies. Similar technique has been used by us for the study of Mt. Pinatubo eruption at a low latitude station, Ahmedabad (23°N, 72°E), India. The results thus obtained are reported in the following sections.

6.4 Observations (Instrumentation)

The scattered flux of the zenith sky received on the ground depends on the wavelength as well as solar depression angle. It has been shown by Rozenberg [1966] that when wavelength increases, the scattering height decreases. At lower wavelength, the layer

has a very distinct shape, practically independent of refraction effects. In the long-wave spectral region, however, part of its profile is severely distorted by refraction. *Rozenberg* [1966] shows that scattering height decreases from about 50 km to about 25 km for a depression angle of 6° when the wavelength increases from 500 nm to 880 nm. In the present study we have concentrated at 800 nm for depression angles less than 5° . We have also taken some observations at 700 and 650 nm wavelengths. The instrument used here is a McPherson monochromator with a grating chosen so that appropriate colour filters provide first order light in the wavelength region of our concern. We have used the red cutoff filter for removing second and higher order spectra. Baffle assembly contains a 45° mirror for the zenith sky measurements. Lock-in amplifier along with a chopper have been used for improving the signal to noise ratio. Chopper frequency was 150 Hz and it was controlled by the Lock-in amplifier. Entrance and exit slit widths were equal and corresponded to 10 nm bandwidth. Current to voltage converter along with voltage amplifier have been used for the output current. R955 Hamamatsu photomultiplier tube with cooling system have been used as a detector. Output signal was recorded in a personal computer. Observations were made from 0 to 8° solar depression angle from November 1991 - February 1992.

6.5 Zenith sky twilight brightness

Fig. 6.1 shows the variation of zenith sky twilight brightness (I) with solar depression angle (α) measured by us at Ahmedabad. Two curves are shown in this figure. Curve 1 corresponds to 11 January 1992 in which Pinatubo effect was present and curve 2 corresponds to 15 September 1993 in which Pinatubo effect had disappeared. One can see from this figure that curve 2 which represents a normal condition, zenith sky intensity (I) shows a monotonic decreases with increase of α due to an increase in the path length. But, an anomalous variation of I with that of α is shown in curve 1.

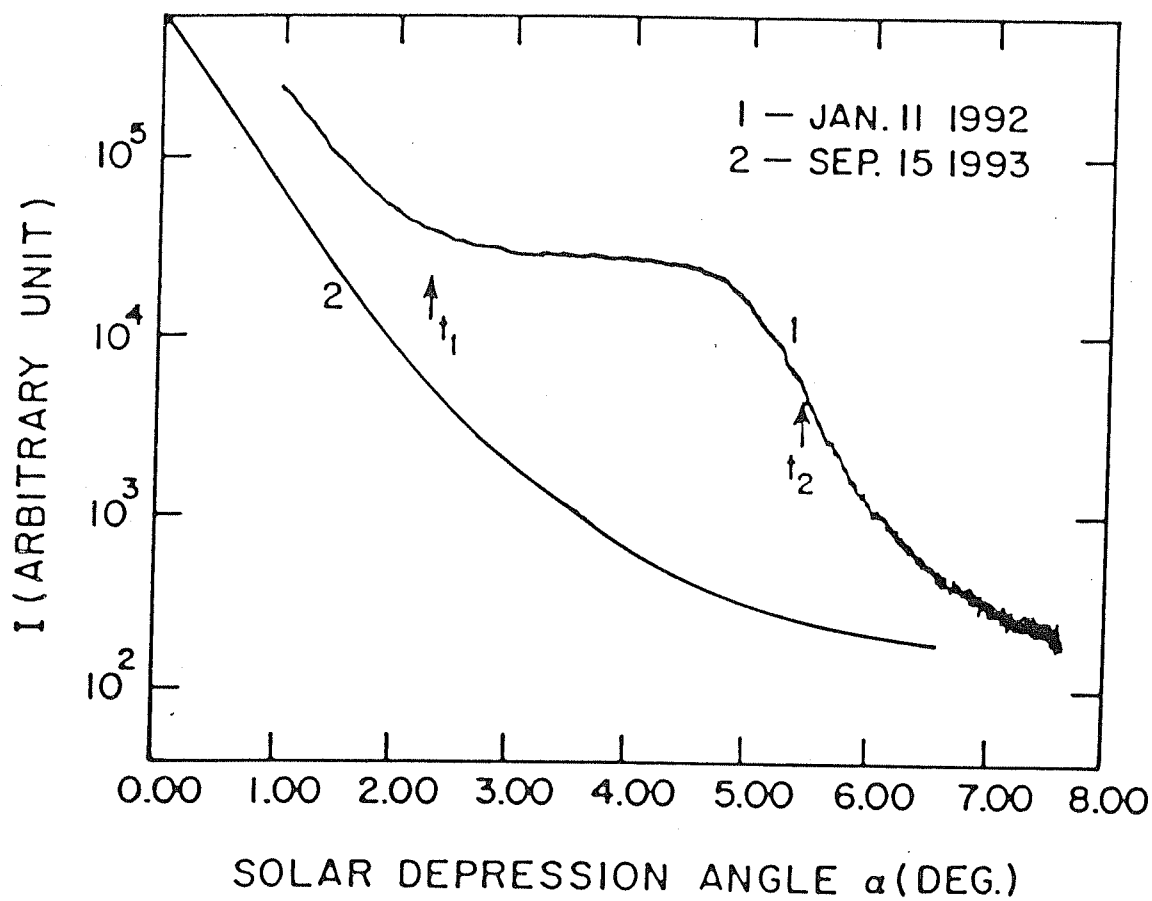


Figure 6.1 Variation of zenith sky twilight brightness with solar depression angle for 11 January 1992 (Curve 1) and 15 September 1993 (curve 2).

This curve (curve 1) shows that a couple of minutes after sunset, the rate of decrease of I with respect to α becomes very slow, remains so for a couple of minutes, then becomes fast and finally merges with the value expected for normal condition. The anomalous behaviour of curve 1 is due to the presence of an aerosol layer produced by the Pinatubo volcano.

To explain the behaviour of curve 1 mentioned above, we have shown the geometry of the solar rays during twilight period in Fig. 6.2. The earth rotates from west to east. It is to be seen from this figure that at sunset ($t = 0$) the aerosol layer at a mean height (\bar{H}) is fully illuminated. With an increase in the solar depression angle below the horizon (α) the normal twilight intensity drops rapidly, but not the contribution of the aerosol layer which continued to be illuminated. The radiation illuminating the aerosol scatterers suffers increasing extinction with time due to its increasingly long passage through the layer. At time t_1 the central light ray has the longest passage through the layer and the extinction is at a maximum, thereby giving rise to a minimum in the observed intensity. Due to the curvature of the earth and the finite thickness of the layer, the total light path through the layer and the extinction are reduced after time t_1 . The observed intensity consequently increases, reaches a plateau and then falls gradually due to the increasing attenuation of light reaching the aerosol scatterers by the lower atmosphere. At time t_2 the shadow of the earth begins cutting off the illumination of the layer from the lower end. At time t_3 , the shadow has completely cut off the layer and the intensity drops to the normal twilight level.

For a normal drop of intensity during twilight, the value of $\frac{-d(\log I)}{d\alpha}$ would be constant with a small change (a few degrees) in the value of α . This has been shown in Fig. 6.3 (curve a). The value of $\frac{-d(\log I)}{d\alpha}$ corresponding to curve 2 shown in Fig. 6.1 comes out to be 0.3 per degree for the change in α from 0° to 2° . However, when

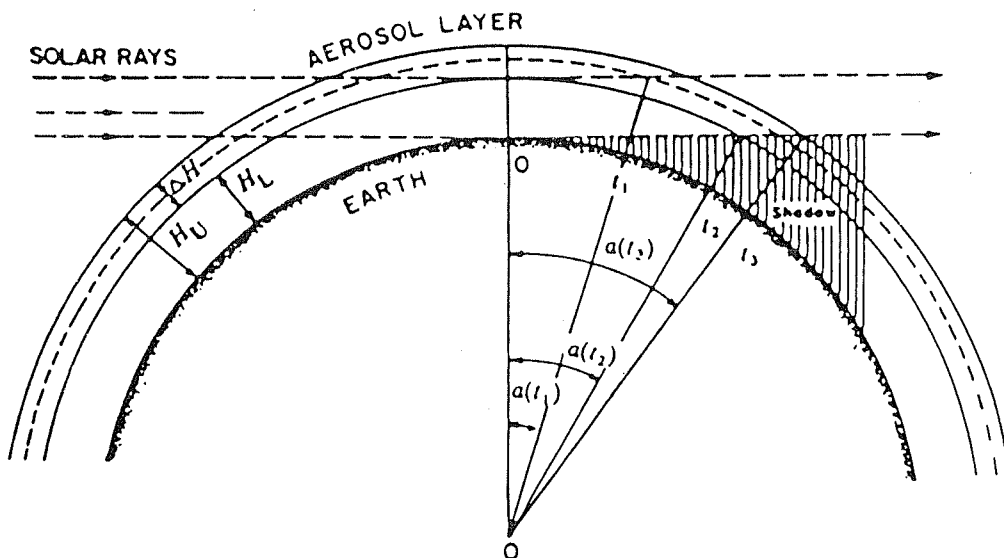


Figure 6.2 Geometry of the situation for zenith observations. Solar rays illuminating the aerosol scatterers suffer attenuation during their passage through the layer (Ashok et al., 1982).

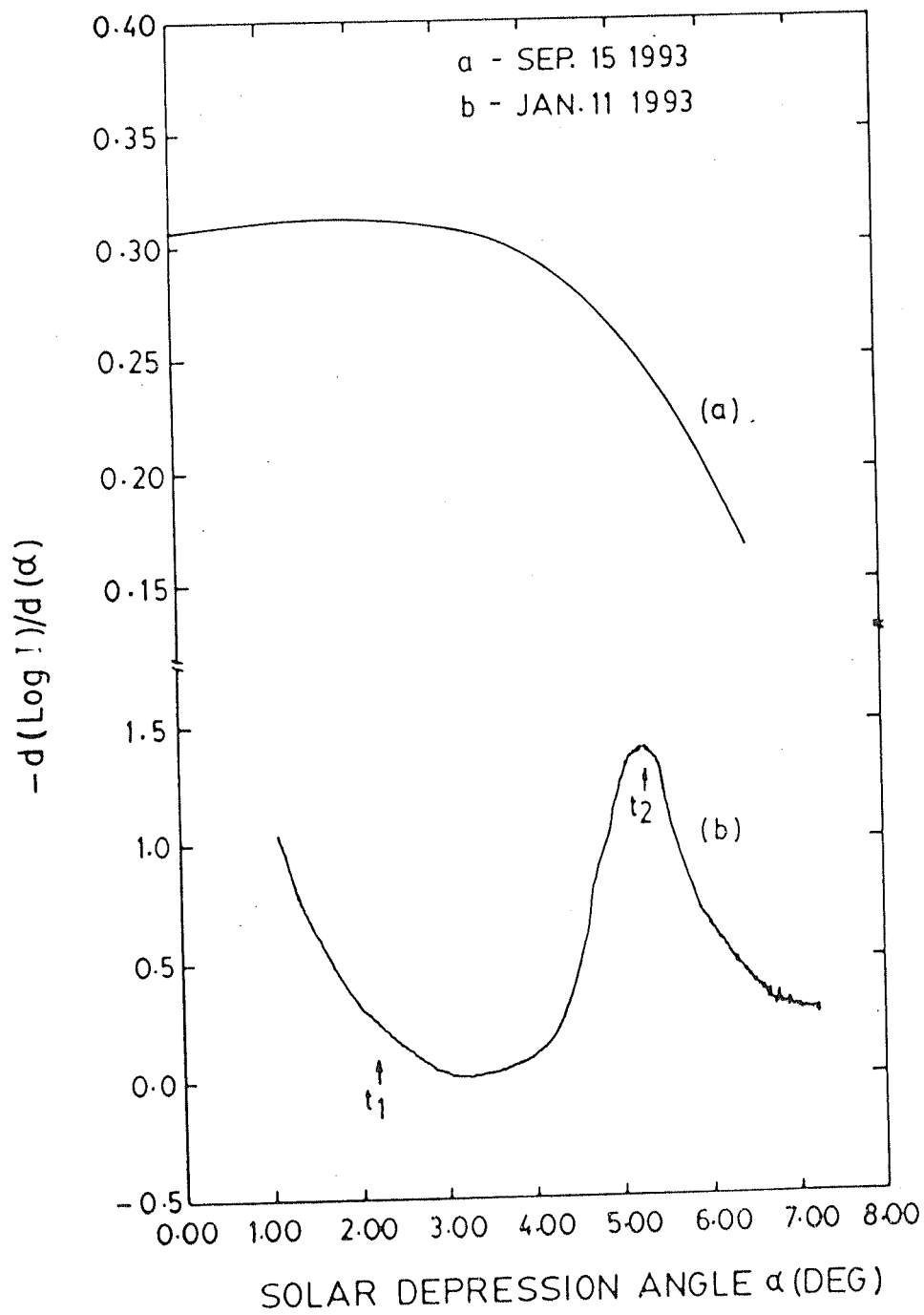


Figure 6.3 Variation of $-\frac{d(\log I)}{d\alpha}$ with solar depression angle (α), (a) for September 15, 1993 and (b) for January 11, 1993

an aerosol layer is present, $\frac{-d(\log I)}{d\alpha}$ does not remain constant with increase of α . Fig. 6.3 (curve b) shows the plot of $\frac{-d(\log I)}{d\alpha}$ vs solar depression angle for 11 January 1992. The positions of time t_1 and t_2 have been marked in this figure. Note the presence of a sharp peak at time t_2 . From the above observations, it is possible to determine several parameters of the aerosol layer, the theory of which have been discussed in the next section.

6.6 Theory

As the solar radiation passes through the earth's atmosphere it undergoes absorption and scattering due to atmospheric species. The main wavelength used for this study is 0.8μ which is almost transparent for water vapour and O_2 absorption [Greenblatt *et al.*, 1990]. The scattered radiation reaching the earth's surface from the zenith direction can be written as :

$$I(t) \propto \int_0^{\Delta H} \exp(-A(x, t)).dx \quad (6.1)$$

where I is the radiation intensity at time t , $A(x, t)$ is the extinction suffered by the radiation at 800 nm, x is the height from the base height of aerosol layer. Suppose that the aerosol layer is a uniform layer with a thickness of ΔH , then the extinction (A) suffered by the light reaching the aerosol can be calculated using the relation :

$$A(x, t) = \begin{aligned} & K.R.([Sin^2\alpha(t) + (2.\frac{\Delta H}{R}).(\frac{1-x}{\Delta H})]^\frac{1}{2} \\ & - 2.[Sin^2\alpha(t) - (2.\frac{\Delta H}{R}).(\frac{x}{\Delta H})]^\frac{1}{2} + Sin\alpha(t)) \\ & \text{for } \alpha(t) > Sin^{-1}(\frac{2.x}{R})^\frac{1}{2} \\ & K.R.([Sin^2\alpha(t) + (2.\frac{\Delta H}{R}).(\frac{1-x}{\Delta H})]^\frac{1}{2} + Sin\alpha(t)) \\ & \text{for } \alpha(t) \leq Sin^{-1}(\frac{2.x}{R})^\frac{1}{2} \end{aligned} \quad (6.2)$$

where K is the extinction per unit length. $A(x,t)$ is the extinction suffered by the radiation reaching the absorber at time t after scattering by an aerosol particle located at a height x above H_L and R is the radius of the earth.

The details of the height calculation have been discussed by *Rozenberg* [1966]. The lower height H_L can be calculated by using the following formula :

$$H_L = R.(1 - \cos\alpha(t_2)). \frac{\cos Z}{\cos\phi} \quad (6.3)$$

where Z is the zenith angle of the observation or look angle and $\phi = (Z - \alpha(t_2))$. $\alpha(t_2)$ is the solar depression angle at time t_2 shown in Fig. 6.3b. Because of the departure in the twilight intensity curve, the shape of the logarithmic gradient of the intensity curve changes. This leads to the formation of a hump in the $\frac{-d(\log I)}{d\alpha}$ vs α curve. t_2 is the time when this hump is formed which can be very easily determined.

The time t_1 , shown in Fig. 6.1 is the time when aerosol layer is fully illuminated by the solar radiation and the radiation reaching the earth's surface is attenuated by the aerosol layer. Thus, the time t_1 in the twilight curve is the indication of transit point of the normal condition to the perturbed condition. By using the time t_1 , the thickness of the aerosol layer has been calculated. The expression for the calculation of aerosol thickness is given by :

$$\Delta H = 2.R.(1 - \cos\alpha(t_1)) \quad (6.4)$$

where $\alpha(t_1)$ is the solar depression angle at time t_1 . ΔH has been calculated only for those days which had a single layer.

To study the time evolution of Pinatubo aerosol layer, a parameter Q has been introduced. It has been defined as

$$Q = \log_{10} \frac{I_{md}}{I_{ss}} \quad (6.5)$$

where I_{md} is the twilight intensity at minimum illumination and I_{ss} is the sunset time twilight intensity. The Q can correspond as an index of aerosol strength and it is proportional to the amount of aerosols present in to the atmosphere. The uncertainty in finding the value of I_{ss} and I_{md} is very small. Therefore the accuracy of Q is very high.

The relation between wavelength and scattered intensity can be represented by the following eqn :

$$I_{scatt} \propto \frac{1}{\lambda^\nu} \quad (6.6)$$

where I_{scatt} is the zenith sky scattered intensity, and ν is the spectral index. The value of the spectral index gives indirectly an idea of the size of the aerosols. To study this aspect, the twilight intensity has been measured at different wavelengths.

6.7 Results and discussion

Pinatubo eruption took place in the month of June 1991. It would have been the best if we could have started taking observations from that month itself. However, at that time the sky was covered by monsoon cloud. The sky became clear in the month of October. Observations were taken from November 1991 to February 1992. The variations of I vs α and $\frac{-d(\log I)}{d\alpha}$ during twilight period have been discussed earlier and shown in Figs. 6.1 and 6.3. The value of α shown in these figures have to be corrected because of the bending of the ray due to refraction in the earth's atmosphere.

6.7.1 Correction due to atmospheric refraction

Fig. 6.4 illustrates the geometry [Shimazaki, 1985] of the ray path near P_i , exaggerating the effect of refraction; the ray path is refracted at P_i with an angle of refraction

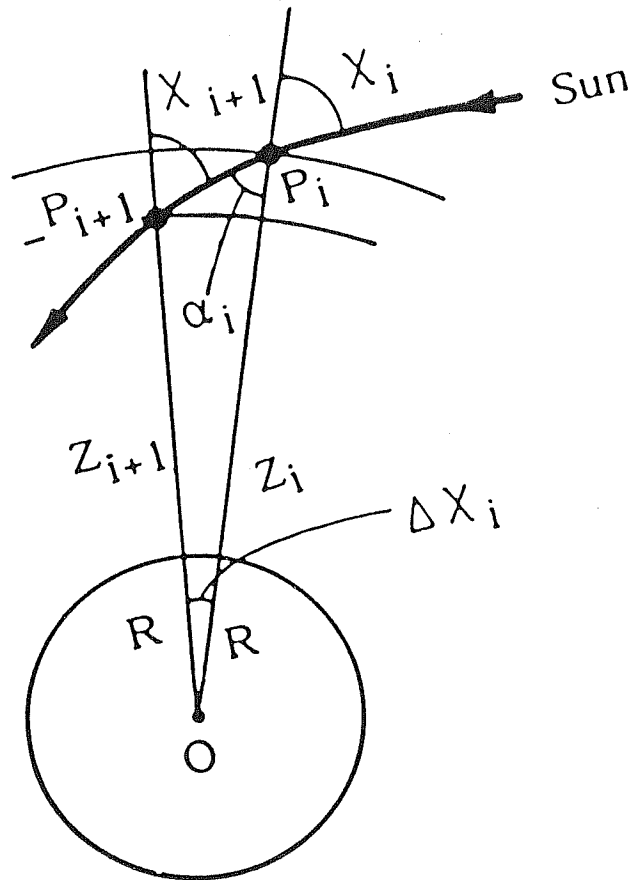


Figure 6.4 A ray path at grazing incidence, P is the observational point (Shimazaki, 1985).

α_i . Applying Snell's law at P_i , we have

$$r_i \cdot \sin \chi_i = r_{i+1} \cdot \sin \alpha_i \quad (6.7)$$

where r_i and r_{i+1} are the mean refractive indices of the layers above P_i and P_{i+1} , respectively. r_i is a function of atmospheric density and wavelength, and it can be written as :

$$r_i^2 = 1 + 2 \cdot (r_o - 1) \cdot \frac{\rho_i}{\rho_o} \quad (6.8)$$

where ρ_i is the air density and the suffix o indicates the value at normal temperature and pressure on the ground surface. r_o is a function of wavelength and its approximate value for the range of $\lambda = 0.2 - 1.35 \mu\text{m}$ is given by [Shimazaki, 1985] :

$$r_o = 1 + 6.4328 \cdot 10^{-5} + \frac{2.94981 \cdot 10^{-2}}{146 - \frac{1}{\lambda^2}} + \frac{2.554 \cdot 10^{-4}}{41 - \frac{1}{\lambda^2}} \quad (6.9)$$

The path length ΔS_i ($=P_i P_{i+1}$) at P_i is related to the angle $\Delta \chi_i$ subtended at the center of the earth by the simple geometrical relation :

$$\frac{\Delta S_i}{\sin(\Delta \chi_i)} = \frac{R + Z_i}{\sin(\chi_{i+1})} = \frac{R + Z_{i+1}}{\sin(\alpha_i)} \quad (6.10)$$

where R is the earth's radius and Z_i is the height of the point P_i from the earth's surface. Using eqn. 6.10, correction has been applied to the solar depression angle values of Figs. 6.1 and 6.3.

6.7.2 Height of the aerosol layer

Lower height of the aerosol layer has been determined by using eqn. 6.3. The value of $\alpha(t_2)$ has been obtained from the plot of $\frac{-d(\log I)}{d\alpha}$ vs α curve. It corresponds to the value of α where a hump is formed in the $\frac{-d(\log I)}{d\alpha}$ vs α curve. The values of H_L thus obtained are shown in Fig. 6.5 for all the days of observation. It appears from this figure that the lower height of the aerosol layer lies between 18 and 25 km

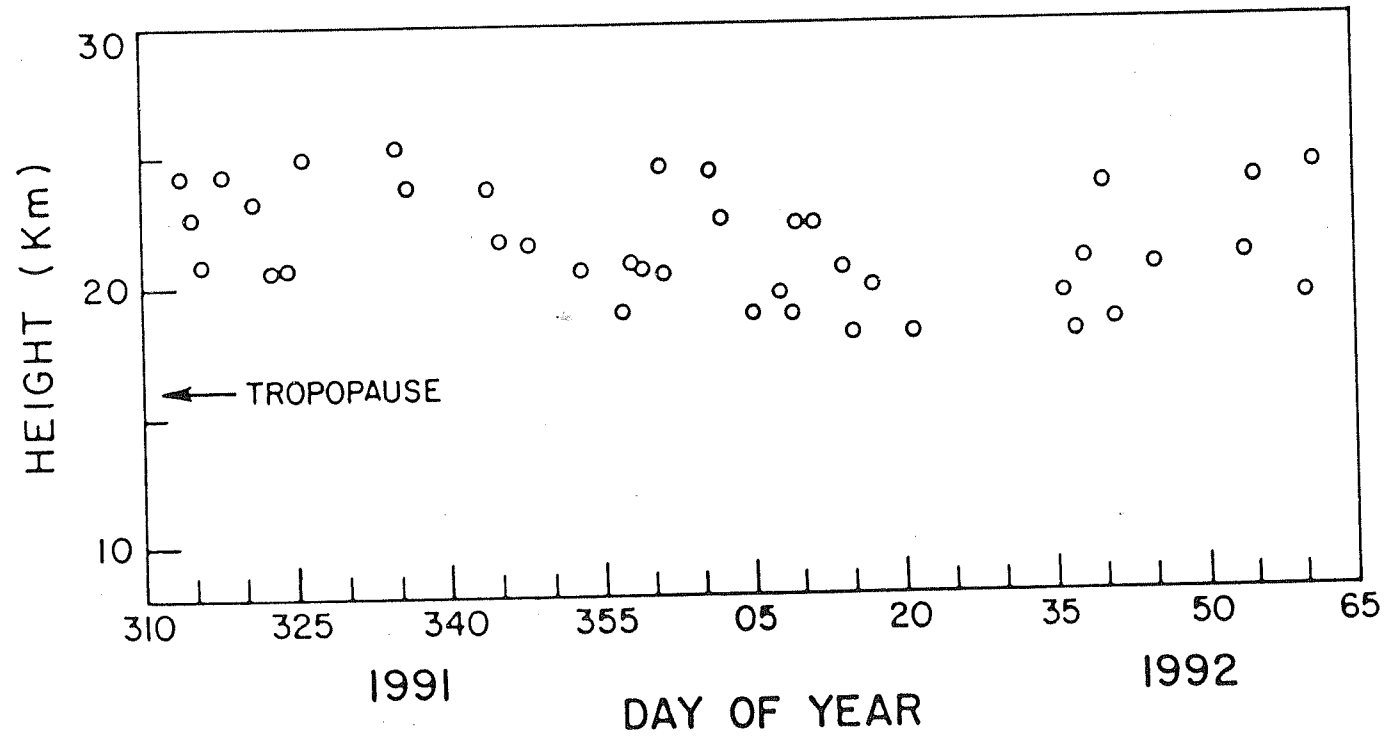


Figure 6.5 Height of the lower end of the aerosol layer (H_L).

with a mean value of 21.5 km. SAGE-II satellite measurements of the Mt. Pinatubo eruption cloud during June, July and early August 1991 show that the aerosols in the tropics reach as high as 29 km with most of the clouds lying between 20 and 25 km [McCormick and Veiga, 1992]. Ground based Lidar data of Mauna Loa showed that the height of the Pinatubo aerosol layer was at about 20-25 km in August 1991 [Deffoor *et al.*, 1992]. Ashok *et al.* [1984] reported this height to be around 18 ± 2 km over a period of one year after the El Chichón eruption.

6.7.3 The aerosol layer thickness

The thickness of the aerosol layer has been calculated by using $\alpha(t_1)$ and the eqn. 6.4. The values thus obtained are shown in Fig. 6.6. The value of $\alpha(t_1)$ can be determined with an accuracy of $\pm 0.3^\circ$. At this time the signal was high. Also the interference due to multiple scattering was relatively low. It can be seen from Fig. 6.6 that during the end of November and beginning of December 1991 the thickness of the aerosol layer was about 12 km. The value of this thickness then started decreasing as the days passed. The layer thickness became minimum (about 6.5 km) in the month of January 1992. After January 1992, again there was an increase in the value of layer thickness which became about 12 km in the last week of February 1992. In comparison, Ashok *et al.* [1982] found after El Chichón eruption, the value of ΔH to lie between 8 and 9.4 km in the month of June 1982.

6.7.4 Aerosol strength variation

To study the time evolution of Pinatubo aerosol layer, a parameter Q has been introduced. It has been defined as

$$Q = \log_{10} \frac{I_{md}}{I_{ss}} \quad (6.11)$$

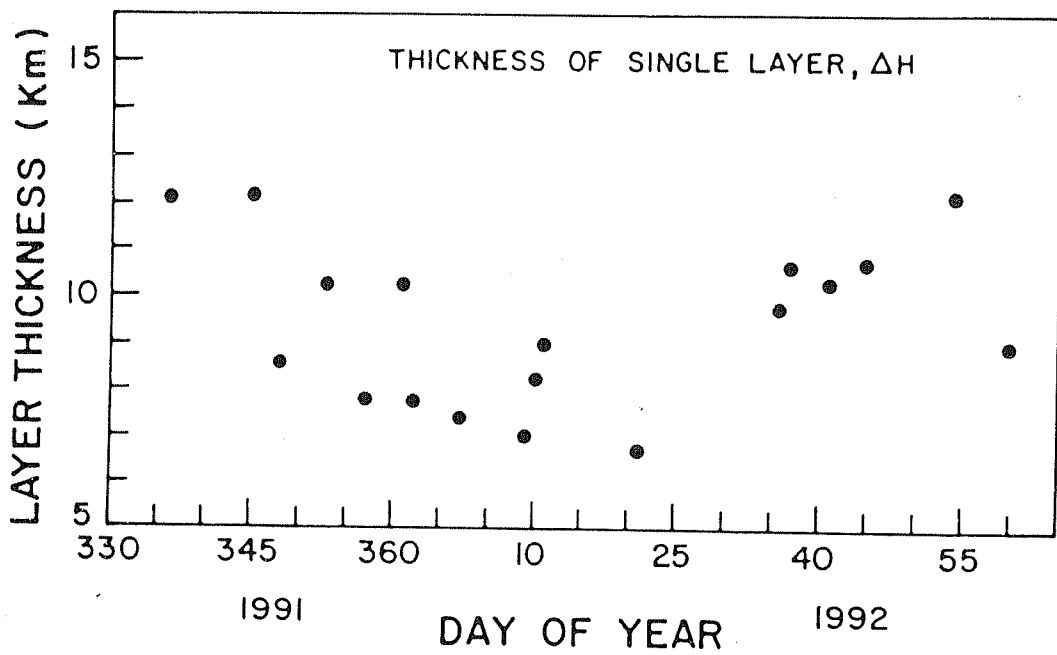


Figure 6.6 Variation of thickness of single layer with days.

where I_{md} is the twilight intensity at minimum illumination and I_{ss} is the sunset time twilight intensity. Q can be considered as an indirect representative of the total mass of aerosols. The values of Q thus obtained since November 1991 have been plotted in Fig. 6.7. For the month of November 1991 the average value of Q was about -0.70. This value increased with the passage of the days. The value of Q became maximum (about -0.45) in the last week of December 1991 and the first week of January 1992 and then started decreasing with the passage of the days. After volcanic eruption, in the beginning, Q is expected to be high, which should slowly decrease with the passage of time as observed by *Ashok et al.* [1982] after El Chichón eruption. The scatter in Q noticed in Fig. 6.7 is due to the presence of multiple aerosol layers. The decreasing trend of Q shows a decreasing trend of total aerosol mass. The anomalous behaviour of Q observed by us agrees with the behaviour of optical depth monitored by AVHRR and SAGE-II [*McCormick and Veiga*, 1992; *Stowe et al.*, 1992]. Q becoming maximum in the last week of December 1991 and the first week of January 1992 after Pinatubo eruption is due to the SO_2 conversion and particle growth time.

The accuracy of Q will depend on how accurately one can determine the value of I_{md} and I_{ss} . There is no difficulty in finding out the value of I_{ss} with good accuracy. At minimum illumination condition, the signal strength is relatively high. Hence the value of I_{md} can also be determined with good accuracy. This condition occurs around 3° solar depression angle. At this depression angle, the effect of multiple scattering is much less than that of single scattering. Uncertainty in Q due to the local meteorological condition or presence of cirrus cloud is further reduced because this is a ratio. Total uncertainty in Q determination is less than 10%.

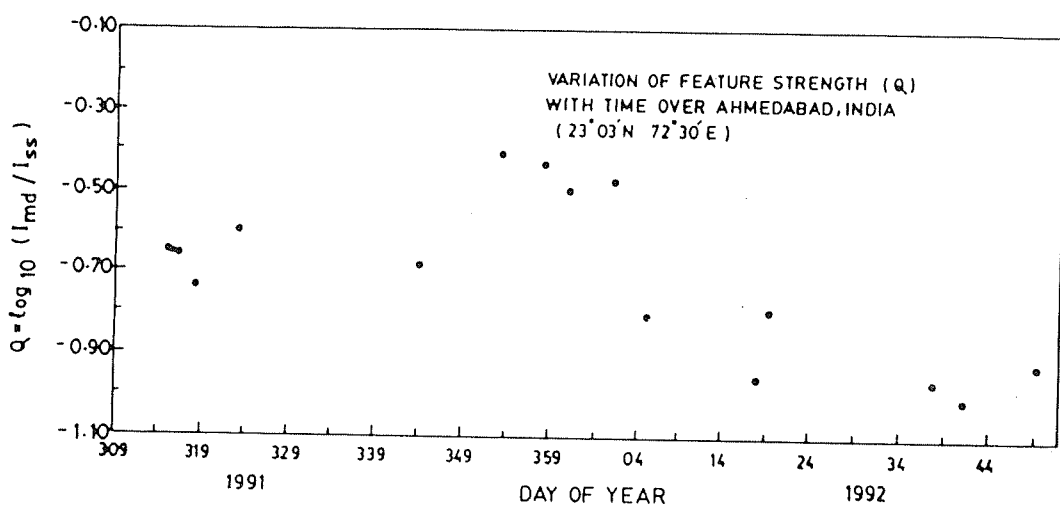


Figure 6.7 Variation of aerosol feature strength index Q with days.

6.7.5 Spectral response of twilight intensity

Twilight intensity curve has also been obtained for different wavelengths. Fig. 6.8 shows a plot for 3 days in February 1992 for wavelengths viz. 800, 700 and 650 nm. In this figure curve a corresponds to 09 February 1992 at 800 nm wavelength, curve b was obtained on 14 February 1992 at 700 nm wavelength and curve c corresponds to 17 February 1992 at 650 nm wavelength. These curves were obtained for the same sky conditions. From this figure one can see that as the wavelength decreases, the degree of departure from the normal twilight intensity curve also decreases. Using these curves and the property that the scattered intensity is proportional to $\lambda^{-\nu}$, where ν is the spectral index, the value of ν has been calculated at the time when the scattered twilight intensity is minimum. The value of ν thus obtained comes out to be in the range of 0.9 to 1.2. This value of ν indicates that the radiation received at that time comes predominantly by scattering from the aerosol layer.

6.7.6 Zenith sky intensity at different look angle

In addition to zenith direction, observations have been taken for few days at different look angles. Fig. 6.9 shows the variation of twilight intensity with solar zenith angle at the same wavelength for two look angles -zenith and off-zenith by 25° . These observations have been taken at an interval of 4 days. The departure time from the normal in the twilight intensity curve which has been taken at 0° zenith angle is less compared to the departure from the normal taken at look angle 25° away from the zenith. Also there is a broadening in the twilight intensity curve. These are due to the variation in the exposure time of the atmosphere at specific heights. *Rozenberg* [1966] has made a theoretical calculation of exposure time at different look angles during twilight period. He shows that If the look angle is $\pm 10^\circ$ with respect to zenith, the exposure time up to about 80 km does not change significantly. But

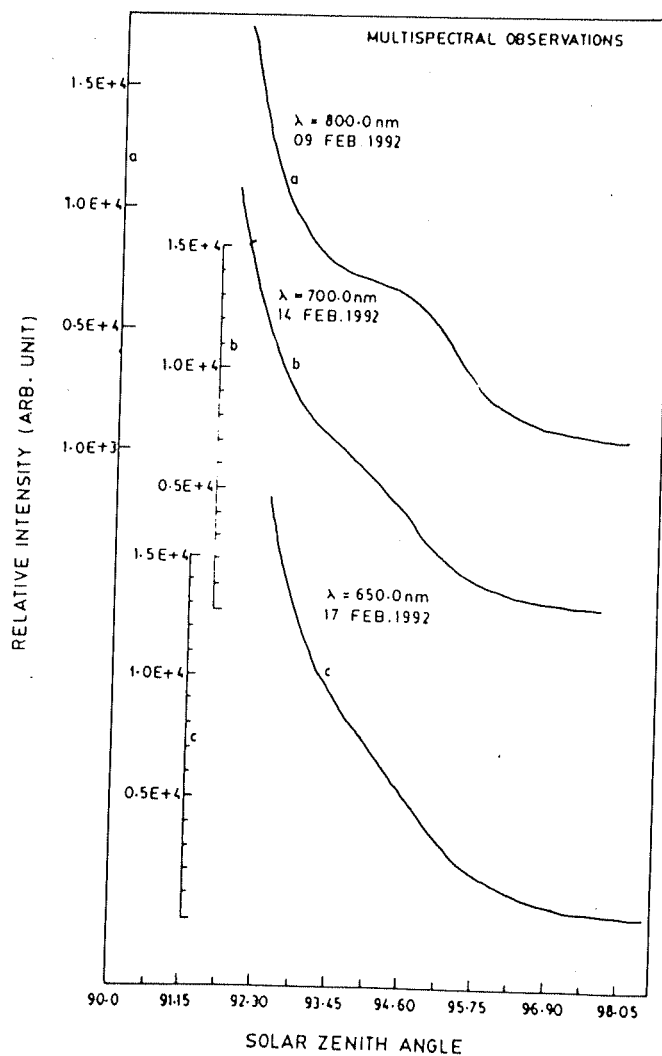


Figure 6.8 Twilight intensity variation with solar zenith angle at 800, 700 and 650 nm.

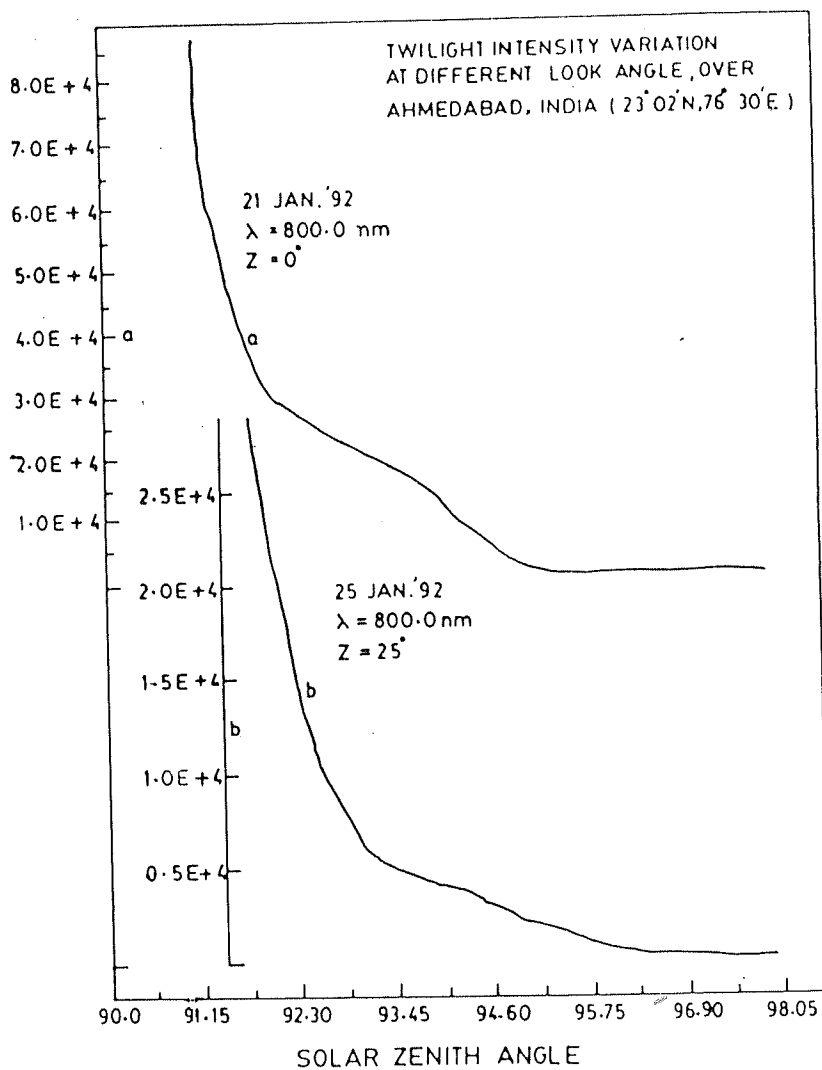


Figure 6.9 Twilight intensity variation with solar zenith angle at two look angles - zenith ($z=0^\circ$) and off-zenith ($z = 25^\circ$).

when the look angle becomes greater than $\pm 10^\circ$ with respect to zenith, the effect of exposure time becomes significant.

6.7.7 Multiple aerosol layer

Analysis of data shows the presence of more than one peak on some days. An example is shown in the Fig. 6.10. In this figure twilight intensity curve has been plotted in the top panel and the logarithmic gradient of twilight intensity has been plotted in the bottom panel against solar depression angle for 10 January 1992. It can be seen from this figure, both from top and bottom curves, that the departure from normal in the twilight intensity curve has taken place twice - around 4° and 5.3° solar depression angles. These correspond to aerosol lower heights, H_L of 11.9 km and 22.4 km after applying refraction correction. One may assume that the number of departures of twilight intensity from the normal, or the number of peaks in the $\frac{-d(\log I)}{d\alpha}$ vs α curve is equal to the number of layers present in the atmosphere. If such were the case then sometimes such peaks were seen much below the tropopause, as low as 6 km. We have, however, ignored them because these could have been due to invisible cirrus cloud or water vapour cloud. Sometimes we have also seen departures at values of α much greater than 5° , which correspond to altitudes higher than 25 km. But these could have been due to the effect of multiple scattering and hence we have ignored them. *Winker and Osborn* [1992 a,b] from airborne lidar observations reported that at times there were many thin, distinct layers in this region, while at other times the layers merged together in various combinations. Both depolarizing and non-depolarizing distinct layers were observed between 17 and 26 km altitudes [*Winker and Osborn*, 1992a,b]. The tropopause was located at about 16 km in their case. Such type of multiple layers were also observed after El Chichón volcanic eruption by *Hofmann* [1987] using balloon-borne particle counter technique. According to him, bigger size particles were present at higher altitude (between 20 and 30 km) region

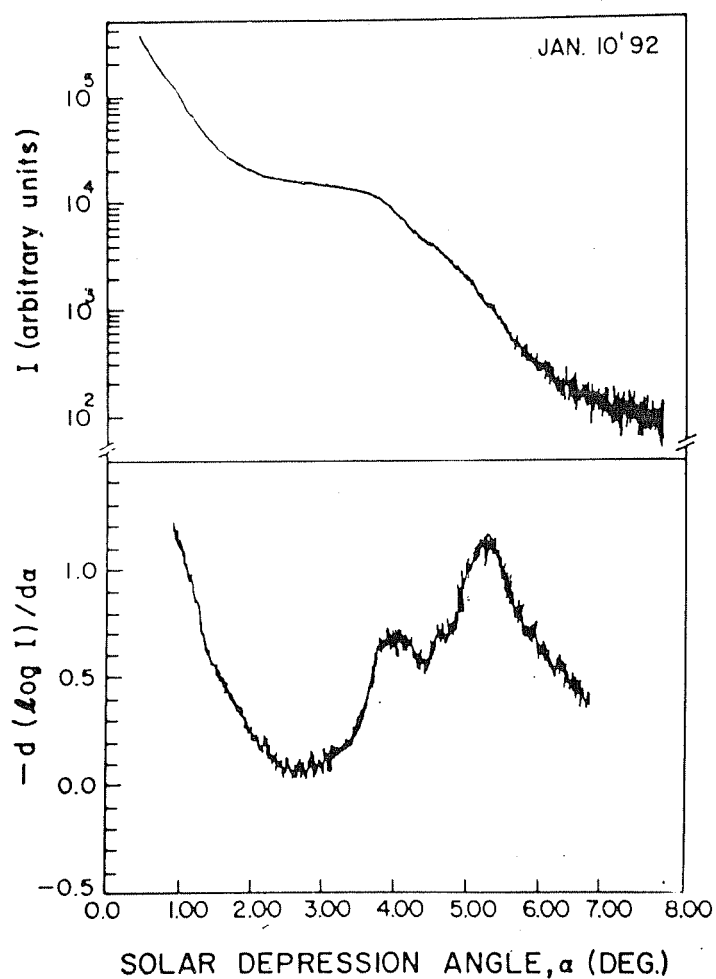


Figure 6.10 Variation of twilight intensity, I , with solar depression angle, α (top panel) and variation of $-d(\log I)/d\alpha$ with solar depression angle, α (bottom panel) for January 10, 1992. An example of double aerosol layers.

and small size particles were present at lower altitudes. Due to gravitational force the large size particles started precipitating downward and merged with the lower layer - finally forming a single layer. Consistent with our findings, *Stowe et al.* [1992] from the NOAA/11 AVHRR data reported that small patches of aerosol broke off from the tropical main layer and moved to higher latitudes, particularly in northern hemisphere. Also they noticed a 16-18 day wave in the variability of aerosol optical thickness. At mid-latitude, *Jäger* [1992] also observed double layered aerosol structure in August 1991 by Lidar system at Garmisch-Partenkirchen (47.5°N , 11.1°E). He related them to the prevailing transport pattern of northern mid-latitude.

Some typical observations of twilight intensity taken on different days and different months have been shown in Fig. 6.11. In the month of November 1991 on more than 50% of the days of observations, multiple layers were seen. Curve f is for multiple layers. Curves e and d show the twilight intensity for 2 and 14 December 1991. All these three curves correspond to 751.8 nm wavelength. In these three curves fluctuations in intensity are seen. These fluctuations could be due to the presence of multiple layers. Curves c, b, and a show the twilight intensity for 27 December 1991, 11 January 1992, and 24 February 1992. These three curves were taken at 800 nm and all of them correspond to single layers. Also, an examination of curves c, b and a shows that the departure from normal in the twilight intensity decreases as the days pass on.

6.8 Uncertainty in results

In this work total aerosol mass variation with time, aerosol layer height, strength of aerosols and total thickness in the stratospheric region, have been studied. All these parameters have been calculated by using the twilight zenith sky intensity variation with solar depression angle. Presence of multiple aerosol layer in the atmosphere can

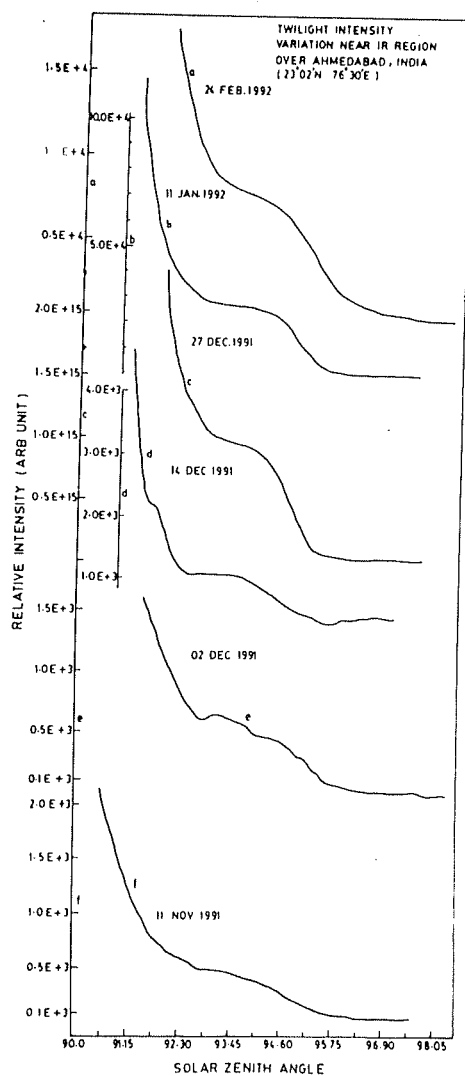


Figure 6.11 Twilight zenith sky intensity curves for different days of observation plotted against solar zenith angle.

cause uncertainty in our results. But multiple scattering becomes important after $\alpha(t_2)$ when the earth's shadow starts cutting off the illumination of the aerosol layers from the lower end. But the value of $\alpha(t)$ used in our calculation are just up to $\alpha(t_2)$ or less. So the effect of multiple scattering can be ignored.

Uncertainty in solar depression angle can cause uncertainty in our results. Solar depression angle has been calculated by using the right ascension, declination, and sidereal time. The starting time of observation was set by the standard clock available through radio signal. Since all the observations have been taken by using the software developed in the laboratory, only starting time of the observation had to be setup manually and other times were recorded through quartz oscillator fixed with personal computer. The error in the solar depression angle calculation comes from the time setting in the beginning and maximum error is less than ± 1 minute and this variation in the time would change the height by less than 1.5 km.

The uncertainty in the height can be understood as follows :

$$H_L = R.(1 - \cos\alpha(t_2)). \frac{\cos Z}{\cos(Z - \alpha(t_2))}$$

A derivative of this equation gives

$$\frac{\delta H_L}{H_L} = \frac{\delta R}{R} + \frac{\delta \cos\alpha(t_2)}{\cos\alpha(t_2)} + \frac{\delta \cos Z}{\cos Z} + \frac{\delta \cos(Z - \alpha(t_2))}{\cos(Z - \alpha(t_2))} \quad (6.12)$$

The reflecting mirror which is kept at 45° in front of monochromator leads to maximum error. Zenith sky and off-zenith sky intensity calculation has been done by Rozenberg [1966] and they found that the variation in $\pm 5^\circ$ off zenith direction leads to the change in height range by about 3 km. Therefore, to minimize experimental error, position of the reflecting mirror has been kept at 45° as accurately as possible. Substituting all the values in eqn. 6.12, the maximum possible error in the height $(\frac{\delta H_L}{H_L} \times 100)\%$ comes out to be 15.8%.

The uncertainty in the layer thickness ΔH can be derived as follows :

$$\Delta H = 2.R.(1 - \text{Cos}\alpha(t_1))$$

Taking a derivative of ΔH one gets

$$\frac{\delta \Delta H}{\Delta H} = \frac{\delta R}{R} + \frac{\delta \text{Cos}\alpha(t_1)}{\text{Cos}\alpha(t_1)} \quad (6.13)$$

Substituting the relevant values in eqn. 6.13, one gets the maximum possible error in aerosol thickness as $(\frac{\delta \Delta H}{\Delta H} \times 100)\% = 4.0\%$. In this expression, the uncertainty is mainly due to the variation in $\alpha(t_1)$. But in the present experiment when single layer is present uncertainty in $\alpha(t_1)$ is very less.

Uncertainty in the aerosol strength can be evaluated as follows :

$$Q = \log(I_{md}/I_{ss}) = \log I_{md} - \log I_{ss}$$

Taking a derivative of this eqn. one gets

$$\frac{\delta Q}{Q} = \frac{\delta(\log I_{md})}{\log I_{md}} + \frac{\delta(\log I_{ss})}{\log I_{ss}} \quad (6.14)$$

After substituting the values of relevant parameters in eqn. 6.14, the maximum possible error comes out to be $(\frac{\delta Q}{Q} \times 100)\% = 6.0\%$.

It appears from above that the maximum uncertainty in this type of work could be as large as 16%. But in our present work this uncertainty was much less than 16%.

Chapter 7

Concluding Remarks

7.1 Achievements

In this thesis some studies have been made on the low latitude middle atmosphere. The studies concentrate on minor neutral species. Both theoretical and experimental studies have been carried out. Experimental studies have been conducted by a ground-based technique.

The minor neutral species that have been measured by us are NO_2 and NO_3 . They belong to the NO_x group of species which catalytically destroy ozone in the stratosphere. We have done these measurements by a ground-based visible absorption spectroscopy technique. For NO_2 , scattered zenith twilight intensity has been measured. This type of measurement has been made by several groups at mid and high latitude stations. But at low latitude data are meagre. In that direction our observed data will be of great contribution to the global data set.

Our main findings on NO_2 are as follows. We find that its averaged AM / PM winter vertical column density is about $2 \times 10^{15} \text{ cm}^{-2}$. This value is about a factor of two lower than the values reported by other workers for low latitude zone. The

evening averaged value of NO_2 is about 1.25 times higher than the morning averaged value. We also found a weak positive correlation (0.7 correlation coefficient) between NO_2 and O_3 . No change in slant column abundance has been noticed after Pinatubo volcanic eruption.

In NO_3 we did not get any consistent results throughout the course of our measurements. At Ahmedabad our measured values of vertical NO_3 column lie between 1 and $5 \times 10^{14} \text{ cm}^{-2}$ in February - March 1991. In December 1991 on the average our NO_3 values are found about a factor of two higher than the February - March values. The above mentioned observations were taken with low lunar zenith angle spectrum as the background spectrum. In January 1992, some measurements were made using large zenith angle solar spectrum as background spectrum. Values of NO_3 obtained this time lie in the range of 1.9 to $2.5 \times 10^{15} \text{ cm}^{-2}$. These values are higher than the December 1991 values by a factor of about two. December 1991 and January 1992 values can not differ by such a large factor.

Since in NO_3 measurements we used direct moon as a source of light, tropospheric contamination was likely. We took our instrumental setup to Gurushikhar, a hill station about 200 km north of Ahmedabad and 1.8 km above the mean sea level. The variability of slant column at Gurushikhar appears to be nearly the same as what has been observed at Ahmedabad. For Gurushikhar we have taken solar spectrum at higher zenith angle as the background spectrum. We find that Gurushikhar NO_3 values do not differ significantly from the Ahmedabad values of February - March, but are lower than the values obtained in the month of December 1991 and January 1992. Gurushikhar being clean sunrise time variation of NO_3 has also been studied here. We find that NO_3 decreases as the sun rises from a value of 4×10^{15} to $6 \times 10^{14} \text{ cm}^{-2}$, after which signal to noise ratio goes beyond the lower limit of the detection of the instrument.

To reproduce the features of NO_2 and NO_3 observed by us an 1 D steady state model study has been made. It has been found that the chemistry of NO_2 and NO_3 is highly sensitive to NO density and temperature profile. We have carefully chosen the values of these two parameters. We find that our observed NO_2 column density agrees with our theoretical daytime NO_2 value. The calculated vertical column abundance of NO_3 is found to be $2 \times 10^{13} \text{ cm}^{-2}$. This is about an order of magnitude less than our observed NO_3 values.

Another species whose vertical distribution has been calculated along with NO_2 and NO_3 is N_2O_5 . By decreasing NO density during nighttime by six orders of magnitude, N_2O_5 total column density is found to be $4.4 \times 10^{14} \text{ cm}^{-2}$. Daytime N_2O_5 calculated column density is $2.33 \times 10^{14} \text{ cm}^{-2}$ which is marginally less than the nighttime N_2O_5 column density after assuming a decrease in NO by six orders of magnitude. Due to the variation in production and loss rate of NO_2 and NO_3 from day to night, N_2O_5 density at night should be about four orders of magnitude larger than the daytime.

Although, we have calculation for steady state condition, the results are to be taken with a little caution. NO_2 at noon reaches a steady state value and hence a steady state calculation of NO_3 and N_2O_5 during day are probably exact. Also NO density during day is reasonably known. At night, however NO is rapidly converted into NO_2 . Then the NO_2 is also quickly converted into NO_3 and N_2O_5 which then decreases throughout the night. Thus a condition of steady state is probably a too simplified an approach to calculate NO_3 and N_2O_5 distribution during nighttime. It could be that in most of the cases, probably by midnight the production is cutoff. This problem, however, can be confirmed, provided we have an accurate nighttime measured profile of NO.

A major volcanic eruption took place in June 1991 from Mt. Pinatubo, Philippines. In this natural phenomenon huge amount of SO_2 was injected into the stratosphere which get converted into $\text{H}_2\text{SO}_4/\text{H}_2\text{O}$ aerosols within a couple of weeks. Normally after sunset twilight intensity decreases exponentially with increase of solar depression angle. However, due to an additional aerosol loading after volcanic eruption twilight radiation intensity variation becomes anomalous. Using this anomalous twilight intensity variation, physical properties of this additional aerosol have been studied. Results are as follows : [1] Height of the aerosol layer was found to be varying. Lower height of the aerosol layer was found to lie between 18 and 25 km. Sometimes another aerosol layer was also found. [2] The thickness of the aerosol layer has been found to lie between ~ 6 km and ~ 12 km. [3] Aerosol strength (Q) which is proportional to total stratospheric aerosol mass, normally starts decreasing after the eruption. But this time it has been found to increase till December 1991 and then start decrease. This increase in Q might be due to gas to particle conversion, which took about six months this time to be completed after eruption.

7.2 Scope and suggestions for future work

[1] For the measurement of NO_2 a background spectrum is needed. In the present study NO_2 have been derived using a constant background spectrum. However this background spectrum is likely to change from day to day and this could be stratospheric or tropospheric or both. This might also affect the scattering height, hence unless this is taken into consideration, real variability of NO_2 can not be ascertained. Hence it is proposed that the variability of background spectrum on the overall variability of NO_2 be examined.

[2] Vertical distribution of NO_2 has been obtained from slant column density by dividing this value by appropriate airmass factor. This value depends on the vertical

distribution of NO_2 . Hence an attempt should be made insitu by balloon to measure NO_2 vertical distribution and calculate the airmass factor. Also the vertical distribution should be derived by measuring zenith sky intensity between 85° and 95° solar zenith angle for the calculation of airmass factor.

[3] NO_3 measurements are very difficult because signal to noise ratio is very low. We have used a Lock-in amplifier to improve the value of this ratio. However, we find a lot of fluctuations in the day to day NO_3 value, whether this is a measurement problem or real variability has to be ascertained. We propose to replace the Lock-in part by diode array detector. However, since NO_3 production is highly temperature dependent, fluctuation in NO_3 could also be real. One important aspect we have noticed in NO_3 when we used lower lunar zenith angle spectrum as background and higher solar zenith angle as background spectrum is that, in the latter case, the value of NO_3 is found to be more by a factor of about two. This needs further careful study.

[4] Vertical distribution of NO_3 has been obtained from slant column density by dividing this value by appropriate airmass factor. This value depends on the vertical distribution of NO_3 . Hence an attempt should be made insitu by balloon to measure NO_3 vertical distribution and calculate the airmass factor. Besides NO_3 variation during dawn can also be used for the derivation of NO_3 vertical distribution which would be useful for calculating NO_3 airmass factor.

[5] Nitric oxide plays a crucial role in the chemistry of NO_2 and NO_3 . In the stratosphere as such its profile is not accurately known. Besides, it has a large day to night (decrease) variation. While explaining our observed NO_2 and NO_3 values theoretically we found that NO density profile during daytime and its rate of decrease after sunset play a very crucial role at least in 1 D model study. Any values of NO_2 and NO_3 are reproducible by playing with these two parameters. Hence we need to have a knowledge of these two parameters for explaining the observed values of NO_2

and NO_3 .

[6] Additional aerosols are formed after volcanic eruption in the stratosphere. We have studied the physical characteristics of aerosols produced after the volcanic eruption of Mt. Pinatubo. The technique used in this study is similar to *Ashok et al.* [1982, 1984] who have derived physical parameters of aerosols produced from ElChichon volcanic eruption. Some of the parameters such as aerosol strength (Q), aerosol thickness (ΔH), and layer height have been calculated by assuming single scattered radiation received on the surface during twilight period, but multiple scattering contribution is also significant during the same time period. Multiple scattering contribution of zenith sky intensity during twilight period can be calculated by using Monte - Carlo radiative transfer model. Such type of model can be used to calculate the multiple scattering contribution in the twilight zenith sky intensity observed over Ahmedabad.

In the present thesis, we have referred to the entire treatment to the atmosphere of the earth, the only planet for which some ground-based observational data are available. However these processes occur on every planet having an atmosphere, where physical processes are governed by essentially the same factors as on earth. Thus the present method and technique can be regarded as preparatory to a study of other planetary atmospheres.

References

1. Ackerman, M., and C. Muller, Stratospheric nitrogen dioxide from infrared absorption spectra, *Nature*, **240**, 300 - 301, 1972.
2. Ackerman, M., and C. Muller, Stratospheric methane and nitrogen dioxide from infrared spectra, *Pure Appl. Geophys.*, **106 - 108**, 1325 - 1335, 1973.
3. Ackerman, M., J. C. Fontanella, D. Frimout, A. Girard, N. Louisnard, and C. Muller, Simultaneous measurements of NO and NO₂ in the stratosphere, *Planet. Space. Sci.*, **23**, 651 - 660, 1975.
4. Ackerman, M., In situ measurements of middle atmosphere composition, *J. Atmos. Terrs. Phys.*, **41**, 723-733, 1979.
5. Allen, M., and M. L. Delitsky, Stratospheric NO, NO₂, and N₂O₅ : A comparison of model results with spacelab 3 Atmospheric Trace Molecule Spectroscopy (ATMOS) measurements, *J. Geophys. Res.*, **95**, 14,077 - 14,082, 1990.
6. Amoruso, A., M. Cacciani, A. Di Sarra, and G. Fiocco, Absorption cross-sections of ozone in the 590- to 610 - nm region at T=230 K and T= 299 K, *J. Geophys. Res.*, **95**, 20,565-20,568, 1990.
7. Anderson, J. G., The absolute concentration of O(³P) in the earth's stratosphere, *Geophys. Res. Lett.*, **2**, 231 - 234, 1975.
8. Ashburn, E. V., The density of the upper atmosphere and the brightness of the twilight sky, *J. Geophys. Res.*, **57**, 85-93, 1952.
9. Ashok, N. M., H. C. Bhatt, T. Chandrasekhar, and J. N. Desai, Twilight IR brightening over India due to El Chichón's eruption in Mexico, *Nature*,

300, 620 - 621, 1982.

10. Ashok, N. M., H. C. Bhatt, T. Chandrasekhar, J. N. Desai, and D. B. Vaidya, Twilight optical studies of the El Chichón volcanic dust over Ahmedabad, India, *J. Atmos. Terr. Phys.*, **46**, 411 - 418, 1984.
11. Barnett, J. J., Satellite measurements of middle atmosphere temperature structure, *Roy. Soc. Lon. Phil. Trans.*, **A296**, 41 - 57, 1980.
12. Barnett, J. J., and M. Corney, Temperature comparisons between the NIMBUS 7 SAMS, Rocket / Radiosondes and the NOAA 6 SSU, *J. Geophys. Res.*, **89**, 5294 - 5302, 1984.
13. Barth, C. A., R. W. Sanders, R. J. Thomas, G. E. Thomas, B. M. Jakosky, and R. A. West, Formation of the El Chichón aerosol cloud, *Geophys. Res. Lett.*, **10**, 993-996, 1983.
14. Barton, I. J., A. J. Prata, I. G. Watterson, and S. A. Young, Identification of the Mount Hudson volcanic cloud over Se Australia, *Geophys. Res. Lett.*, **19**, 1211-1214, 1992.
15. Bass, A. M., A. E. Ledford, Jr., and A. H. Laufer, Extinction coefficients of NO_2 and N_2O_4 , *J. Res. Nat. Bur. Stand., Sect. A*, **80**, 143, 1976.
16. Baulch, D. L., R. A. Cox, R. F. Hampson, Jr., J. A. Kerr, J. Troe, and R. T. Watson, Evaluated kinetic and photochemical data for atmospheric chemistry, *J. Phys. Chem. Ref. Data*, **9**, 295 - 471, 1980.
17. Bhartia, P. K., K. F. Klenk, A. J. Fleig, C. G. Wellemeyer, and D. Gordon, Intercomparison of NIMBUS 7 solar backscattered ultraviolet ozone profiles with rocket, balloon and umkehr profiles, *J. Geophys. Res.*, **89**, 5227 - 5238, 1984.
18. Bhonde, S. D., P. Mehra, S. Bose, A. L. Londhe, and D. B. Jadhav, Simultaneous measurements of low latitude NO_2 and O_3 from zenith sky observations in visible region, *Indian J. of Radio Space Phys.*, **21**, 18-25, 1992.

19. Bigg, E. K., Detection of atmospheric dust and temperature inversions by twilight scattering, *Nature*, **177**, 77-79, 1956.
20. Blatherwick, R. D., A. Goldman, D. G. Murcray, F. J. Murcray, G. R. Cook, and J. W. Van Allen, Simultaneous mixing ratio profiles of stratospheric NO and NO₂ as derived from balloon - borne infrared solar spectra, *Geophys. Res. Lett.*, **7**, 471 - 473, 1980.
21. Bluth, G. J. S., S. D. Doiron, C. C. Schnetzler, A. J. Krueger, and L. S. Walter, Global tracking of the SO₂ clouds from the June 1991, Mount Pinatubo eruptions, *Geophys. Res. Lett.*, **19**, 151-154, 1992.
22. Boughner, R., J. C. Larsen, and M. Natarajan, The influence of NO and ClO variations at twilight on the interpretation of solar occultation measurements, *Geophys. Res. Lett.*, **7**, 231 - 234, 1980.
23. Brasseur, G., D. Cariolle, A. de Rudder, L. J. Gray, J. A. Pyle, E.- P. Roth, U. Schmailzl, and D. J. Wuebbles, Odd nitrogen during the MAP / GLOBUS 1983 Campaign : Theoretical considerations, *Planet. Space Sci.*, **35**, 637 - 645, 1987.
24. Brewer, A. W., C. T. McElroy, and J. B. Kerr, Nitrogen Dioxide concentrations in the atmosphere, *Nature*, **246**, 129-133, 1973.
25. Burkhardt, E. G., C. A. Lambert, and C. K. N. Patel, Stratospheric nitric oxide : measurements during daytime and sunset, *Science*, **188**, 1111 - 1113, 1975.
26. Burrows, J. P., G. S. Tyndall, and G. K. Moortgat, Absorption spectrum of NO₃ and kinetics of the reactions of NO₃ with NO₂, Cl, and several stable atmospheric species at 298 K, *J. Phys. Chem.*, **89**, 4848 - 4856, 1985.
27. Cadle, R. D., and G. W. Grams, Stratospheric aerosol particles and their optical properties, *Rev. Geophys. and Space Phys.*, **13**, 475-501, 1975.
28. Cantrell, C. A., J. A. Davidson, R. E. Shetter, B. A. Anderson, and J. G. Calvert, The temperature invariance of the NO₃ absorption cross section

in the 662 nm region, *J. Phys. Chem.*, **91**, 5858-5863, 1987.

29. Carroll, M. A., D. D. Montzka, G. Hubler, K. K. Kelly, and G. L. Gregory, In situ measurements of NO_x in the Airborne Arctic Stratospheric Expedition, *Geophys. Res. Lett.*, **17**, 493-496, 1990.
30. Carroll, M. A., B. A. Ridley, D. D. Montzka, G. Hubler, J. G. Walega, R. B. Norton, B. J. Huebert, and F. E. Grahek, Measurements of nitric oxide and nitrogen dioxide during the Mauna Loa observatory photochemistry experiment, *J. Geophys. Res.*, **97**, 10,361-10,374, 1992.
31. Chakrabarty, D. K., and P. Chakrabarty, The evolution of ozone with changing solar activity, *Geophys. Res. Lett.*, **9**, 76 - 78, 1982.
32. Chandra, S., and R. S. Stolarski, Recent trends in stratospheric total ozone : Implications of dynamical and El Chichón perturbations, *Geophys. Res. Lett.*, **18**, 2277-2280, 1991.
33. Chappuis, J., Sur le spectre d'absorption de l'ozone, *C. R. Acad. Sci.*, **91**, 985, 1980.
34. Chappuis, J., Sur le spectre d'absorption de l'ozone, *C. R. Acad. Sci.*, **94**, 858 - 891, 1982.
35. Chu, W. P., and M. P. McCormick, SAGE observations of stratospheric nitrogen dioxide, *J. Geophys. Res.*, **91**, 5465 - 5476, 1986.
36. Coffey, M. T., W. G. Mankin, and A. Goldman, Simultaneous spectroscopic determination of the latitudinal, seasonal, and diurnal variability of stratospheric N₂O, NO, NO₂, and HNO₃, *J. Geophys. Res.*, **86**, 7331-7341, 1981.
37. Coffey, M. T., W. G. Mankin, and A. Goldman, Airborne measurements of stratospheric constituents over Antarctica in the Austral spring, 1987 2. Halogen and nitrogen trace gases, *J. Geophys. Res.*, **94**, 16,597 - 16,613, 1989.
38. Cogley, A. C., and W. J. Borucki, Exponential approximation for daily average solar heating or photolysis, *J. Atmos. Sci.*, **33**, 1347 - 1356, 1976.

39. Coulson, K. L., Polarization and intensity of light in the atmosphere (Book), *A. Deepak Publishing*, 1988.
40. Cox, R. A., R. A. Barton, E. Ljungstrom, and D. W. Stocker, The reactions of Cl and ClO with NO₃ radical, *Chem. Phys. Lett.*, **108**, 228 - 232, 1984.
41. Creel, C. L., and J. Ross, Photodissociation of NO₂ in the region 458 - 630 nm, *J. Chem. Phys.*, **64**, 3560 - 3566, 1976.
42. Crutzen, P. J., The influence of nitrogen oxides on the atmospheric ozone content, *Quart. J. Roy. Meteorol. Soc.*, **96**, 320 - 325, 1970.
43. Crutzen, P. J., SST's - A threat to the earth's ozone shield, *Ambio*, **1**, 41 - 51, 1972.
44. Crutzen, P. J., A discussion of the chemistry of some minor constituents in the stratosphere and troposphere, *Pure Appl. Geophys.*, **106 - 108**, 1385 - 1399, 1973.
45. Crutzen, P. J., Physical and chemical processes which control the production, destruction and distribution of ozone and some other chemically active minor constituents, *Garp Publ.*, **16**, Global Atmos. Res. Program, Geneva, April 1975.
46. Crutzen, P. J., I. S. A. Isaksen, and J. R. McAfee, The impact of the chlorocarbon industry on the ozone layer, *J. Geophys. Res.*, **83**, 345 - 363, 1978.
47. Cunnold, D. M., J. M. Zawodny, W. P. Chu, J. P. Pommereau, F. Goutail, J. Lenoble, M. P. McCormick, R. E. Veiga, D. Murcray, N. Iwagami, K. Shibasaki, P. C. Simon, and W. Peetermans, Validation of SAGE II NO₂ measurements, *J. Geophys. Res.*, **96**, 12,913-12,925, 1991.
48. Curcio, J. A., L. F. Drummeter, and T. H. Cosden, The absorption spectrum of the atmosphere from 4400 to 5500 A, *NRL Report 4669*, Naval Research Laboratory, Washington, D. C., 1955.

49. Dave, J. V., and C. L. Mateer, The effect of stratospheric dust on the colour of the twilight sky, *J. Geophys. Res.*, **73**, 6897-6913, 1968.
50. Davidson, J. A., C. A. Cantrell, A. H. McDaniel, R. W. Shetter, S. Madronich, and J. G. Calvert, Visible ultra-violet absorption cross sections for NO₂ as a function of temperature, *J. Geophys. Res.*, **93**, 7105 - 7112, 1988.
51. Davidson, J. A., C. A. Cantrell, R. E. Schetter, A. H. McDaniel, and J. G. Calvert, The NO₃ radical decomposition and NO₃ scavenging in the troposphere, *J. Geophys. Res.*, **95**, 13,963 - 13,969, 1990.
52. Davenport, J. E., Determination of NO₂ photolytic parameters for stratospheric modeling, **Report FAA - EQ - 74 - 14** (Federal Aviation Administration, Washington, D. C.), 1977.
53. Defoor, T. E., E. Robinson, and S. Ryan, Early LIDAR observations of the June 1991 Pinatubo eruption plume at Mauna Loa observatory, Hawaii, *Geophys. Res. Lett.*, **19**, 187-190, 1992.
54. Deluisi, J. J., E. G. Dutton, K. L. Coulson, T. E. Defoor, and B. G. Mendonca, On some radiative features of El Chichón volcanic stratospheric dust cloud and a cloud of unknown origin observed at Mauna Loa, *J. Geophys. Res.*, **88**, 6769 - 6772, 1983.
55. Demore, W. B., M. J. Molina, S. P. Sander, D. M. Golden, R. F. Hampson, M. J. Kurzlo, C. J. Howard, and A. R. Ravishankara, Chemical kinetics and photochemical data for use in stratospheric modeling, Evaluation No. 8, *JPL Publications*, **87 - 41**, 1987.
56. Dickinson, P. H. G., W. C. Bain, L. Thomas, E. R. Williams, D. B. Jenkins, and N. D. Twiddy, The determination of the atomic oxygen concentration and associated parameters in the lower ionosphere, *Proc. Roy. Soc. London, A*, **369**, 379 - 408, 1980.
57. Douglass, A. R., C. H. Jackman, and R. S. Stolarski, Comparison of model results transporting the odd nitrogen family with results transporting separate odd nitrogen species, *J. Geophys. Res.*, **94**, 9862-9872, 1989.

58. Drummond, J. W., J. M. Rosen, and D. J. Hofmann, Balloon borne chemiluminescent measurement of NO to 45 km, *Nature*, **265**, 319 - 320, 1977.
59. Elterman, L., UV, Visible and IR attenuation for altitudes to 50 km, 1968, **AFCRL - 68 - 0153**, *Environmental Research Paper No. 285*, U. S. Air Force Cambridge Research Laboratories, Massachusetts, 1968.
60. Evans, W. F. J., H. Fast, J. B. Kerr, C. T. McElroy, R. S. O'Brien, D. I. Wardle, J. C. McConnell, and B. A. Ridley, Stratospheric constituent measurements from project stratoprobe, Proc. of WMO symposium on the geophysical aspects and consequences of changes in the composition of the stratosphere, *WMO Pub. 511*, World Meteorological Organization, Geneva, 55 - 60, 1978.
61. Evans, W. F. J., J. B. Kerr, C. T. McElroy, R. S. O'Brien, and J. C. McConnell, Measurement of NO, NO₂ and HNO₃ during a stratospheric warming at 54°N in February, 1979, *Geophys. Res. Lett.*, **9**, 493 - 496, 1982.
62. Fabian, P., J. A. Pyle, and R. J. Wells, Diurnal variations of minor constituents in the stratosphere modeled as a function of latitude and season, *J. Geophys. Res.*, **87**, 4981 - 5000, 1982.
63. Fabian, P., G. Flentje, and W. A. Matthews, Stratospheric NO profiles measured simultaneously using two chemiluminescent balloon - borne sondes, *Planet. Space Sci.*, **35**, 609 - 614, 1987.
64. Farman, J. C., B. G. Gardiner, and J. D. Shanklin, Large losses of total ozone in Antarctica reveal seasonal ClO_x/NO_x interaction, *Nature*, **315**, 207-210, 1985.
65. Farmer, C. B., Infrared measurements of stratospheric composition, *Can. J. Chem.*, **52**, 1544, 1974.
66. Flaud, J.- M., C. Camy- Peyret, J. W. Brault, C. P. Rinsland, and D. Car-
iolle, Nighttime and daytime variation of atmospheric NO₂ from ground-
based infrared measurements, *Geophys. Res. Lett.*, **15**, 261-264, 1988.

67. Fontanella, J. C., A. Girard, L. Gramont, and N. Louisnard, Vertical distribution of NO, NO₂, and HNO₃ as derived from stratospheric absorption infrared spectra, *Appl. Opt.*, **14**, 825 - 839, 1975.
68. Froidevaux, L., M. Allen, S. Berman, and A. Daughton, Analysis of LIMS observations in the upper stratosphere and lower mesosphere, 1. The mean O₃ profile and its temperature sensitivity at midlatitudes in May, 1979, paper presented at the stratospheric satellite data analysis meeting, *Natl. Cent. for Atmos. Res.*, Boulder, Colo., Sept 24 -26, 1984.
69. Garcia, R. R., and S. Solomon, A numerical model of the zonally averaged Dynamical and Chemical structure of the middle atmosphere, *J. Geophys. Res.*, **88**, 1379-1400, 1983.
70. Gelinas, R. J., and J. P. Vajk, Diurnal analysis of local variabilities in atmospheric NO₃, *J. Geophys. Res.*, **86**, 7369-7377, 1981.
71. Gil, M., and J. Cacho, NO₂ total column evolution during the 1989 spring at Antarctica Peninsula, *J. Atmos. Chem.*, **15**, 187-200, 1992.
72. Girard, A., J. Besson, R. Giraudet, and L. Gramont, Correlated seasonal and climatic variations of trace constituents in the stratosphere, *Pure. App. Geophys.*, **117**, 381 - 394, 1978.
73. Goldman, A., F. G. Fernald, W. J. Williams, and D. G. Murcray, Vertical distribution of NO₂ in the stratosphere as determined from balloon measurements of solar spectra in the 4500 Å region, *Geophys. Res. Lett.*, **5**, 257 - 260, 1978.
74. Goldman, A., F. J. Murcray, C. P. Rinsland, R. D. Blatherwick, S. J. David, F. H. Murcray, and D. G. Murcray, Mt. Pinatubo SO₂ cloumn measurements from Mauna Loa, *Geophys. Res. Lett.*, **19**, 183-186, 1992.
75. Graham, R. A., and H. S. Johnston, The photochemistry of NO₃ and the kinetics of the N₂O₅-O₃ system, *J. Phys. Chem.*, **82**, 254-268, 1978.
76. Grainger, J. F., and J. Ring, Anomalous Fraunhofer line profiles, *Nature*, **193**, 762, 1962.

77. Granier, C., and G. Brasseur, Impact of heterogeneous chemistry on model predictions of ozone changes, *J. Geophys. Res.*, **97**, 18,015 - 18,033, 1992.
78. Grant, W. B., J. Fishman, E. V. Browell, V. G. Brackett, D. Nganga, A. Minga, B. Cros, R. E. Veiga, C. F. Butler, M. A. Fenn, and G. D. Nowicki, Observations of reduced ozone concentrations in the tropical stratosphere after the eruption of Mt. Pinatubo, *Geophys. Res. Lett.*, **19**, 1109-1112, 1992.
79. Greenblatt, G. D., J. J. Orlando, J. B. Burkholder, and A. R. Ravishankara, Absorption measurements of oxygen between 330 and 1140 nm, *J. Geophys. Res.*, **95**, 18,577-18,582, 1990.
80. Griggs, M., Absorption coefficient of ozone in the ultraviolet and visible regions, *J. Chem. Phys.*, **49**, 857 - 859, 1968.
81. Hall, T. C., Jr., and F. E. Blacet, Separation of the absorption spectra of NO_2 and N_2O_4 in the range 2400 - 5000 Å, *J. Chem. Phys.*, **20**, 1745, 1952.
82. Harker, A. B., W. Ho, and J. J. Ratto, Photodissociation quantum yield of NO_2 in the region 375 to 420 nm, *Chem. Phys. Lett.*, **50**, 394 - 397, 1977.
83. Harries, J. E., Measurements of some hydrogen - oxygen - nitrogen compounds in the stratosphere from Concorde 002, *Nature*, **241**, 515, 1973.
84. Harrison, A. W., and D. J. W. Kendall, Fraunhofer line Filling In (3855-4455 Å), *Can. J. Phys.*, **52**, 940-944, 1974.
85. Harrison, A. W., Midsummer stratospheric NO_2 at latitude 45°S, *Can. J. Phys.*, **57**, 1110-1117, 1979.
86. Heath, D. F., and B. H. Schlesinger, Global response of stratospheric ozone to natural perturbations on climatological time scales by variations of UV solar flux and the eruption of El Chichón, *Eos Trans. AGU*, **65**, 836 - 837, 1984.
87. Helten, M., W. Patz, D. H. Ehhalt, and E. P. Roeth, Measurements of nighttime NO_3 and NO_2 in the stratosphere by matrix isolation and ESR

- spectroscopy, in *Atmospheric Ozone*, edited by C. S. Zerefos and A. Ghazi, pp. 196 - 200, D. Reidel, Dordrecht, 1984.
88. Herman, J. R., The problem of nighttime stratospheric NO₃, *J. Geophys. Res.*, **84**, 6336-6338, 1979.
 89. Herman, J. R., Reply, *J. Geophys. Res.*, **85**, 4558 - 4559, 1980.
 90. Hicks, E., B. Leroy, P. Rigaud, J. L. Jourdain, and G. Le Bras, Spectres d'absorption dans le proche ultraviolet et le visible des compose's mine'ri-taires atmosphe'riques NO₂ et SO₂ entre 200 et 300 K, *J. Chem. Phys.*, **76**, 693, 1979.
 91. Hirono, M., and T. Shibata, Enormous increase of stratospheric aerosols over Fukuoka due to volcanic eruption of El Chichón in 1982, *Geo-phys. Res. Lett.*, **10**, 152-154, 1983.
 92. Hofmann, D. J., and J. M. Rosen, Stratospheric sulfuric acid fraction and mass estimate for the 1982 volcanic eruption of El Chichon, *Geophys. Res. Lett.*, **10**, 313-316, 1983.
 93. Hofmann, D. J., and R. M. Rosen, On the temporal variation of strato-spheric aerosol size and mass during the first 18 months following the 1982 eruptions of El Chichón, *J. Geophys. Res.*, **89**, 4883 - 4890, 1984.
 94. Hofmann, D. J., Perturbations to the global atmosphere associated with the El Chichón volcanic eruption of 1982, *Rev. of Geophys.*, **25**, 743-759, 1987.
 95. Hofmann, D. J., and S. Solomon, Ozone destruction through heteroge-neous chemistry following the eruption of El Chichon, *J. Geophys. Res.*, **94**, 5029-5041, 1989.
 96. Horvath, J. J., J. E. Frederick, N. Orsini, and A. R. Douglass, Nitric oxide in the upper stratosphere : Measurements and geophysical interpretation, *J. Geophys. Res.*, **88**, 10809 - 10817, 1983.

97. Hsu, D. K., D. L. Monts, and R. N. Zare, Spectral atlas of nitrogen dioxide 5580 to 6480 Å, *Academic Press*, New York, 1978.
98. Humphrey, G. L., and R. M. Badger, The absorption spectrum of ozone in the visible, I, Examination for fine structure, II, The effect of temperature, *J. Phys. Chem.*, **15**, 794 - 798, 1947.
99. Inn, E. C. Y., and Y. Tanaka, Absorption coefficient of ozone in the ultra-violet and visible regions, *J. Opt. Soc. Am.*, **43**, 870 - 873, 1953.
100. Jäger, H., and W. Carnuth, The decay of the El Chichon stratospheric perturbation, observed by LIDAR at northern midlatitudes, *Geophys. Res. Lett.*, **14**, 696-699, 1987.
101. Jäger, H., The Pinatubo eruption cloud observed by LIDAR at Garmisch-Partenkirchen, *Geophys. Res. Lett.*, **19**, 191-194, 1992.
102. Jayaraman, A., S. Lal, M. Lal, B. H. Subbaraya, S. C. Garg, T. John, K. S. Zalpuri, N. Seshadri, C. R. Sreedharan, R. Vijaykumar, V. M. Ignatov, G. A. Kokin, S. P. Perov, O. V. Shtrikov, S. V. Tishin, and A. F. Chizhov, The Indo- Soviet collaborative experiment at Thumba to study diurnal variations in the ozone vertical distribution over the tropics, in *Atmospheric Ozone*, edited by R. D. Bojkov and P. Fabian, pp. 113 - 116, *A. Deepak Publishing*, U S A, 1989.
103. JPL, Chemical kinetic and photochemical data for use in stratospheric modeling, Evaluation No. 4, NASA panel for data evaluation, *JPL pub.* **81 -3**, 123 pp., Jet Prop. Labor., Pasadena, C A, 1981.
104. JPL, Chemical Kinetic and photochemical data for use in stratospheric modeling, Evaluation No. 5, NASA panel for data evaluation, *JPL pub.* **82 - 57**, 186 pp., Jet Prop. Labor., C A. 1982.
105. JPL, Chemical kinetics and photochemical data for use in stratospheric modeling, *JPL publication 87 - 27*, Pasadena, Calif., 1987.
106. Jet Propulsion Laboratory, (JPL) chemical kinetics and photochemical data for use in stratospheric modeling, *JPL Publ.* **90 - 1**, 1990.

107. Johnston, H. S., and R. A. Graham, Photochemistry of NO_x and HNO_x compounds, *Can. J. Chem.*, **52**, 1415 - 1423, 1974.
108. Johnston, F. S., Transport processes in the upper atmosphere, *J. Atmos. Sci.*, **32**, 1658 - 1662, 1975.
109. Johnston, P. V., and R. L. McKenzie, Long - path absorption measurements of tropospheric NO_2 in rural New Zealand, *Geophys. Res. Lett.*, **11**, 69 - 72, 1984.
110. Johnston, P. V., and R. L. McKenzie, NO_2 observations at 45°S during the decreasing phase of solar cycle 21, from 1980 to 1987, *J. Geophys. Res.*, **94**, 3473-3486, 1989.
111. Johnston, P. V., R. L. McKenzie, J. G. Keys and W. A. Matthews, Observations of depleted stratospheric NO_2 following the Pinatubo volcanic eruption, *Geophys. Res. Lett.*, **19**, 211-213, 1992.
112. Jones, E. J., and O. R. Wulf, The absorption coefficient of nitrogen pentoxide in the ultraviolet and the visible absorption spectrum of NO_3 , *J. Chem. Phys.*, **5**, 873 - 877, 1937.
113. Keating, G. M., and D. F. Young, Interim reference ozone models for the middle atmosphere, in *Handbook for MAP*, Vol. 16, edited by K. Labitzke, J. J. Barnett, and B. Edwards, pp. 205 - 229, SCOSTEP Secretariat, Univ. of Illinois, Urbana, 1985.
114. Keating, G. M., M. C., Pitts, and D. F. Young, Ozone reference models for the middle atmosphere, *Adv. Space Res.*, **10**, (12)317 - (12)355, 1990.
115. Kerr, J. B., and C. T. McElroy, Measurement of stratospheric nitrogen dioxide from the AES stratospheric balloon program, *Atmosphere*, **14**, 166 - 171, 1976.
116. Kerr, J. B., W. F. J. Evans, and J. C. McConnell, The effect of NO_2 changes on tangent ray NO_2 measurements, *Geophys. Res. Lett.*, **4**, 577 - 579, 1977.

117. Kerr, J. B., C. T. McElroy, and W. F. J. Evans, Mid-latitude summertime measurements of stratospheric NO₂, *Can. J. Phys.*, **60**, 196-200, 1982.
118. Keys, J. G., and P. V. Johnston, Stratospheric NO₂ and O₃ in Antarctica : Dynamic and Chemically controlled variations, *Geophys. Res. Lett.*, **13**, 1260-1263, 1986.
119. Knollenberg, R. G., and D. Huffman, Measurements of the aerosol size distributions in the El Chichón cloud, *Geophys. Res. Lett.*, **10**, 1025 - 1028, 1983.
120. Knight, W., D. R. Hastie, and B. A. Ridley, Measurements of nitric oxide during a stratospheric warming, *Geophys. Res. Lett.*, **9**, 489 - 492, 1982.
121. Kondo, Y., W. A. Matthews, A. Iwata, and M. Takagi, Measurements of nitric oxide from 7 to 32 km and its diurnal variation in the stratosphere, *J. Geophys. Res.*, **90**, 3813 - 3820, 1985.
122. Kondo, Y., W. A. Matthews, A. Iwata, Y. Morita, and M. Takagi, Aircraft measurement of oxides of nitrogen along the eastern rim of the Asian continent: Winter observations, *J. Atmos. Chem.*, **5**, 37 - 58, 1987.
123. Kondo, Y., A. Iwata, M. Pirre, R. Ramaroson, C. Delannoy, W. A. Matthews, M. Koike, and K. Suzuki, *Geophys. Res. Lett.*, **16**, 867-870, 1989.
124. Kondo, Y., P. Amedieu, W. A. Matthews, W. R. Sheldon, and J. R. Benbrook, A mid - latitude balloon - borne observation of total odd nitrogen, *Geophys. Res. Lett.*, **17**, 73 - 76, 1990.
125. Labitzke, K., B. Naujokat, and M. P. McCormick, Temperature effects on the stratosphere of the April 4, 1982 eruption of El Chichón, Mexico, *Geophys. Res. Lett.*, **10**, 24-26, 1983.
126. Labitzke, K., On the variability of the stratosphere in the Arctic regions in winter, *Ber. Bunsenges. Phys. Chem.*, **96**, 496-501, 1992.
127. Labitzke, K., and M. P. McCormick, Stratospheric temperature increases due to Pinatubo aerosols, *Geophys. Res. Lett.*, **19**, 207-210, 1992.

128. Lefebvre, L., Low temperature absorption spectrum of ozone, *C. R. Acad. Sci.*, **200**, 653 - 702, 1935.
129. Livingston, W., and G. W. Lockwood, Astronomical observations relating to the transit of volcanic ash over Arizona, Spring 1982, *Science*, **220**, 300 - 302, 1983.
130. Llewellyn, E. J., and G. Witt, The measurement of ozone concentrations at high latitude during the twilight, *Planet. Space Sci.*, **25**, 165 - 172, 1977.
131. Logan, J. A., M. J. Prather, S. C. Wofsy, and M. B. McElroy, Atmospheric chemistry : Response to human influence, *Phil. Trans. Roy. Soc. London*, **A 290**, 187 - 234, 1978.
132. Louisnard, N., G. Fergant, A. Girard, L. Gramont, O. Lado - Bordowsky, J. Laurent, S. Le Boiteau, and M. P. Lemaître, Infrared absorption spectroscopy applied to stratospheric profiles of minor constituents, *J. Geophys. Res.*, **88**, 5365 - 5376, 1983.
133. Madronich, S., D. R. Hastic, H. I. Schiff, and B. A. Ridley, Measurement of the photodissociation coefficient of NO_2 in the atmosphere, II, stratospheric measurements, *J. Atmos. Chem.*, **3**, 233 - 245, 1985.
134. Magnotta, F., and H. S. Johnston, Photodissociation quantum yields for the NO_3 free radical, *Geophys. Res. Lett.*, **7**, 679 - 772, 1980.
135. Maier, E. J., A. C. Aikin, and J. E. Ainsworth, Stratospheric nitric oxide and ozone measurements using photoionization mass spectrometry and UV absorption, *Geophys. Res. Lett.*, **5**, 37 - 40, 1978.
136. Mankin, W. G., M. T. Coffey, A. Goldman, M. R. Schoeberl, L. R. Lait, and P. A. Newman, Airborne measurements of stratospheric constituents over the Arctic in the winter of 1989, *Geophys. Res. Lett.*, **17**, 473-476, 1990.
137. Mankin, W. G., M. T. Coffey, and A. Goldman, Airborne observations of SO_2 , HCl , and O_3 in the stratospheric plume of the Pinatubo volcano in July 1991, *Geophys. Res. Lett.*, **19**, 179-182, 1992.

138. Marinelli, W. J., D. M. Swanson, and H. S. Johnston, Absorption cross sections and line shapes for NO_3 (O-O) band, *J. Chem. Phys.*, **76**, 2864 - 2870, 1982.
139. Mateer, C. L., and H. U. Duetsch, Uniform evaluation of Umkehr observations from the world ozone network : Part 1, Proposed standard Umkehr evaluation technique, *Nat'l Center for Atmos. Res.*, Boulder, Colorado, 1964.
140. McCormick, M. P., T. J. Swissler, E. Hilsenrath, A. J. Krueger, and M. T. Osborn, Satellite and correlative measurements of stratospheric ozone; Comparison of measurements made by SAGE, ECC balloons, Chemiluminescent and optical rocket - sondes, *J. Geophys. Res.*, **89**, 5315 - 5320, 1984.
141. McCormick, M. P., Initial assessment of the stratospheric and climatic impact of the 1991 Mount Pinatubo eruption: Prologue, *Geophys. Res. Lett.*, **19**, 149, 1992.
142. McCormick, M. P., and R. E. Veiga, SAGE-II measurements of early Pinatubo aerosols, *Geophys. Res. Lett.*, **19**, 155-158, 1992.
143. McCormick, M. P., R. E. Veiga, and W. P. Chu, Stratospheric ozone profile and total ozone trends derived from the SAGE I and SAGE II data, *Geophys. Res. Lett.*, **19**, 269-272, 1992.
144. McElroy, T., The measurement of temperature, ozone and water vapour, *Handbook for MAP*, **15**, 1 - 36, 1985.
145. McFarland, M., B. A. Ridley, M. H. Proffitt, D. L. Albritton, T. L. Thompson, W. J. Harrop, R. H. Winkler, and A. L. Schmeltekopf, Simultaneous In situ measurements of nitrogen dioxide, nitric oxide, and ozone between 20 and 31 km, *J. Geophys. Res.*, **91**, 5421-5437, 1986.
146. McKenzie, R. L., and P. V. Johnston, Ground-based measurements of stratospheric trace gases from New Zealand, **Report No. 783** (Physics and Engineering Laboratory), 1982a.

147. McKenzie, R. L., and P. V. Johnston, Seasonal variations in stratospheric NO₂ at 45°S, *Geophys. Res. Lett.*, **9**, 1255-1258, 1982b.
148. McKenzie, R. L., and P. V. Johnston, Stratospheric ozone observations simultaneous with NO₂ at 45°S, *Geophys. Res. Lett.*, **10**, 337-340, 1983.
149. McKenzie, R. L., and P. V. Johnston, Springtime stratospheric NO₂ in Antarctica, *Geophys. Res. Lett.*, **11**, 73-75, 1984.
150. McKenzie, R. L., W. A. Matthews, and P. V. Johnston, The relationship between erythemal UV and ozone, derived from spectral irradiance measurements, *Geophys. Res. Lett.*, **18**, 2269-2272, 1991a.
151. McKenzie, R. L., P. V. Johnston, C. T. McElroy, J. B. Kerr, and S. Solomon, Altitude distributions of stratospheric constituents from ground-based measurements at twilight, *J. Geophys. Res.*, **96**, 15,499-15,511, 1991b.
152. McMahon, B. B., and E. L. Simmons, Ground-based measurements of atmospheric NO₂ by differential optical absorption, *Nature*, **287**, 710-711, 1980.
153. Megrelishvili, T. G., I. G. Mel'nikova, G. V. Rozenberg, and A. V. Khovanskiy, Mean twilight at the zenith and vertical profile of scattering coefficient according to observations at the Abastumani Astrophysical Observatory (1942-1952), *Izvestiya, Atmospheric and Oceanic Physics*, **14**, 805-812, 1978.
154. Michelangeli, D. V., M. Allen, and Y. L. Yung, El Chichón volcanic aerosols : Impact of radiative, thermal, and chemical perturbations, *J. Geophys. Res.*, **94**, 18,429-18,443, 1989.
155. Miller, C., D. L. Filkin, A. J. Owens, J. M. Steed, and J. P. Jesson, A two-dimensional model of stratospheric chemistry and transport, *J. Geophys. Res.*, **86**, 12039 - 12065, 1981.
156. Mitchell, D. N., R. P. Wayne, P. J. Allen, R. P. Harrison, and R. P. Twin, Kinetic and photochemistry of NO₃, *J. Chem. Soc., Faraday Trans. 2*, **76**, 785 - 793, 1980.

157. Mitra, A. P., Minor constituents in the middle atmosphere, *Scientific Note* (ISRO - INCOSPAR - SN - 03 - 77), 1977.
158. Mount, G. H., R. W. Sanders, A. L. Schmeltekopf, and S. Solomon, Visible spectroscopy at McMurdo station, Antarctica, 1. Overview and daily variations of NO₂ and O₃ during austral Spring, 1986, *J. Geophys. Res.*, **92**, 8320 - 8326, 1987.
159. Murcray, D. G., A. Goldman, W. J. Williams, F. H. Murcray, J. N. Brooks, J. Van Allen, R. N. Stocker, J. J. Kusters, D. B. Barker, and D. E. Snider, Recent results of stratospheric trace gas measurements from balloon - borne spectrometers, *Proc. Third CIA P Conf.*, A. J. Broderick and T. M. Hard, editors, **DOT - TSC - OST - 74 - 15**, U. S. Dept. of Transportation, Washington, D. C., pp. 184 - 192, 1974.
160. Nagata, T., T. Tohmatsu, and T. Ogawa, Sounding rocket measurement of atmospheric ozone density, 1965 - 1970, *Space Res.*, **11**, 849 - 855, 1971.
161. Nakayama, T., M. Y. Kitamura, and K. Watanabe, Ionization potential and absorption coefficients of nitrogen dioxide, *J. Chem. Phys.*, **30**, 1180 - 1186, 1959.
162. NASA, The stratosphere : Present and Future, ed. by R. D. Hudson and E. I. Reed, 432 pp., *NASA Ref. publ.* **1049**, 1979.
163. Naudet, J. P., P. Rigaud, and D. Huguenin, Stratospheric NO₂ at night from stellar spectra in the 440 nm region, *Geophys. Res. Lett.*, **7**, 701 - 703, 1980.
164. Naudet, J. P., D. Huguenin, P. Rigaud, and D. Cariolle, Stratospheric observations of NO₃ and its experimental and theoretical distribution between 20 and 40 km, *Planet. Space. Sci.*, **29**, 707-712, 1981.
165. Naudet, J. P., D. W. Rusch, R. J. Thomas, R. T. Clancy, C. A. Barth, J. Wedding, J. M. Zawodny, P. Fabian, and M. Helten, Stratospheric NO₂ from the solar mesosphere explorer during MAP/GLOBUS 1983, *Planet. Space Sci.*, **35**, 631 - 635, 1987.

166. Naudet, J.- P., P. Rigaud, M. Pirre, and D. Huguenin, Altitude distribution of stratospheric NO_3 1. Observations of NO_3 and related species, *J. Geophys. Res.*, **94**, 6374 - 6382, 1989.
167. Nicolet, M., The chemical equations of stratospheric and mesospheric ozone; pp. 823 - 864, in: Nicolet, M. and Aikin, A. C. (eds), *proceedings of the NATO Advanced Study Institute on Atmospheric ozone : Its variation and human influences*, U. S. Department of Transportation, Washington, D. C. 20591, 1980.
168. Norton, R. B., and J. F. Noxon, Dependence of stratospheric NO_3 upon latitude and season, *J. Geophys. Res.*, **91**, 5323-5330, 1986.
169. Noxon, J. F., Nitrogen dioxide in the stratosphere and troposphere measured by ground-based absorption spectroscopy, *Science*, **189**, 547-549, 1975.
170. Noxon, J. F., R. B. Norton, and W. R. Henderson, Observation of atmospheric NO_3 , *Geophys. Res. Lett.*, **8**, 675-678, 1978a.
171. Noxon, J. F., Stratospheric NO_2 in the Antarctic winter, *Geophys. Res. Lett.*, **5**, 1021-1022, 1978b.
172. Noxon, J. F., Stratospheric NO_2 , 2. Global behaviour, *J. Geophys. Res.*, **84**, 5067-5076, 1979.
173. Noxon, J. F., E. C. Whipple, Jr., and R. S. Hyde, Stratospheric NO_2 , 1. Observational method and behaviour at mid-latitude, *J. Geophys. Res.*, **84**, 5047-5065, 1979.
174. Noxon, J. F., R. B. Norton, and E. Marovich, NO_3 in the troposphere, *Geophys. Res. Lett.*, **7**, 125-128, 1980a.
175. Noxon, J. F., R. B. Norton, and W. R. Henderson, Comment on " The problem of nighttime stratospheric NO_3 " by J. R. Herman, *J. Geophys. Res.*, **85**, 4556-4557, 1980b.

176. Noxon, J. F., NO_x in the mid-pacific troposphere, *Geophys. Res. Lett.*, **8**, 1223 - 1226, 1981.
177. Noxon, J. F., W. R. Henderson, and R. B. Norton, Stratospheric NO₂ : 3, The effects of large-scale horizontal transport, *J. Geophys. Res.*, **88**, 5240-5248, 1983.
178. Noxon, J. F., NO₃ and NO₂ in the mid-pacific troposphere, *J. Geophys. Res.*, **88**, 11,017-11,021, 1983.
179. Orme, W. A. Jr., Review on El Chichón volcanic eruption, *Res. Dev. Mexico*, **1982**, September, 22, 1982.
180. Patel, C. K. N., E. G. Burkhardt, and C. A. Lambert, Spectroscopic measurements of stratospheric nitric oxide and water vapour, *Science*, **174**, 1173, 1974.
181. Penner, J. E., and J. S. Chang, Possible variations in atmospheric ozone related to the eleven year solar cycle, *Geophys. Res. Lett.*, **5**, 817 - 820, 1978.
182. Penney, C. M., Study of temperature dependence of the chappuis band absorption of ozone, *NASA contract. Rep.* **158977**, 1979.
183. Perliski, L. M., and S. Solomon, Radiative influences of Pinatubo volcanic aerosols on twilight observations of NO₂ column abundances, *Geophys. Res. Lett.*, **19**, 1923-1926, 1992.
184. Perliski, L. M., and S. Solomon, On the evaluation of airmass factors for atmospheric near-ultraviolet and visible absorption spectroscopy, *J. Geophys. Res.*, **98**, 10,363 - 10,374, 1993.
185. Perner, D., A. Schmeltekopf, R. H. Winkler, H. S. Johnston, J. G. Calvert, C. A. Cantrell, and W. R. Stockwell, A laboratory and field study of the equilibrium $\text{N}_2\text{O}_5 \rightleftharpoons \text{NO}_3 + \text{NO}_2$, *J. Geophys. Res.*, **90**, 3807 - 3812, 1985.
186. Pirre, M., P. Rigaud, and D. Huguenin, Mesure de l'absorption par la haute atmosphere dans le domaine de longueurs d'onde de la fenetre atmospherique au voisinage de 200 nm, in *Atmospheric Ozone*, edited by C. S. Zerefos

and A. Ghazi, pp. 630 - 634, G. Reidel, Dordrecht, 1985.

187. Pirre, M., R. Ramaroson, J.- P. Naudet, and P. Rigaud, Altitude distribution of stratospheric NO_3 , 2. Comparison of observations with model, *J. Geophys. Res.*, **94**, 6383 - 6388, 1989.
188. Pitts, J. N., Jr., H. W. Biermann, R. Atkinson, and A. M. Winer, Atmospheric implications of simultaneous nighttime measurements of NO_3 radicals and HONO, *Geophys. Res. Lett.*, **11**, 557-560, 1984.
189. Platt, U., D. Perner, and H. W. Patz, Simultaneous measurement of atmospheric CH_2O , O_3 , and NO_2 by differential optical absorption, *J. Geophys. Res.*, **84**, 6329-6335, 1979.
190. Platt, U., and D. Perner, Direct measurements of atmospheric CH_2O , HNO_2 , O_3 , NO_2 , and SO_2 by differential optical absorption in the near UV, *J. Geophys. Res.*, **85**, 7453-7458, 1980.
191. Platt, U., D. Perner, A. M. Winer, G. W. Harris, and J. N. Pitts, Jr., Detection of NO_3 in the polluted troposphere by differential optical absorption, *Geophys. Res. Lett.*, **7**, 89-92, 1980.
192. Platt, U., D. Perner, J. Schroder, C. Kessler, and A. Toennissen, The diurnal variation of NO_3 , *J. Geophys. Res.*, **86**, 11,965-11,970, 1981.
193. Platt, U., and D. Perner, Measurements of atmospheric trace gases by long path differential UV/visible absorption spectroscopy in Optical and Laser Remote Sensing, edited by D. K. Killinger and A. Mooradian, **39**, *Springer Series in Optical Sciences*, Springer-Verlag, 97 - 105, 1983.
194. Platt, U., A. M. Winer, H. W. Biermann, R. Atkinson, and J. N. Pitts, Jr., Measurement of nitrate radical concentrations in continental air, *Environ. Sci. Technol.*, **18**, 365 - 369, 1984.
195. Platt, U., G. LeBras, G. Poulet, J. P. Burrows, and G. Moortgat, Peroxy radicals from night-time reaction of NO_3 with organic compounds, *Nature*, **348**, 147-149, 1990.

196. Pollack, J. B., O. B. Toon, C. Sagan, A. Summers, B. Baldwin, and W. V. Camp, Volcanic explosions and climatic change : A Theoretical assessment, *J. Geophys. Res.*, **81**, 1071-1083, 1976.
197. Pollack, J. B., and T. P. Ackerman, Possible effects of the El Chichon volcanic cloud on the radiation budget of the northern tropics, *Geophys. Res. Lett.*, **10**, 1057-1060, 1983.
198. Pommereau, J. P., Observations of NO₂ diurnal variations in the stratosphere, *Geophys. Res. Lett.*, **9**, 850 - 853, 1982.
199. Pommereau, J. P., P. Fabian, G. Flentje, M. Helten, H. W. Patz, D. H. Ehhalt, F. Karcher, G. Froment, G. Armand, W. A. Matthews, D. Offermann, H. Rippel, P. Rigaud, J. P. Naudet, D. Huguenin, P. C. Simon, W. Peetermans, P. Vandeneede, R. Zander, and G. Roland, Inter-comparison of stratospheric NO₂ and NO₃ measurements during MAP/GLOBUS 1983, *Planet. Space Sci.*, **35**, 615 - 629, 1987.
200. Pommereau, J. P., and F. Goutail, O₃ and NO₂ ground-based measurements by visible spectrometry during Arctic winter and spring 1988, *Geophys. Res. Lett.*, **15**, 891 - 894, 1988a.
201. Pommereau, J. P., and F. Goutail, Stratospheric O₃ and NO₂ observations at the southern polar circle in summer and fall 1988, *Geophys. Res. Lett.*, **15**, 895-897, 1988b.
202. Post, M. J., C. J. Grund, A. O. Langford, and M. H. Proffitt, Observations of Pinatubo ejecta over Boulder, Colorado by LIDARS of three different wavelengths, *Geophys. Res. Lett.*, **19**, 195-198, 1992.
203. Ramsey, D. A., *Proc. Colloq. Spectrosc. Int.*, **10**, 583, 1962.
204. Rao- Vupputuri, R. K., Numerical experiments on the steady state meridional structure and ozone distribution in the stratosphere, *Mon. Weather Rev.*, **101**, 510 - 527, 1973.
205. Ravishankara, A. R., and P. H. Wine, Absorption cross sections for NO₃ between 565 and 673 nm, *Chem. Phys. Lett.*, **101**, 73 - 78, 1983.

206. Ravishankara, A. R., and R. L. Mauldin III, Temperature dependence of the NO_3 cross section in the 662-nm region, *J. Geophys. Res.*, **91**, 8709-8712, 1986.
207. Ridley, B. A., and L. C. Howlett, An instrument for nitric oxide measurements in the stratosphere, *Rev. Sci. Instrum.*, **45**, 742 - 746, 1974.
208. Ridley, B. A., J. T. Bruin, H. J. Schiff, and J. C. McConnell, Altitude profile and sunset decay measurements of stratospheric nitric oxide, *Atmosphere*, **14**, 180 - 188, 1976.
209. Ridley, B. A., M. McFarland, J. T. Bruin, H. I. Schiff, and J. C. McConnell, Sunrise measurements of stratospheric nitric oxide, *Can. J. Phys.*, **55**, 212 - 221, 1977.
210. Ridley, B. A., and D. R. Hastie, Stratospheric odd nitrogen : NO measurements at 51°N in summer, *J. Geophys. Res.*, **86**, 3162 - 3166, 1981.
211. Ridley, B. A., and H. I. Schiff, Stratospheric odd nitrogen : Nitric oxide measurements at 32°N in autumn, *J. Geophys. Res.*, **86**, 3167 - 3172, 1981.
212. Ridley, B. A., S. H. Luu, D. R. Hastie, H. I. Schiff, J. C. McConnell, W. F. J. Evans, C. T. McElroy, J. B. Kerr, H. Fast, and R. S. O' Brien, Stratospheric odd nitrogen : Measurements of HNO_3 , NO, NO_2 and O_3 near 54°N in winter, *J. Geophys. Res.*, **89**, 4797-4820, 1984.
213. Ridley, B. A., M. McFarland, A. L. Schmeltekopf, M. H. Proffitt, D. L. Albritton, R. H. Winkler, and T. L. Thompson, Seasonal differences in the vertical distribution of NO, NO_2 , and O_3 in the stratosphere near 50°N , *J. Geophys. Res.*, **92**, 11,919-11,929, 1987.
214. Rigaud, P., J. P. Naudet, and D. Huguenin, Simultaneous measurements of vertical distributions of stratospheric NO_3 and O_3 at different periods of the night, *J. Geophys. Res.*, **88**, 1463 - 1467, 1983.
215. Rinsland, C. P., R. E. Boughner, J. C. Larsen, G. M. Stokes, and J. W. Brault, Diurnal variations of atmospheric nitric oxide: Ground-based infrared spectroscopic measurements and their interpretation with time -

dependent photochemical model calculations, *J. Geophys. Res.*, **89**, 9613 - 9622, 1984.

216. Robbins, D. E., and J. G. Carnes, Variations in the upper stratosphere's ozone profile, WMO symposium on the geophysical aspects and consequences of changes in the composition of the stratosphere, Toronto, Canada, Pub. 511, *World Meteorological Organization*, Geneva, pp. 131 - 137, 1978.
217. Roscoe, H. K., J. R. Drummond, and R. F. Jarnot, Infrared measurements of stratospheric composition III. The daytime changes of NO and NO₂, *Proc. Roy. Soc. London A*, **375**, 507 - 528, 1981.
218. Roscoe, H.K., B. J. Kerridge, S. Pollitt, M. Bangham, N. Louisnard, C. Alamichel, J. P. Pommereau, T. Ogawa, N. Iwagami, M. T. Coffey, W. Mankin, J. M. Fland, C. Camay - Peret, F. J. Murcray, A. Goldman, W. F. J. Evans, and T. McElroy, Intercomparison of stratospheric measurements of NO and NO₂, in *Atmospheric Ozone*, edited by C. S. Zerefos and A. Ghazi, pp. 149 - 156, D. Reidel, Dordrecht, 1985.
219. Roscoe, H. K., B. J. Kerridge, L. J. Gray, R. J. Wells, and J. A. Pyle, Simultaneous measurements of stratospheric NO and NO₂ and their comparison with model predictions, *J. Geophys. Res.*, **91**, 5405 - 5419, 1986.
220. Rosen, J. M., Stratospheric dust and its relationship to meteoric influx, *Space Sci. Rev.*, **9**, 58 - 89, 1969.
221. Rozenberg, G. V., *Twilight : A study in Atmospheric Optics*, state press for physicomathematical literature, Moscow, 1963. Translated by Richard B. Rodman, 358 pp., *Plenum Press*, New York, 1966.
222. Russell, J. M., III, J. C. Gille, E. E. Remsberg, L. L. Gordley, P. L. Bailey, S. R. Drayson, J. Fischer, A. Girard, J. E. Harries, and W. F. J. Evans, Validation of nitrogen dioxide results measured by the Limb Infrared Monitor of the Stratosphere (LIMS) experiment on Nimbus 7, *J. Geophys. Res.*, **89**, 5099 - 5107, 1984

223. Russell, III, J. M., S. Solomon, M. P. McCormick, A. J. Miller, J. J. Barnett, R. L. Jones, and D. W. Rusch, Middle atmosphere composition revealed by satellite observations, in *Handbook for MAP*, Vol. 22, edited by J. M. Russell III, pp. 1 - 302, SCOSTEP Secretariat, Univ. of Illinois, Urbana, 1986.
224. Sander, S. P., Temperature dependence of the NO_3 absorption spectrum, *J. Phys. Chem.*, **90**, 4135, 1986.
225. Sanders, R. W., S. Solomon, G. H. Mount, M. W. Bates, and A. L. Schmeltekopf, Visible spectroscopy at McMurdo Station, Antarctica, 3. Observations of NO_3 , *J. Geophys. Res.*, **92**, 8339-8342, 1987.
226. Sanders, R. W., S. Solomon, M. A. Carroll, and A. L. Schmeltekopf, Visible and near-ultraviolet spectroscopy at McMurdo station, Antarctica 4. Overview and daily measurements of NO_2 , O_3 , and OCIO during 1987, *J. Geophys. Res.*, **94**, 11,381-11,391, 1989.
227. Sarkissian, A., J. P. Pommereau, and F. Goutail, Identification of polar stratospheric clouds from the ground by visible spectrometry, *Geophys. Res. Lett.*, **18**, 779-782, 1991.
228. Shimabukuro, F. I., P. L. Smith, and W. J. Wilson, Estimation of the ozone distribution from millimeter wavelength absorption measurements, *J. Geophys. Res.*, **80**, 2957 - 2959, 1975.
229. Shibasaki, K., N. Iwagami, and T. Ogawa, Stratospheric nitrogen dioxide observed by ground-based and balloon-borne techniques at Syowa station (69°S , 39.6°E), *Geophys. Res. Lett.*, **13**, 1268-1271, 1986.
230. Shibata, T., M. Fujiwara, and M. Hirono, The El Chichón volcanic cloud in the stratosphere: Lidar observation at Fukuoka and numerical simulation, *J. Atmos. Terr. Phys.*, **46**, 1121 - 1146, 1984.
231. Shimazaki, T., The photochemical time constants of minor constituents and their families in the middle atmosphere, *J. Atmos. Terr. Phys.*, **46**, 173 - 191, 1984.

232. Shimazaki, T., Minor constituents in the middle atmosphere (Book), *Terra Scientific Publishing Company*, Tokyo, Japan, 1985.
233. Smith III, F. L., and C. Smith, Numerical evaluation of Chapman's Grazing Incidence Integral $ch(X,\chi)$, *J. Geophys. Res.*, **77**, 3592-3597, 1972.
234. Smith, J. P., and S. Solomon, Atmospheric NO_3 , 3. Sunrise disappearance and the stratospheric profile, *J. Geophys. Res.*, **95**, 13,819-13,827, 1990.
235. Smith, J. P., S. Solomon, R. W. Sanders, H. L. Miller, L. M. Perliski, J. G. Keys, and A. L. Schmeltekopf, Atmospheric NO_3 4. vertical profiles at middle and polar latitudes at sunrise, *J. Geophys. Res.*, **98**, 8983 - 8989, 1993.
236. Solomon, S., and R. R. Garcia, On the distribution of nitrogen dioxide in the high-latitude stratosphere, *J. Geophys. Res.*, **88**, 5229-5239, 1983a.
237. Solomon, S., and R. R. Garcia, Simulation of NO_x partitioning along isobaric parcel trajectories, *J. Geophys. Res.*, **89**, 5497 - 5501, 1983b.
238. Solomon, S., J. M. Russell III, and L. L. Gordley, Observations of the diurnal variation of nitrogen dioxide in the stratosphere, *J. Geophys. Res.*, **91**, 5455-5464, 1986.
239. Solomon, S., A. L. Schmeltekopf, and R. W. Sanders, On the interpretation of zenith sky absorption measurements, *J. Geophys. Res.*, **92**, 8311-8319, 1987.
240. Solomon, S., H. L. Miller, J. P. Smith, R. W. Sanders, G. H. Mount, A. L. Schmeltekopf, and J. F. Noxon, Atmospheric NO_3 , 1. Measurement technique and the annual cycle at 40°N, *J. Geophys. Res.*, **94**, 11,041-11,048, 1989a.
241. Solomon, S., R. W. Sanders, G. H. Mount, M. A. Carroll, R. O. Jakoubek, and A. L. Schmeltekopf, Atmospheric NO_3 , 2. Observations in polar regions, *J. Geophys. Res.*, **94**, 16,423-16,427, 1989b.
242. Solomon, S., and J. G. Keys, Seasonal variations in Antarctic NO_x chemistry, *J. Geophys. Res.*, **97**, 7971-7978, 1992.

243. Solomon, S., J. P. Smith, R. W. Sanders, L. Perliski, H. L. Miller, G. H. Mount, J. G. Keys, and A. L. Schmeltekopf, Visible and near-ultraviolet spectroscopy at McMurdo station, Antarctica, 8. Observations of night-time NO_2 and NO_3 from April to October 1991, *J. Geophys. Res.*, **98**, 993 - 1000, 1993.
244. Somayajulu, Y. V., K. S. Zalpuri, and S. Sampath, Rocket measurement of ozone density distribution in the equatorial stratosphere and mesosphere, *Indian J. Radio Space Phys.*, **10**, 197 - 200, 1981.
245. Spinhirne, J. D., and M. D. King, Latitude variation of spectral thickness and columnar size distribution of the El Chichón stratospheric aerosol layer, *J. Geophys. Res.*, **90**, 10,607-10,619, 1985.
246. Stommel, H., and E. Stommel, Volcano weather, 177 pp., *Seven Seas Press*, New Port, R. I., 1983.
247. Stowe, L. L., R. M. Carey, and P. P. Pellegrino, Monitoring the Mt. Pinatubo aerosol layer with NOAA/11 AVHRR data, *Geophys. Res. Lett.*, **19**, 159-162, 1992.
248. Subbaraya, B. H., S. Lal, and A. Jayaraman, In - situ measurement of ozone concentration profiles at stratospheric and mesospheric altitudes over Thumba, (Abstract), *IMAP Third Scientific Assembly*, Hamburg, Federal Republic of Germany, August, 1981.
249. Subbaraya, B. H., and A. Jayaraman, The vertical distribution of ozone in the equatorial zone, *Adv. Space Res.*, **7**, (9)119 - (9)112, 1987.
250. Syed, M. Q., and A. W. Harrison, Ground based observations of stratospheric nitrogen dioxide, *Can. J. phys.*, **58**, 788-802, 1980.
251. Syed, M. Q., and A. W. Harrison, Seasonal trend of stratospheric NO_2 over Calgary, *Can. J. Phys.*, **59**, 1278-1279, 1981.
252. Thomas, G. E., B. M. Jakosky, R. A. West, and R. W. Sanders, Satellite LIMB-scanning thermal infrared observations of the El Chichon stratospheric aerosol : First results, *Geophys. Res. Lett.*, **10**, 997-1000, 1983.

253. Toon, G. C., C. B. Farmer, and R. H. Norton, Detection of stratospheric N_2O_5 by infrared remote sounding, *Nature*, **319**, 570 - 571, 1986.
254. Toon, G. C., C. B. Farmer, L. L. Lowes, P. W. Schaper, J. - F. Blavier, and R. H. Norton, Infrared aircraft measurements of stratospheric composition over Antarctica during September 1987, *J. Geophys. Res.*, **94**, 16,571 - 16,596, 1989.
255. Uehara, K., and H. Sasada, High resolution spectral atlas of nitrogen dioxide 559 - 597 nm, *Series in Chemical Physics*, Vol. **41**, Springer, New York, 1985.
256. Vassy, A., and E. Vassy, Effect of temperature on the absorption spectrum of ozone : Chappuis band, *J. Chem. Phys.*, **16**, 1163 - 1164, 1948.
257. Vigroux, E., Contribution a' l'e'tude experimentale de l'absorption de l'ozone, *Ann. Phys.*, **8**, 709 - 762, 1953.
258. Volz, F. E., and R. M. Goody, The intensity of the twilight and upper atmospheric dust, *J. Atmos. Sci.*, **19**, 385-406, 1962.
259. Volz, F. E., Twilight and stratospheric dust before and after the Agung eruption, *App. Opt.*, **8**, 2505-2517, 1969.
260. Volz, F. E., Spectral skylight and solar radiance measurements in the Caribbean: Maritime aerosols and sahara dust, *J. Atmos. Sci.*, **27**, 1041 - 1047, 1970.
261. Volz, F. E., Infrared optical constants of Ammonium sulfate, Sahara dust, Volcanic pumice, and Flyash, *Applied Optics*, **12**, 564-568, 1973.
262. Volz, F. E., The stratospheric dust event of October 1971, *J. Geophys. Res.*, **79**, 479-482, 1974.
263. Wahner, A., R. O. Jakoubek, G. H. Mount, A. R. Ravishankara, and A. L. Schmeltekopf, Remote sensing observations of daytime column NO_2 during the airborne Antarctic ozone experiment, August 22 to October 2, 1987, *J. Geophys. Res.*, **94**, 16,619-16,632, 1989.

264. Wahner, A., J. Callies, H. P. Dorn, U. Platt, and C. Schiller, Near UV atmospheric absorption measurements of column abundances during Airborne Arctic stratospheric expedition, January- February 1989 : 1. Technique and NO₂ observations, *Geophys. Res. Lett.*, **17**, 497-500, 1990.
265. Webster, C. R., and R. T. Menzies, In situ measurements of stratospheric nitric oxide using a balloon-borne tunable diode laser spectrometer, *Appl. Opt.*, **23**, 1140 - 1142, 1984.
266. Weiler, K. H., P. Fabian, G. Flentje, and W. A. Mathews, Stratospheric NO measurements: A new balloon-borne chemiluminescence instrument, *J. Geophys. Res.*, **85**, 7445 - 7452, 1980.
267. Wilkes, M. W., A table of Chapman's grazing incidence integral $Ch(X, \chi)$, *Proc. Phys. Soc. London, Sect. B*, **67**, 304 - 305, 1954.
268. Wilson, J. C., M. R. Stolzenburg, W. E. Clark, M. Loewenstein, G. V. Ferry, K. R. Chan, and K. K. Kelly, Stratospheric sulfate aerosol in and near the northern hemisphere polar vortex : The morphology of the sulfate layer, multimodal size distributions, and the effect of denitrification, *J. Geophys. Res.*, **97**, 7997-8013, 1992.
269. Winker, D. M., and M. T. Osborn, Airborne LIDAR observations of the Pinatubo volcanic plume, *Geophys. Res. Lett.*, **19**, 167-170, 1992a.
270. Winker, D. M., and M. T. Osborn, Preliminary analysis of observations of the Pinatubo volcanic plume with a polarization - sensitive LIDAR, *Geophys. Res. Lett.*, **19**, 171-174, 1992b.
271. Wofsy, S. C., and M. B. McElroy, HO_x, NO_x and ClO_x: their role in atmospheric photochemistry, *Can J. Chem.*, **52**, 1582 - 1591, 1974.
272. Wofsy, S. C., Temporal and latitudinal variations of stratospheric trace gases: a critical comparison between theory and experiment, *J. Geophys. Res.*, **83**, 364 - 378, 1978.
273. World Meteorological Organization, The stratosphere 1981; Theory and measurements, **Report No. 11**, WMO global ozone research and monitoring project, Geneva, 1981.

274. World Meteorological Organization, Atmospheric ozone 1985; assessment of our understanding of the processes controlling its present distribution and change, **Report No. 16**, pp. 1095, *WMO Global ozone Res. and Monitoring Project*, Geneva, 1986.
275. Yao, F., I. Wilson, and H. Johnston, Temperature dependent ultraviolet absorption spectrum for dinitrogen pentoxide, *J. Phys. Chem.*, **86**, 3611 - 3615, 1982.